PREDICTION OF STRONG GROUND MOTION FOR PARTS OF NORTH INDIA

A THESIS

Submitted in fulfilment of the requirements for the award of the degree

of

DOCTOR OF PHILOSOPHY

in

APPLIED GEOPHYSICS

By

ABHA MITTAL

DEPARTMENT OF EARTH SCIENCES
INDIAN INSTITUTE OF TECHNOLOGY ROORKEE
ROORKEE–247 667 (INDIA)

DECEMBER, 2002

Nothing can happen
without Master's Grace,
and that Grace and our effort
go side by side.
The more effort we make,
the more Grace He showers on us
to make more effort,
He is all powerful
and no laws apply to Him.

INDIAN INSTITUTE OF TECHNOLOGY ROORKEE

CANDIDATE'S DECLARATION

I hereby certify that the work which is being presented in the thesis entitled ***"Prediction of Strong Ground Motion for Parts of North India"*** in fulfilment of the requirement for the award of the Degree of Doctor of Philosophy and submitted in the Department of Earth Sciences of the Indian Institute of Technology, Roorkee is an authentic record of my own work carried out during a period from January 1997 to December 2002 under the supervision of Prof. V.N. Singh and Dr. Tanuja Srivastava.

The matter presented in this thesis has not been submitted by me for the award of any other degree of this or any other Institute/University.

Abha Mittal

(Abha Mittal)
Signature of the Candidate

This is to certify that the above statement made by the candidate is correct to the best of our knowledge.

Tanuja

(Dr. Tanuja Srivastava)
Asstt. Professor
Department of Mathematics
Indian Institute of Technology
Roorkee – 247667 (INDIA)

V.N. Singh

(Prof. V.N.Singh)
Professor
Department of Earth Sciences
Indian Institute of Technology
Roorkee – 247667 (INDIA)

Date : 26.12.2002

Signature of Supervisors

The Ph.D. Viva-Voce examination of **Abha Mittal,** Scientist, CBRI Roorkee, has been held on 7-9-2005

Tanuja

Signature of Supervisor(s)

V.N. Singh

Signature of H.O.D.

RP Singh

Signature of External Examiner

V.N. Singh

ABSTRACT

The development of appropriate preventive measures to minimize the risk of damage from earthquakes is dependent on the proper evaluation of seismic hazard in the region. The source of damage lies most often with the strong shaking caused by the waves set up by the earthquakes. The records of strong ground motions from past earthquakes can serve to provide a wealth of information that will be indispensable in the design of earthquake resistant structures. In many regions like Himalayas, such records generated by past earthquakes are few or absent and one needs to use theoretical predictions for estimating the peak ground acceleration or complete time history of ground from expected earthquakes in order to assess the seismic hazard. However synthetic accelerograms are now increasingly being used in earthquake engineering. A knowledge of regional and local seismicity and seismotectonics, a suitable earth model and source characteristics of the design earthquake are required for this purpose.

The work carried out in the present thesis has been divided into two parts. In the first part, new empirical attenuation relationships for estimating peak ground acceleration have been derived for Himalaya and northeast regions of India. In the second part, an improved method of generating synthetic accelerograms has been presented and discussed based on the convolution model of seismogram.

The peak values of horizontal acceleration is one of the important parameter that is considered in the earthquake safe design of structures. In the present study, the strong motion data from eight earthquakes (three in Himalayan region and five in Shillong area) has been used. The Himalayan region and

Shillong area are characterised by two different tectonic environments, so two different attenuation relationships are developed. An integrated attenuation relationship has also been developed based on the relationships available in literature. An exercise has also been done to find out the attenuation relationship available in literature which predicts PGA values nearer to the observed ones. After comparing these three attenuation relationships it is observed that our developed relationships gives the good fit with the observed values.

In the second part, a simple and fast method has been discussed and presented for generating synthetic accelerograms based on the convolution model of the seismogram. The spectrum of the ground motion expected at recording site are first computed from the knowledge of source parameters (source mechanism, size, geometry, time function, slip distribution on fault plane, radiation pattern etc.) and medium properties (elastic properties of earth materials in the immediate vicinity of the fault, geometrical spreading, frequency dependent attenuation, local site geology etc.). This spectrum is then inverse Fourier transformed to yield the desired synthetic accelerogram.

The suitability of the method has been demonstrated by comparing the synthetic accelerograms with the observed accelrograms for two earthquake events of Uttarkashi, 1991 and Chamoli, 1999. The synthetic and observed accelerograms are compared at eight sites for Uttarkashi earthquake and at five sites in case of Chamoli earthquake. The observed and synthetic accelerograms are compared for selected portions of high amplitudes. The extent of matching has been quantitatively expressed by computing the r.m.s. errors. It has been found that matching between the synthetic and observed is quite comparable.

ACKNOWLEDGEMENTS

I feel to express my profound indebtness, deep sense of gratitude and sincere thanks to Prof. V.N. Singh, Department of Earth Sciences and Dr. Tanuja Srivastava, Department of Mathematics, Indian Institute of Technology, Roorkee who not only imparted valuable instructions but also instilled in me a constant fountain of inspirational courage and evoked a keener sense of responsibility and devotion, during this endeavor. It is due to their inspiring novel ideas, expert and constant guidance, invaluable advice, constructive criticism without which it would not have been possible to complete this research work. I am highly obliged to both of them.

I am extremely grateful to the Head and other faculty members of Department of Earth Sciences, IIT, Roorkee and to the Director and other officials of the Central Building Research Institute, Roorkee for providing the required facilities during the course of present work.

Heart-felt thanks are due to my friends and colleagues Dr. Pradeep Kumar, Dr. Atul Kr. Agarwal, Scientists and Ms. Deepti Agarwal, B.S. Bisht, Tech. Staff of CBRI who have helped and co-operated me at various stages of the present work. Thanks are also due to Dr. K. K. Srivastava, Director, CESER, Roorkee for their constant encouragement and suggestions during the course of this work. Thanks are due to Ms. Himani, Vandana and Priyamvada, Research Scholars of IIT, Roorkee who helped me time to time.

The good wishes, honest blessings, moral support and encouragement of my mother, sisters, brothers and other relatives in various ways are deeply appreciated and gladly acknowledged for completion of this task.

I take pleasure in acknowledging my debt to all my colleagues and friends named or un-named , who provided me the environment in casting my work to present stage.

No words, no language is ever adequate to express my heart-felt veneration for my dear husband Shri M.C. Mittal and sons Master Achal and Nishchal for their willing co-operation, whole hearted moral support, painstaking patience and continued understanding.

Last but not the least, my heart goes to the memory of my father Late Shri J.P. Jain who had always desired and wished for my attaining a distinguished status. With profound love and regards, I dedicate this work to his cherished memories which are always with me.

Abha Mittal

(Abha Mittal)

December 2002

CONTENTS

LIST OF FIGURES

LIST OF TABLES

CHAPTER 1

Introduction

1.1 Preamble

Earthquakes pose a grave risk to life and property in seismically active areas. Mitigating the risk of damage from imparting earthquakes in such areas is of paramount importance. Prediction of the next big earthquake may be a solution in this direction. However, methodologies of earthquake prediction are not advanced to a stage where an accurate prediction can be made. One important way which will substantially reduce the risk of damage is earthquake resistant design and construction of all civil structures in earthquake prone areas. This will greatly reduce, if not eliminate, the risk of total collapse of a building.

Earthquake resistant design of a civil structure depends critically on the quality and accuracy of seismological data. A good and reliable knowledge of some key parameters of strong ground motion such as peak ground acceleration, duration of strong shaking, frequency content will enable one to make a better estimate of design spectrum. This will be adequate for designing ordinary structures. For a detailed dynamic analysis of an important civil structure, a complete specification of entire time history of expected ground motion will be more desirable.

For estimating peak ground acceleration at a site, available strong motion data has been used to propose a number of attenuation relationships. Generation of synthetic accelerograms is, however, a much more formidable problem. It made a reliable estimate of source

parameters of an earthquake along with its location parameters. A number of methods have been proposed for this purpose both in time and frequency domains. These methods differ from each other in the details of rupture process, velocity and attenuation models whether a detailed waveform modelling is used or not. These methods are quite successful in predicting strong ground motion sufficiently accurately.

1.2 A Review of Literature

In strong motion seismology, earthquakes of magnitude 5 or more are considered important in view of their damage potential. The ground motion recorded in the near field of large earthquakes is essentially of high frequency. Such ground motion is not recorded very often. Peak ground acceleration (PGA) is often used to characterise strong ground motion. It is an important parameter in arriving at an acceptable design spectrum which is considered for designing ordinary structures. However, for earthquake resistant design of other important structures like dams and nuclear power plants, located in seismically active areas, it is desirable to have a reliable site specific acceleration time history.

On the basis of strong motion data available of past earthquake events worldwide, a number of attenuation relationships are available in literature to calculate the PGA values. A comparison of various attenuation characteristics clearly shows that they are region specific due to different geological characteristics and the seismic source properties. This demands the careful examination of any available relationship prior to use in a seismic design.

A number of computational methods have been presented in the literature for solving the forward problem in strong motion seismology,

viz., predicting the synthetic accelerogram i.e. the acceleration time history at a given point on the earth's surface for an earthquake with prescribed source mechanism. The source mechanism includes specification : location and orientation of the fault plane in terms of dip and strike angles, distribution of slip on the fault plane, source time function, dimension of the fault plane and the location of the point on the fault plane (i.e. the focus) at which the rupture initiates. The medium properties between the fault and receiving point on the earth's surface, details of the recording instruments, properties of the intervening medium in terms of velocity structure, Q structure etc. are the other specifications which effect the source mechanism. In addition the topography near the point of observation may also be considered.

A brief literature review has been given in subsequent sub-sections.

1.2.1 Development of Predictive Relationships

The ground motion is described commonly in the form of time histories of acceleration, velocity and displacement. The directly obtained parameters from time histories of accelerograms are their peak values. Therefore, peak acceleration (a), peak velocity (v) and peak displacement (d) are most widely used parameters. Apart from peak values, the characterisation of earthquake ground motion in terms of its response spectra are also used for earthquake resistant design. The response spectra is obtained from ground motion and is related with frequency content of accelerogram.

The correlation of peak ground acceleration with earthquake magnitude and distance is characterised by large scattering and uncertainties. Ritcher (1958) stated that the earthquake magnitude is conventionally

defined from the peak amplitude of intermediate or long term seismic waves, whereas the peak acceleration is mostly associated with the high frequency waves. Brune (1970) had came out with the result that in the near field, very close to the seismic source, the peak acceleration is mainly governed by the stress drop and not by the magnitude. Due to the use of different data bases, various published empirical attenuation relationships for peak ground acceleration produce widely varying results. Further, the use of particular relationship for an area with different geological and tectonic features would lead to the results which may differ significantly from the actual values. Esteva & Rosenblueth (1963), Milne et. al (1969), Donovan (1973), McGuire (1977) and Cornell et. al (1979) have given attenuation relationships based on the strong motion data for different parts of the world. Idriss (1979), has given a comprehensive review of ground motion predictive relationship developed before the 1979 Imperial Valley, California, earthquake. Joyner & Boore (1981) has worked on world wide data for rock sites and gave a reasonable values for distances less than 50 km. Hasagava et. al. (1981) worked on Western & Eastern Data of Canada. Campbell (1985) have reviewed the attenuation relationship published up to 1984. Peng et.al (1985) have worked on data of China region. Sabetta & Pugliese (1987) have given a relationship based on Italian Data.

In 1989, Abrahamson & Litehiser have worked on worldwide data. They used the two step regression procedure that is a hybrid approach of Joyner & Boore (1981) & Campbell (1981) regression methods. They found that site geology had a profound effect on peak acceleration recorded during earthquake.

In 1990, Fukushima & Tanaka developed the relationship for the standardised ground condition. They used the large amount of acceleration data available in Japan supplemented by near sources data from the United State and other part of the world. Campbell (1991) used Loma Prieta, California earthquake data to study the empirical analysis. He concluded that source directivity, radiation pattern and local site conditions could be partly responsible for peak acceleration.

Anderson & Lei (1994) & Anderson (1996) developed a non-parametric model for PGA for sub-duction zone event using data from Guerrero, Mexico, accelerograph network. Abrahamson & Silva (1997) derived empirical response spectral attenuation relationship for both the horizontal & vertical components for ground motion. They used the data of Western coastal regions of North America. Sadigh et.al (1997) developed attenuation relationship for shallow crustal earthquakes based on California Strong Motion Data. Youngs et. al (1997) developed relationship for sub-duction zone events primarily based on recordings from Japan & South America. Atkinson & Boore (1997 a,b) developed attenuation relation for stable continent region, the input data spans thousands of records from hundreds of Eastern North America earthquakes in the magnitude range from 3-7 at distances from 10 to 1000 km. All the data was taken from hard-rock sites.

Based on the Indian strong motion data an attenuation relationship for peak horizontal acceleration has been given by Gupta et.al. (1991) for Koyna region and relationships for Himalayan region has been developed by Singh et.al. (1996) and Sharma (1998).

1.2.2 Stochastic Simulation of Ground Motion

The earthquake ground motion is to be treated as random process. The parameters of random process model could be determined directly by statistical analysis provided ensemble of earthquake records are available. This was not possible earlier because of availability of few strong motion records. This forced researchers to propose various stochastic models of ground motion based on few records. They can be broadly classified into three categories (i) white noise (ii) stationary process and (iii) non-stationary process.

Initially Housner (1947) had modeled earthquake acceleration as random process. The acceleration was idealised, as a series of pulses, which in fact is white noise. Housner (1955) improved the model by taking accelerograms as sum of full period sine wave pulses with frequency and amplitude taken from a calculated probability distribution. Some investigators such as Hudson (1956), Rosenblueth (1956), Bycroft (1960) identified earthquake accelerograms as white noise and showed that velocity spectra obtained were similar to those of actual earthquake records. Housner (1959) stated that despite the fact that the white noise processes are unrealistic it was quite popular because of its simplicity to use.

The stationary process models were an improvement over the white noise model as they can be shaped to represent the frequency characteristics of the actual ground motion closely. Nevertheless, because of non-stationary and transient nature of earthquake ground motion, engineers have tried to include it in strong ground motion modelling by introducing non-stationary random process models. A simplest of its kind, non-stationary model can be constructed by

multiplying a deterministic modulating function with stationary process having specified auto-correlation or power spectral density.

Bolotin (1960) was perhaps the first to suggest modulated stationary process. Maruyama (1963) and Burridge and Knopoff (1964) showed that the body force equivalent of a point shear dislocation is a double couple and that a synthetic seismogram can be constructed by a space-time convolution of the slip function and Green's function. The slip function describes the form of the fault displacement as a function of time and position of the fault plane. Green's function is the response of earth when an impulsive double couple is applied at a point on the fault plane. The slip function and Green's function express quantitatively the source and propagation effect, respectively, on seismic motion.

Housner & Jennings (1964), modeled earthquake accelerograms as stationary Gaussian random process with a given power spectral density and generated a ensemble of artificial earthquakes. Shinozuka and Sato (1967) generated accelerograms by passing white noise through a second order filter and imparting non-stationerity by an enveloping function. Amin and Ang (1968) also suggested non-stationary filtered Gaussian white noise process with a second order filter as a suitable model for strong motion earthquake. Iyengar & Iyengar (1969) included number of zero crossings and time dependent variance function in to a modulated stationary random process. Penzein & Liu (1969) used filtered stationary white noise process with given filter parameters to model accelerograms.

The most fundamental synthesis of strong ground motion was carried out by Aki (1968) and Haskell (1969) based on Green's function

approach. The response of horizontally layered crustal structure to a double couple point source has been computed using a number of techniques e.g., generalized ray theory (Helmberger, 1968; Heaton and Helmberger, 1977, 1978), reflectivity method (Fuchs and Mueller, 1971), direct frequency domain integration (Herrmann, 1977), the normal mode method (Swanger and Boore, 1978) and the discrete wave-number method (Bouchon, 1979) and by the descrete wave number/ finite element method (Olson, 1982). Some of these methods generate the complete response of the medium, including all types of body and surface waves.

The earthquake ground motion accelerograms consist of essentially three phases namely a weak initial phase, a strong phase followed by a weak phase, so it should be treated as non-stationary random process. The popular approach has been to assume the strong motion to be Gaussian stationary random process. The motion at any given time can be considered as the superposition of a large number of wave forms. Thus, the Central Limit Theorem may be invoked to argue that the ground motion must be tending to be Gaussian. Gaussian random process can be completely defined in terms of mean, standard deviation and second order correlation function. The mean is generally taken to be zero because of the to and fro of the oscillation.

Apart from these direct models, indirect modelling of strong ground motion is also proposed in the literature. The earth is characterised by lateral heterogenities, attenuation properties and local topographical site effects in the vicinity of the faults. Due to these complexities complete modelling with any of the given methods is difficult. To overcome this difficulty, Hartzell (1978) presented a semi-empirical

approach in which strong ground motions from a large earthquake are modeled by using the aftershocks as an empirical earth response. The ground motion associated with a small event may be treated as Green's function if its source can be approximated as a point source on the fault on which a large earthquake takes place.

The models of earthquake source in the methods described above are kinematic in nature. In these models some simplifying assumptions are made in a arbitrary manner on the rupture propagation over the fault plane and the displacement time history. For a comprehensive understanding of complex ground motions in the near field in a event of large earthquake, modelling of the actual rupture process must be done. Haskell (1966) introduced a model involving statistical randomness of fault slip along the fault plane. Das and Aki (1977 a,b) considered a fault plane having various barriers distributed over it. Rupture starts near one of the barriers and then propagates over the fault plane until it is brought to rest or slowed to the next barrier.

Stochastic source model is the first realistic theoretical predictions of strong ground motion. Two stochastic source models are available in the literature, the barrier model of Papageorgiou and Aki (1983a,b) and stochastic ω-square model of Hanks and McGuire (1981). In the barrier model a rectangular fault plane is covered by circular cracks of equal diameter separated by unbroken barriers. This model is specified by five basic parameters, fault length, fault width, maximum slip, rupture velocity and barrier interval. A sixth parameter, the cohesive zone size, is introduced to explain the cutoff of high frequencies in the spectrum.

The cutoff frequency f_m (Hanks, 1982) is considered by Papageorgiou and Aki (1983a) to be a source parameter that may vary with other source parameter.

According to the Hanks-McGuire (1981) model, earthquake accelerations are band-limited white noise in the band between the corner frequency f_o and f_m, and the spectral shape is given by the Brune (1970, 1971) spectrum. Hanks and McGuire (1981) used this model with the aid of random vibration theory to predict horizontal peak acceleration and rms acceleration and obtained excellent agreement with empirical data over the magnitude range from 4.0 to 7.0. Boore (1983) made use of both stochastic simulations and random vibration theory to test the predictions of the Hanks- McGuire (1981) model for peak horizontal velocity and response spectra as well as for peak acceleration. Hanks and Boore (1984) showed that the model predictions reproduce the correlation between log moment and local magnitude M_L for California earthquakes in the M_L range form 0 to 7. Boore (1986) compared model predictions with peak teleseismic P-wave amplitudes given by Houston and Kanamori (1986) for earthquakes with moment magnitude up to 9.5 and showed good agreement.

Boore and Atkinson (1986) has given the spectral model by considering the various factors such as, nature of earthquake source, distance to the point of observation, geometrical spreading, frequency dependent attenuation along the path of propagation of energy, local site geology etc. Gaussian white noise is generated with a random number generator. This noise is windowed with shaping function whose duration is related to the source corner frequency. The amplitude of the window

is chosen such that the mean level of the spectrum is unity. Filtering is then performed in the frequency domain by multiplying the spectrum of the white noise by the spectral shape calculated previously. Fourier transformation back to the time domain then yields the desired time series.

Some of the recent attempts on new approaches to synthesize strong ground motion and to obtain source parameters include those of Somerville et.al. (1990, 1991), Abrahamson et.al. (1990), Makaris et.al. (1992), Barker et.al. (1988,1989), Wald (1991), Zeng et.al. (1993 a,b), Zeng et.al. (1994 a,b), Khattri et.al. (1994 a), Yu et.al. (1995) and Kumar et.al. (1999).

Khattri et.al. (1994 b) and Yu et.al. (1995) carried out synthesis of strong motion for the Uttarkashi earthquake. Khattri et.al. (1994 b) carried out the forward modelling using the isochrone method and inverted the observed accelerograms by recursive stochastic inverse algorithm to obtain the earthquake source slip function. Yu et.al (1995) generated synthetics using the composite source model and synthetic green's function. The solution of forward problem carried out by Yu et.al. (1995) have taken into account the velocity structure in the Uttarkashi area and its Q structure. The method of generating synthetics, depend on the knowledge of many input parameters like velocity and Q structure of the layered earth model. Kumar et.al. (1999) used semi-empirical method for calculating synthetic accelerogram. He divided the fault plane into the sub-faults. They generated envelop waveform, instead of actual time history, corresponding to each element of the fault plane.

1.3 Plan of the Thesis

The plan of thesis is briefly as follow:

In **Chapter 2** a generalised form of the attenuation model has been presented. Subsequently, an attempt has been made to develop two attenuation relationships for Himalayan and Northeast (Shillong) regions of India.

In **Chaper 3** gives the details of a simple method for generating the synthetic accelerograms has been presented and some aspects of computational strategy have been discussed.

In **Chapter 4**, the results of the computations in the form of synthetic accelerograms have been presented and discussed. A comparison between the synthetic and observed ground motion has been given and it is found to be quite comparable. Synthetic accelerograms for a hypothetical earthquake in Himalayan region have also been generated and presented at few sites in Garhwal Himalaya.

In **Chapter 5**, a summary and conclusions are given. Few suggestions for further research work have also been included.

CHAPTER 2

Empirical Attenuation Relationships

2.1 Introduction

Due to severe earthquake, the prediction of peak ground acceleration (PGA) is necessary for the assessment of seismic effects on structures and their mitigation. The peak values of horizontal acceleration is one of the important parameter that is considered in the earthquake safe design of engineered structure. Accordingly, a number of studies have been done to obtain the attenuation relations for peak ground acceleration for various region of the world. Many of these relationships are region specific and cannot be applied elsewhere. It has been recognised that attenuation of strong ground motion with distance from the source are also governed by tectonic environment of the region, among other factors. Most of these studies are based on regression or multiple regression analysis of large data sets of strong motion acceleration records. Paucity of adequate set of strong motion data, very few attempts have been made to develop attenuation relationship for strong motion data of Indian region.

In the present Chapter, an attempt has been made to develop two attenuation relationships for Himalayan region and Shillong area of India because both the regions are governed by different tectonic environment.

2.2 Strong Motion Arrays in India

The earliest record of strong motion in India were obtained from 1967 Koyna Earthquake. These were manually digitized and analyzed by Jai Krishna and Chandrasekaran (1969). The strong motion instrumentation programme of the Department of Earthquake Engineering, I.I.T., Roorkee has led to the installation of strong motion arrays in Himalayan region of India, namely, the Kangra array in the Himachal Pradesh (NW India), the Uttar Pradesh (UP) array (N-C India), the Shillong array in Meghalaya and Assam (N-E India) and the Bihar array in Bihar. Recently, a network of Strong Motion Accelerograph has been installed in in Delhi region. Figure 2.1 shows the locations of the arrays.

Kangra array has fifty strong motion accelerographs installed in the region trends to NW to NE having a dimension of about 240 km. Most of the stations in this array are located in Lesser Himalayas. There are numerous faults and thrusts, but along these two are of Prominence and can be traced all essentially thrust sheets. The tectonic feature separating Tertiaries from Mesozoic is the main boundary thrust (MBT) and Mesozoic from central crystalline of the Main Central Thrust (MCT).

Uttar Pradesh (U.P.) array or Uttaranchal array has 40 analog accelerographs installed in the region. Physiographically the Uttaranchal Himalayan region is represented by high hills and most of the northern part of this Himalayan region is above perpetual snow line and some peaks rises to more than 7500 m high.

Himalayan ranges in Uttaranchal represent a wide variety of tectonic features. Broadly the main tectonic features of this region is similar to that of Himachal Himalayas. This array is deployed around main boundary thrust (MBT) and main central thrust (MCT) in the Uttaranchal Himalayas. The region has experienced high stress condition which resulted in the formation of several tectonic features/ lineaments namely, the Tons thrust, the Srinagar thrust, the Uttarkashi thrust and many other.

Shillong array is deployed with 45 analog accelrographs in the Shillong massif in the states of Meghalaya and Assam. Northeastern region of India has undergone various stages of tectonic activities and present day seismicity is the testimony of the complex seismotectonic setup. Two prominent tectonic features forming the boundary of the Shillong plateau towards west, north Cachar hills and south are the Dhubri and Dauki faults respectively.

The entire region has experienced intense compressive stress which are attributed to slow movements of the Indian plate towards north and east directions. This array primarily covers the central portion of northeast India. The Shillong plateau forms a wedge shaped triangular crustal block bounded by the Arunachal Himalaya towards north and northeast, the Indo-Burma folded belt towards east and southeast, the Bengal basins on the south and Rajmahal-Garo-Syhlet gap towards the west. It comprises of Shillong massif and Mikir hills massif, which are separated by an alluvial tract.

Bihar array has been installed in Bihar region. 15 strong motion accelerographs are installed at various locations in Bihar.

Recently, Central Building Research Institute, Roorkee has been operating **Strong Motion Accelerograph (SMA) Network in Delhi** and nearby region to collect the strong motion data generated in the region as Delhi, the National capital, lies in Seismic zone IV and is fast growing mega city. 16 triaxial digital strong motion acceelrographs are installed within and aroung Delhi (Pandey et.al., 2001)

2.3 Strong Motion Data

There are eight earthquakes contributing data for the study undertaken, one of which has been recorded by Kangra array, two by Uttaranchal array and five by the Shillong array.

The arrays and the strong motion data of the above earthquakes are well documented (Chandrasekaran and Das, 1990; 1995, IMD, 2000). Some salient features of the above earthquakes are listed in Table 2.1. The last column indicates the number of stations considered in the present analysis.

The primary source of focal parameters for all Indian events is Indian Meteorological Department (IMD). The SMA data is collected from Department of Earthquake Engineering, IIT, Roorkee. The locations of eight earthquakes under study are shown in Figure 2.2 which give the tectonic features of the Himalayas. Figures 2.3 – 2.6 show the locations of the epicenter of the earthquakes along-with the recording stations.

The peak ground accelerations (PGA), epicentral distance of these earthquakes at various stations are tabulated in Appendix A. The site type in the form of rock (R) or soil (S) is given. The sites marked "R"

are generally deployed on granite/ quartize/ sandstone. The sites marked "S" are those that are deployed on exposed soil cover on the basement.

Table 2.1 : Locations of the earthquake events under study

Earthquake	Magnitude (m_b)	Epicenter		Focal depth (km.)	No. of stations
		Latitude	Longitude		
Dharmsala (26 April 1986)	5.5	32.18°N	76.28°E	7	9
Shillong (10 Sept. 1986)	5.5	25.42°N	92.08°E	28	12
N.E. (18 May 1987)	5.7	25.27°N	94.20°E	50	14
N.E. (6 Feb. 1988)	5.8	24.64°N	91.51°E	15	18
N.E. (6 Aug. 1988)	5.8	25.14°N	95.12°E	91	33
N.E. (1 Jan. 1990)	6.1	24.75°N	95.24°E	119	14
Uttarkashi (20 Oct. 1991)	6.6	30.78°N	78.78°E	12	13
Chamoli (29 Mar. 1999)	6.8	30.41°N	79.42°E	21	10

Source : Indian Meteorological Department (IMD), Delhi

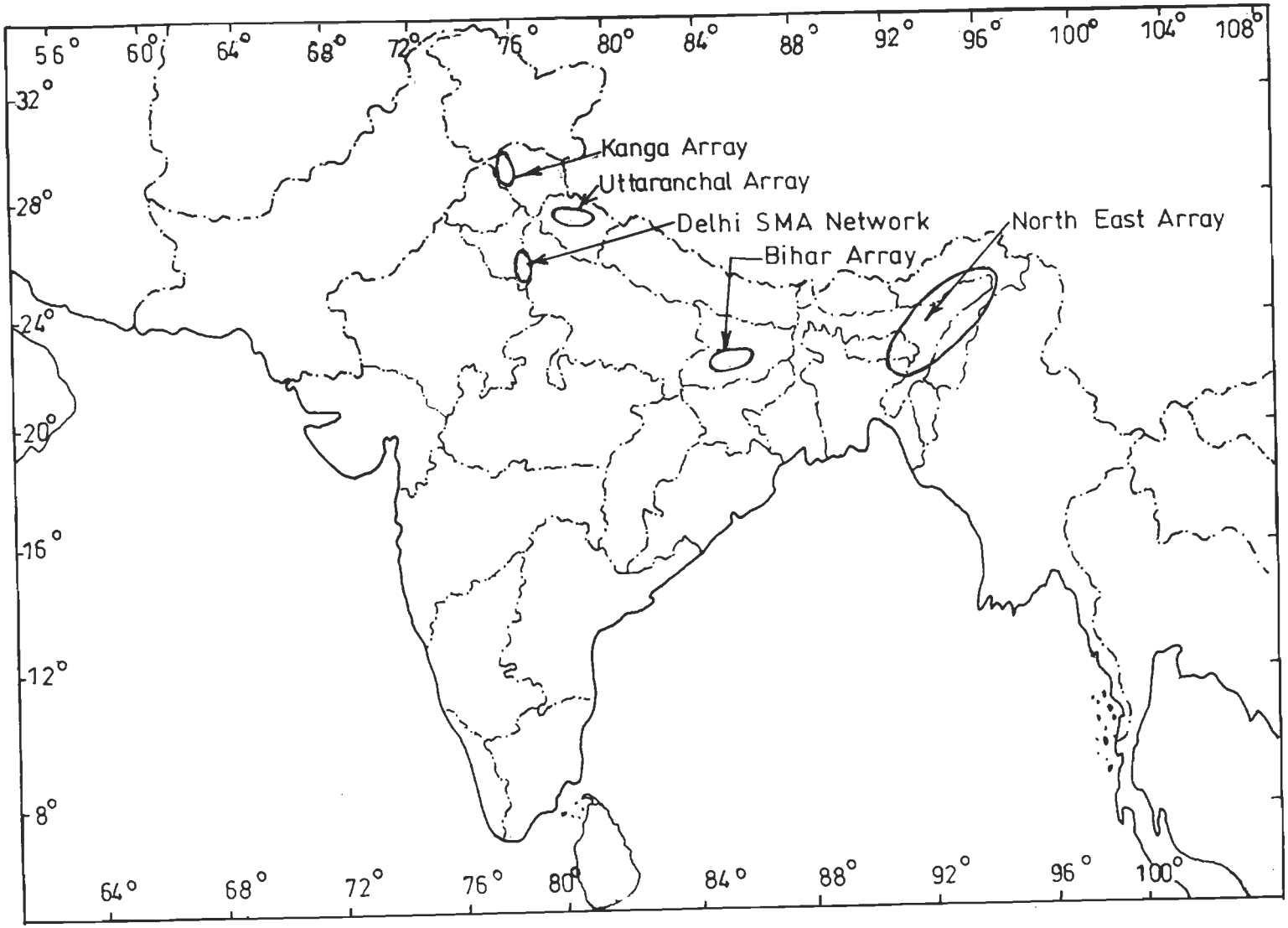

Fig. 2.1 : Locations of the strong motion arrays in India

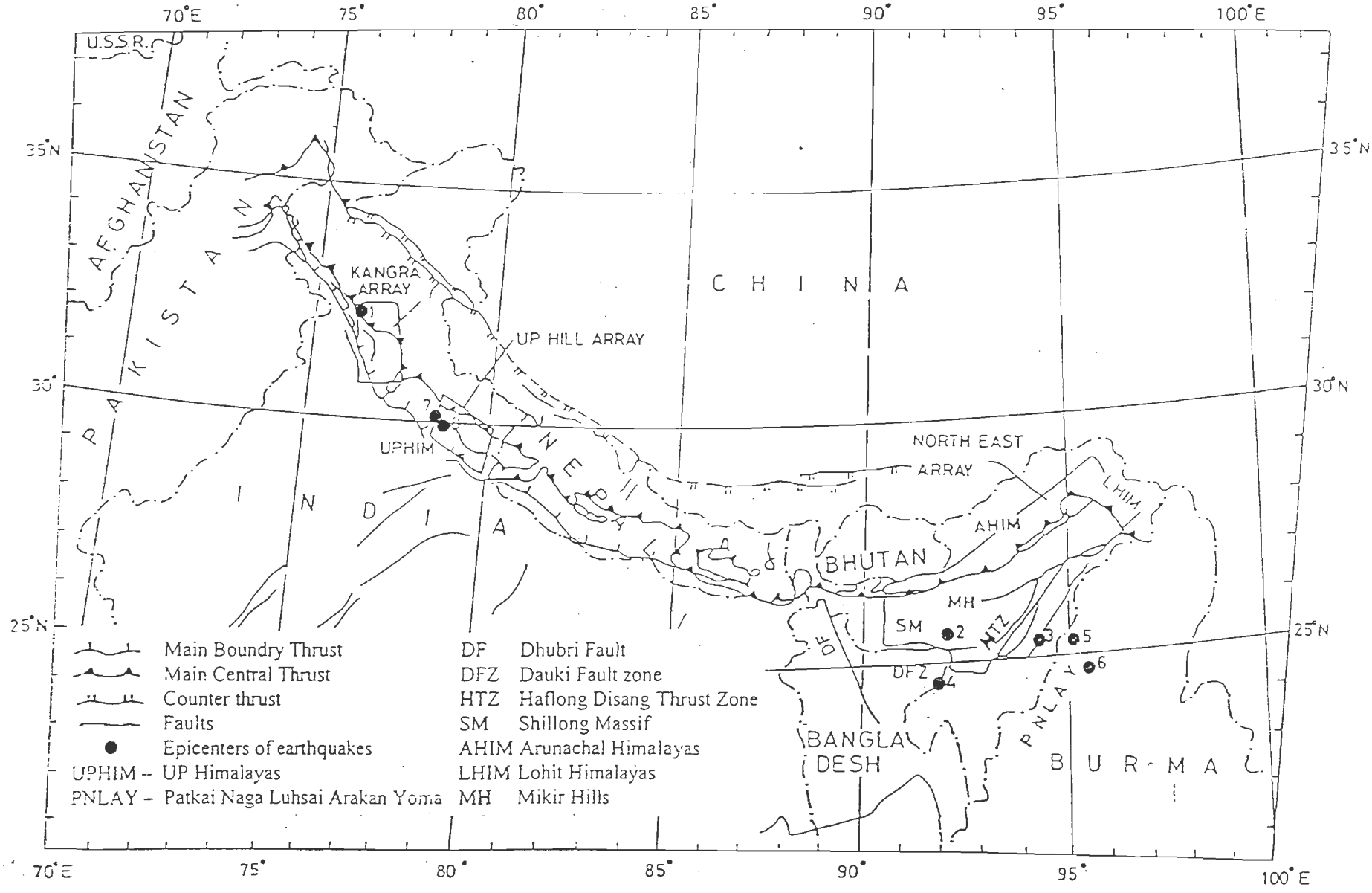

Fig. 2.2 : Locations of the earthquakes undertaken for study (after Sharma, 1998)

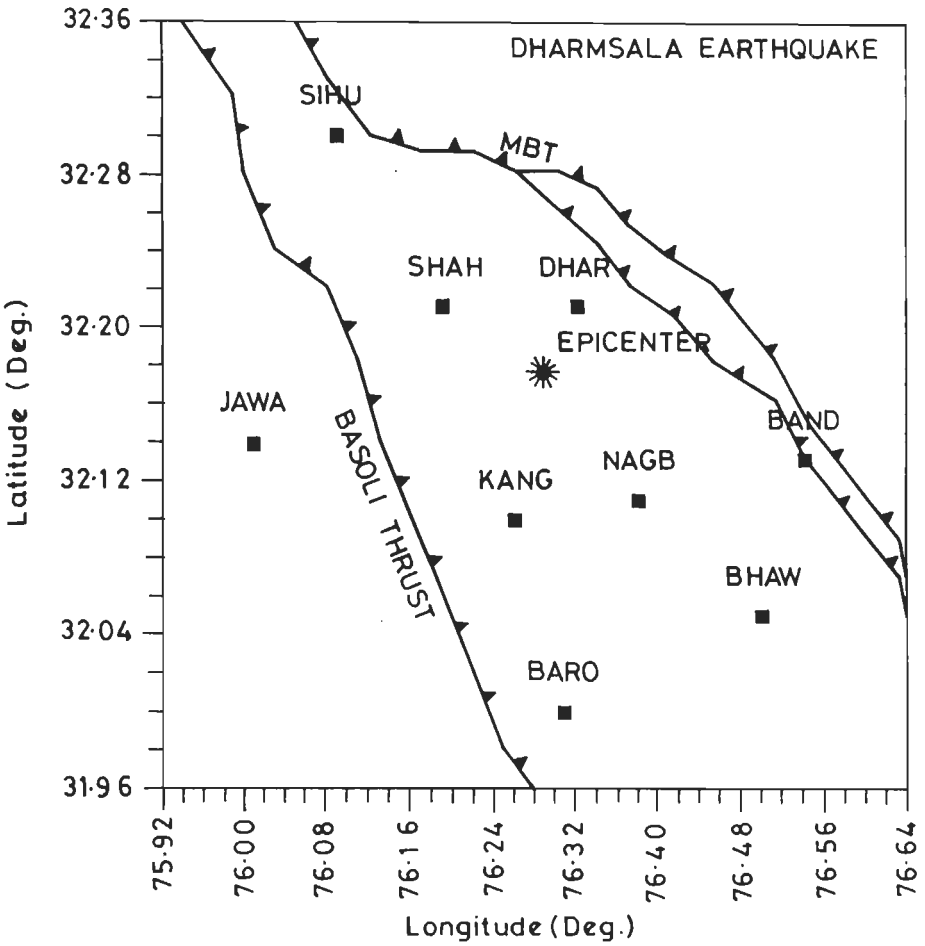

Fig. 2.3 : Locationof the Dharmsala, 1986 earthquake and recording stations alongwith main tectonic features of the region.

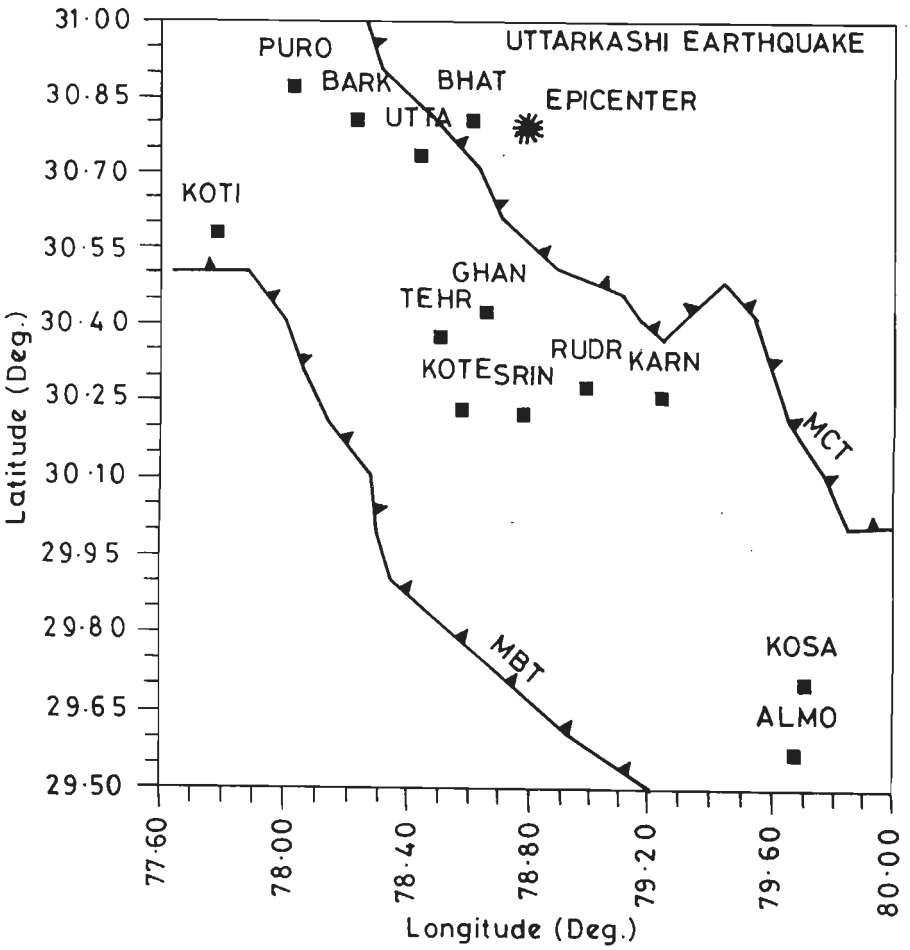

Fig. 2.4 : Location of the Uttarkashi, 1991 earthquake and recording stations alongwith main tectonic features of the region.

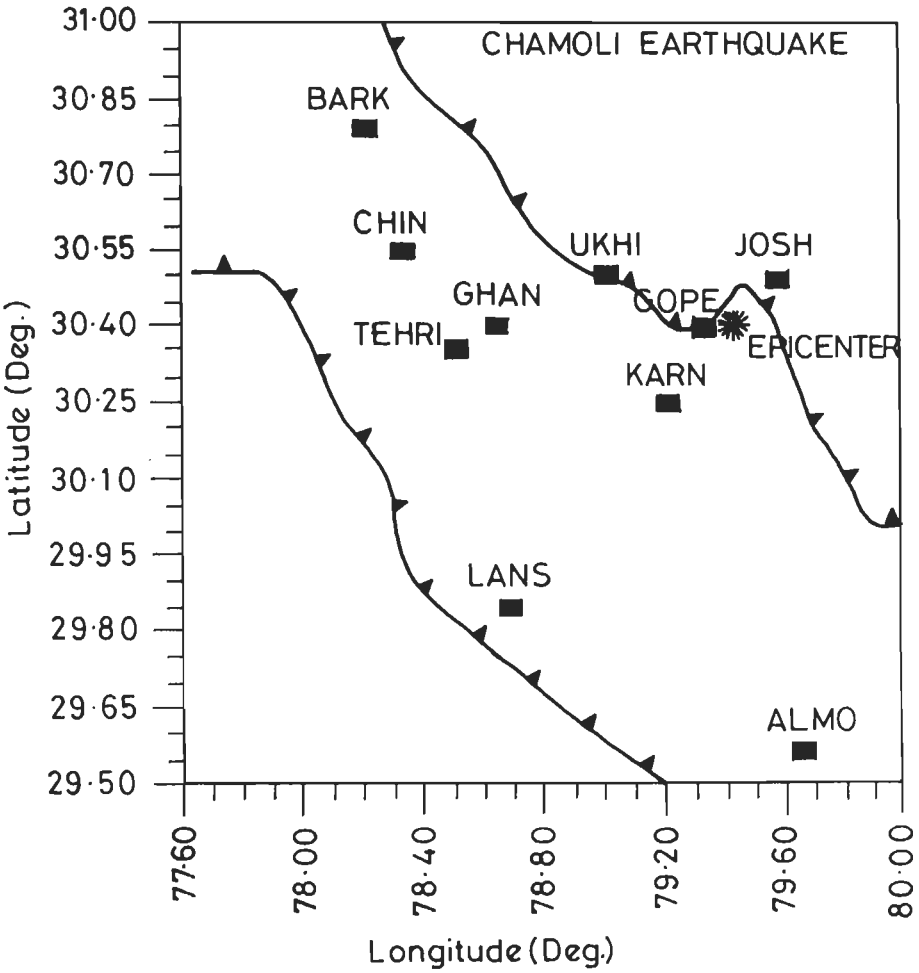

Fig. 2.5 : Location of the Chamoli, 1999 earthquake and recording stations alongwith main tectonic features of the region.

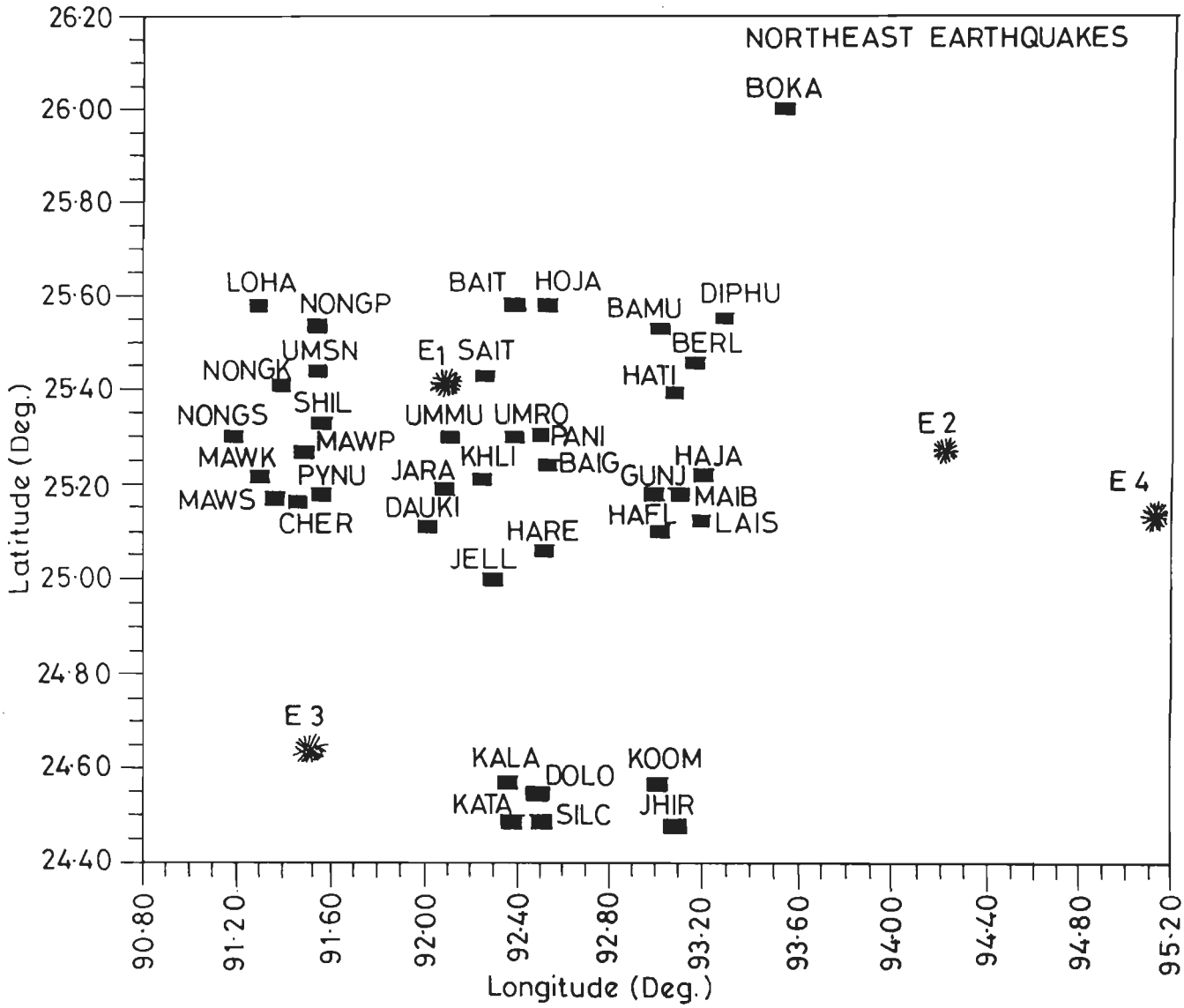

Fig. 2.6: Locations of the five earthquakes and recording stations of the northeast region

2.4 Ground Motion Attenuation Model

The peak ground acceleration at a site is affected by many factors. These include

(i) the size of earthquake (represented by its magnitude)

(ii) distance of the site from the source

(iii) site conditions (whether rock or soil)

(iv) fault type (strike slip, normal or reverse) and

(v) tectonic environment (interplate or intraplate).

A number of attenuation models have been suggested to incorporate the various parameters noted above. The basic functional form of the attenuation model, as defined by Campbell (1985), is :

$$f(Y)= b_1 f_1 (M) f_2 (R) f_3 (M,R) f_4 (S) \varepsilon \quad \ldots (2.1)$$

Where Y is the response variable (dependent variable), b_1 is a constant scaling factor, $f_1 (M)$ is a function of magnitude M, $f_2 (R)$ is a function of source to site distance R, $f_3 (M,R)$ is a joint function of M and R, $f_4 (S)$ is a function representing parameters of earthquake path, site or structure and ε is a random variable representing the uncertainty in Y.

The estimated transformation of distance and PGA show a logarithmic behavior, whereas the transformation of magnitude is seen to be approximately linear. The functions of equation (2.1) were therefore formulated as

$$f(Y)= \log A \ ; \ f_1 (M) = b_2 M \ ; \ f_2 (R) = b_3 \log R \quad \ldots (2.2)$$

After applying relations (2.2) to relation (2.1), one gets the following generalized form (Gupta et al., 1991)

$$log\ A = b_1 + b_2 M + b_3 log\ R + b_4 S + \varepsilon \quad \ldots (2.3)$$

To develop an attenuation relation of the type of equation (2.3) for a region of interest, coefficients b_1, b_2, etc. are evaluated by regression analysis of the strong-motion data available. However, due to strong dependence on regional geology, use of an attenuation relation for another area with different geological and tectonic features may lead to PGA values which are usually unacceptable for earthquakes resistant design of amplitudes at close distances.

The geometrical spreading term $b_3 \log R$ in some of the attenuation relations is taken as $b_3 \log(R+d)$ or $b_3 \log(R^2+d^2)^{1/2}$ or in some other relations as $b_3 \log(R+\alpha e^{\beta M})$, where the additional parameters α and β or d are also evaluated by regression analysis of the recorded data. But, in general, there are not enough near source data on large magnitude earthquakes to get realistic values for these parameters. Further, to account for the effect of magnitude saturation, in some of the empirical attenuation relations, the magnitude dependence is taken in the quadratic form, $b_4 M + b_5 M^2$. But, again, due to limited number of data on very large magnitude earthquakes, it is normally not possible to get realistic estimate for the additional coefficient b_5.

2.5 Attenuation Relationships for Indian Region

The observed acceleration values from eight earthquakes (three in Himalayan region and five in Shillong region) have been analysed. To work out the attenuation relation, as a first step, a linear regression analysis was carried out by considering a relation as

$$log\ (A) = b_1 - b_2\ log\ (R) \quad \ldots (2.4)$$

where A is the acceleration in g, R is the epicentral distance and b_1 and b_2 are the regression coefficients. The results for eight earthquakes are tabulated in Table 2.2, the figures in the brackets are the standard error of each coefficient. The average value of decay parameter i.e. of b_2 is computed to be 1.24.

Table 2.2 : b_1 and b_2 values computed using equation (2.4)

Earthquake	b_1	b_2
Dharmsala 1986	1.036 (0.725)	1.649 (0.576)
NE Sept. 1986	0.702 (0.770)	1.067 (0.443)
NE May 1987	1.843 (0.786)	1.469 (0.365)
NE Feb. 1988	0.189 (1.207)	0.722 (0.567)
NE Aug. 1988	1.196 (1.234)	1.195 (0.504)
NE Sept. 1990	2.436 (2.344)	1.461 (0.258)
Uttarkashi 1991	1.543 (0.348)	1.436 (0.190)
Chamoli 1999	0.373 (0.746)	0.904 (0.403)

Next, a general multiple regression analysis was performed for the whole data set by assuming the basic regression model as

$$log\ (A) = b_1 - b_2\ log\ (R) + b_3\ M \qquad \ldots (2.5)$$

where M is the magnitude and b_1 , b_2 ,and b_3 are the regression coefficients. The value of the decay parameter b_2 come out to be 0.351(0.059), which is much less than the average value. To overcome this, two-step stratified regression analysis is used as suggested by Fukushima and Tanaka (1990). This method also minimizes the interaction of b_1 estimates (Joyner and Boore, 1988).

The attenuation model considered is based on equation (2.3), which is the general form of the attenuation relationship. The focal mechanism

term is not considered here because that is not well reported. The regression model thus selected for the attenuation relation is as follows:

$$log\ (A) = c_1 + c_2\ M - b\ log\ (R+e^{C3M}) + +c_4\ S \qquad \ldots (2.6)$$

where c_1 , c_2 , c_3, c_4 and b are the regression coefficients. In first step b is estimated using equation (2.4) as 1.24. In second step, b is fixed as 1.24 and coefficients c_1, c_2, c_3 and c_4 are estimated applying non-linear regression analysis using relation (2.6) with whole data set. The following attenuation relationship is obtained:

$$log\ A = -1.962+0.659\ M - 1.24\ log\ (R+e^{0.888M}) - 0.0674S \quad \ldots (2.7)$$

where A is PGA in units of g, the acceleration due to gravity, R is the epicentral distance in km, M is the surface wave magnitude and S is the site type. The residual sum of squares and standard error for coefficients are given in Table 2.3.

Table 2.3 : Residual sum & standard error for equation (2.7)

R squared = 1 - Residual SS / Corrected SS = .19808				
Parameter	Estimate	Asymptotic Std. Error	Asymptotic 95 % Confidence Lower	Interval Upper
C_1	-1.9621659	.0619201	-2.0847845	1.8395472
C_2	.6592139	.0000000	.6592139	.6592139
C_3	.8883680	.0568071	.7758745	1.0008616
C_4	-.0673746	.0656339	-.1973477	.0625984

The observed peak ground accelerations for all eight events are plotted with the predicted values of PGA given by the relationship (2.7) with the same magnitudes in Fig. 2.7.

In general, the seismotectonic regions are characterised by their specific focal mechanisms of earthquakes and attenuation relations are governed by the regional geology. The strong motion data from eight earthquakes used are from two different regions namely, Himalayan region and Shillong region. These regions are characterised by distinctly different tectonic environment. Hence, the strong motion data from these regions has been treated separately and new relationships developed. The regression model thus selected is of the form:

$$log\ (A) = c_1 + c_2\ M - b\ log\ (R+e^{C3M}) + +c_4\ R \qquad \ldots\ (2.8)$$

For strong motion data of three Himalayan earthquakes (Dharmsala, Uttarkashi and Chamoli) the attenuation relationship using (2.8) with 2-step stratified non-linear analysis taking the value of b as 1.0 in I^{st} step, is obtained as follows:

$$log\ A) = -1.345 + 0.309\ M - log(R+e^{0.312M}) - 0.0006\ R \qquad \ldots\ (2.9)$$

The residual sum of squares and standard error for coefficients are given in Table 2.4.

The observed PGA values for all three earthquake events are plotted with the predicted values of PGA as given by the relationships (2.9) with the same magnitudes in Fig. 2.8.

Table 2.4 : Residual sum & standard error for equation (2.9)

R squared = 1 – Residual SS / Corrected SS = .48416				
Parameter	Estimate	Asymptotic Std. Error	Asymptotic 95 % Confidence Interval Lower	Upper
C_1	-1.3449242	.0000000	-1.3449242	-1.3449242
C_2	.3089307	.1192298	.0642912	.5535702
C_3	.3122633	.0021984	.3077525	.3167741
C_4	-.0005776	.2665110	-.5474131	.5462578

Then, after analysing the strong motion data of five earthquakes of northeast region using equation (2.8) with geometrical spreading term as $c_3 log\ (R^2+d^2)$ instead of $b\ log\ (R+e^{C3M})$, the following attenuation relationship is obtained:

$$log\ A = -2.995 + 0.513\ M - .577\ log\ (R^2+15^{\ 2})^{1/2} - 0.0002\ R \quad \ldots (2.10)$$

The residual sum of squares and standard error for coefficients are given in Table 2.5 for the above attenuation relationship.

Table 2.5 : Residual sum & standard error for equation (2.10)

R squared = 1 – Residual SS / Corrected SS = .37307				
Parameter	Estimate	Asymptotic Std. Error	Asymptotic 95 % Confidence Interval Lower	Upper
C_1	-2.9952990	.9805847	-4.9446370	-1.0459610
C_2	.5130838	.0784630	.3571045	.6690631
C_3	-.5770221	.5174821	-1.6057431	.4516988
d	15.1599191	4.3453673	-2.9957534	23.3155918
C_4	-.0001731	.0012402	-.0026385	.0022923

The observed PGA values are plotted with the predicted values of PGA as given by the relationships (2.10) with the same magnitudes in Fig. 2.9.

2.6 Integrated Attenuation Relationship

To get consistently stable estimates of the PGA values with minimal deviations from the real values for a wide range of earthquake parameters, several well published attenuation relationships (listed in Appendix B) have been integrated together to develop an average attenuation relationship. This relationship has been then modified for the near source saturation effects to get realistic values of PGA at very close source to site distances.

A typical plot of the attenuation relations for different regions of the world evaluated with magnitude 6.0 is given in the Fig. 2.10. From the figure it is observed that there may be large regional variations in the attenuation characteristics. The use of any attenuation relation for some other region may not be suitable and does not come out with considerable results. To minimize the error, the regional differences have been averaged out by developing an integrated attenuation relationship using all the well behaved relationships.

To scrutinize the behavior of the attenuation relations, the peak acceleration values are computed for M = 4.0, 5.0, 6.0, 7.0 and 8.0 and plotted as a function of distance for each of the relationships. Some relationships have shown abnormal behavior such as increase linearly to very large values with decrease in distance, some relations over estimate the near-field acceleration values. The mean value, μ, and the standard deviation σ, of the peak ground acceleration (PGA) values obtained from these relationships were computed for five magnitude

values M= 4.0, 5.0, 6.0, 7.0 and 8.0 and 196 distances from 5 km. to 200 km. at an interval of 1.0 km. By plotting these relationship along with the ($\mu \pm \sigma$) band for each of the five magnitudes. It is observed from the Figs. 2.11(a) to 2.11(c) plotted against the magnitude values M=4.0, 6.0 and 8.0 that some of the relations lie outside the ($\mu \pm \sigma$) band or deviate significantly from the mean trend of attenuation for certain magnitude and distance ranges. Thus, after deleting those relationships, only 16 well-behaved remaining relations have been used for further study as listed in Table 2.6.

The mean values of PGA have been obtained for above mentioned five magnitudes and 196 distance levels from 5 km to 200 km which forms the data set for further analysis. The following attenuation model has been chosen for integrated relationship:

$$log\ (A) = c_1 + c_2\ log(R) + c_3\ R + c_4\ M + c_5\ M^2 \qquad \ldots (2.11)$$

In the above relationship, A is the peak acceleration in units of acceleration due to gravity (g), M is the earthquake magnitude and R is the measure of the source-to-site distance.

The mathematical form of equation (2.11) is based on the physical principal of seismology and elastic wave propagation. First term is related to the strength of earthquake source, second term accounts for geometrical spreading of wave energy, third term describes the anelastic attenuation and the fourth and fifth terms give the magnitude scaling, where quadratic dependence has been selected to achieve the magnitude saturation effects.

Table 2.6 : Attenuation relations for different regions of the World

Sl. No.	Attenuation Relation	Region	Reference
1	$a(cm/s^2) = 1230\, e^{0.8M} (R+25)^{-2}$	Firm ground condition	Esteva, L. (1970)
2	$a(cm/s^2) = 274\, e^{0.8M} R^{-1.64}$; Not applicable for R ≤ 15 km.		Devenport A.G. (1972)
3	$a(cm/s^2) = 1080\, e^{0.5M} (R+25)^{-1.32}$	Rocky ground	Denovan, N.C. (1973)
4	$a(cm/s^2) = 64.75 \times 10^{0.4M} R^{-1.39}$; $\sigma_{\ln a} = 0.69$ Not applicable for R ≤ 15 km.	California region, Rock and Alluvium	Orphal, D.L. & J.A. Lahoud (1974)
5	$a(cm/s^2) = 1.03\, h^{0.6} \times 10^{0.54M} R^{-1.5}$; R ≥15	Tanzania region	Bath, M. (1975)
6	$a(cm/s^2)=472.0\times10^{0.278M}(R+25)^{-1.301}$ $\sigma_{\ln a}$ = 0.62, Not applicable for R ≤ 15km	Rock and Alluvium	McGuire R.K. (1977)
7	$a(g) = 0.0306e^{0.89M} R^{-1.301} e^{-0.020s}$ $\sigma_{\ln a}$ = 0.62 for rock sites	Western U.S.	McGuire R.K. (1978)
8	$a(g) = 0.0160e^{0.868M} (R+0.61e^{0.7M})^{-1.09}$; $\sigma_{\ln a}$ = 0.37	Worldwide data	Campbell (1981)
9	$a(g) = 0.3480e^{1.21M} (R+25)^{-2.08}$; $\sigma_{\ln a}$ = 0.71	California region	Battis, J. (1981)
10	$a(g)= 0.0239e^{1.24M} (R+25)^{-1.24}$; $\sigma_{\ln a}$ = 0.71 ,	Central U.S.	Battis, J. (1981)
11	$a(g)= 3.79\times10^{-3}e^{1.15M}(R^2 +0.000346e^{2.1M})^{-0.415}e^{-0.00159R}$; $\sigma_{\ln a}$ =0.55	Mississippi Valley	Nuttli, O.W. and R.B. Herrmann (1984)
12	$\log a(cm/s^2) = -0.474 + 0.613M - 0.873 \log R - 0.00206 R$	NE China	Peng K.Z., et.al. (1985)
13	$\log a(cm/s^2) = -0.437 + 0.454M - 0.739 \log R - 0.00279 R$	NW China	Peng K.Z., et. al. (1985)
14	$\log a(g) = -0.62 + 0.177M - 0.982 \log (R + e^{0.284M}) + 0.132F - 0.0008E_r$ $\sigma_{\ln a}$ = 0.277, F=1 for reverse or reverse oblique fault, 0 otherwise, Er=1 for interplate and 0 for intraplate events.	Worldwide	Abrahamson, N.A. and J.J. Litehiser (1989)
15	$\log a(cm/s^2) = 2.64 - 0.01197 R - 0.0995\log R - 0.6476M + 0.10634M^2$	Koyna region, India	Gupta I.D., Rambabu V. & Joshi R.G. (1991).
16	$\log a(g) = -0.87 + 0.217M - \log R - 0.00117R$; $\sigma_{\log a}$ = 0.26,	Europe	Ambraseys N.M. & Bommer J.J. (1991)

The least square multiple regression analysis is applied to above mentioned data set and the following integrated attenuation relationship has been obtained:

$$\log A = -1.72 - 0.878 \log(R) - 0.0016R + 0.288M + 0.0095M^2 \quad \ldots (2.12)$$

The residual sum of squares and standard error for coefficients are given in Table 2.7.

Table 2.7 : Residual sum & standard error for equation (2.12)

R squared = 1 - Residual SS / Corrected SS = 0.855				
Parameter	Estimate	Asymptotic Std. Error	Asymptotic 95 % Confidence Interval Lower	Upper
c_1	-1.720000	2.363E-10	-1.720000	-1.719999
c_2	-.878000	5.918E-12	-.878000	-.878000
c_3	-.001600	5.066E-13	-.001600	-.001600
c_4	.288000	.0000000	.288000	.288000
c_5	.009500	8.620E-11	.009500	.009500

The relationship (2.12) is found to describe very well the attenuation of PGA for intermediate and large distances, but the peak acceleration is seen to blow up for very small distances. Comparison of peak acceleration values (solid curves) with the corresponding values obtained from equation (2.12) (dashed curves) have been shown in Fig. 2.12.

This relationship is not able to consider the effect of near distance saturation of the peak accelerations. Most of the published attenuation relations used to develop the relationship of eqn. (2.12) are based on

strong motion data recorded at distances greater than about 20 km. Thus, extrapolation of eqn (2.12) to small distances gives unrealistically high values of PGA, particularly for large magnitudes. To compute the peak acceleration in the near field, eqn. (2.12) is required to be modified to consider the saturation effects.

2.7 Modified Integrated Attenuation Relationship

Almost all the available empirical attenuation relations are based on the point source approximation, according to which the entire seismic energy is assumed to originates from a point, and the source-to-site distance, R, refers to that point only. This assumption doesn't make much difference at large distances, but as one approaches closer to the source, the size of the fault starts exhibiting its effect. The point of observation is influenced by the energy radiated from a limited portion of the fault. By idealizing the fault plane by a circular area of radius R_o and assuming the site of observation to lie at a distance R on the axis of the circle, the effect of the finite size of the fault can be accounted by replacing the distance R with an equivalent distance R_{eq}, defined as (Gupta et.al. 1997)

$$R_{eq} = R_o \left[\ln\left(\frac{R^2 + R_o^2}{R^2} \right) \right]^{-\frac{1}{2}} \qquad \ldots (2.13)$$

The peak ground acceleration in the near field is not governed by the total area of the fault, such relations are not suitable to define the radius R_o for computing the equivalent source-to-site distance. Thus to get a realistic estimate of the equivalent distance from eqn. (2.12), it is necessary to use the effective size of the fault, rather than its actual physical size. Though there is no way to find the effective size of the fault generating an earthquake, the empirical relations due to Trifunac

and Lee (1990) can be used to conveniently obtain it for practical applications.

In the present study, the effective radius R_o of the fault has been taken equal to half the source size S for lowest period range (0.04 - 0.10 sec) defined as

$$S = 0.2 + 8.23\,(M-3)\,;\quad R_o = S/2$$

The equivalent distance R_{eq} evaluated using this R_o would be able to account for the near distance saturation effects in a very simple way. Fig. 2.12 shows the comparison of the peak acceleration values (dashed curve) obtained directly from the attenuation relationship (2.12) with those (solid curves) obtained by substituting R_{eq} in place of R in relationship (2.12). The introduction of equivalent distance based on the effective source size is able to give the near source saturation effect in a very realistic way. To avoid the explicit computation of equivalent distance for use in the relationship (2.13), the data corresponding to the solid curves in Fig. 2.12 have been used to obtain the following attenuation regression relationship

$$\log A = -1.567 - 0.969\log(R+e^{0.107M}) - 0.0017R + 0.288M + 0.0098M^2 \qquad \ldots (2.14)$$

which is of the form

$$\log(A) = c_1 + c_2\log(R+e^{C3M}) + c_4 R + c_5 M + c_6 M^2$$

Here geometric spreading term is $c_2\log(R+e^{C3M})$ in place of $c_2\log(R)$ which gives better estimates as clear from the following Table. The residual sum of squares and standard error for coefficients are given in Table 2.8.

Table 2.8 : Residual sum & standard error for equation (2.14)

R squared = 1 – Residual SS / Corrected SS = .6543				
Parameter	Estimate	Asymptotic Std. Error	Asymptotic 95 % Confidence Interval Lower	Upper
c_1	-1.567212	2.363E-10	-1.567212	-1.567210
c_2	-.969000	8.632E-10	-.969000	-.969000
c_3	.107000	.0021400	.109150	.104870
c_4	-.001700	2.012E-09	-.001700	-.001700
c_5	.288000	.0000000	.288000	.288000
c_6	.009800	5.880E-14	.009800	.009800

The PGA values predicted from relationship of eqn. (2.14) plotted by dashes curves in Fig. 2.13, is seen to approximate very closely the solid curves of Fig. 2.12. Thus the attenuation relationship of equation (2.14) is able to account for the near-distance saturation effects and it also gives the results which are the average values of the PGA obtained from the 16 selected relationships. This equation can, therefore, be considered independent of regional influences and biases.

2.8 Results and Discussion

Different authors have worked on different set of strong motion data available worldwide and number of attenuation relationships for PGA are available in literature. As discussed above a set of strong motion data is available for Indian region. The observed acceleration data for eight earthquake events have been plotted with the sixteen empirical relationships as given in Table 2.7. As relationships use different magnitude scales and distances, an appropriate conversion has been made while preparing these graphs for proper comparisons.

Observed acceleration values for Dharmsala, 1986, Uttarkashi, 1991 and Chamoli, 1999 earthquakes and five earthquakes events from Northeast region (Sept. 1986, May 1987, Feb. 1988, Aug. 1988 and Jan. 1990) are compared with the sixteen relationships and depicted in Figures 2.14(i) to 2.14(xvi), 2.15(i) to 2.15(xvi), 2.16(i) to 2.16(xvi), 2.17(i) to 2.17(xvi), 2.18(i) to 2.18(xvi), 2.19(i) to 2.19(xvi), 2.20(i) to 2.20(xvi) and 2.21(i) to 2.21(xvi). Some relationships predicts higher values at lower distances and others do the same at higher distances. It is clear from the figures that none of the sixteen relations is adequate to closely predict the observed acceleration values at all the distances. Some relations show a slower rate as compared to the observed values and over predict at large distances of 20-30 km. Other relations over predict even at shorter distances as well.

The root mean square error (rmse) between the observed acceleration values and the values predicted by the sixteen relations available have been calculated for each of the earthquake studies using the following formula:

$$rmse = \left[(1/N)\sum \left(A_{obs} - A_{cal}\right)^2\right]^{\frac{1}{2}} \qquad \ldots (2.15)$$

where A_{obs} and A_{cal} are the observed and the calculated accelerations respectively and N is the number of data points. Figures 2.22(a) to 2.22(c) show the rms error versus the relationships listed in Table 2.6 for Dharmsala, Uttarkashi and Chamoli earthquakes and the figures 2.23(a) to 2.23(e) show the rms error for five earthquake events for Northeast region. The numbers on X-axis are corresponding to the serial number (Sl. No.) of the Table 2.6.

It is noted from the Fig. 2.22(a) and Figs. 2.14(i) to (xvi) that the relationship given by Battis (1981) for California region (at Sl. No. 9 in table 2.6) predicts satisfactorily for Dharmsala, 1986 earthquake as the rms error produced by the attenuation relation 9 is minimum. Similarly, from Figs. 2.23(b), 2.23(c) and Figs. 2.15(i) to (xvi) and Figs. 2.16(i) to (xvi) it is clear that for two earthquakes i.e. Uttarkashi, 1991 and Chamoli, 1999, the attenuation relationship given by Peng (1985) for North west China (at Sl. No. 13 in table 2.6) give good prediction values of PGAs.

It is clear from the Figs. 2.24(a) to (e) and similarly from the Figs. 2.17(i) to (xvi), 2.18(i) to (xvi), 2.19(i) to (xvi), 2.20(i) to (xvi) and 2.21(i) to (xvi), that for the NE event of Sept. 1986 the attenuation relationship given by McGuire (1977) predicts satisfactorily (at Sl. No. 6 in Table 2.6), for two events of May 1987 and Feb. 1988 the attenuation relationship given by Battis (1984) for Central U.S. (at Sl. No. 10 in Table 2.6) show the rms error as minimum. For the remaining two NE events of ~~Feb.~~ Aug. 1988 and Jan 1990 the attenuation relationship given by ~~McGuire~~ Donovan (1973) (1977) (at Sl. No. 6 in Table 2.6) predict satisfactorily. at (Sl no 3 in Table 2.6)

The rmse are also calculated for developed relationships (2.9) and (2.10), integrated relationship (2.14) and attenuation relationships found suitable in literature as discussed above, for the observed data of the three earthquake events of Himalayan region and five earthquake events of Northeast region of India. These are shown in Table 2.9. These observed PGA values were plotted against these attenuation relationships in Figs. 2.24 to 2.31.

Table 2.9 : RMS errors calculated for different earthquakes

Region	*RMS errors for developed relationship*	*RMS errors for integrated Relationship*	*RMS errors for best fit available in literature*
Dharmsala, 1986	0.0470	0.0508	0.0489
Uttarkashi, 1991	0.0464	0.0473	0.0468
Chamoli, 1999	0.0720	0.0841	0.0737
NE Sep. 1986	0.0300	0.0483	0.0342
NE May 1987	0.0168	0.0462	0.1550
NE Feb. 1986	0.0300	0.0483	0.0323
NE Aug.1986	0.1270	0.1255	0.1150
NE Jan. 1990	0.0631	0.0642	0.0551

On the basis of minimum rmse and observations from Figs. 2.24 to 2.31, the following conclusions have been drawn:

- The attenuation relationships derived in the present study give the best fit with the observed peak acceleration values of strong motion data.

- The integrated relationship (generalized relationship) is at par with the best fitted relationship and can be used by computing PGA values for earthquake resistant design particularly at sites and regions where strong motion data is not available.

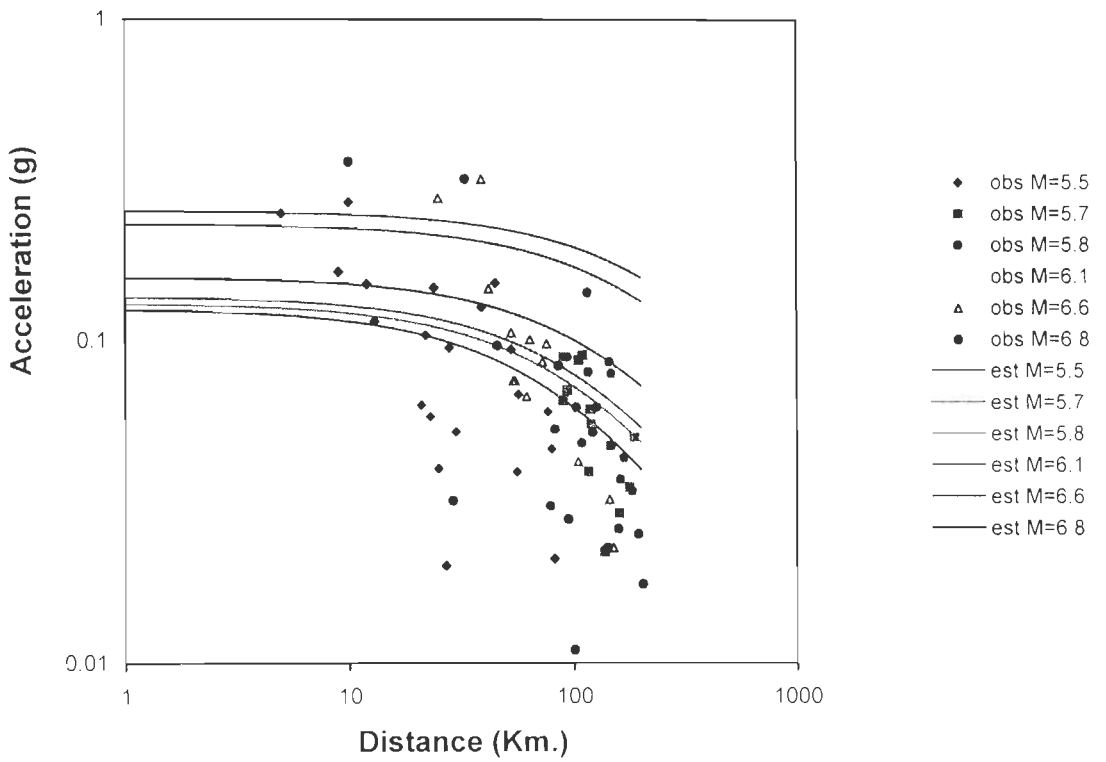

Fig. 2.7: Developed relationship (2.7) plotted with observed data of all eight earthquake events

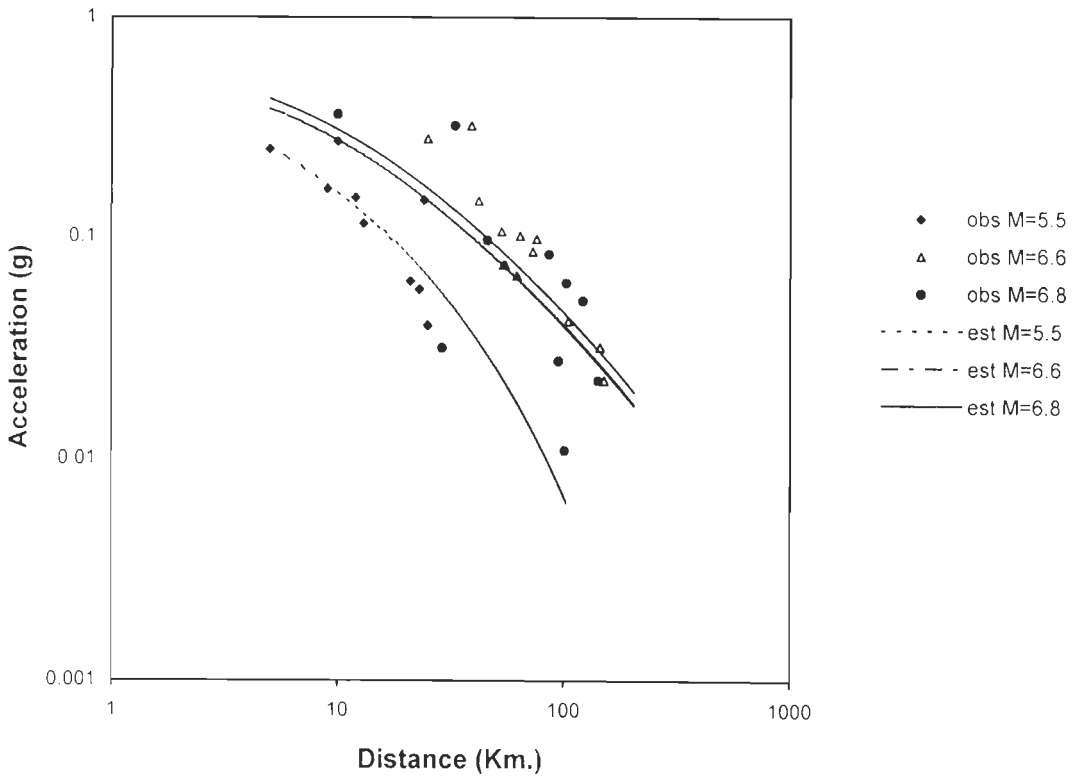

Fig. 2.8: Developed relationship (2.9) plotted with observed data of three earthquake events of Himalayan region

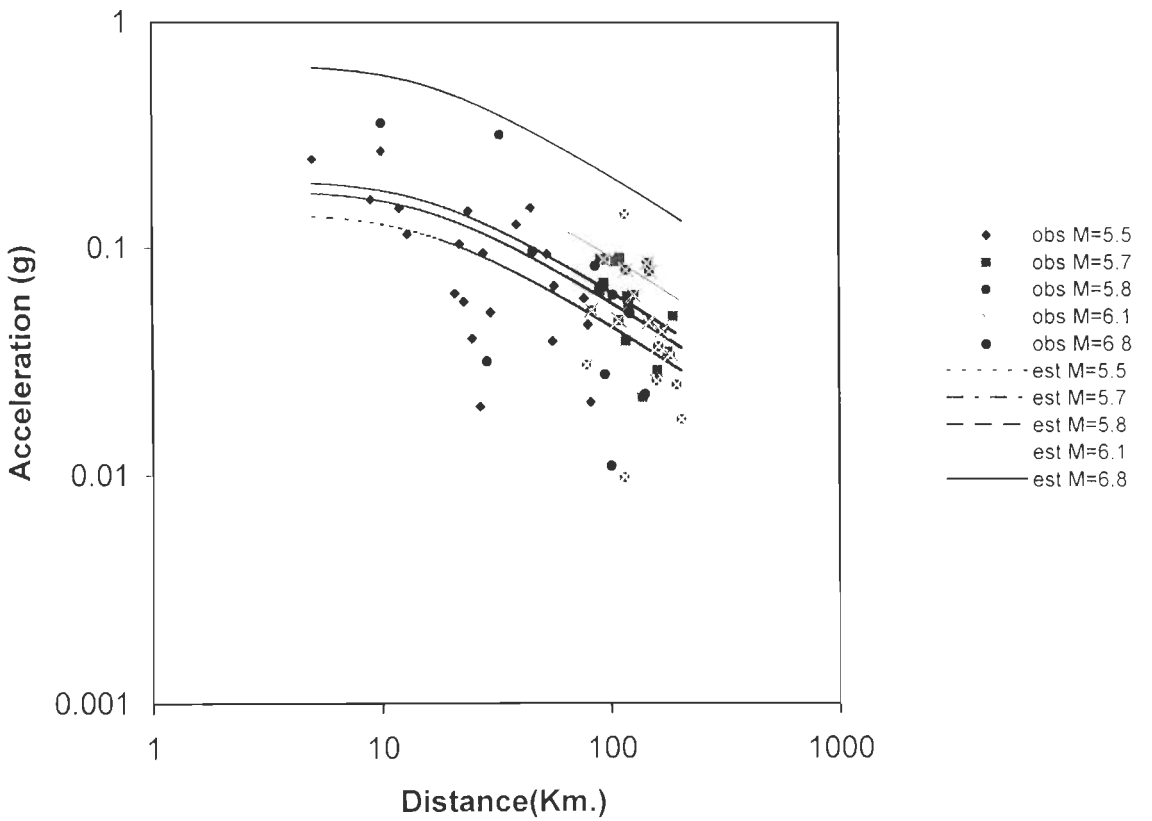

Fig. 2.9: Developed relationship (2.10) plotted with observed data of five earthquake events of Northeast region

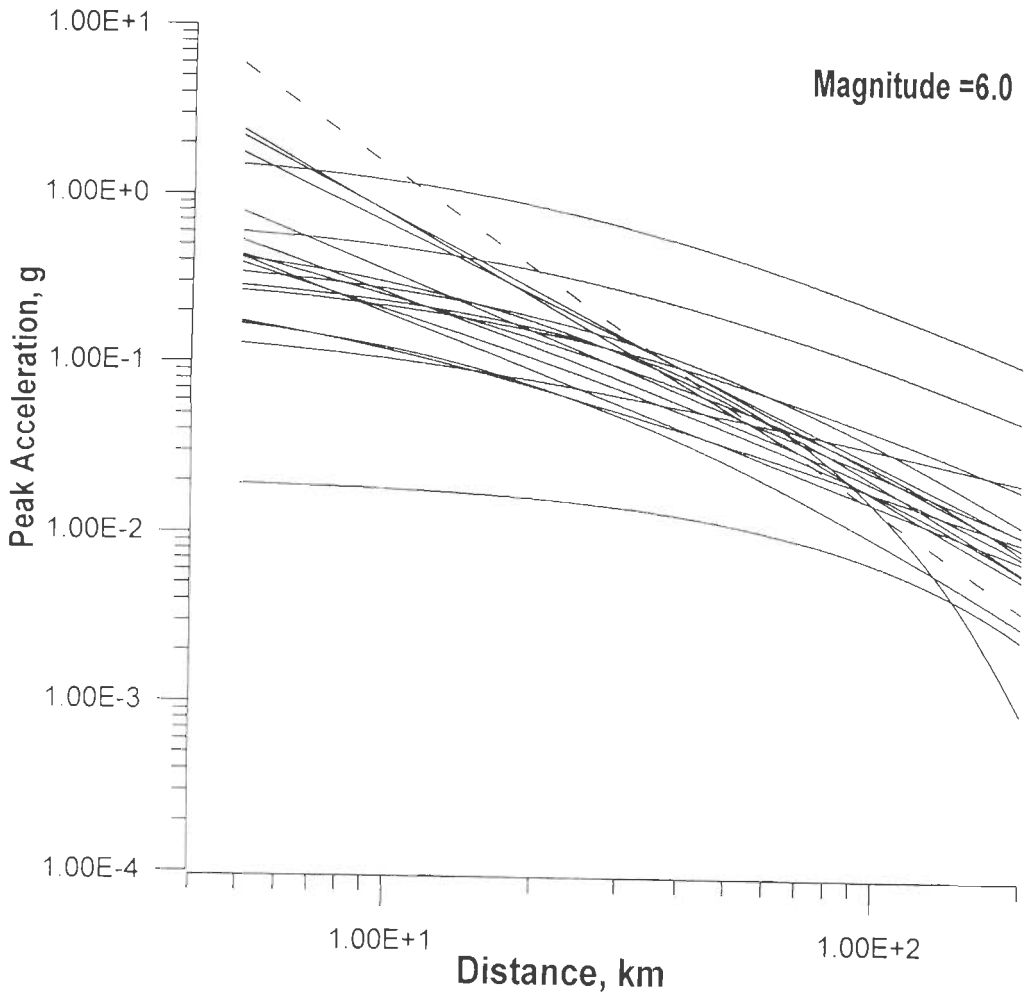

Fig. 2.10 : A typical plot of the Attenuation relations for different regions of the world (Mag = 6.0)

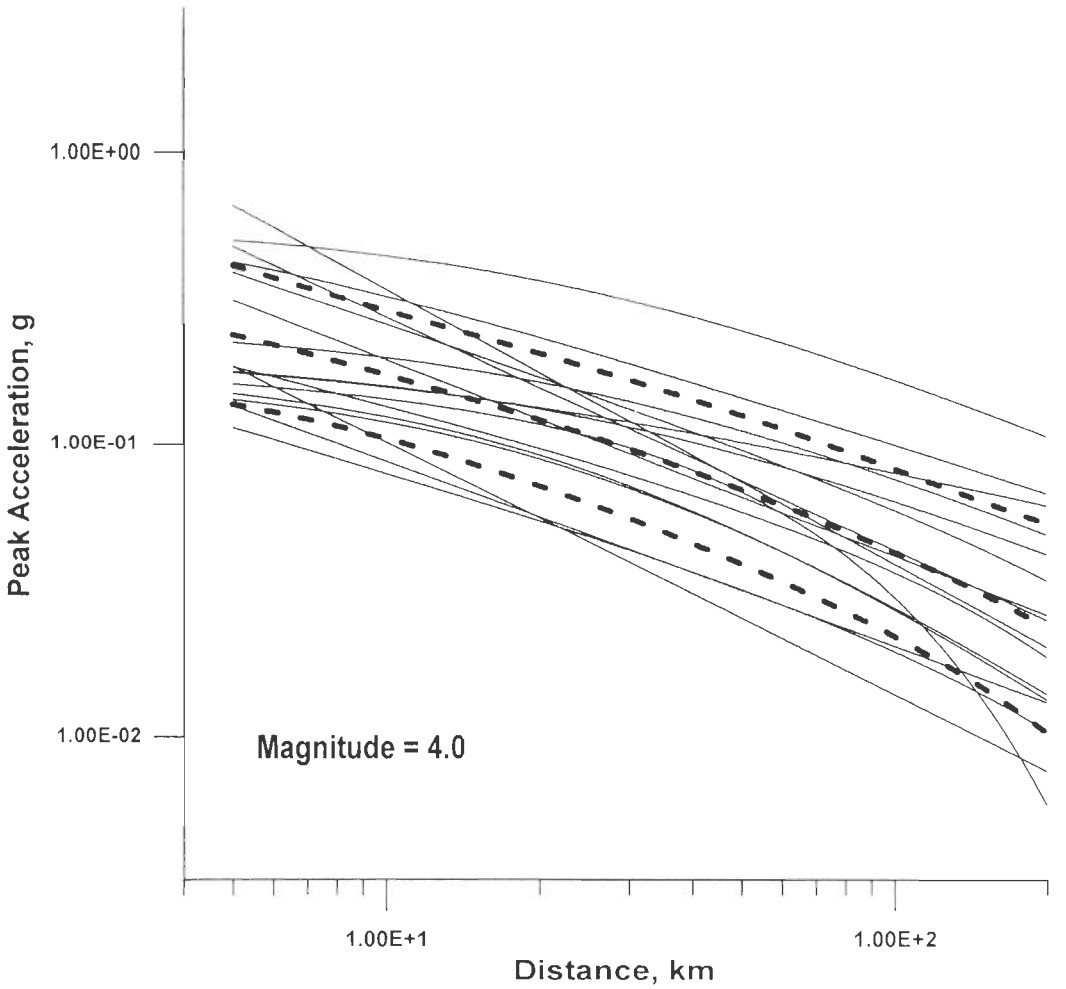

Fig. 2.11(a) : Comparison of well behaved relation with their ($\mu \pm \sigma$) band (dark dotted line) for m = 4.0

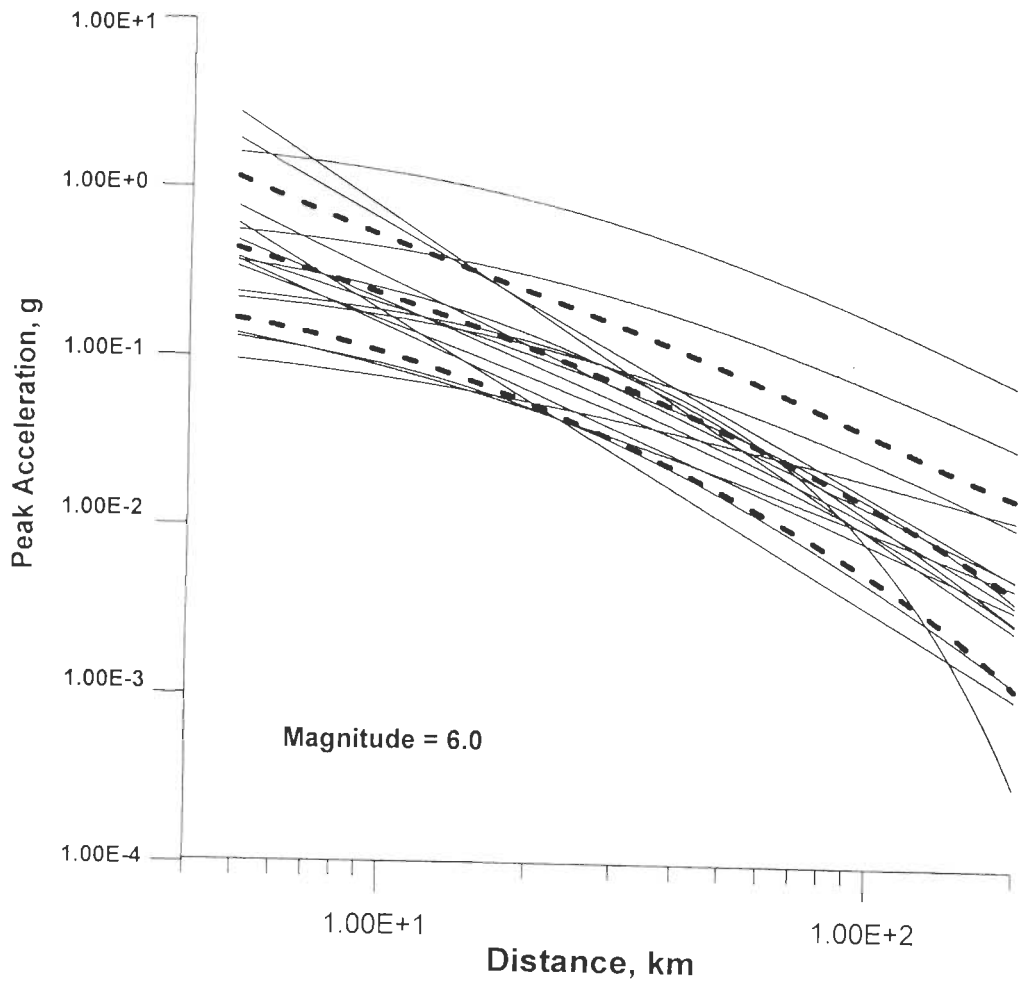

Fig. 2.11(b) : Comparison of well behaved relation with their ($\mu \pm \sigma$) band (dark dotted line) for m = 6.0

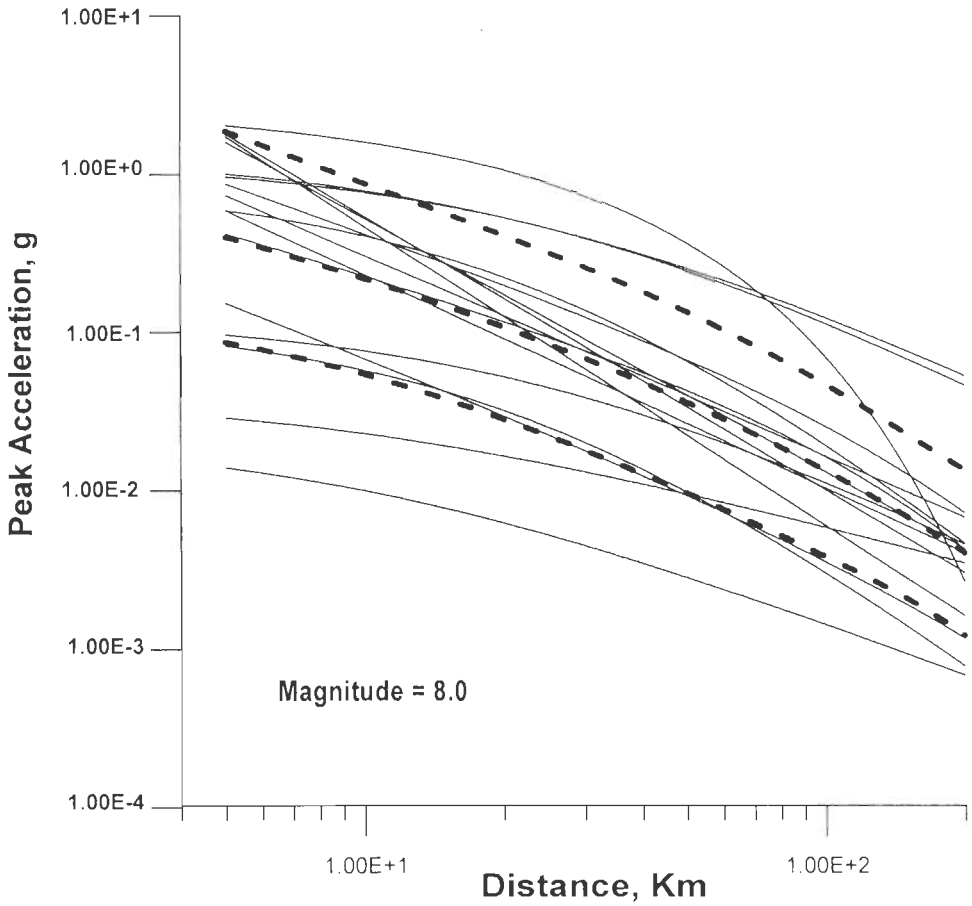

Fig. 2.11(c) : Comparison of well behaved relation with their ($\mu \pm \sigma$) band (dark dotted line) for m = 8.0

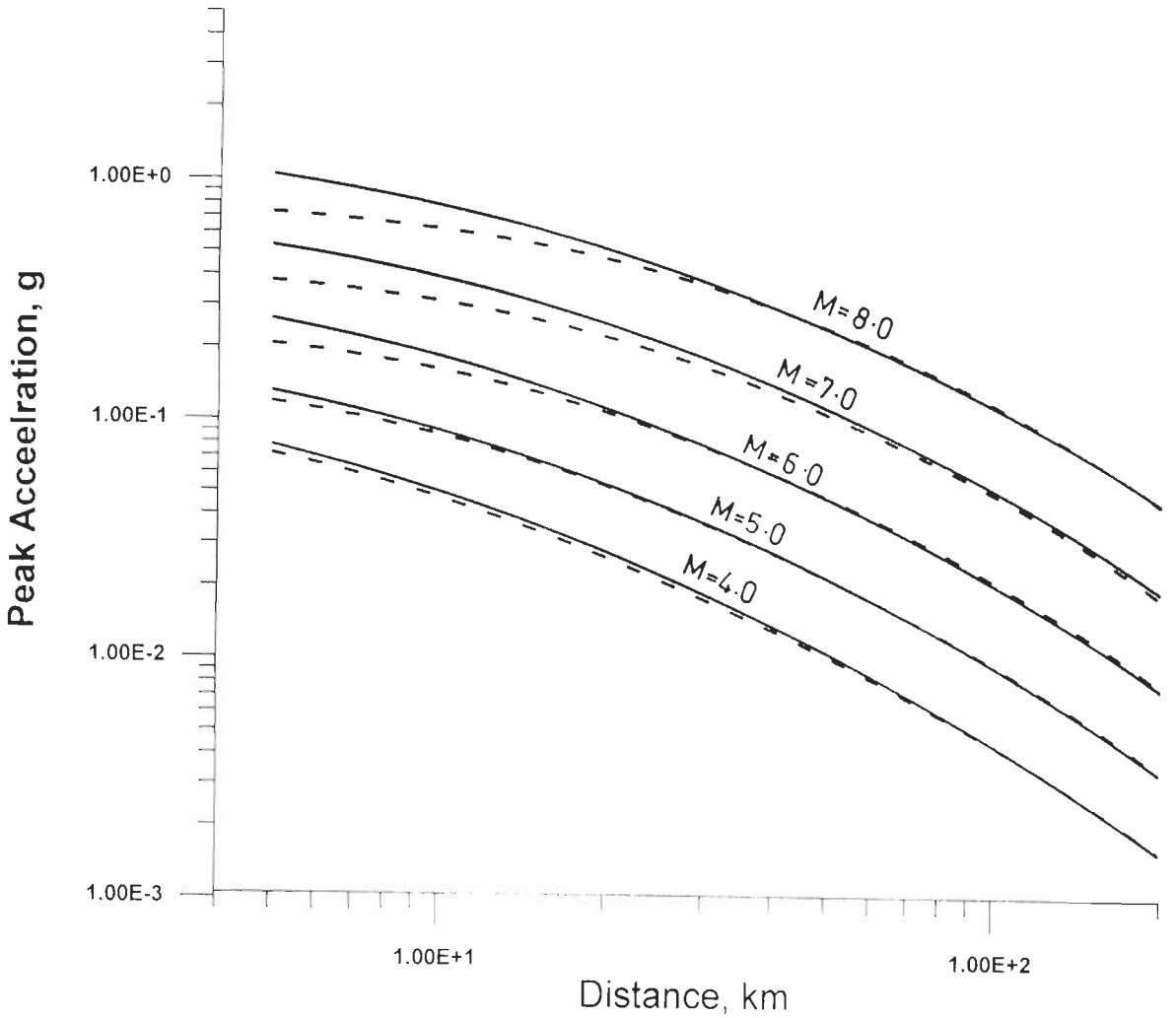

Fig. 2.12 : Comparison of peak acceleration values with the corresponding values obtained from equation (2.12) for m = 4.0, 5.0, 6.0, 7.0, and 8.0

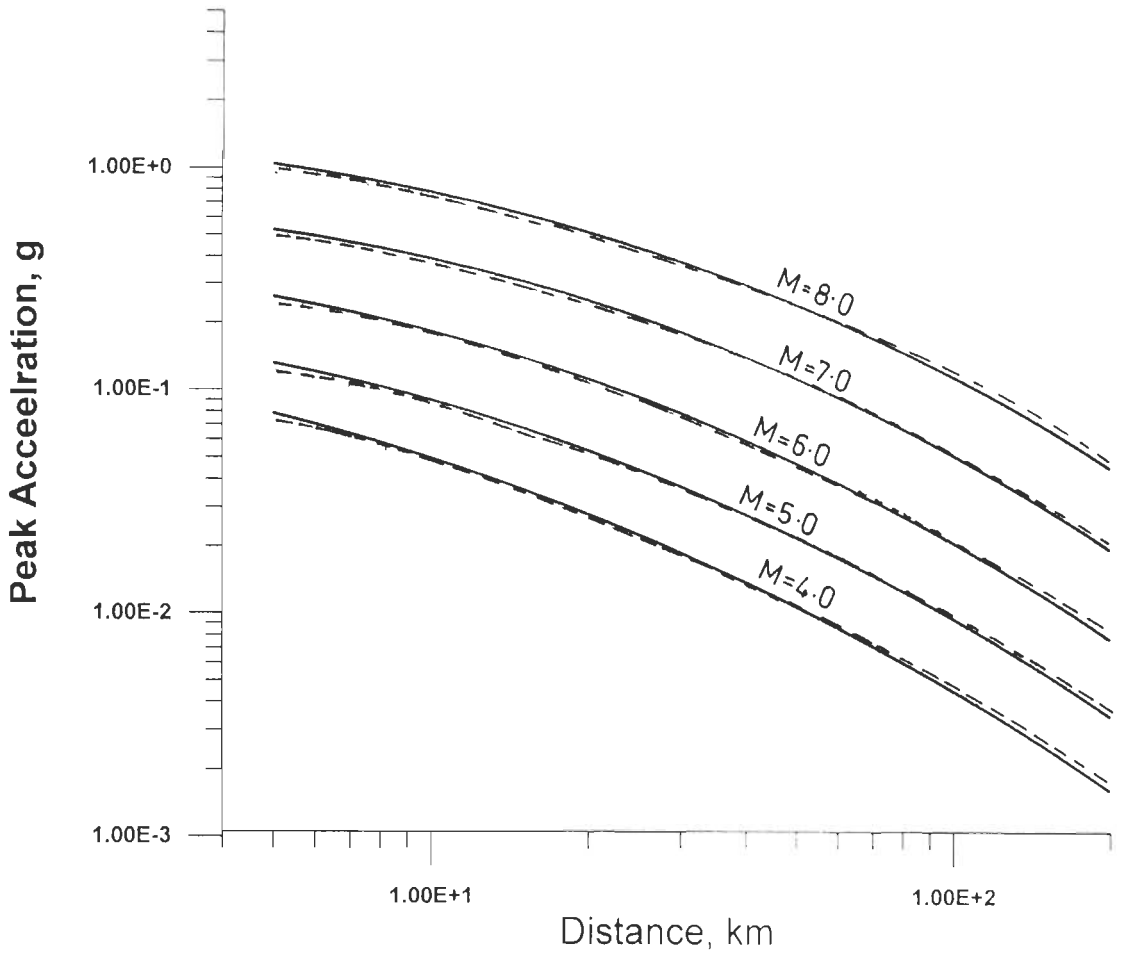

Fig. 2.13 : Comparison of peak acceleration values with the corresponding values obtained from equation (2.14) for m = 4.0, 5.0, 6.0, 7.0, and 8.0 by considering the saturation effect

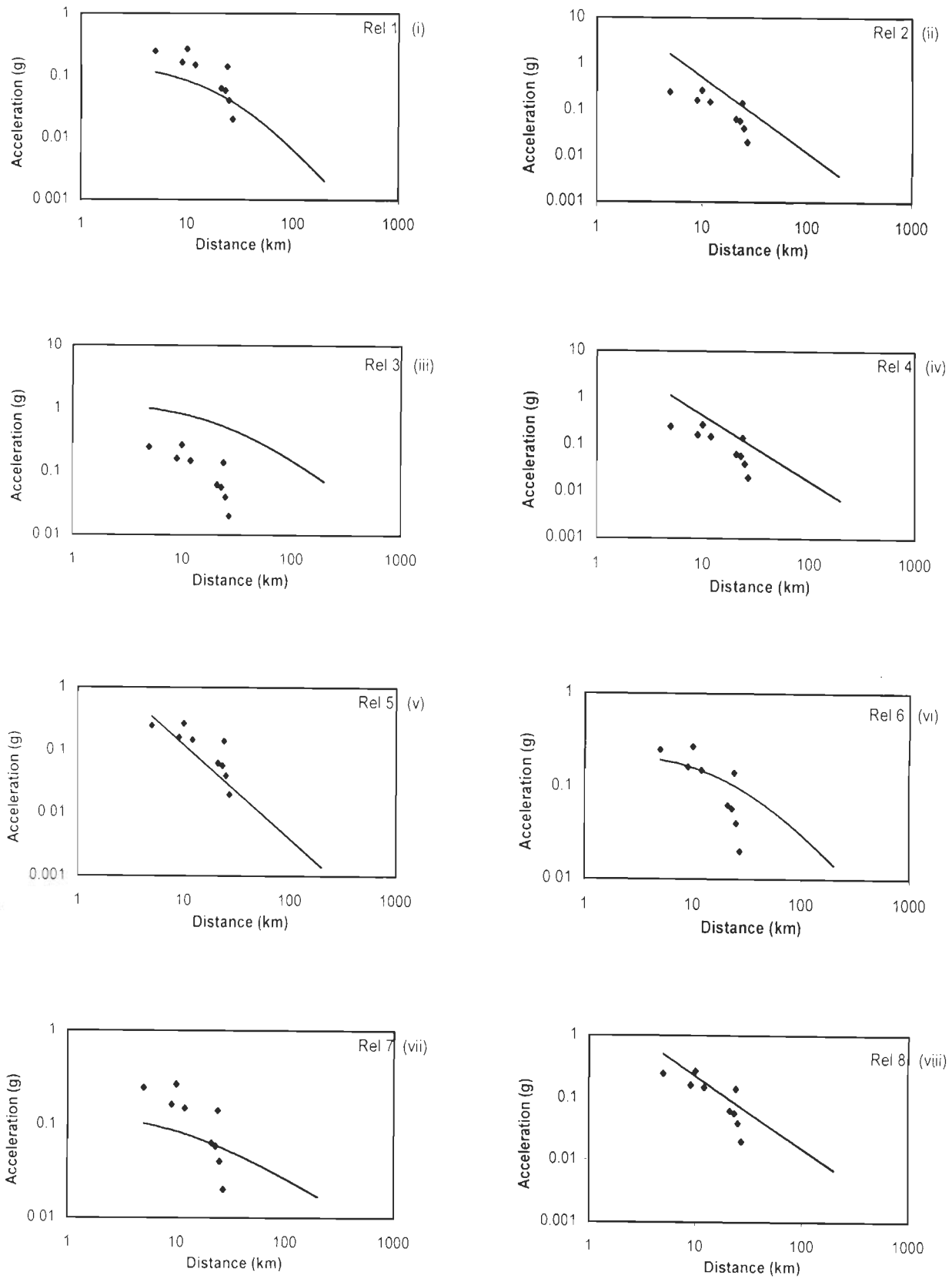

Fig. 2.14(i- viii) : Plot of the observed acceleration with distance for Dharmsala, 1986 earthquake and the regression curves of the empirical relations for Table 2.6

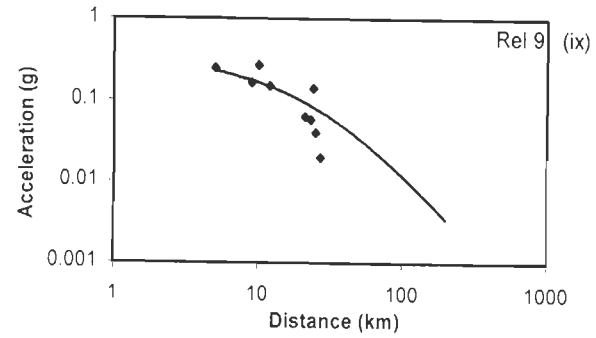

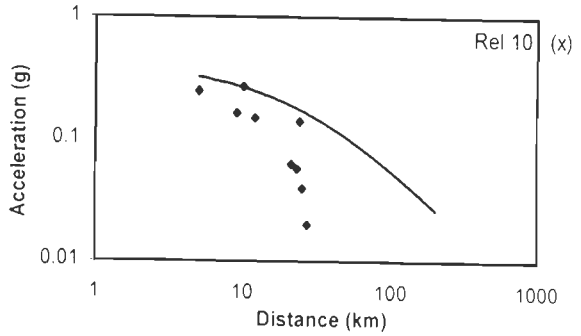

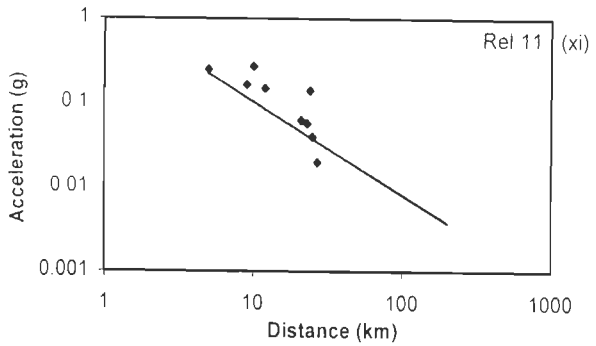

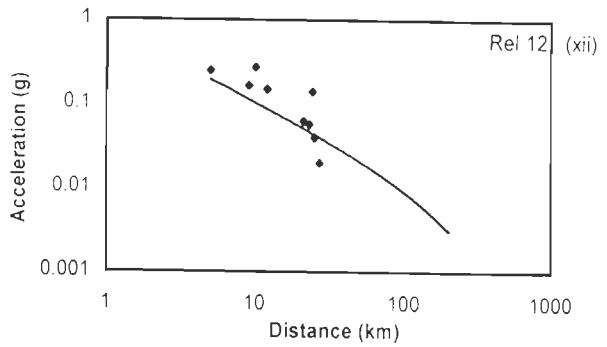

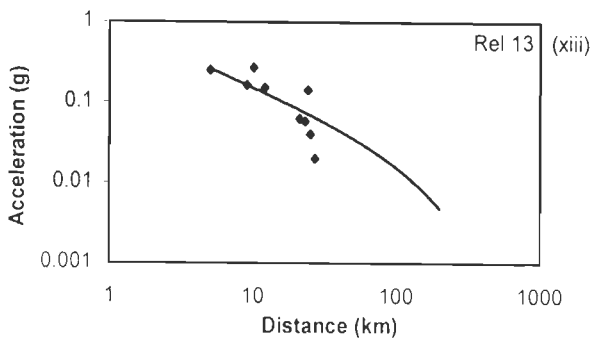

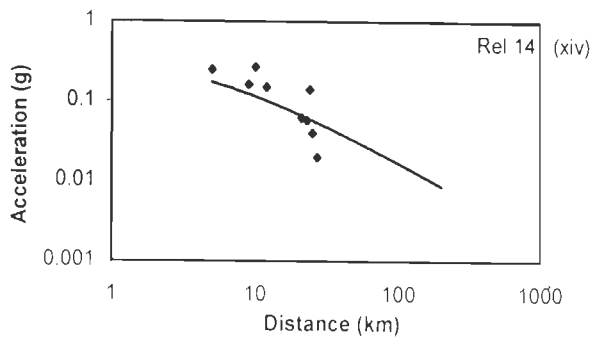

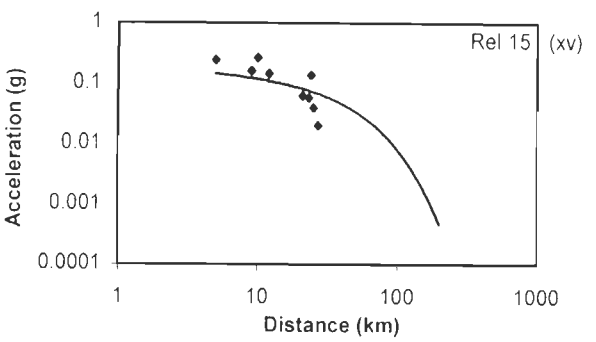

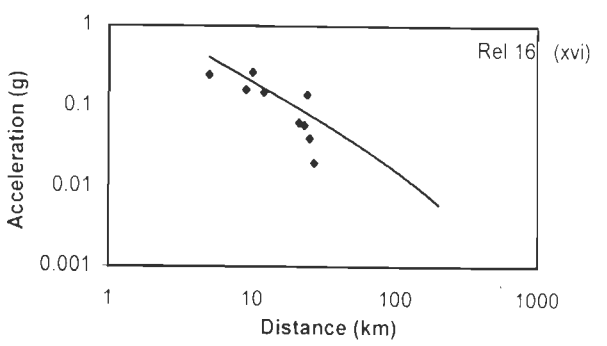

Fig. 2.14(ix-xvi) : Plot of the observed acceleration with distance for Dhamsala, 1986 earthquake and the regression curves of the empirical relations for Table 2.6

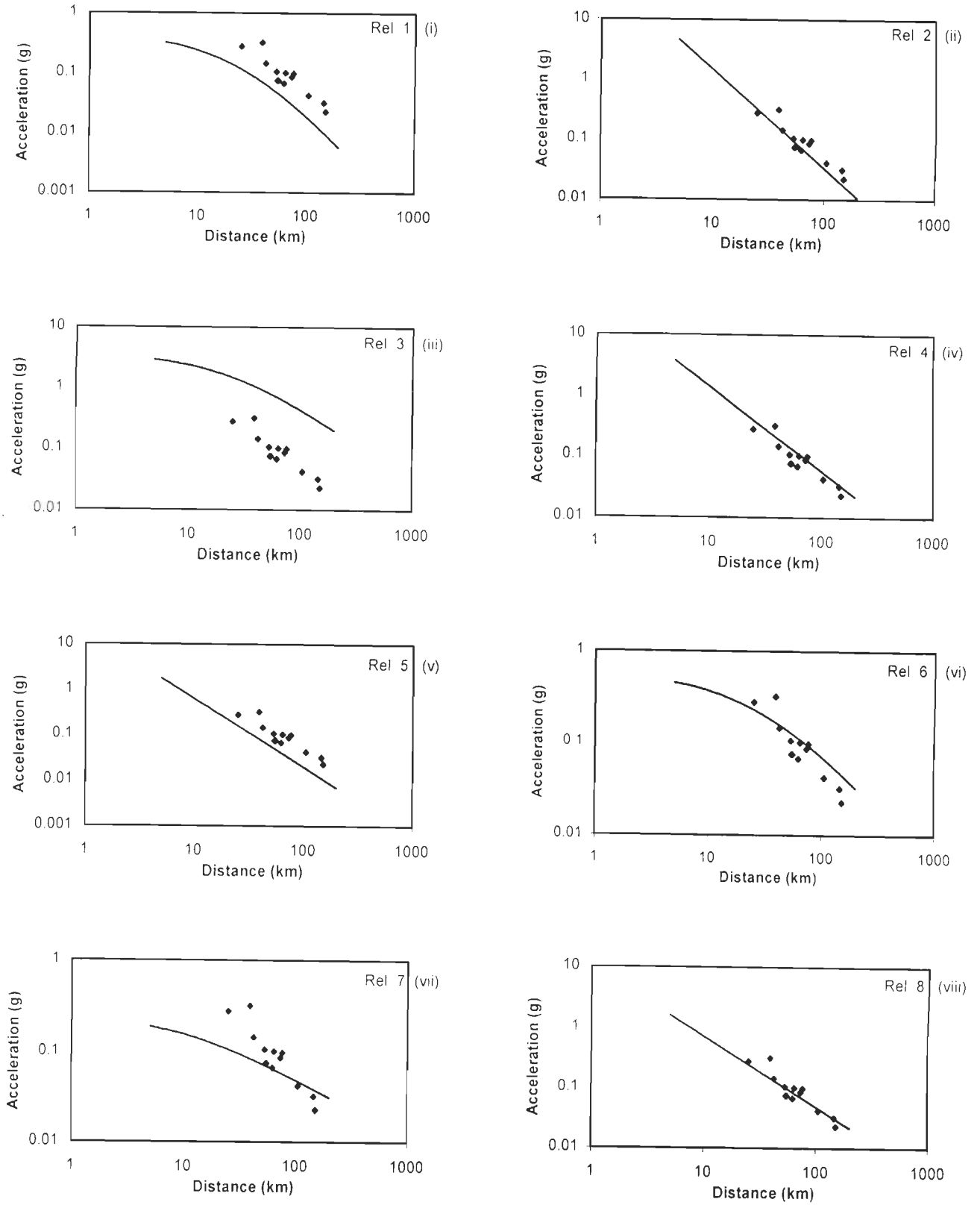

Fig. 2.15(i-viii) : Plot of the observed acceleration with distance for Uttarkashi, 1991 earthquake and the regression curves of the empirical relations for Table 2.6

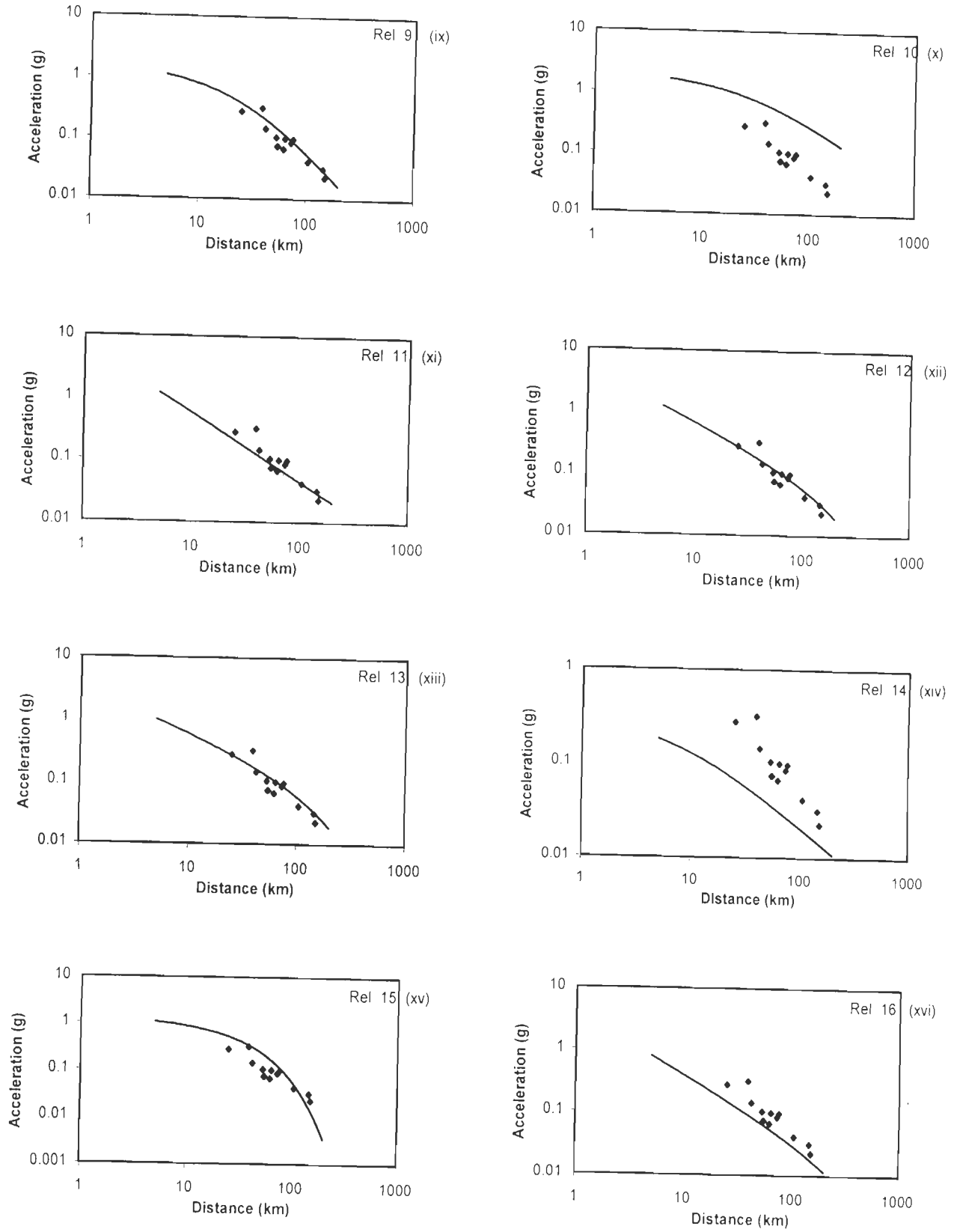

Fig. 2.15(xi-xvi) : Plot of the observed acceleration with distance for Uttarkashi, 1991 earthquake and the regression curves of the empirical relations for Table 2.6

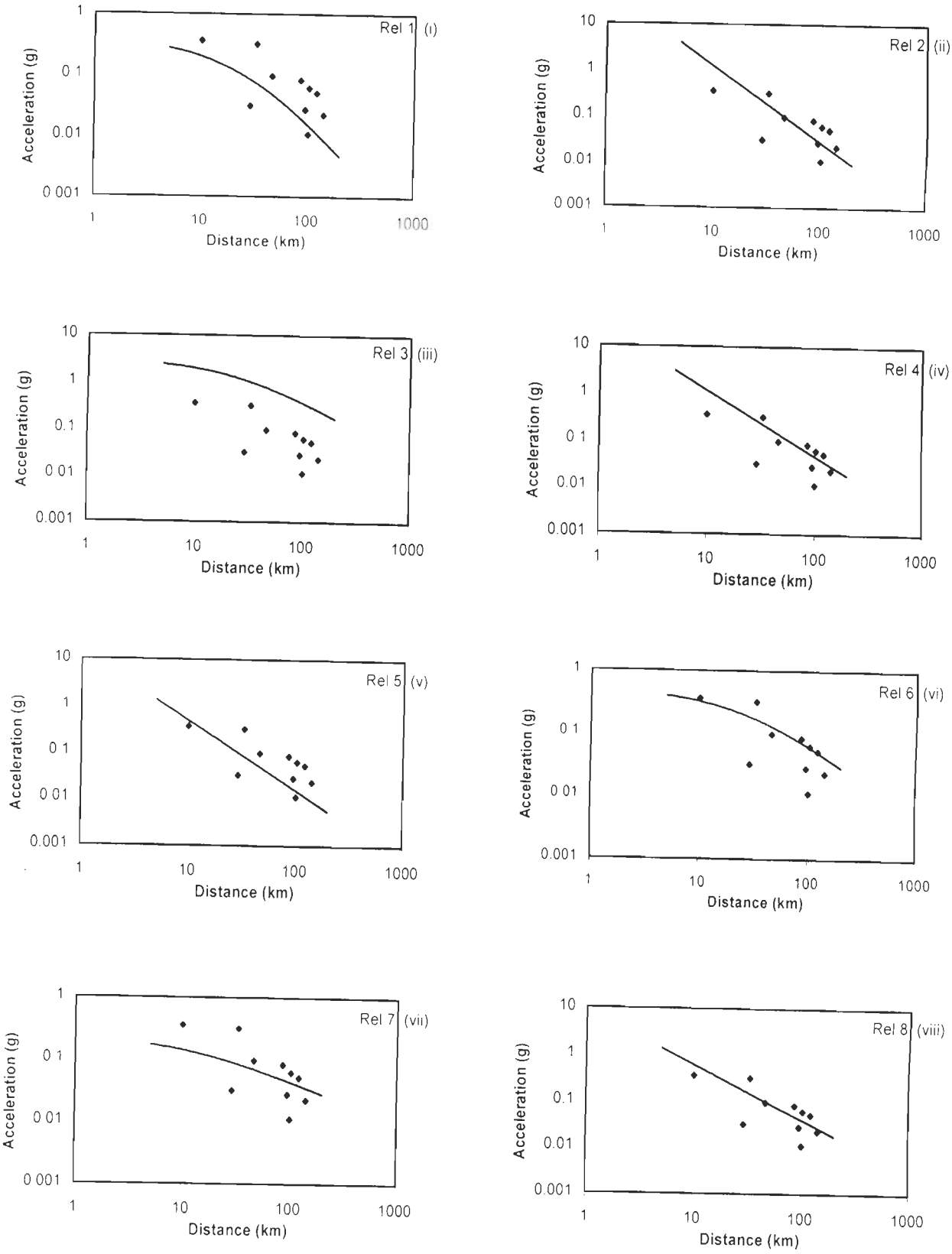

Fig. 2.16(i-viii) : Plot of the observed acceleration with distance for Chamoli, 1999 earthquake and the regression curves of the empirical relations in Table 2.6

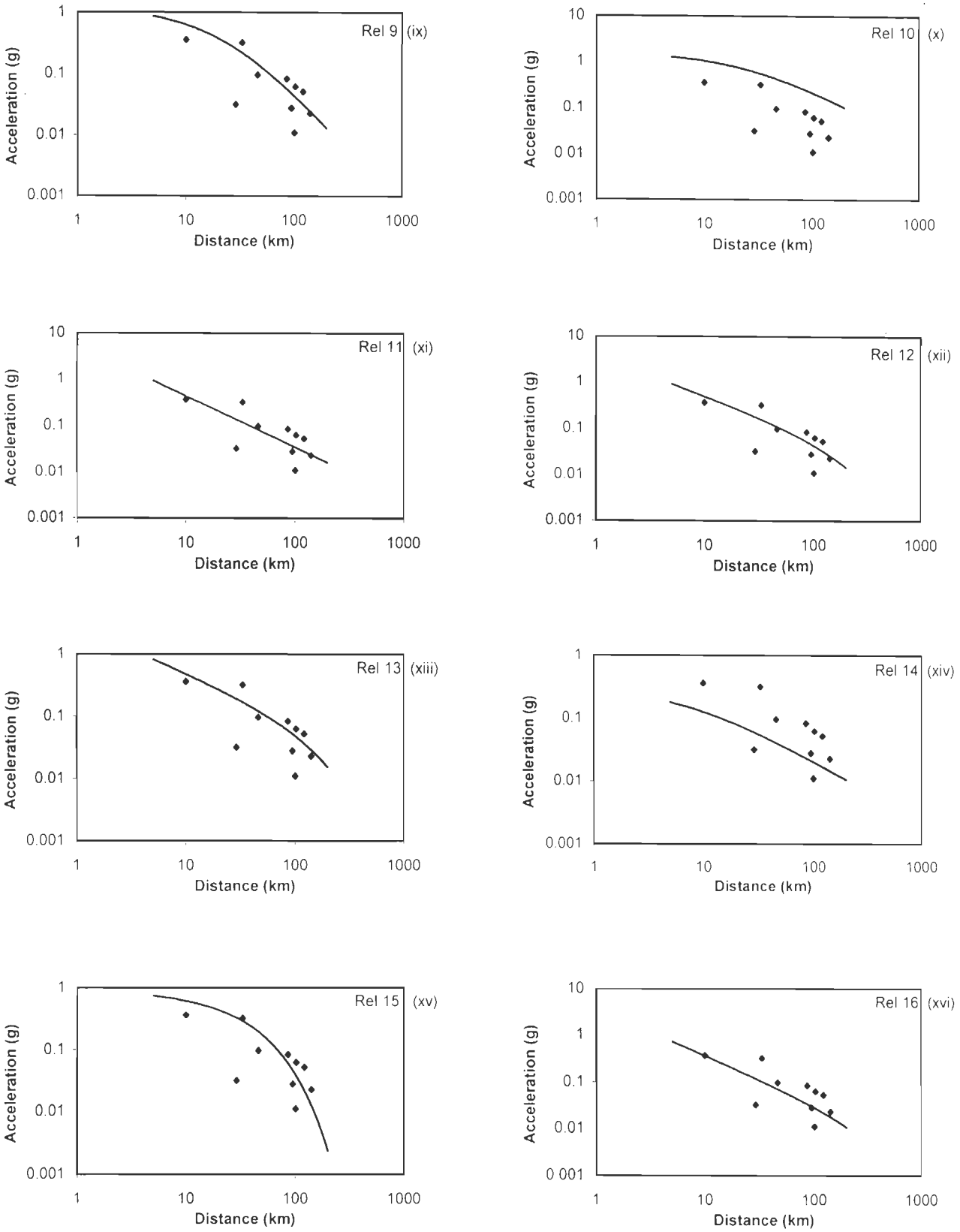

Fig. 2.16(ix-xvi) : Plot of the observed acceleration with distance for Chamoli, 1999 earthquake and the regression curves of the empirical relations in Table 2.6

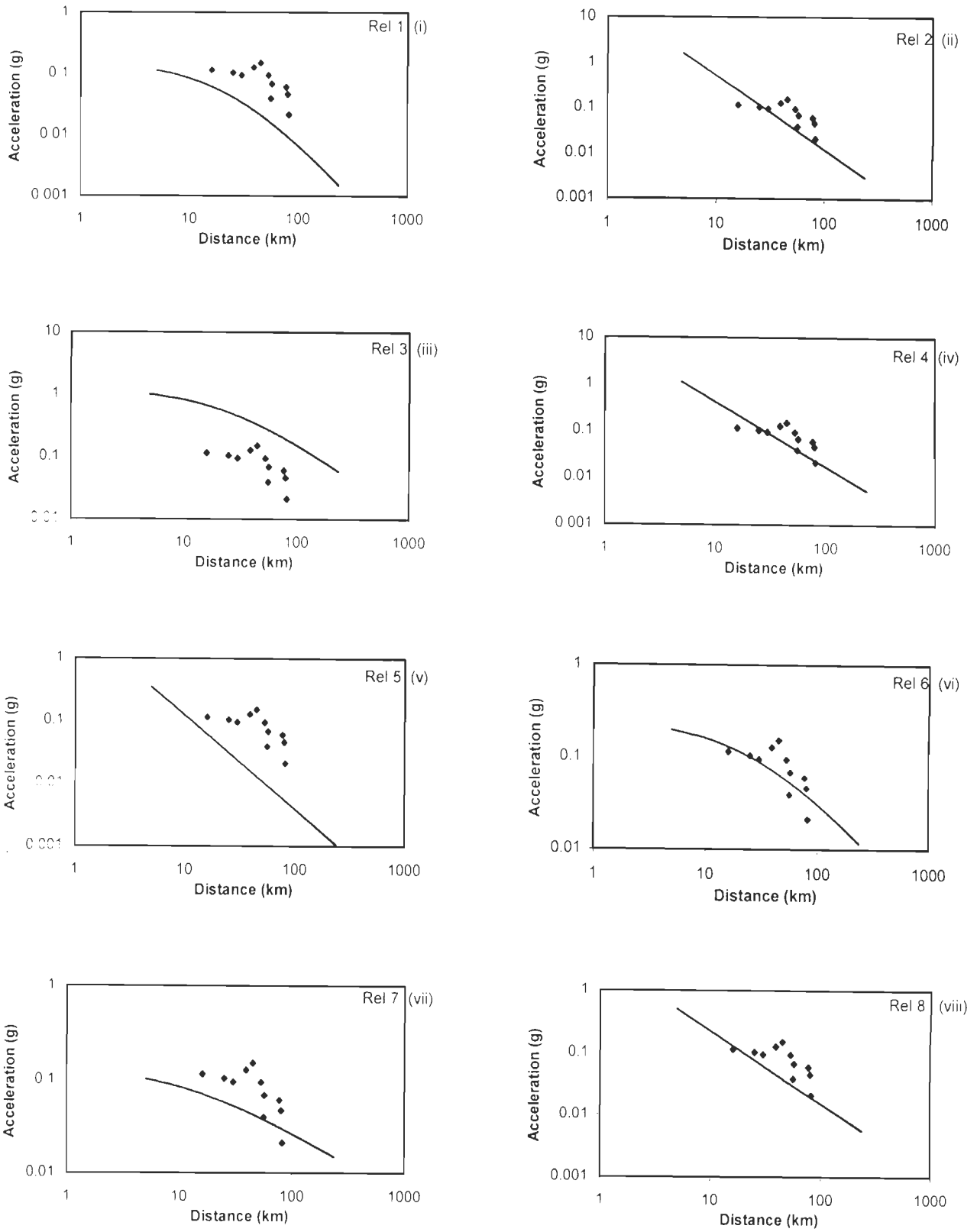

Fig. 2.17(i-viii) : Plot of the observed acceleration with distance for Northeast Earthquake of Sept.1986 and the regression curves of the empirical relations in Table 2.6

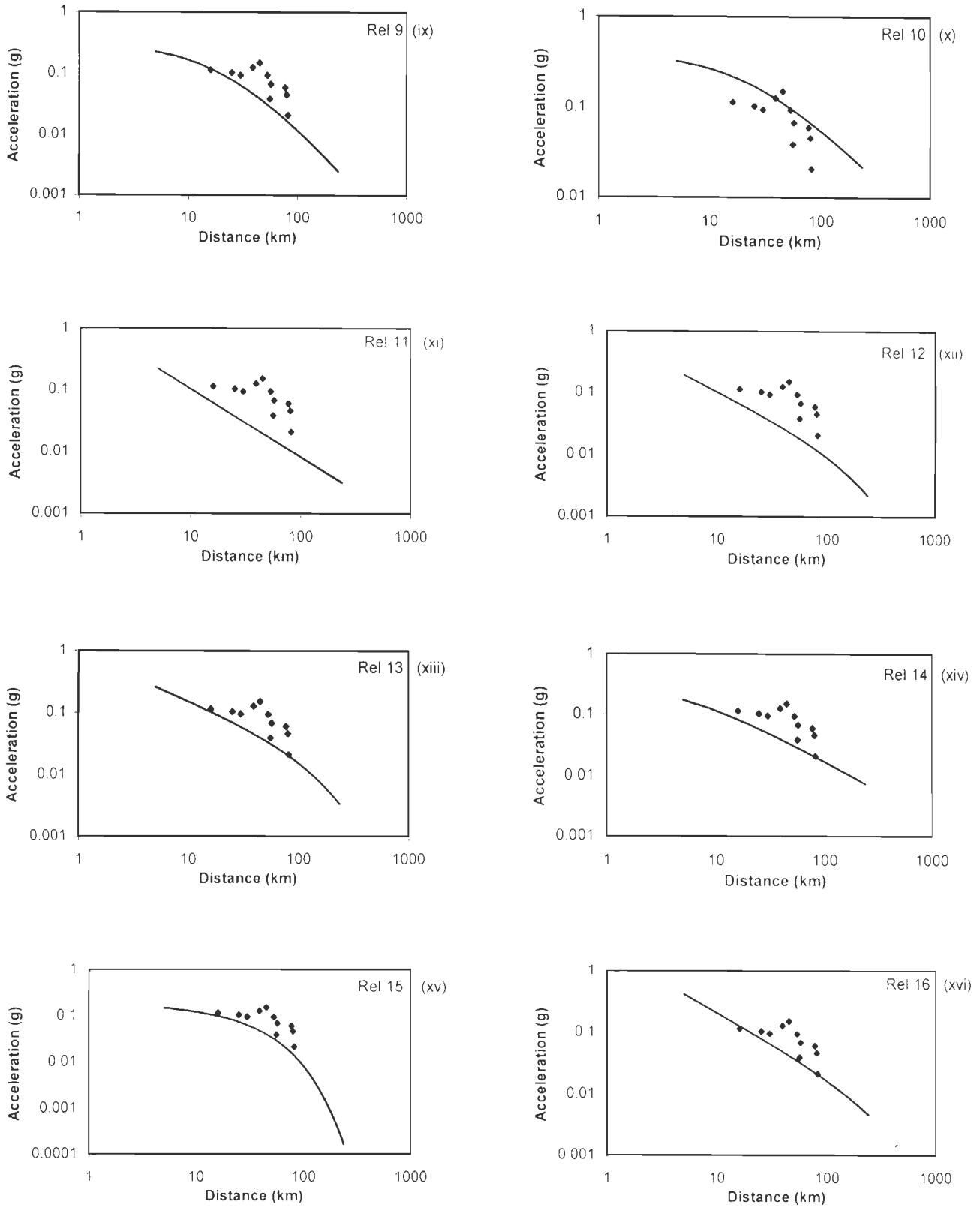

Fig. 2.17(ix-xvi) : Plot of the observed acceleration with distance for Northeast Earthquake of Sept.1986 and the regression curves of the empirical relations in Table 2.6

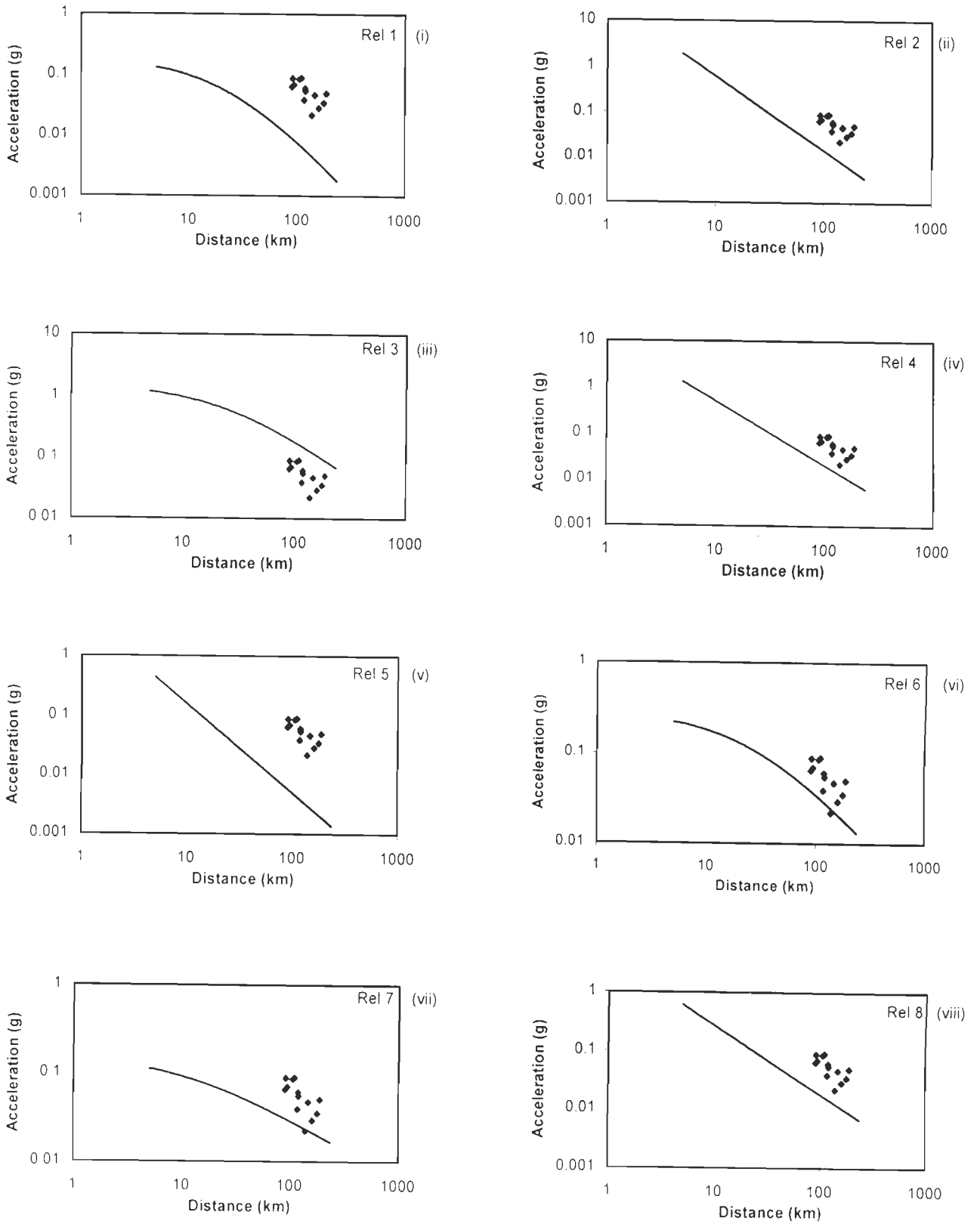

Fig. 2.18(i–viii) : Plot of the observed acceleration with distance for Northeast earthquake of May 1987 and the regression curves of the empirical relations in Table 2.6

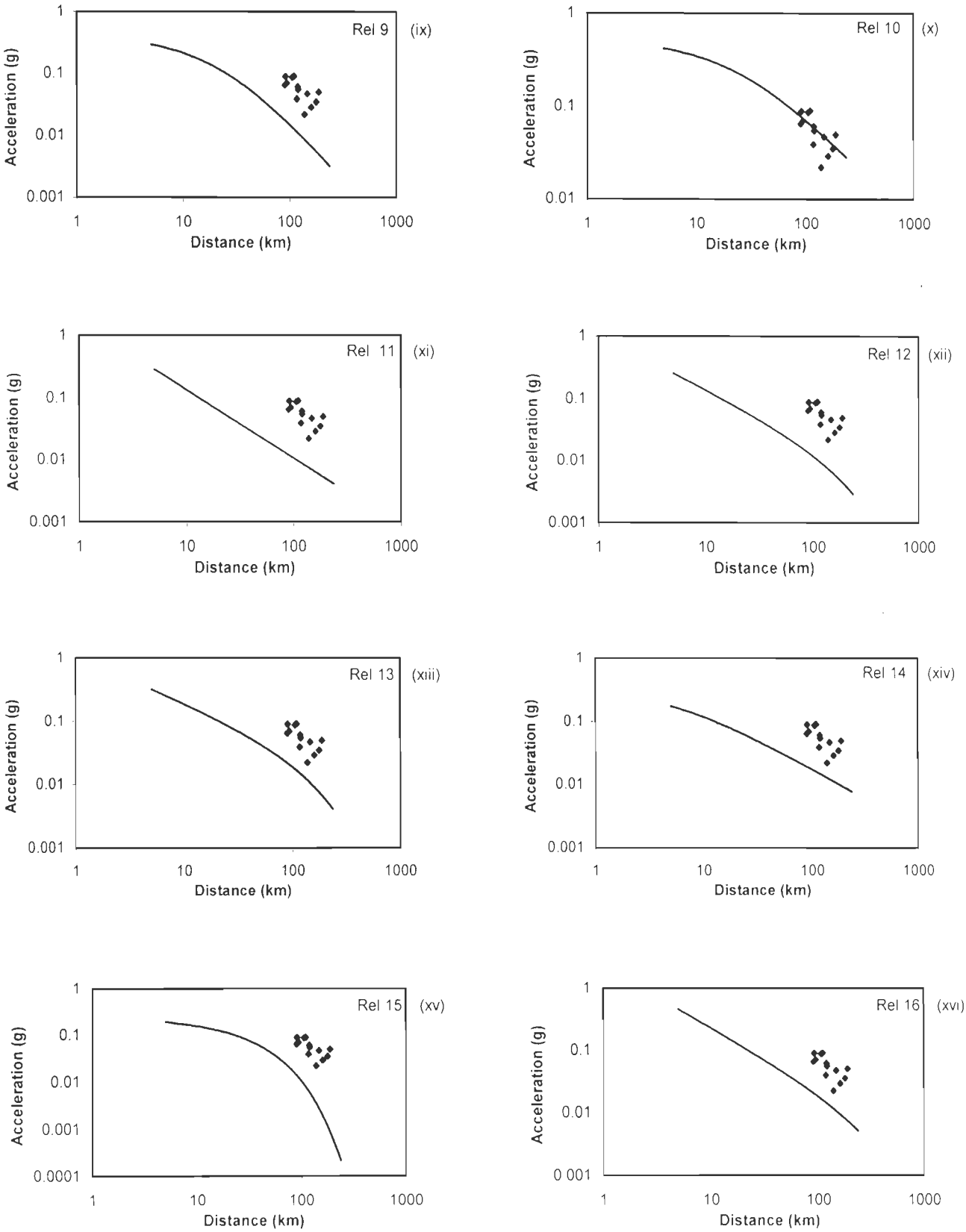

Fig. 2.18(ix–xvi) : Plot of the observed acceleration with distance for Northeast earthquake of May 1987 and the regression curves of the empirical relations in Table 2.6

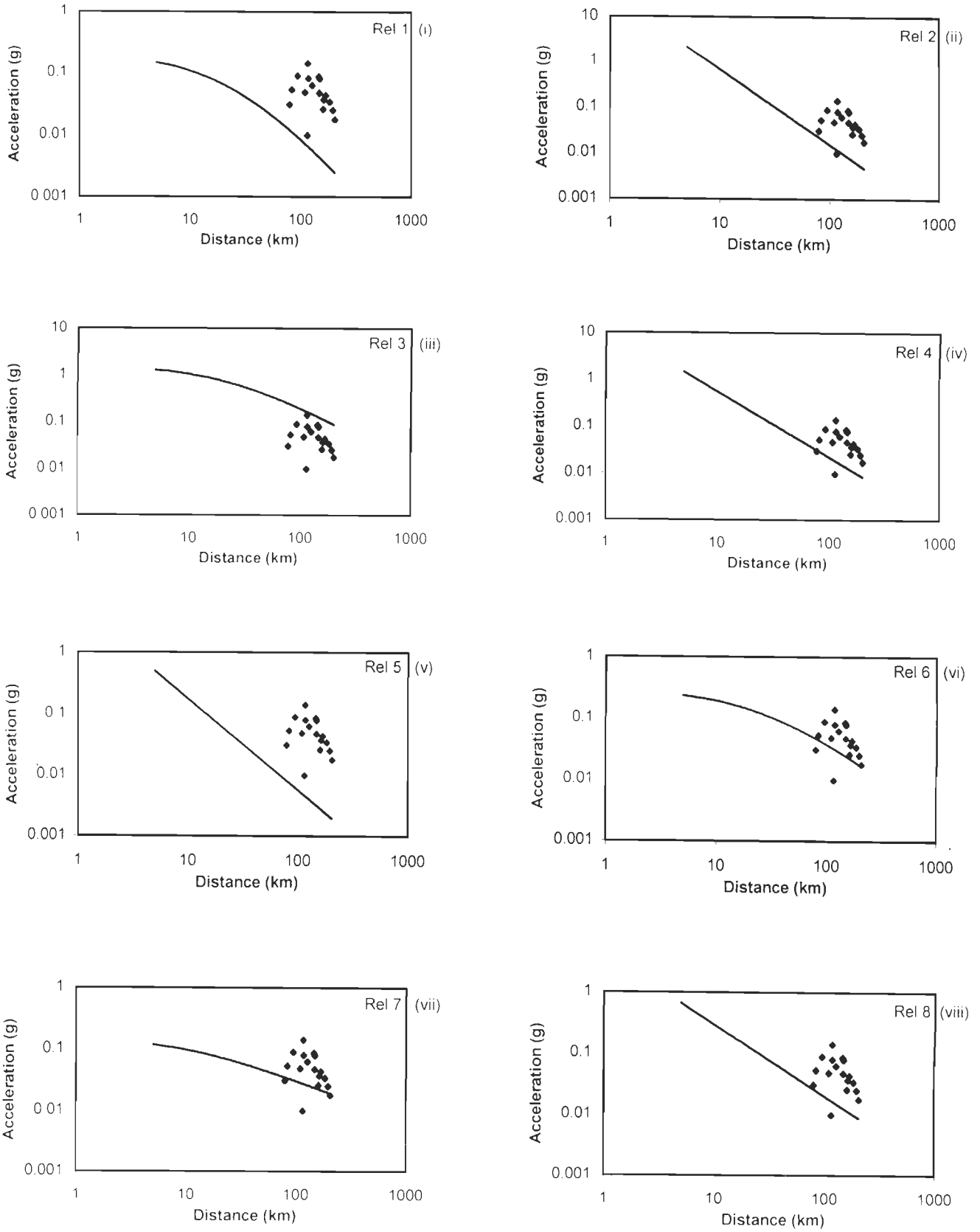

iFig 2.19(i-viii) : Plot of the observed acceleration with distance for Northeast earthquake of Feb.1988 and the regression curves of the empirical relations fin Table 2.6

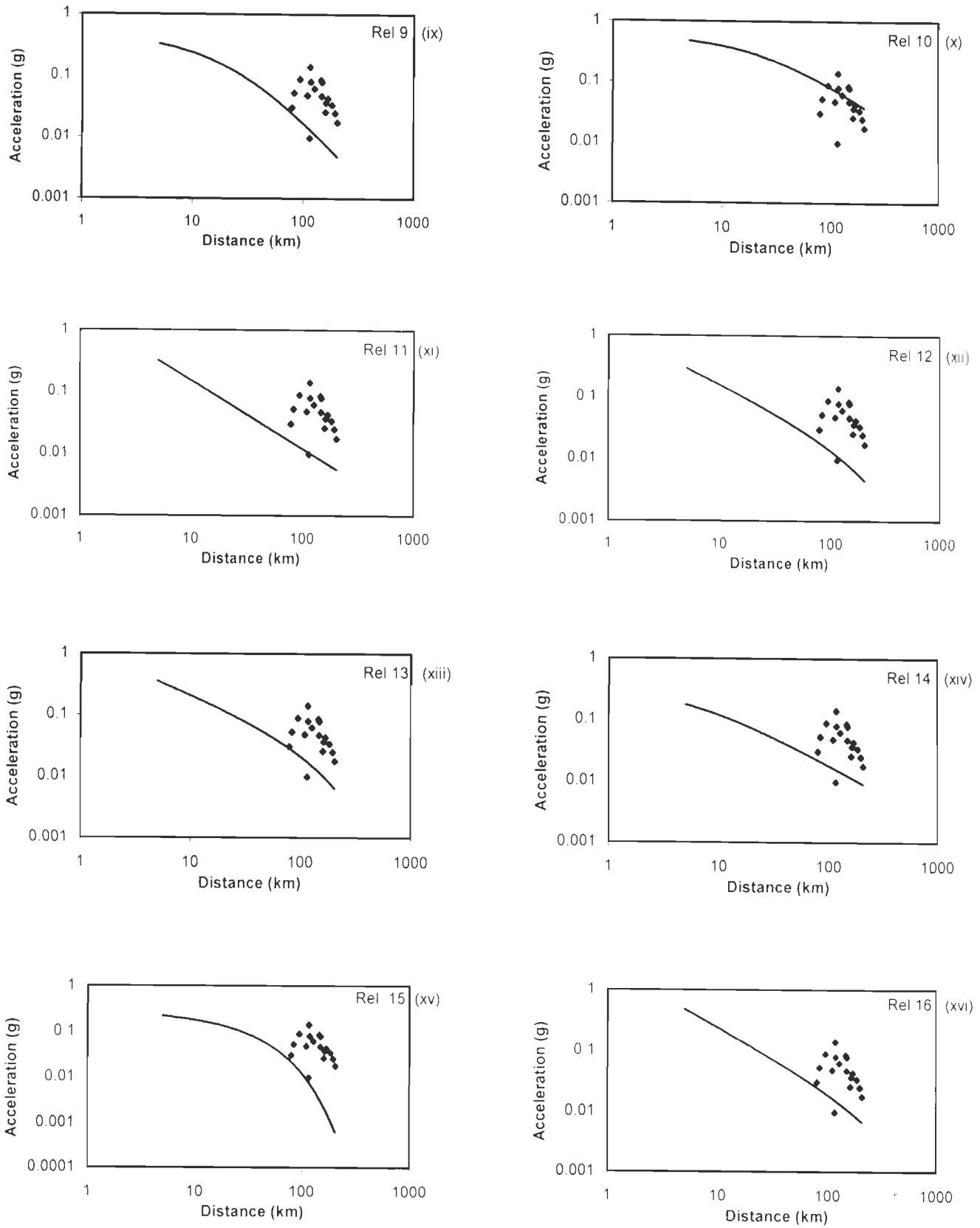

Fig. 2.19(ix-xvi): Plot of the observed acceleration with distance for Northeast Earthquake of Feb.1988 and the regression curves of the empirical relations fin Table 2.6

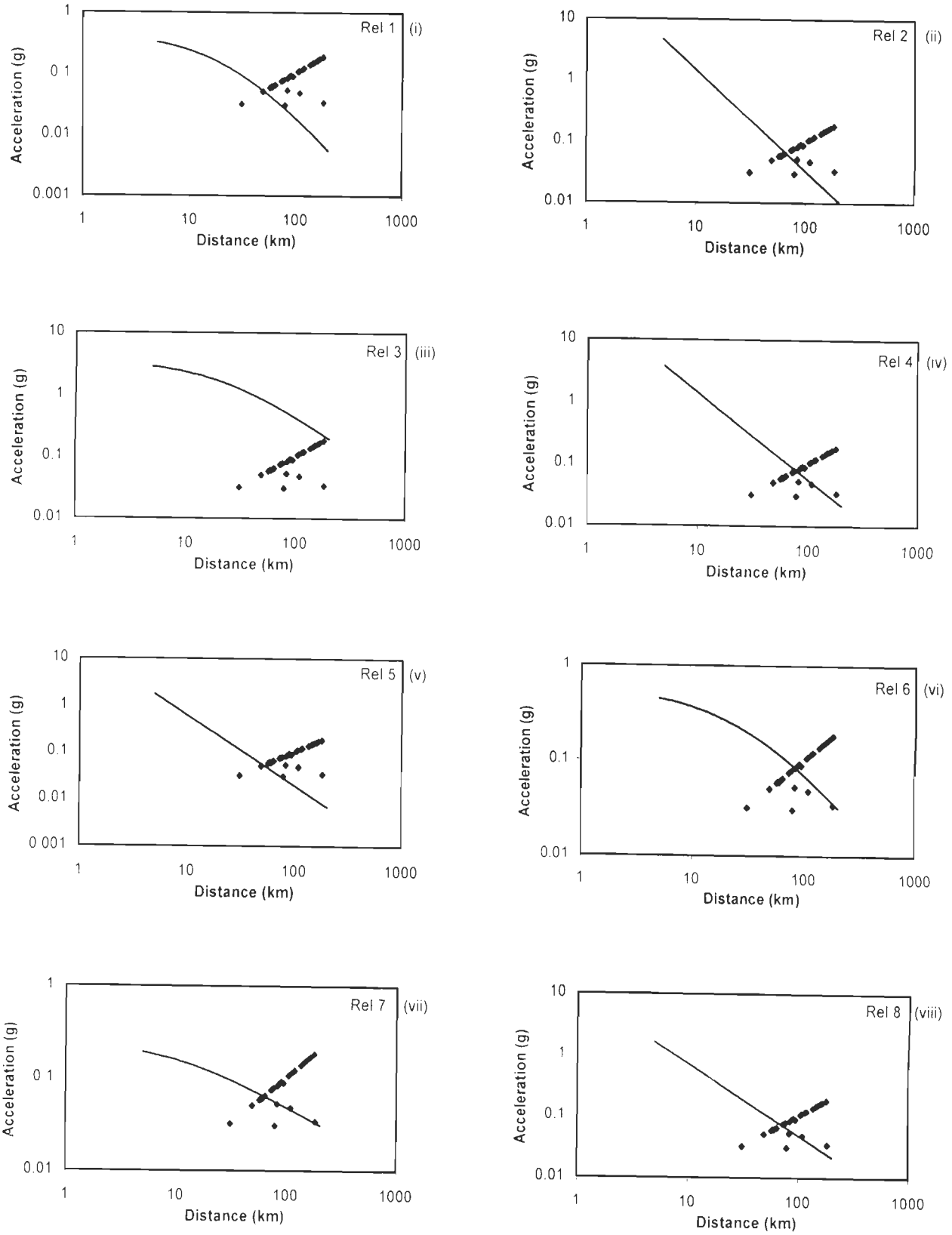

Fig. 2.20(i-viii) : Plot of the observed acceleration with distance for Northeast earthquake of Aug.1988 and the regression curves of the empirical relations for Table 2.6

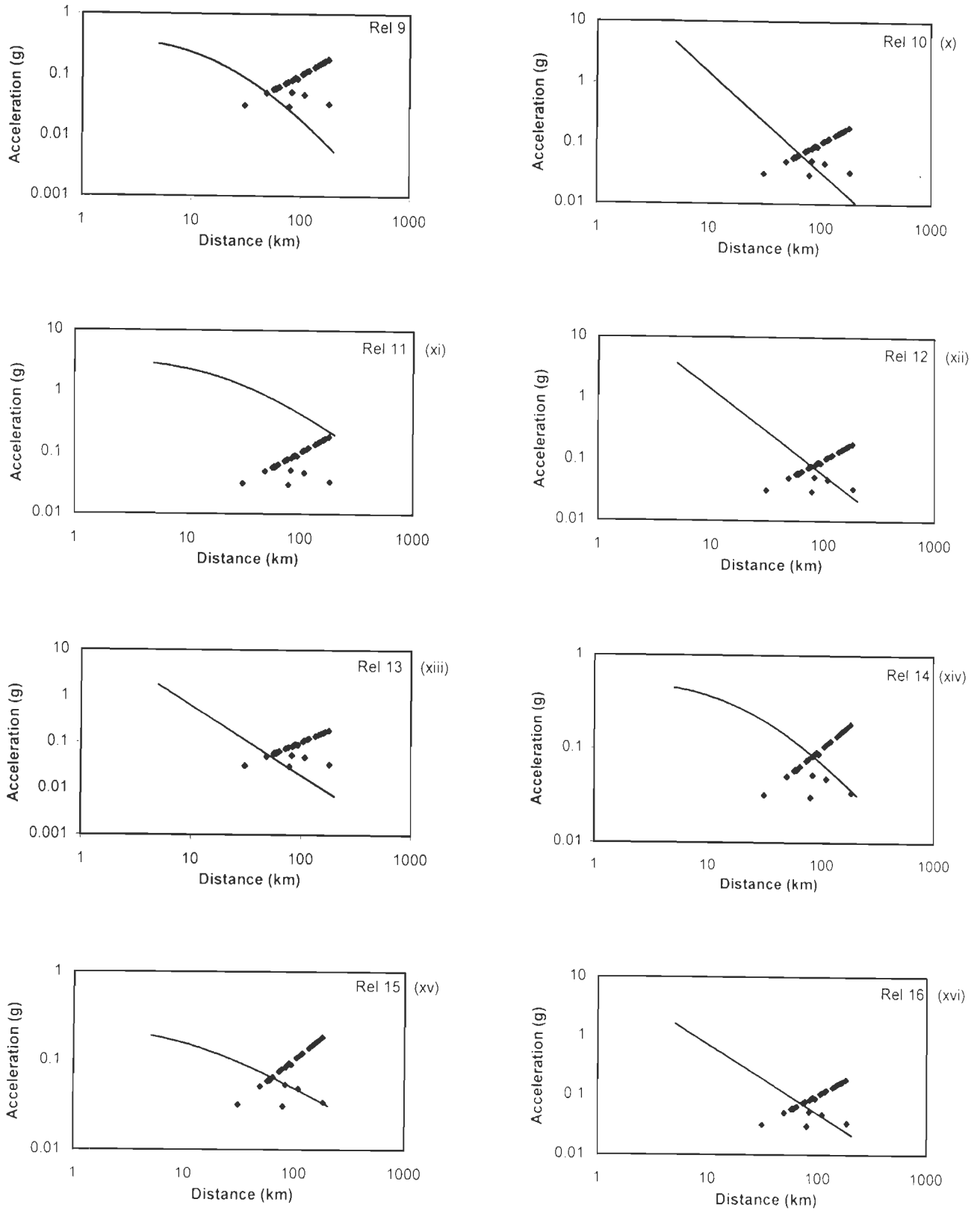

Fig. 2.20(ix-xvi) : Plot of the observed acceleration with distance for Northeast earthquake of Aug.1988 and the regression curves of the empirical relations for Table 2.6

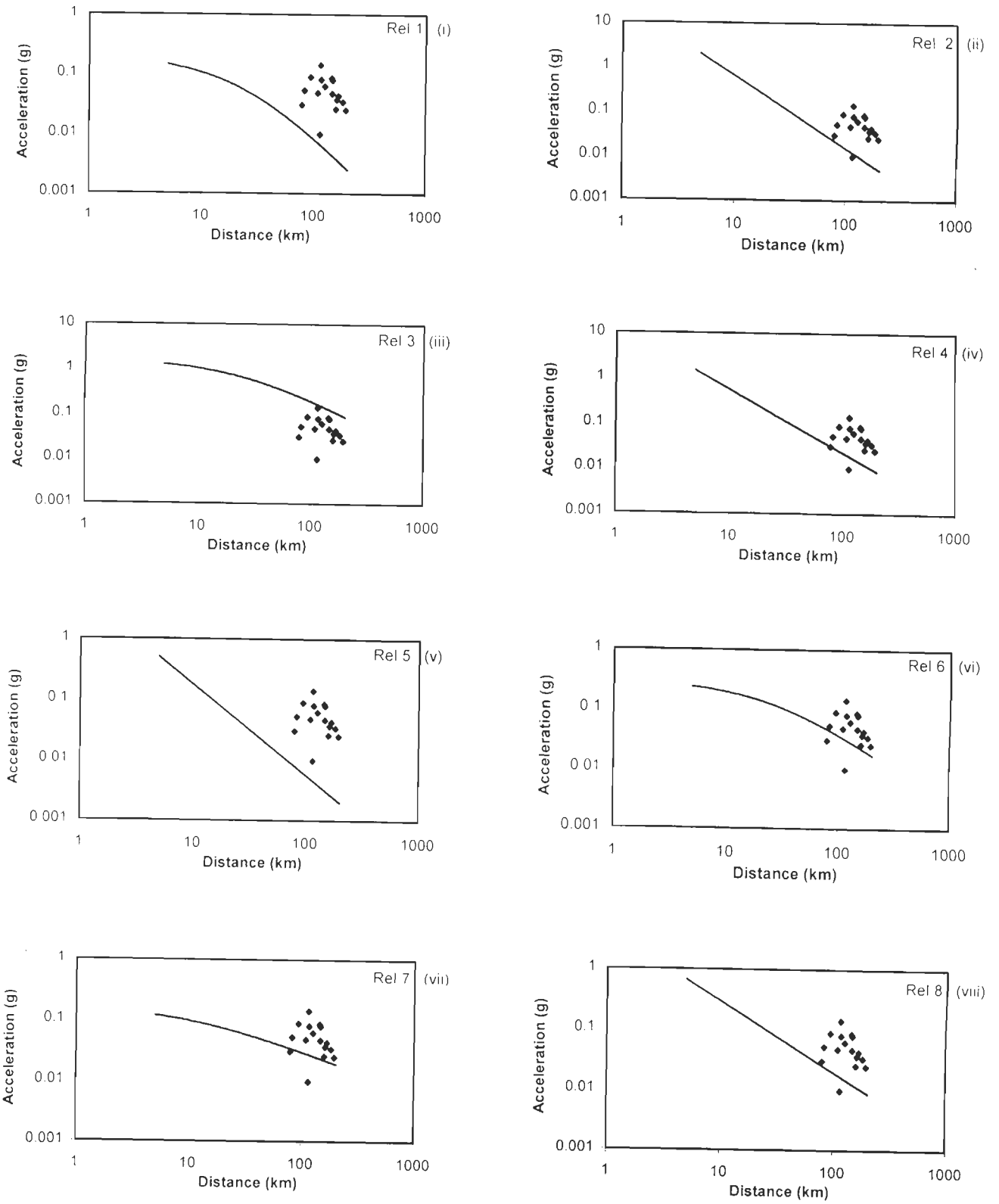

Fig. 2.21(i-viii) : Plot of the observed acceleration with distance for Northeast earthquake of Jan.1990 and the regression curves of the empirical relations for Table 2.6

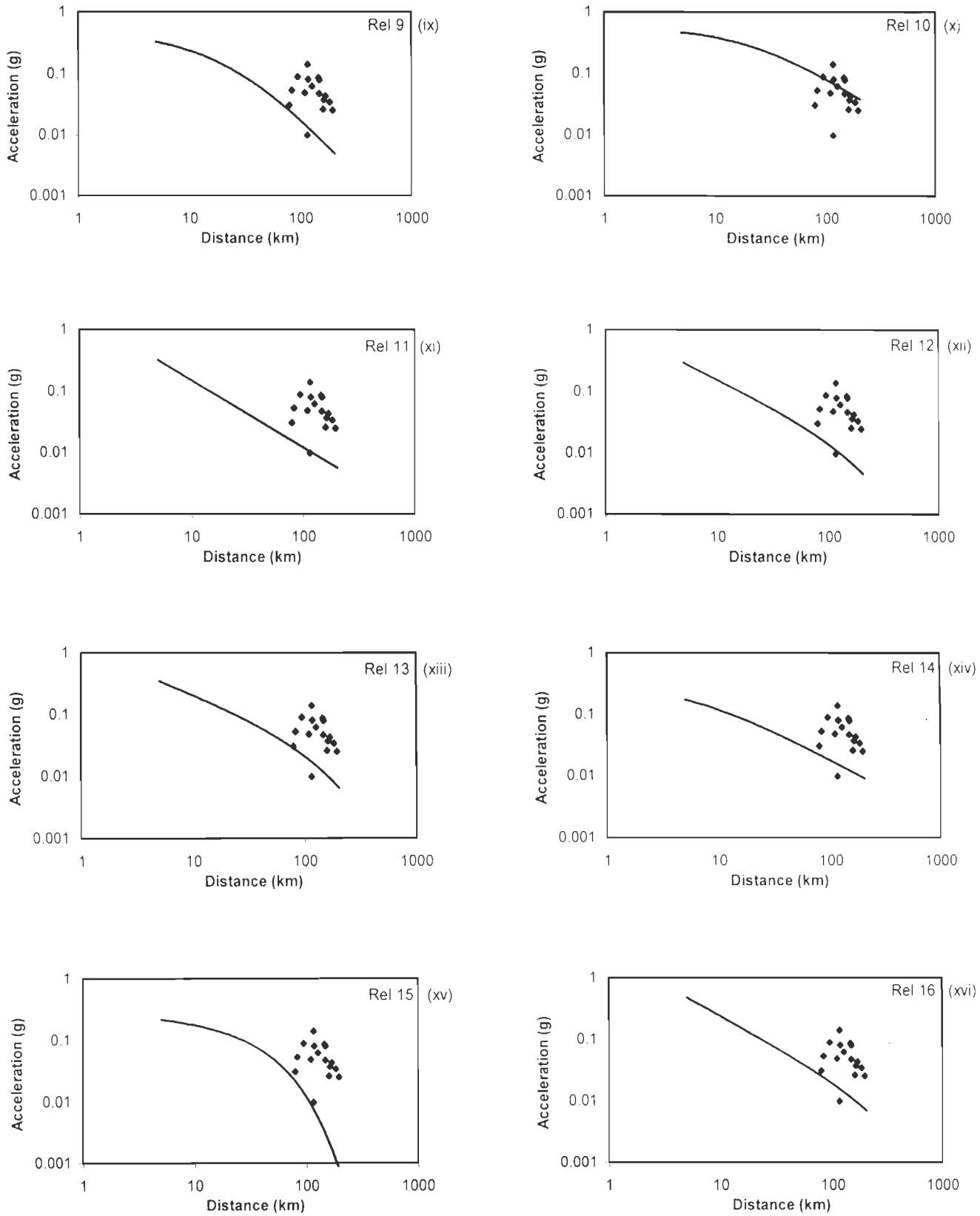

Fig. 2.21(ix-xvi) : Plot of the observed acceleration with distance for Northeast earthquake of Jan.1990 and the regression curves of the empirical relations for Table 2.6

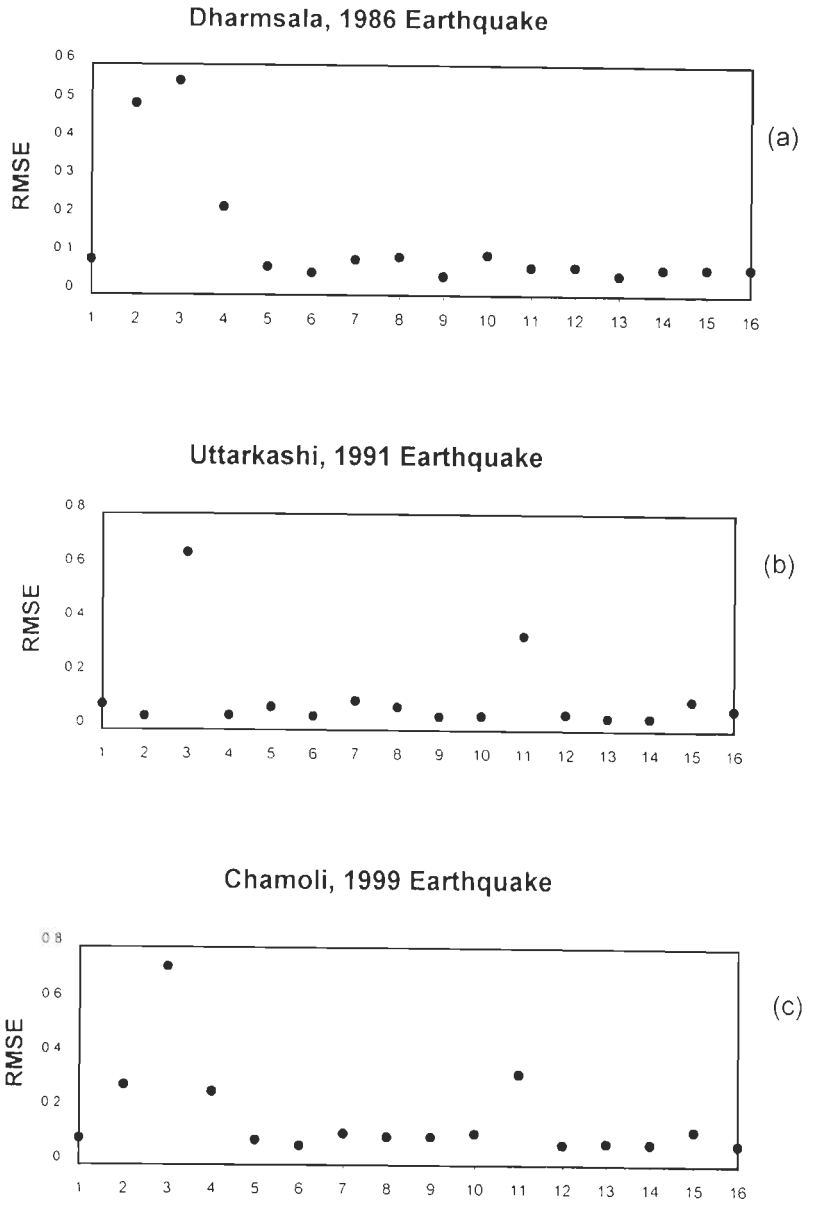

Fig. 2.22(a-c) : Root mean square error versus empirical relations listed in Table 2.6

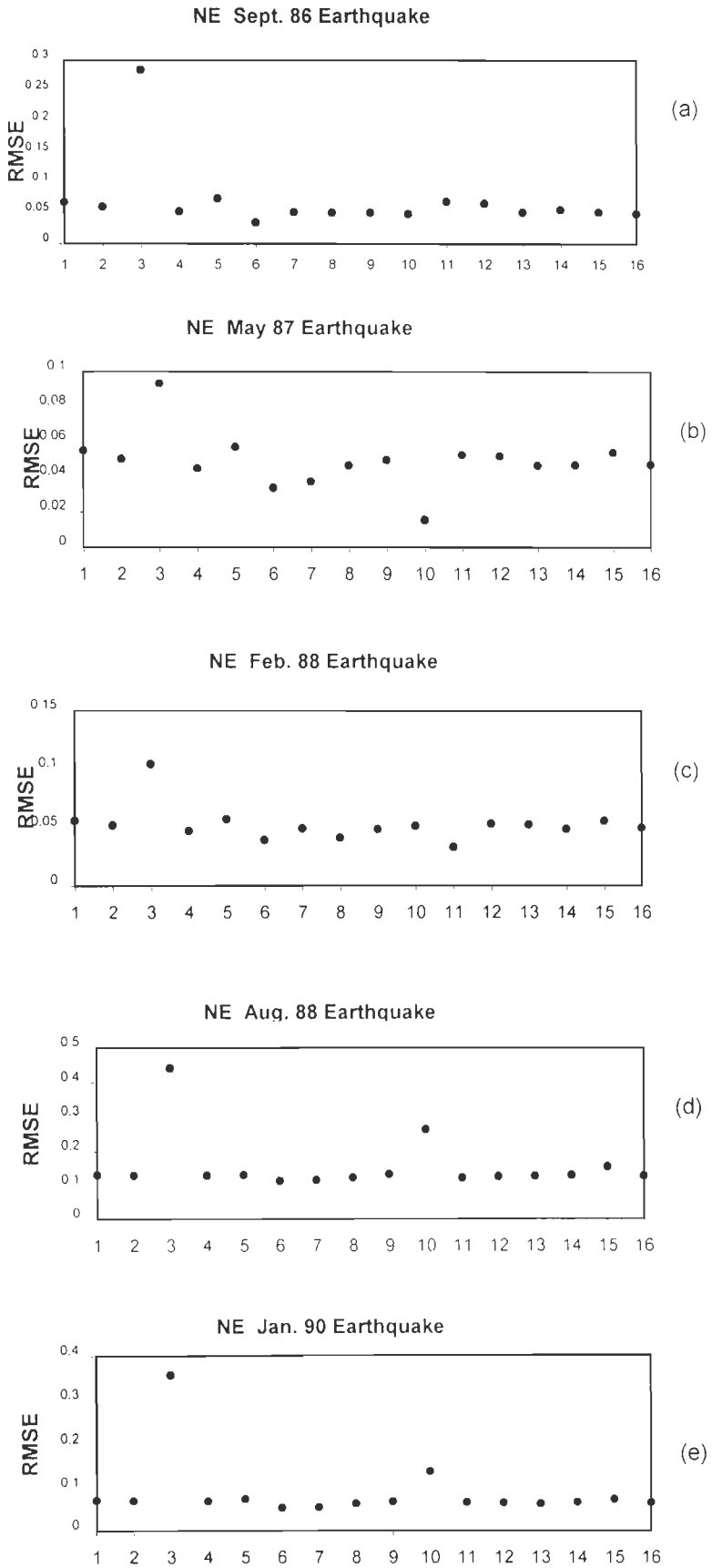

Fig. 2.23(a-e) : Root mean square error versus empirical relations listed in Table 2.6

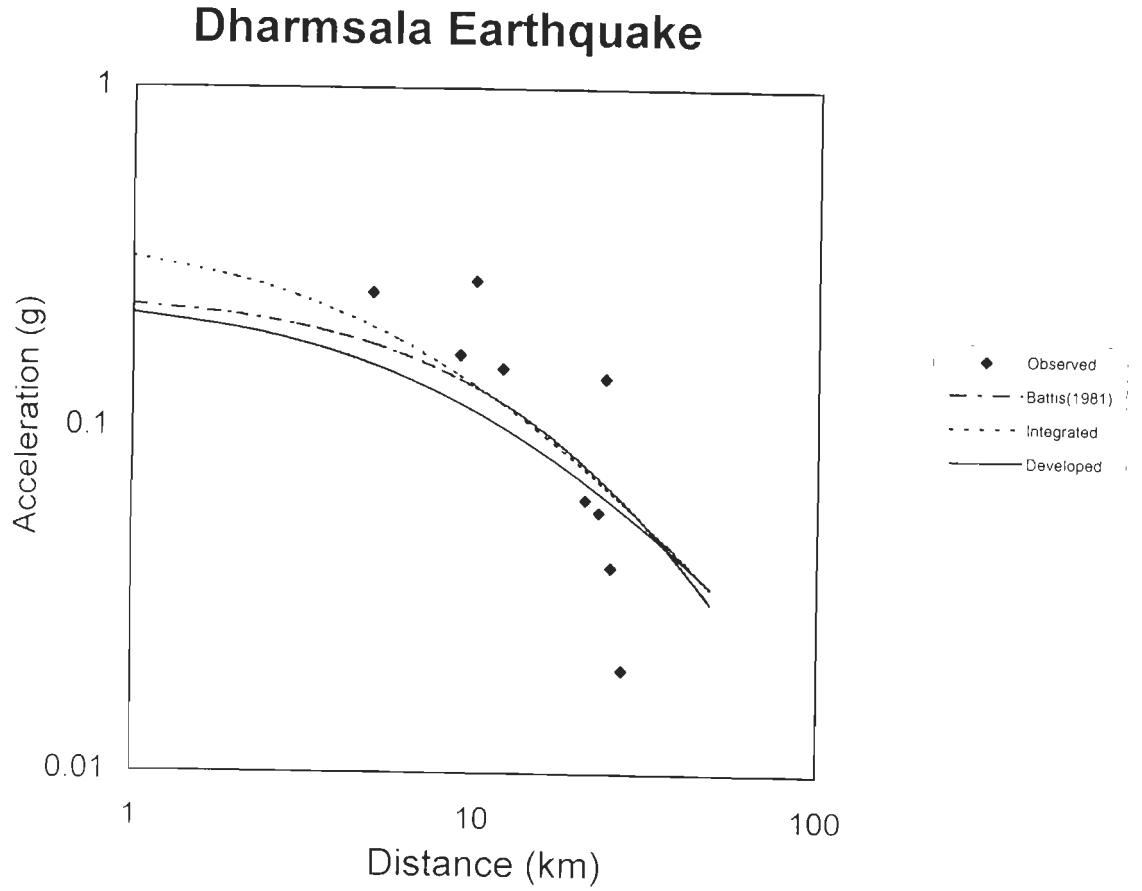

Fig. 2.24 : Comparison of observed data with developed relationship, integrated relationship and relationship from literature found min rmse (Dharmsala, 1986 earthquake)

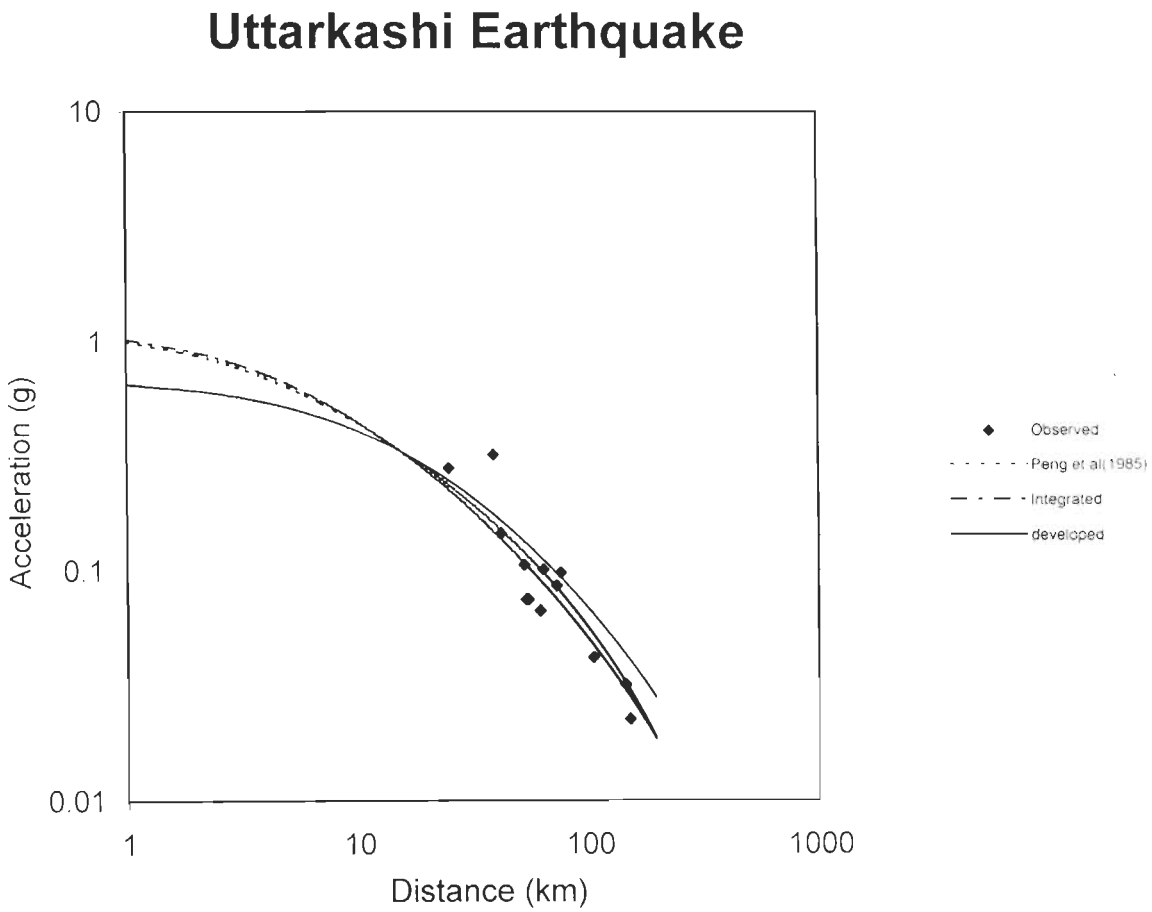

Fig. 2.25 : Comparison of observed data with developed relationship , integrated relationship and relationship from literature found min rmse (Uttarkashi, 1991 earthquake)

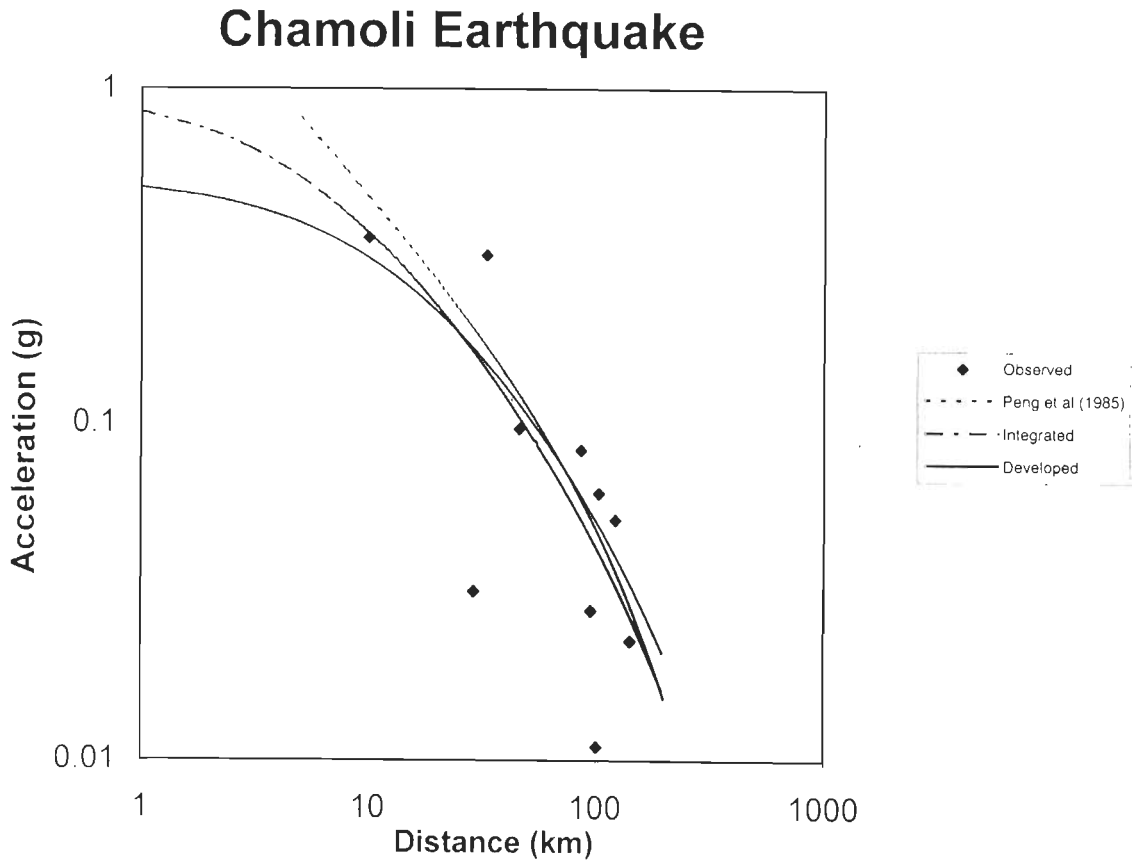

Fig. 2.26 : Comparison of observed data with developed relationship, integrated relationship and relationship from literature found min rmse (Chamoli, 1999 earthquake)

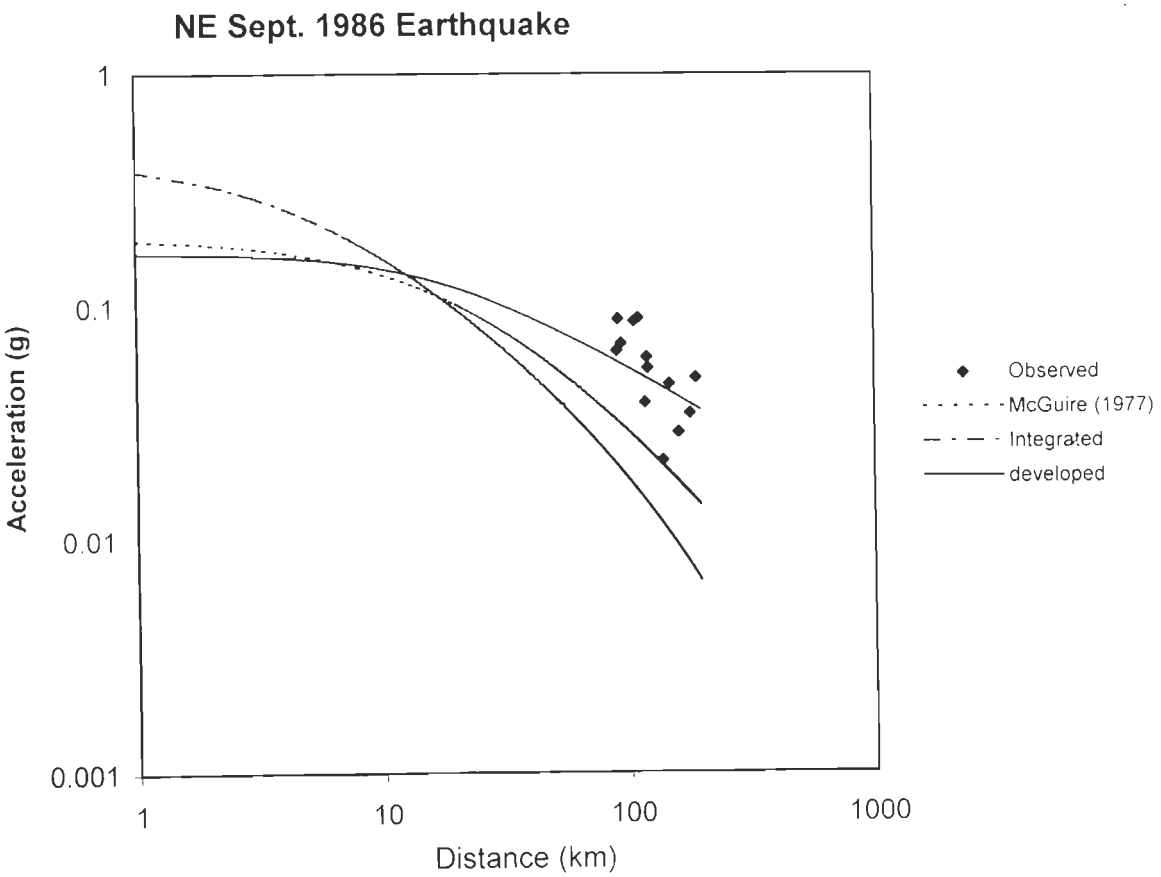

Fig. 2.27 : Comparison of observed data with developed relationship, integrated relationship and relationship from literature found min rmse (Northeast earthquake of Sept. 1986)

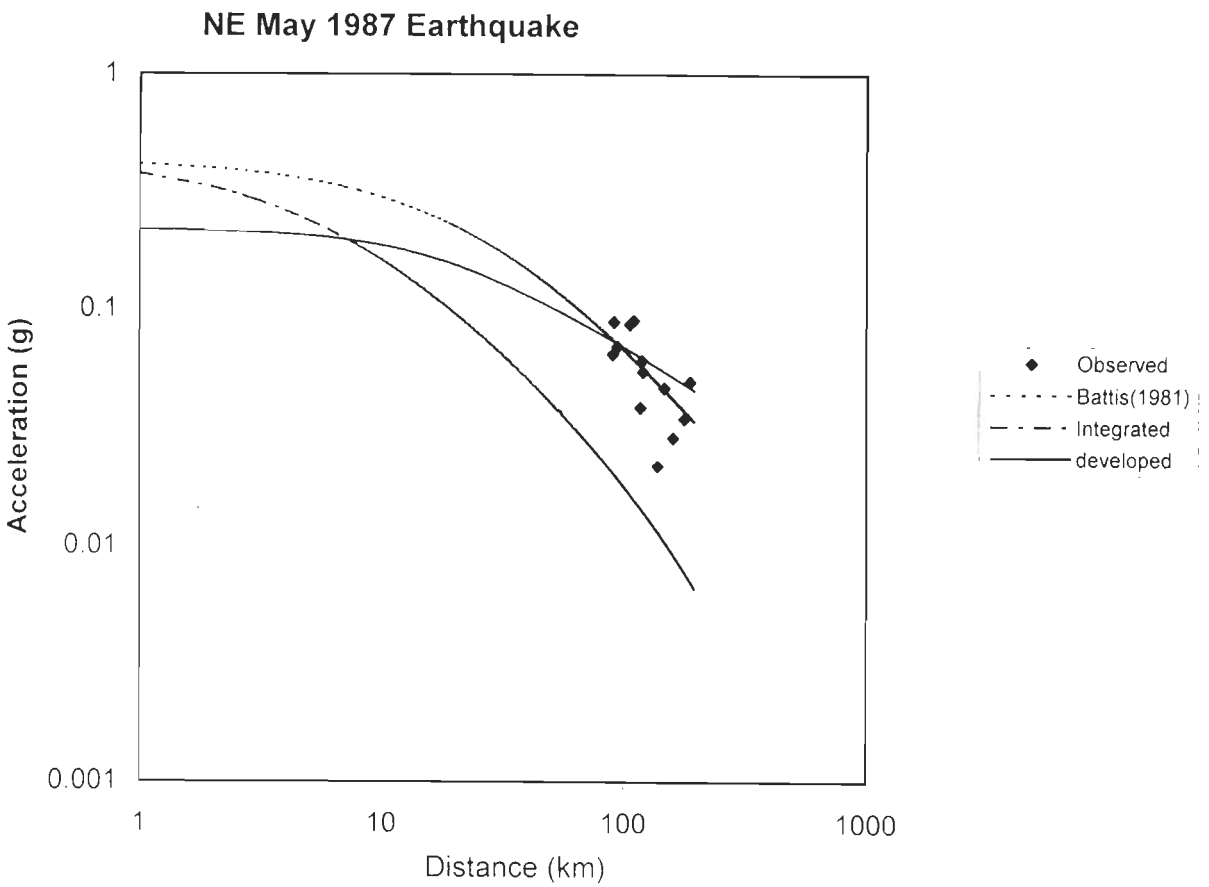

Fig. 2.28 : Comparison of observed data with developed relationship, integrated relationship and relationship from literature found min rmse (Northeast earthquake of May 1987)

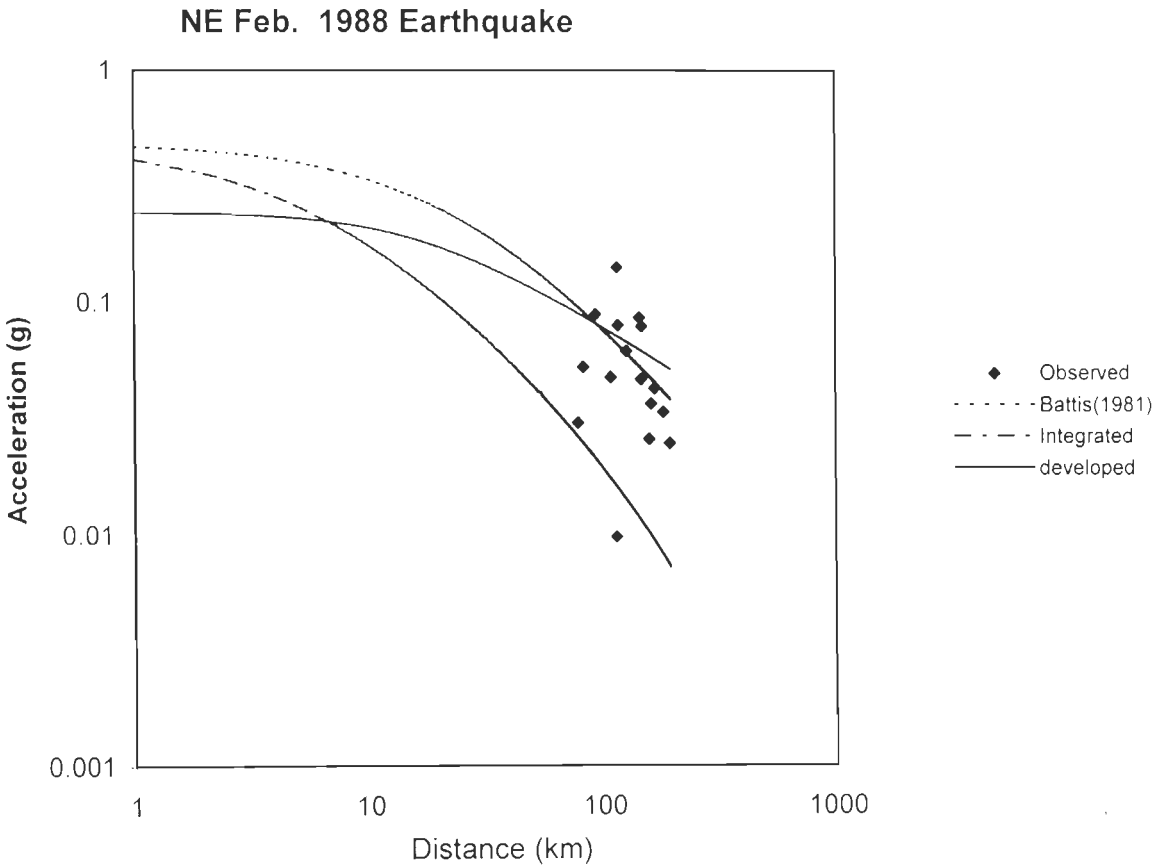

Fig. 2.29 : Comparison of observed data with developed relationship, integrated relationship and relationship from literature found min rmse (Northeast earthquake of Feb. 1988)

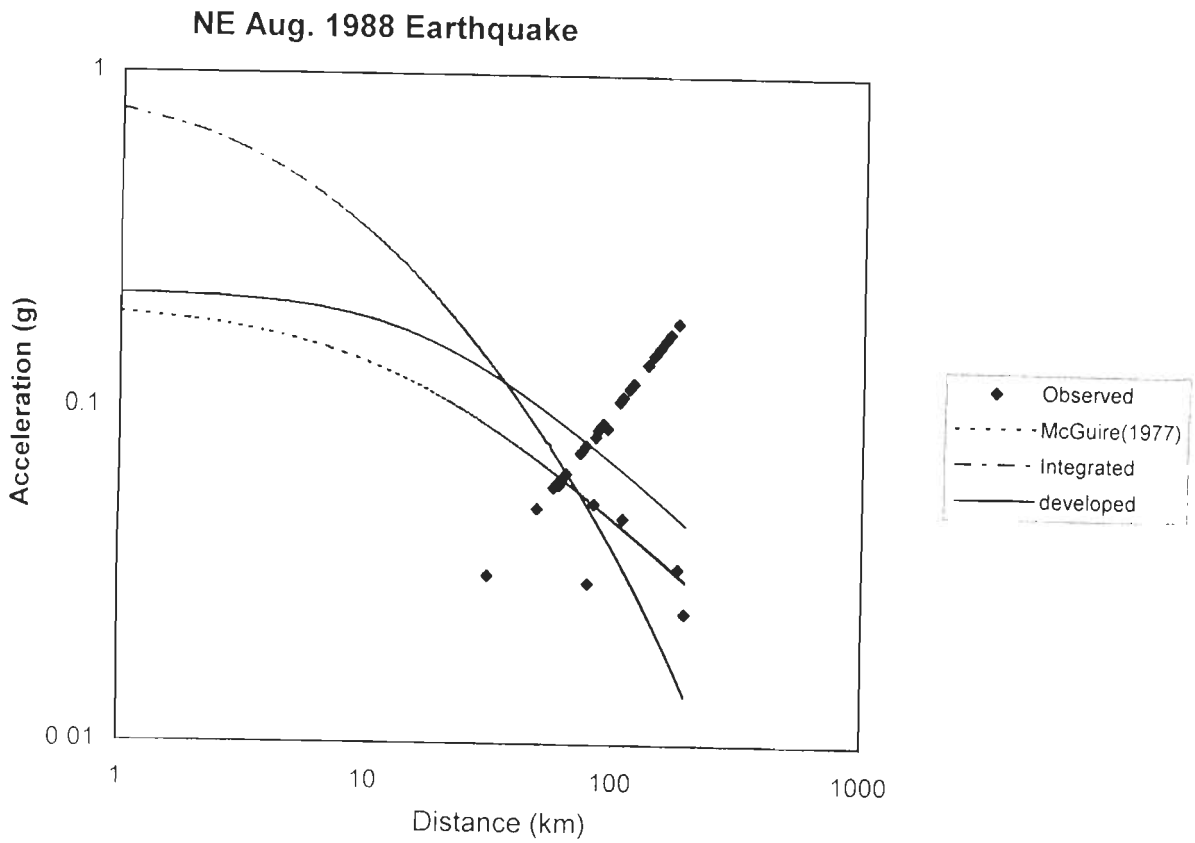

Fig. 2.30 : Comparison of observed data with developed relationship, integrated relationship and relationship from literature found min rmse (Northeast earthquake of Aug. 1988)

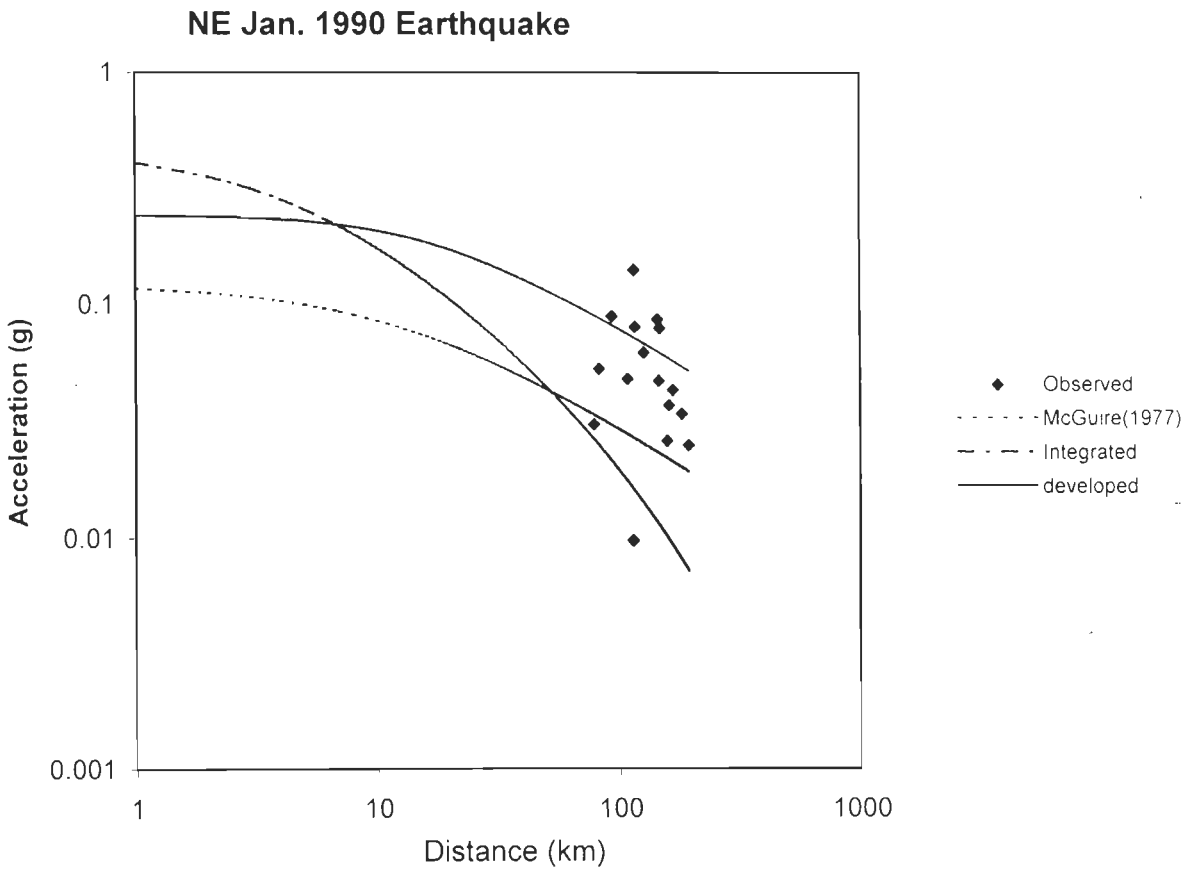

Fig. 2.31 : Comparison of observed data with developed relationship, integrated relationship and relationship from literature found min rmse (Northeast earthquake of Jan.1990)

CHAPTER 3

Synthetic Seismogram Generation - Basics

3.1 Introduction

The elastic rebound model was proposed by H.F. Reid after the 1906 San Francisco earthquake. According to this model strains are built up in the faulted rocks until a failure point is reached. Rupture then takes place and the strained rocks rebound on each side of the fault under its own elastic stress until the strain is largely or wholly relieved. The whole movement is not instantaneous but proceeds in irregular steps. Rupture starts suddenly and also stops suddenly producing vibrations which propagate to large distances. The rupture propagation over the fault is not smooth but is subject to irregular variations related to roughness of the fault plane (Abrahamson and Bolt, 1986). This model forms the basis for generation of synthetic accelerograms.

The generation of the synthetic accelerograms in the near field is based on a dislocation moving over a fault plane. The computed ground motions have to take into account the nature of rupture propagation over the fault plane, radiation pattern effects, presence of free surface, layering in the earth between the source and free surface and effect of finite moving source. The slip on the causative fault is specified in terms of shape, rise time and amplitude of the source time function. In addition velocity of rupture propagation and final area over which slip occurs are also specified.

The computation of synthetic accelerograms in the present work is based on the convolution model of the seismogram. The spectrum of ground motion expected at a recording site are first computed from a knowledge of source parameters and medium properties. This spectrum is then inverse Fourier transformed to yield the desired synthetic accelerogram.

This method has been successfully used by Boore (1983), and has been further extended in the present thesis.

3.2 Convolution model of Seismogram

Let Y(t) represent the recorded seismogram at a point on the surface of a layered half space produced by a point shear dislocation. This can be written as

$$y(t) = C \cdot s(t) \cdot a(t) \cdot d(t) \cdot i(t) \qquad \ldots (3.1)$$

where C is a scalar, $s(t)$ is the source time function, $a(t)$ represents the impulse response of the layered medium between source and receiver, $d(t)$ accounts for frequency dependent attenuation and $i(t)$ is the impulse response of the seismograph. In frequency domain equation (3.1) can be written as

$$Y(\omega) = C\, S(\omega)\, A(\omega)\, D(\omega)\, I(\omega) \qquad \ldots (3.2)$$

where each function of angular frequency ω represents the Fourier transform of the corresponding time function. All these functions are complex in ω. In this way the phase of the above functions of ω is also taken into account.

Scalar C used in the synthesis is given by

$$C = {M_o R_p F_s} / {4\pi\rho c^3 r} \qquad \ldots (3.3)$$

where M_o is the seismic moment which itself is the product of fault area, average dislocation and rigidity of the medium in which fault is embedded. (Kasahara, 1981). R_p is the radiation pattern term (for details, see Appendix C) and F_s represents the effect of the presence of free surface i.e. the factor by which ground motions are amplified by the presence of free surface (for details, see Appendix D). The term ρ is density of the medium, C represents the P or S-wave velocity (α or β) and r is the source-to-receiver distance (i.e. hypocentral distance).

S(ω) represents the source spectral function and is discussed later.

The function A(ω) accounts for the effect of intervening medium between source and receiver. It can be expressed as the frequency–dependent transfer function that results from wave propagation in a stack of layers with a strong impedance contrast at the base of the stack. As acoustic impedance decreases towards the earth's surface, conservation of energy for waves travelling through materials with decreasing velocity requires an increase in wave amplitude as the wave speed slows down. Thus, as seismic waves approach the earth's surface they are amplified by gradual decrease in seismic impedance. In case of a homogeneous elastic half space, the amplification factor A(ω) can be taken as unity.

Diminution function D(ω) accounts for the frequency dependent attenuation due to the nature of the medium along the path followed by

the seismic waves. The amplitude of the seismic waves from an earthquake source decreases with increasing distance because of geometrical spreading, energy partitioning at layer boundaries, diffraction, scattering and frequency dependent attenuation resulting from the absorption and conversion of seismic energy into heat.

The attenuation properties expressed by quality factor Q. The attenuation coefficient *a* is given by

$$a = \frac{\omega}{2CQ} \qquad \ldots (3.4)$$

So attenuation for a given wave type (P or S) is defined as the inverse of quality factor Q. Q has been found to be a function of frequency. A form of Q that fits a number of observations is given by (Boore, 1987)

$$Q = 29.4 \frac{\left[1 + \frac{\omega}{0.6\pi}\right]^{2.9}}{\left[\frac{\omega}{0.6\pi}\right]^{2}} \qquad \ldots (3.5)$$

The following form has been chosen for the diminution factor $D(\omega)$ (Rovelli, 1987).

$$D(\omega) = \exp [- a r] P (\omega,\omega_m) \qquad \ldots (3.6)$$

where $P(\omega,\omega_m)$ is a kind of high cut filter of arbitrary shape given by

$$P(\omega,\omega_m) = [1 + (\omega/\omega_m)^n]^{-1/2} \qquad \ldots (3.7)$$

where n is the power of a filter. The high-cut filter P is needed to account for the general observation that acceleration spectra often

shows an abrupt depletion of high-frequency energy above some frequency, ($\omega_m = 2\pi f_{max}$).

Instrumentation response **I(ω)** is a kind of filter used to shape the spectrum so that the predicted motion correspond to the particular ground motion measure of interest. It is given by

$$I(\omega) = \frac{V\omega^2}{[(\omega^2 - \omega_r^2)^2 + 4\eta^2\omega^2]^{1/2}} \qquad \ldots (3.8)$$

where V = static magnification

ω_r = natural frequency of seismograph

η = fractional damping

3.3 Source Spectral Function

The shape of the spectrum of recorded ground motion is greatly influenced by the spectral content of source time function, form of the rupture process (unilateral, bilateral or circular rupture), velocity of rupture propagation and finiteness of seismic source. In the convolution model used by Boore (1983), a point earthquake source was used and details of the rupture process were omitted. In the present work the finiteness of the earthquake source has been considered. The spectrum of source time function S(ω) has been so defined that it includes the effect of finiteness of the source.

S(ω) is defined as

$$S_o(\omega) = \left(-i\omega/\tau_c\right) F(\omega) \frac{\sin X_c}{X_c} \exp\left[i\left(\frac{\omega r_o}{c} + X_c\right)\right] \qquad \ldots (3.9)$$

$$where \quad X_c = \frac{\omega L}{2}\left(\frac{1}{v} - \frac{\cos\psi}{c}\right)$$

$f(\omega)$ = spectrum of the source time function.

ν = rupture velocity

L = length of the fault rupture

$\tau_c = \frac{L}{c}\left(\frac{c}{\nu} - \cos\psi\right)$

(r_o, ψ) = as defined in Fig. 3.1

The above form of source spectral function takes into account source finiteness, the travel time r_o/c from radiating point to the source and the fact that in the far field the displacement is proportional to time derivative of the source time function f(t).

The equation (3.2) for $Y(\omega)$ can now be written in a modified form

$$Y(\omega) = \frac{M_o}{4\pi\rho r_o}\left[\left\{\frac{R^P F_s^P}{\alpha^3 \tau_\alpha}\frac{\sin X_\alpha}{X_\alpha}\exp\left(-a_\alpha r_o + i\left(\frac{\omega r_o}{\alpha} + X_\alpha\right)\right)\right\} + \left\{\frac{R^{SV} F_s^{SV} + 2R^{SH}}{\beta^3 \tau_\beta}\frac{\sin X_\beta}{X_\beta}\exp\left(-a_\alpha r_o + i\left(\frac{\omega r_o}{\beta} + X_\beta\right)\right)\right\}\right] X$$

$$(-i\omega\, F(\omega)).\ P(\omega,\omega_m).\ I(\omega) \qquad \ldots\ (3.10)$$

The fault plane is divided into a number of elementary faults or sub-faults. The dimension of each sub-fault is so chosen that the observation point is effectively in the far-field, in order to use the above formulation that is valid only in the far field. The observation point will be effectively in the far field if the distance between the nearest radiating point on the fault and the observation point is several times the dimension of the sub-fault.

3.4 Synthetic Accelerograms in Garhwal Himalayas

The theoretical basis of computing synthetic accelerograms has been discussed above. Now the computational procedure has been discussed and presented to generate the synthetic accelerograms.

3.4.1 Seismotectonic Setup of Garhwal Himalayas

The Garhwal Himalaya falls in the main Himalayan Seismic Zone. This region forms part of the boundary between the colliding Indian and the Eurasian Plates. The region is characterised by three major northward dipping thrust zones separated by geological/ physiographic sub-provinces. The northern most province is the greater Himalaya which has an average elevation of 5 km and is composed of crystalline metamorphic and igneous rocks brought up along the Main central Thrust (MCT). The sedimentary rocks in the south, which are mostly of Paleozoic age, define the Lesser Himalaya sub-province, which is delimited by the Main Boundary Thrust (MBT) to its south (Valdiya, 1988). The average elevation in this part is 2.5 km. These slightly metamorphosed sediments are overlain, in places, by a thrust sheet of the crystalline rocks. South of MBT lies Outer Himalaya or Sub-Himalaya region with average elevation of a few hundred meters. This zone consists of folded and faulted Siwalik mollase sediments of Miocene age.

In a widely accepted tectonic model (Seeber at.al., 1981), a detachment of fault represents the top surface of the northward underthrusting Indian plate over which the wedges of Himalayan rock units are thrusted southwards. The detachment fault represents a decollement

dipping gently less than 10° below the Outer and Lesser Himalaya at depth about 15-20 km. The local seismic activity in this region is largely concentrated in a relatively narrow belt, close to and primarily south of the surface trace of MCT. Most earthquakes are located between part of Lesser Himalaya and immediate south of Higher Himalaya extending from Nepal through Kumaun and Garhwal and Western Himachal Pradesh. The tectonic features of the Garhwal region are shown in Fig. 3.2.

3.4.2 Velocity Model

Two layer P velocity model has been based on result of micro earthquake investigations (Khattri, 1992). According to this model the P wave velocity in the top layer is 5.2 km/sec and that in the second layer, 6.0 km/sec. The top later is 16 km thick. The density of half space is chosen to be 2700 kg/m^3. These velocities correspond to a material with Poisson's ratio of 0.25 which signifies that half space is made up of well consolidated rocks.

3.4.3 Source Model

For the purpose of generating synthetic accelerograms, a source model has to be specified. This includes spatio-temporal parameters of earthquake focus, fault geometry (dip and strike of the fault), slip distribution over the fault plane and source time geometry. For the sake of simplicity source is supposed to be a rectangular fault buried in a homogeneous half space.

3.4.4 The Source Time Function

For the purposes of present study a ramp function with rounded shoulders is chosen as the source time function. The formula for the same is given below (Ben-Menahem and Singh, 1981):

$$f(t) = \begin{cases} 0 & , \quad t \le 0 \\ (t/T_o)(1 - \sin \omega_o t / \omega_o t) & , \quad 0 \le t \le T_o \\ 1 & , \quad t \ge T_o \end{cases} \qquad \ldots (3.11)$$

where T_o. is the rise time and $\omega_o = 2\pi/T_o$. This function is continuous everywhere and is easily differentiable. The above form is chosen to model slip as a function of time at a point on the fault. The velocity and acceleration pulses emanating from the source are given below

$$v(t) = (1/T_o)(1 - \cos\omega_o t), \qquad 0 \le t \le T_o \qquad \ldots (3.12)$$

$$a(t) = (\omega_o / T_o) \sin\omega_o t, \qquad 0 \le t \le T_o \qquad \ldots (3.13)$$

The three wave functions f(t), v(t) and a(t) are shown in Fig 3.3 for T_o = 0.25 sec and sampling interval of 0.02 sec, the same as for recorded accelerograms. In Fig. 3.4, the amplitude spectra of these functions are also shown. This type of source time function has been used by Ben-Menahem and Singh (1981) for generating synthetic accelerograms.

3.4.5 Source Size

For generating synthetic accelerograms in the near field, the size of the source i.e. the fault plane, has to be specified. The following method was followed.

Firstly, an estimate of the length of the fault was obtained. For this the following relation was used (Kasahara,1981):

$$\log L_m = 3.2 + 0.5\ M \qquad \ldots (3.14)$$

where L_m is in cm and denotes the upper limit of the fault length for a given magnitude M. M is the surface wave magnitude. Using the following M_b - M (body wave - surface wave magnitude) relationship given by Richter (1958)

$$M = 1.59\ M_b - 3.97 \qquad \ldots (3.15)$$

the above relation can also be rewritten as

$$\log L_m = 1.215 + 0.795\ M_b \qquad \ldots (3.16)$$

3.4.6 Slip Distribution over the Fault Plane

For the purpose of generating synthetic accelerograms, the whole fault has been considered to be made of a number of sub-faults each of size 1 km x 1 km. To properly model the ground acceleration at the recording site which is nearby to the epicentre, the slip distribution over the fault plane should be specified. In the present work the slip is assumed to be distributed randomly. For such a slip distribution a set of random numbers has been generated with mean zero and standard deviation unity. The average slip over the fault has been calculated or estimated separately. A suitable value was selected for standard deviation of slip over the fault. So the set of random numbers was converted into another set of random numbers with mean equal to the average slip and suitably distributed over the fault plane. Many such distributions are possible having the same mean. The objective was to model the

chaotic nature of fault slip in an approximate manner. The direction of slip was however kept constant all over the fault plane.

3.4.7 Choice of Coordinate System

Global

The coordinates of epicenter and stations locations are available in terms of their latitudes and longitudes. These were converted into Cartesians coordinates x_1 and x_2 with epicenter as origin, x_1 positive towards north and x_2 positive towards east. The third coordinates x_3 was taken positive downwards. All the stations were considered to be situated on the same elevation as the epicentre (above sea level) and the difference between their elevations was ignored. Following formula given by Lee and Stewart (1981) were used to obtain coordinates of stations on x_1 - x_2 plane.

$$x_1 = 60\ A\ (\lambda - \lambda_o) \qquad \ldots (3.17)$$

$$x_2 = 60\ B\ (\phi - \phi_o) \qquad \ldots (3.18)$$

where λ and ϕ are the longitude and latitude of the station and λ_o and ϕ_o are the longitude and latitude of the epicentre in the equations (3.17) and (3.18) respectively. The values for A and B in these equations are obtained as given below:

$$A \approx 1.8553654 + 0.0062792 \sin^2 \Phi + 0.0000319 \sin^4 \Phi \qquad \ldots (3.19)$$

$$A \approx 1.8428071 + 0.0187098 \sin^2 \Phi + 0.0001583 \sin^4 \Phi \qquad \ldots (3.20)$$

where $\Phi = \frac{1}{2} (\phi + \phi_o)$

Local

A local (i.e.fault based) coordinate system (y_1, y_2 y_3) was chosen in the following manner. The focus which lies on the foot-wall side of the fault, is chosen as the origin. A line on the fault plane parallel to strike of the fault is chosen as the y_1-axis with y_2-axis in the up dip direction and perpendicular to the y_1-axis. The y_3-axis is chosen perpendicular to the fault plane and penetrating the hanging wall. Fig. 3.5 shows the global and local coordinate systems on a fault with ϕ_s as strike angle and δ as the angle of dip. The seismic ray makes an angle i_o at the focus. The line joining the origin to the recording station makes an angle ϕ with the x_1-axis.

Let (y_1, y_2, 0) be the location of a point on the fault plane. The following relations convert these local coordinates (y_1, y_2, 0) to global coordinates (x_1, x_2, 0)

$$x_1 = y_1 \cos \phi_s - y_2 \sin \phi_s \cos \delta \quad \ldots (3.21)$$

$$x_2 = y_1 \sin \phi_s - y_2 \cos \phi_s \cos \delta \quad \ldots (3.22)$$

$$x_3 = y_1 \sin \delta + h \quad \ldots (3.23)$$

where ϕ_s is the strike, δ is the dip and h is the depth of focus.

3.4.8 Rotation of the Axes

The horizontal components of the generated synthetic accelerograms are in the north and east directions which are also the directions of x_1 - and x_2 - axes respectively of the global coordinate system. The horizontal components of the recorded accelerograms are not in these directions. These have been termed longitudinal (L) and transverse (T)

components, the directions of which vary from station to station as given in Table 3.2 and 3.3. For the purpose of comparison, the synthetic accelerograms were rotated so that the rotated components lie in the L and T directions for the given recording station. The following relations have been used for rotation from x_1 and x_2 directions to L and T directions:

$$u_L = u_{x1} \cos \phi_r - u_{x2} \sin \phi_r \quad \ldots (3.24)$$

$$u_T = u_{x1} \sin\phi_r + u_{x2} \cos \phi_r \quad \ldots (3.25)$$

Where ϕ_r is the angle which the L component makes with the north measured clockwise, u_{x1} and u_{x2} are horizontal components of the synthetic accelerograms and u_L and u_T are those of the recorded data by L for longitudinal and T for transverse respectively.

3.4.9 Generation of Gaussian Random Noise

To generate a Gaussian random noise, a random number seed is needed initially. An approximation to a normally distributed or Gaussian random sequence can be obtained by summing uniformly distributed random numbers with mean zero and variance one (Stearns and david (1988). The final random series obtained is normalised against its peak value. A number of seeds are specified to generate number of random series and the resulted series was finally used after summed and averaged.

3.4.10 Source Parameters for Uttarkashi & Chamoli Earthquakes

For the purpose of applying the proposed method for generating synthetic accelerograms, two earthquake events are selected which were recorded at number of recording station in Uttaranchal region (as

discussed in detail in Chapter 2). These earthquakes are the Uttarkashi earthquake of October 20, 1991 and Chamoli earthquake of March 29, 1999. A short account of relevant features of these two earthquakes are given below:

Uttarkashi Earthquake

The **Uttarkashi earthquake** occurred on October 20, 1991 at 02:53 (IST) in the Uttarkashi region in the northwestern Himalayas. The focal mechanism solution is given in Table 3.1. The centroid Moment Tensor focal mechanism solution by Harvard University (PDE, Monthly, Oct. 1991) has been chosen in this study as the initial model. The fault plane chosen for modelling strong ground motion is the one having parameters corresponding to NP1 as given in Fig. 3.6. Fig. 3.7 shows the fault in vertical section parallel to strike of the fault along with the two layer P velocity model obtained as described above. The fault plane lies entirely in the top layer. Fig. 3.8 shows a three dimensional view of the fault plane.

Chamoli Earthquake

Chamoli earthquake occurred on March 29, 1999 at 03:55 hrs (IST) north of Chamoli in Lesser Himalayas. The focal mechanism solution is given in Table 3.1. Fig. 3.9 shows the fault in vertical section parallel to strike of the fault.

The hypocentral distance and other parameters for some of the recording stations are given in Table 3.2 and 3.3 for both the earthquakes. The fault plane lies entirely in the top layer for this earthquake event also same as in the case of Uttarkashi earthquake. Fig. 3.10 shows a three dimensional view of the fault plane.

The body wave magnitude for the Uttarkashi earthquake has been given as 5.5 M_b, which gave an estimate of fault length as 24.13 km using equation (3.16). Accordingly a value of 24 km was chosen as the length of the fault. Since the fault is found to be dipping at a low angle (14^o). Accordingly the causative fault is taken to be 24 km long and 16 km wide. In this way the size of the causative fault has been obtained. Similarly, the fault size for Chamoli earthquake has been taken as 36 km long and 20 km wide. The amount of dislocation was adjusted with estimates of the length and width of causative fault in such a way that correct value of seismic moment is obtained. Source parameters for both the earthquakes are given in Table 3.4.

3.4.11Computational Procedure

To generate the synthetic accelerograms, a number of numerical experiments were conducted to arrive at the optimum values of some key parameters which greatly affect the arrival times and phases of recorded pulses. These source parameters are rise time (T_o), rupture velocity (ν), slip angle (λ) and focal depth h. Three rupture models were used, namely, unilateral, bilateral and circular rupture. Finally it was found that circular rupture gives most satisfactory results.

The slip distribution patterns are given in Figs. 3.11 and 3.12 for Uttarkashi and Chamoli earthquakes. The slip angle is kept same in each sub-fault. The inverse of quality factor Q versus frequency is shown in Fig. 3.13 as given by equation (3.5).

As discussed earlier that a rectangular fault has been taken and divided into number of sub-faults. To determine the duration of strong ground

motion at the recording site, P and S-wave travel times were computed from each of the four corners of the fault. The largest S - wave travel time and the smallest P-wave travel time were selected. The travel time of P-wave directly from the focus was also computed which is smallest. If the smallest P travel time from any of the corners of the fault happened to be smaller than that directly from focus, that time was taken as the smallest P-wave travel time.

Amplitude spectrum of ground acceleration as shown in Fig. 3.14, is then calculated by summing contribution from each sub-fault. It takes into account slip distribution (assumed random) on the fault plane, slip angle (assumed constant all over the fault), finiteness of the source, diminution factor and instrument response.

This spectrum is then multiplied by the spectrum of Gaussian white noise to give the spectrum shown in Fig. 3.15. This is inverse Fourier transformed to yield the time history shown in Fig. 3.16. This represents the synthetic accelerogram as if each point on the fault had radiated an impulse. Convoluting this with source time function shown in Fig. 3.17 (the acceleration pulse) yields the final synthetic accelerogram shown in Fig. 3.18(b). This procedure is repeated for every site where synthetic accelerogram has been generated.

Table 3.1 : Focal mechanism of Uttarkashi and Chamoli earthquakes

Sl. No	Source	Focal Mechanism	Size (M_o) (dyne-cm.)
1.		**Uttarkashi Earthquake**	
	CMT (Harvard)	Centroid Moment Tensor Solution NP1 : strike 317°, dip 14°, slip 115° NP2 : strike 112°, dip 78°, slip 84°	1.8×10^{26}
2.		**Chamoli Earthquake**	
		NP1 : strike 274°, dip 8°, slip 100°	1.8×10^{26}

M_o : Seismic moment

Table 3.2 : Details of the selected stations for Uttarkashi earthquake

Sl. No.	Station	Station Coordinates	Epicentral Distance (Δ) (km)	Components
1.	Almora	29.58° N 79.65° E	162.30	L N53W T N37E
2.	Barkot	30.80° N 78.22° E	61.55	L N10E T N80W
3.	Bhatwari	30.80° N 78.60° E	19.40	L N85E T N05W
5.	Karnprayag	30.25° N 79.23° E	77.75	L N05W T N85E
6.	Koteshwar	30.23° N 78.57° E	65.03	L N30W T N60E
7.	Purola	30.87° N 78.08° E	77.78	L N65W T N25E
8.	Tehri	30.36° N 78.50° E	55.61	L N63W T N27E
9.	Uttarkashi	30.73° N 78.45° E	36.41	L N15W T N75E

Δ : Epicentral distance, L : Longitudinal, T : Transverse

Table 3.3 : Details of the selected stations For Chamoli earthquake

Sl. No.	Station	Station Coordinates	Epicentral Distance Δ (km)	Components
1.	Almora	29.58° N 79.65° E	94.44	L N53W T N37E
2.	Barkot	30.80° N 78.22° E	141.58	L N10E T N80W
3.	Gopeshwar	30.25° N 79.23° E	27.92	L N70W T N20E
4.	Ukhimath	30.50° N 79.01° E	46.76	L N15E T N75W
5.	Tehri	30.36° N 78.50° E	102.65	L N63W T N27E

Δ : Epicentral distance, L : Longitudinal, T : Transverse

Table 3.4 : Source parameters for Uttarkashi and Chamoli earthquake

Sl. No.	Parameter	Value	
		Uttarkashi	Chamoli
1	Length of the Fault	24 km	36 km
2	Width of the Fault	16 km	20 km
3	Focal Depth	10 km	15 km
3	Dip of the Fault	14°	8°
4	Strike of the Fault	317° N	274° N
5	Rise Time	0.25 sec	0.25 sec
6	Rupture Velocity	2.30 km/sec	2.50 km/sec
7	P-wave velocity	5.2 km/sec	5.2 km/sec
8	S-wave velocity	3.0 km/sec	3.0 km/sec
9	Slip Angle	115°	100°
10	Rupture Model	Circular Rupture	Circular Rupture
11	Source Time Function	Modulated Ramp	Modulated Ramp
12	Average Slip	80 cm	75 cm
13	Maximum Slip	170 cm	160 cm
14	Natural Freq. of Instrument	25 Hz	25 Hz
15	Damping Constant	0.70	0.70

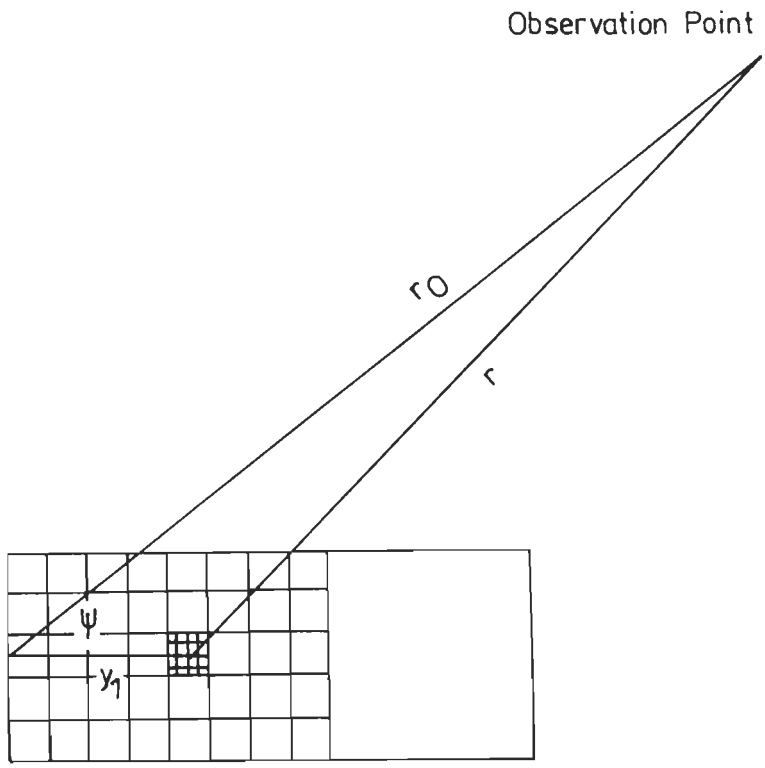

Fig. 3.1 : ψ is the angle between the direction to the receiver and the direction of rupture propagation and r is the hypocentral distance

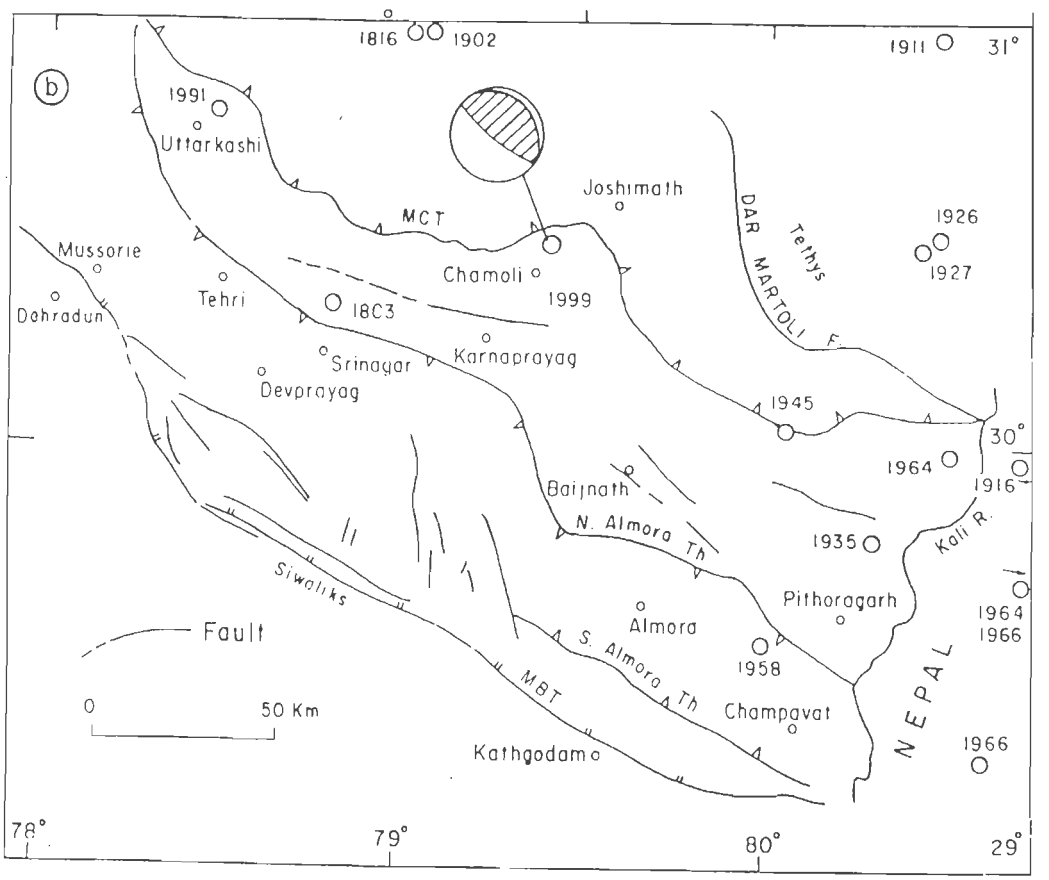

Fig. 3.2 : Tectonic features of the Garhwal Himalayan region (after Kumar, 1981)

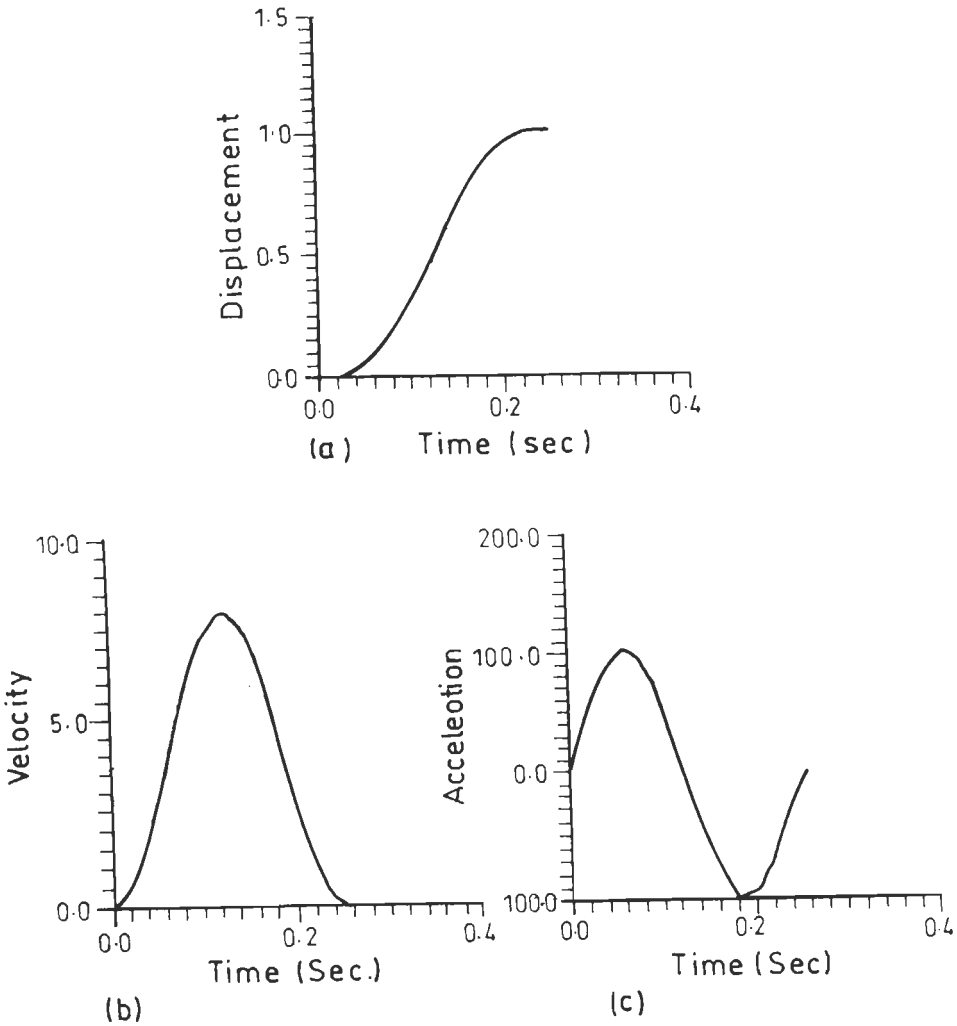

Fig. 3.3 : Source time function (a) slip displacement (b) slip velocity (c) slip acceleration

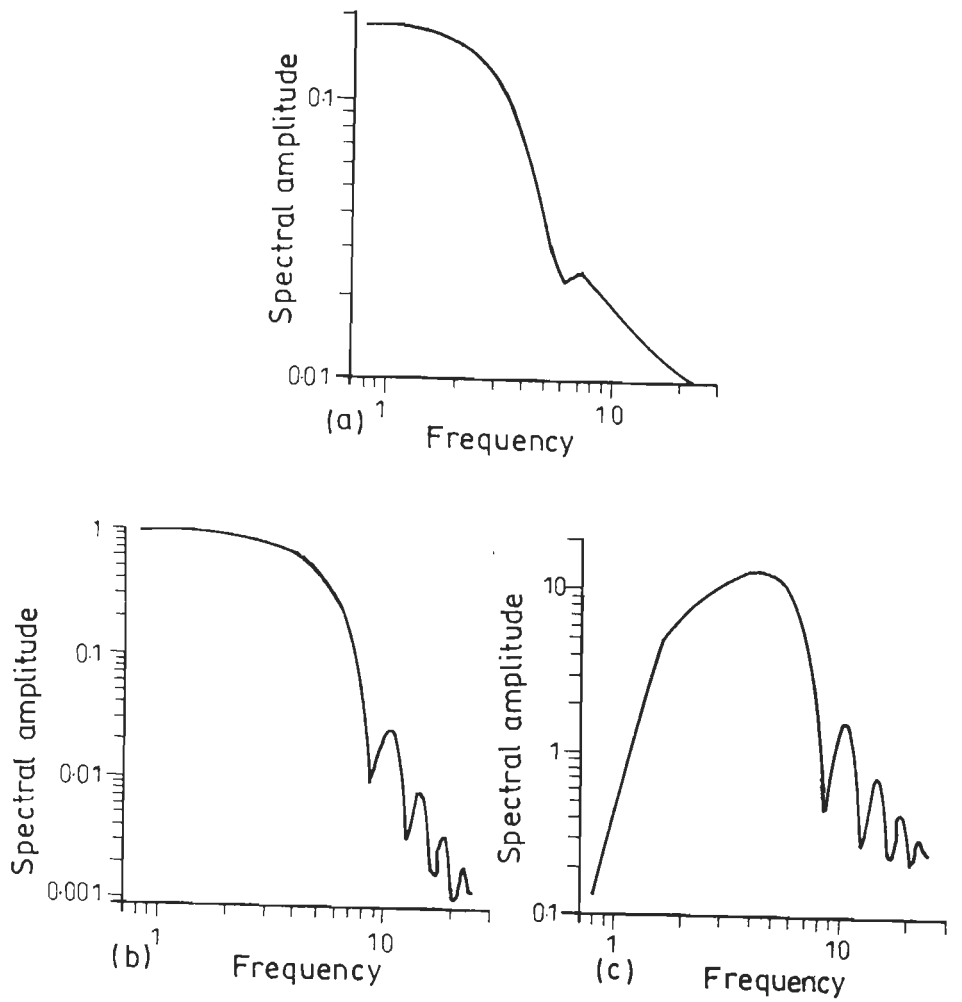

Fig. 3.4 : Spectrum of source time function (a) slip displacement spectrum (b) slip velocity spectrum (c) slip acceleration spectrum

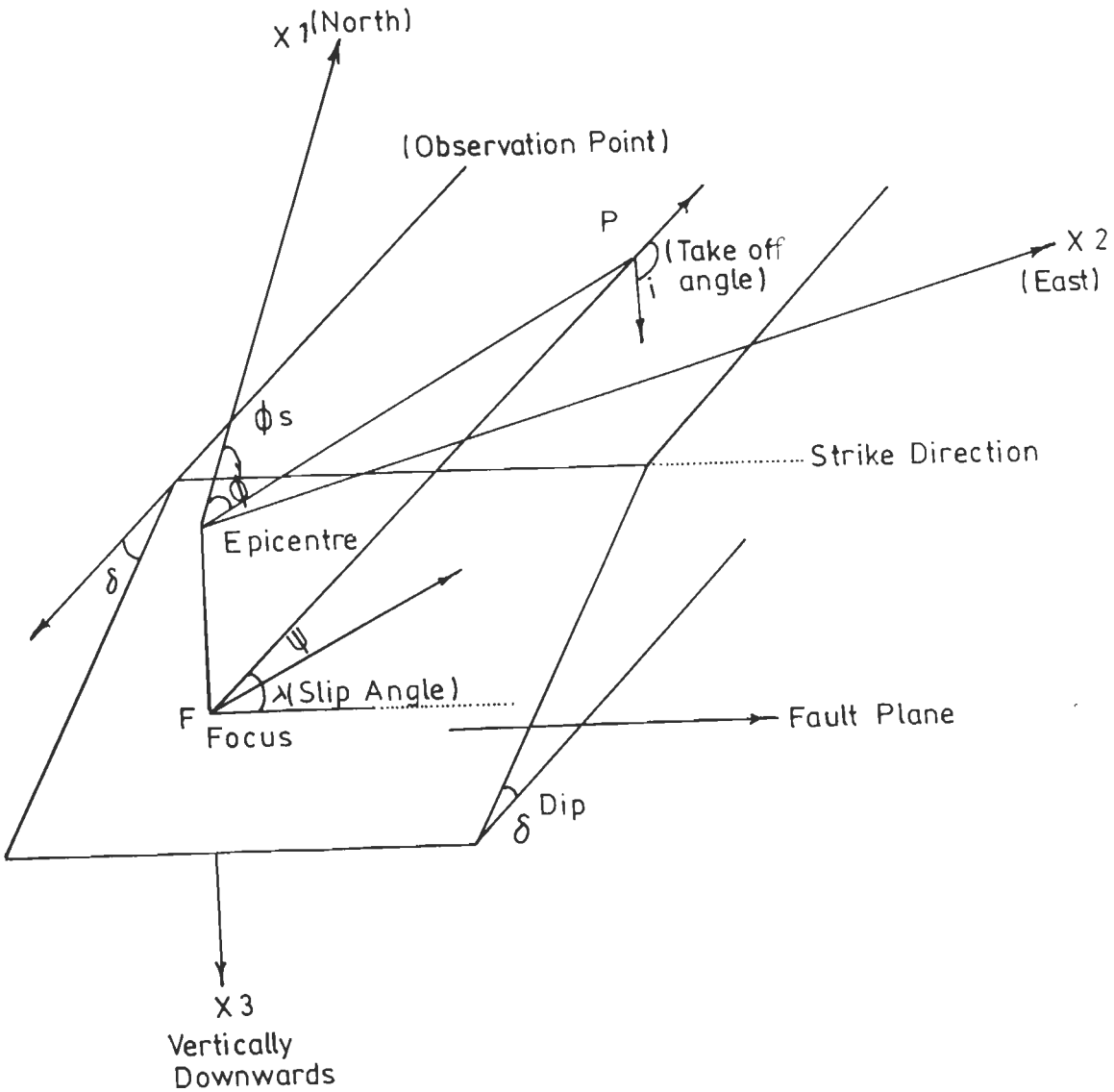

Fig. 3.5 : Global and local coordinate systems ϕ_s : strike, δ : dip, λ : slip angle, i_o : take off angle, ϕ : azimuth of recording station, Δ : epicentral distance E : epicentre and ν : fault normal

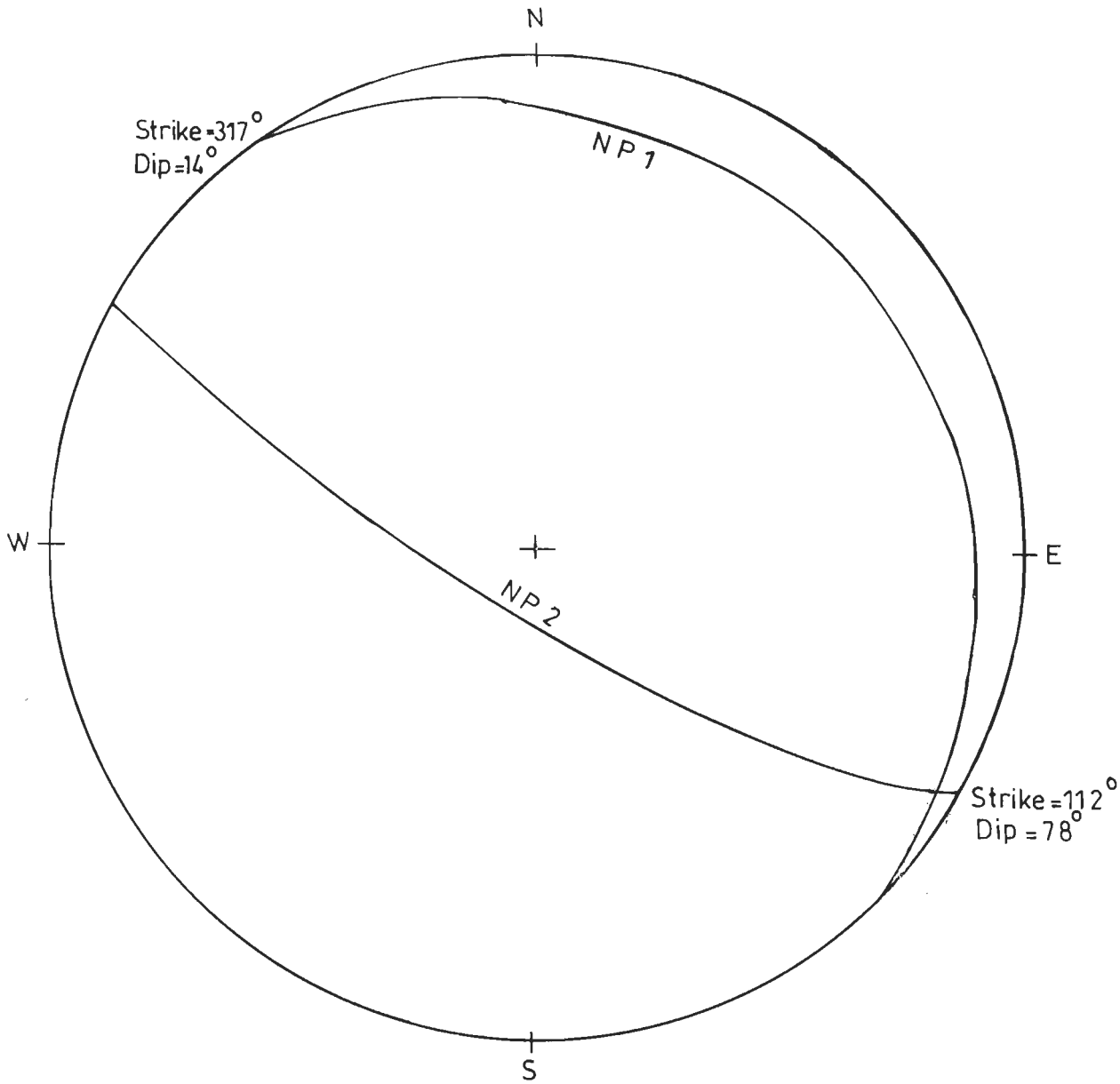

Fig. 3.6 : Fault plane solution, NP1 : strike 317°, dip 14°, NP2 : strike 112°, dip 78°, for Uttrakashi, 1991 earthquake, as used in this study.

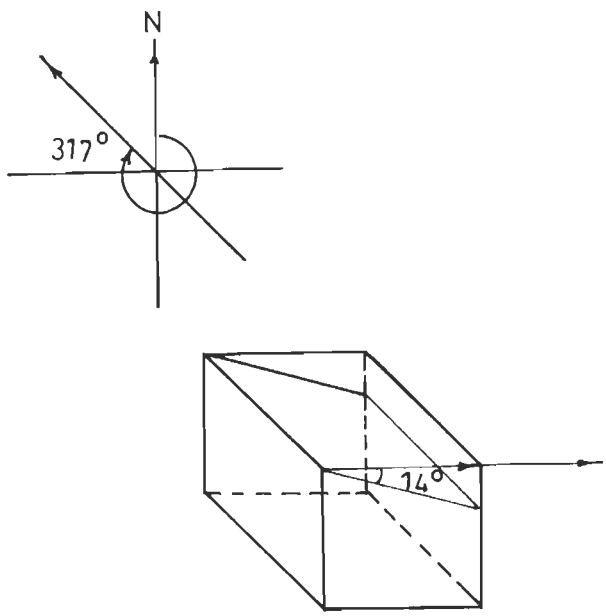

Fig. 3.7 : Vertical section perpendicular to the strike of the Fault showing that the fault lies in the first layer (Uttarkashi earthquake)

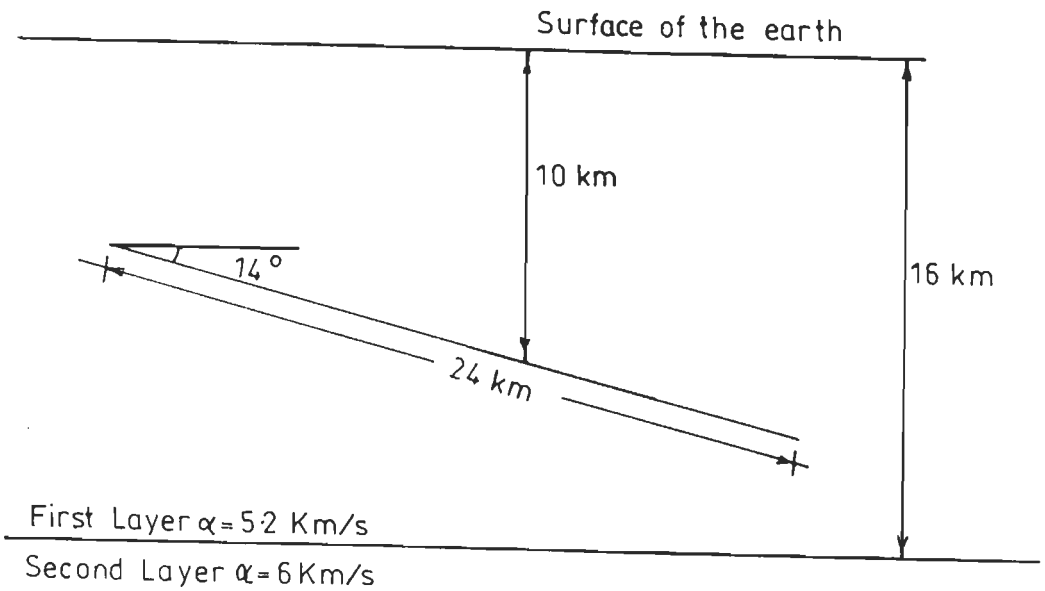

Fig. 3.8 : Strike of the fault plane and dip in three dimensional view (Uttarkashi earthquake)

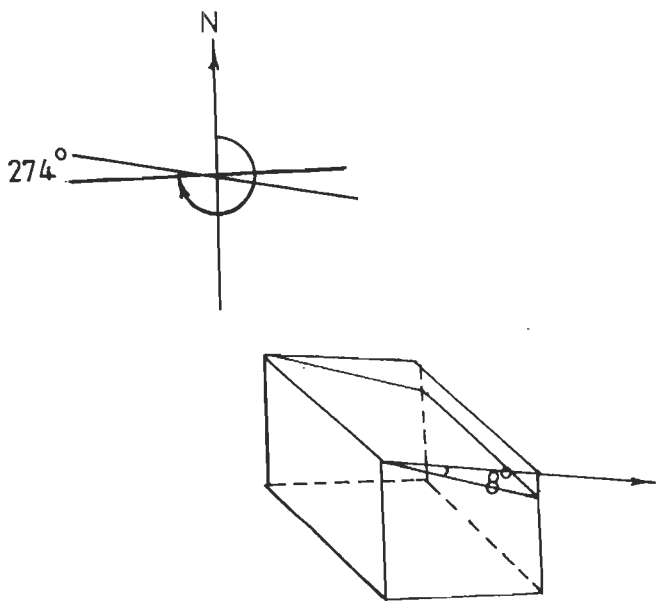

Fig. 3.9 : Vertical section perpendicular to the strike of the fault showing that the fault lies in the first layer (Chamoli earthquake)

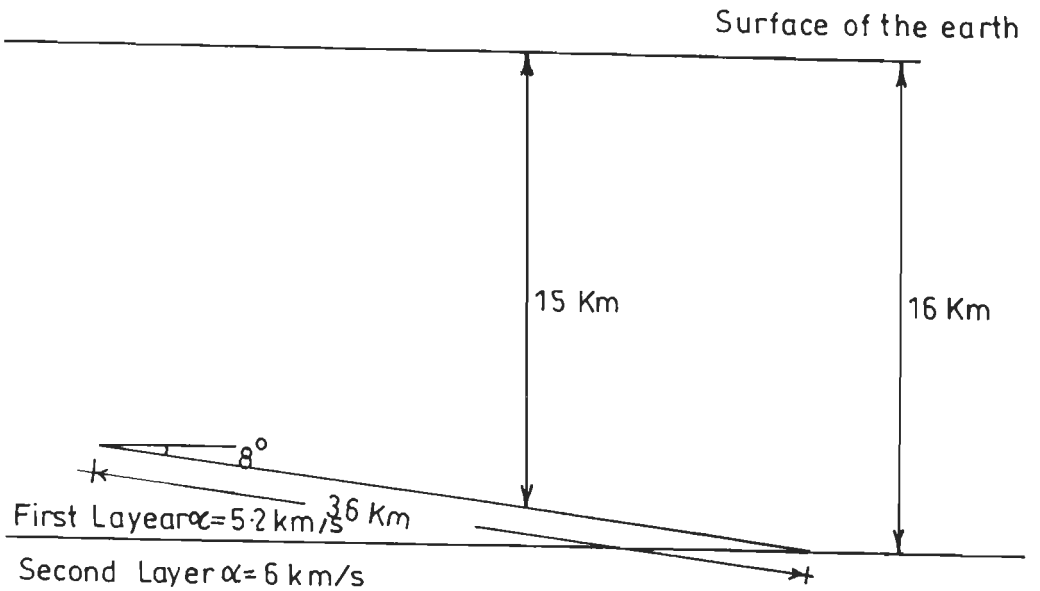

Fig. 3.10 : Strike of the fault plane and dip in three dimensional view (Chamoli earthquake)

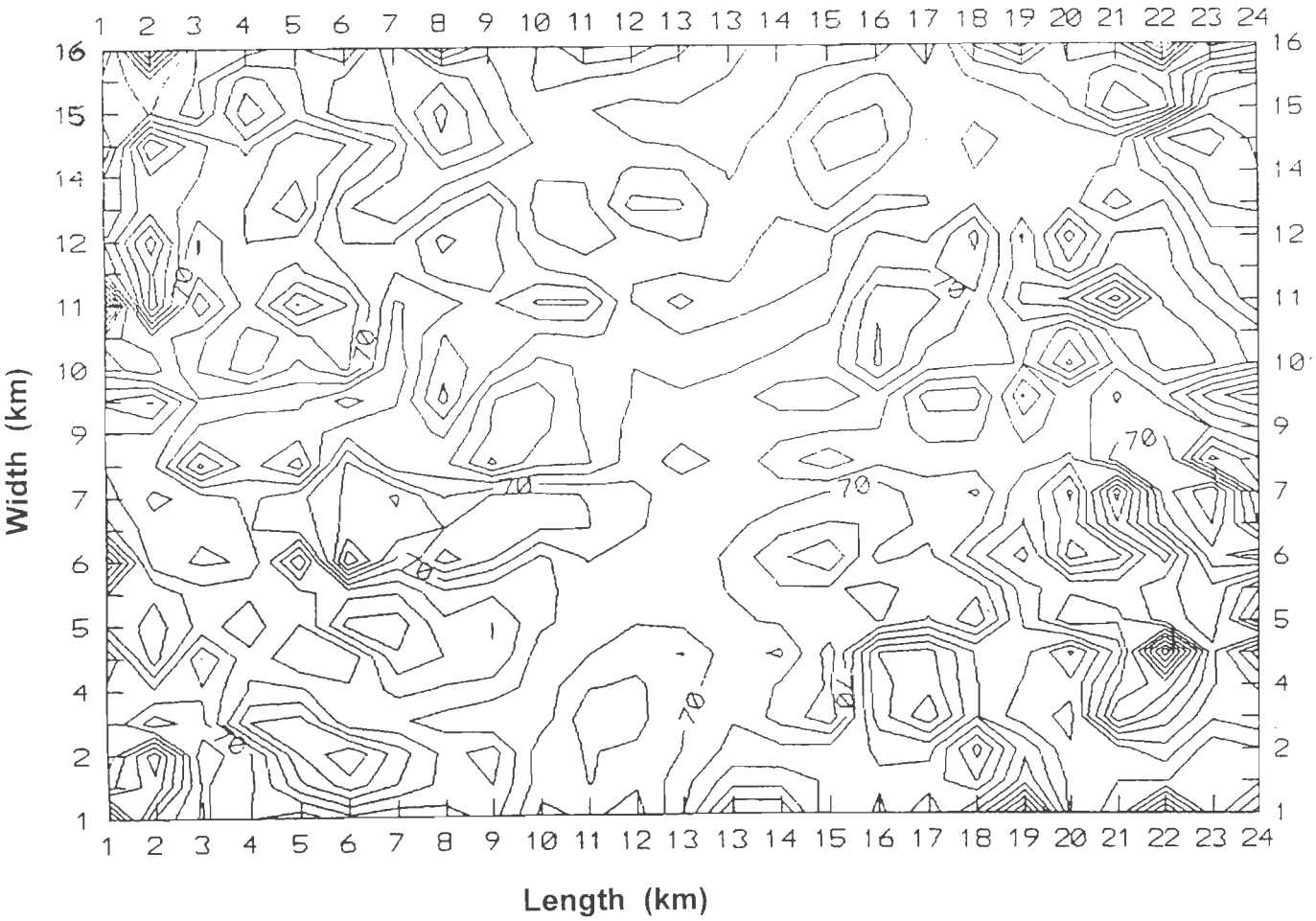

Fig.3.11 : Slip distribution pattern over the fault plane for Uttarkashi earthquake

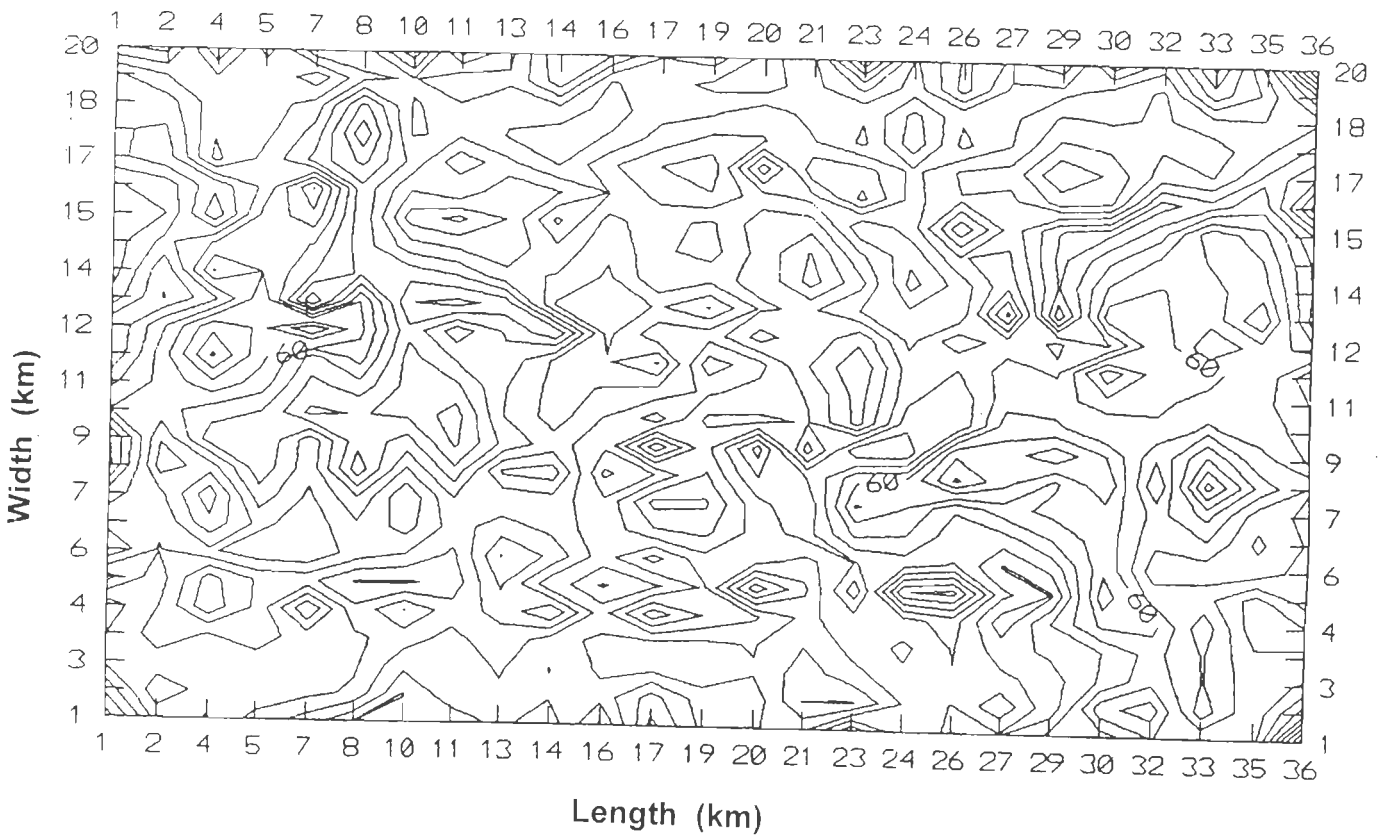

Fig.3.12 : Slip distribution pattern over the fault plane for Chamoli earthquake

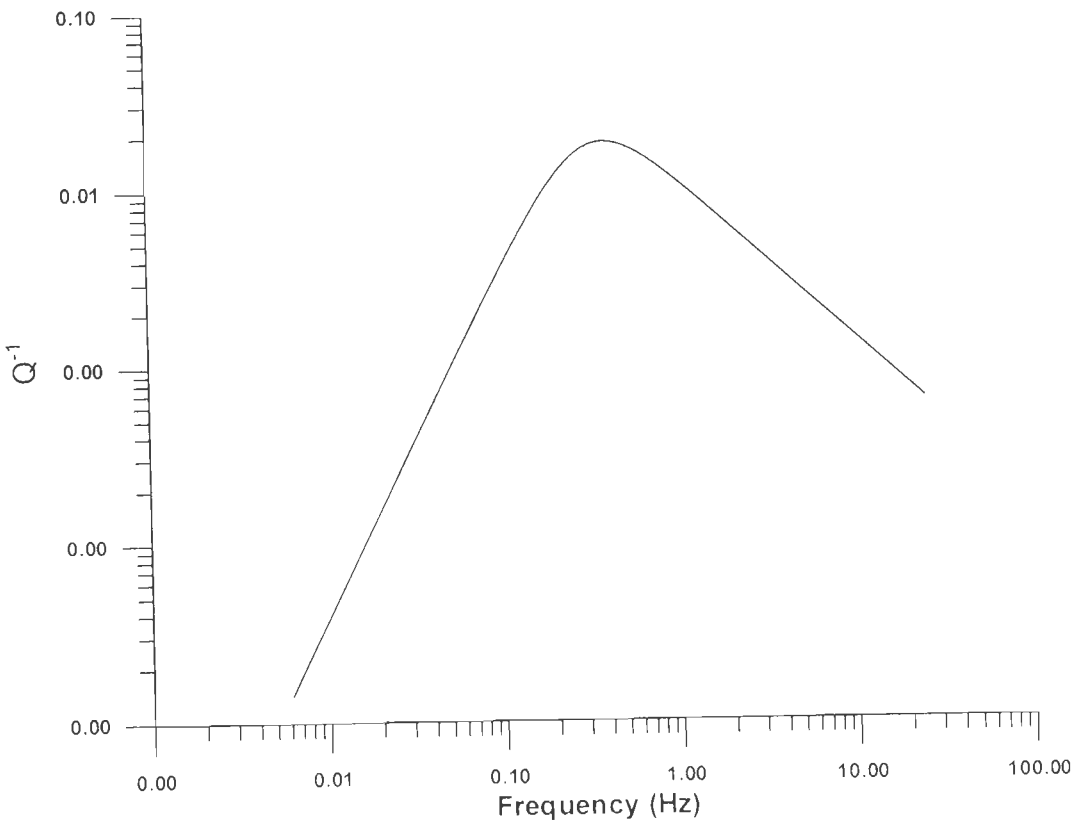

Fig. 3.13 : Observed inverse Q versus frequency (Boore, 1987)

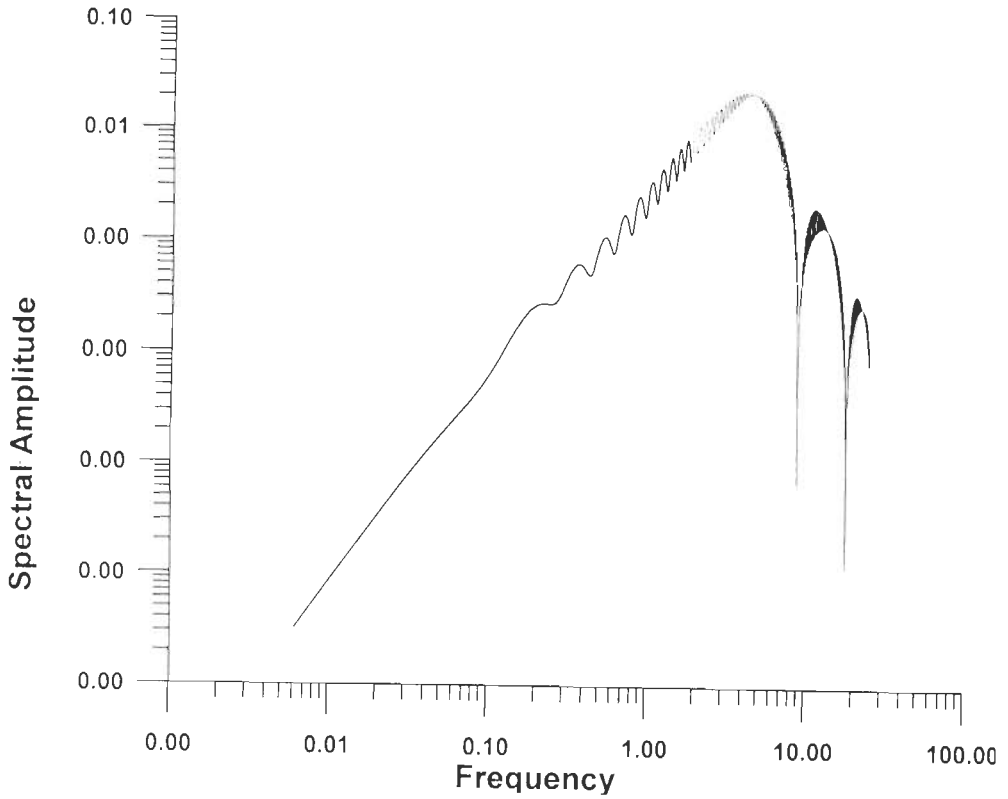

Fig. 3.14 : Amplitude spectrum of ground acceleration

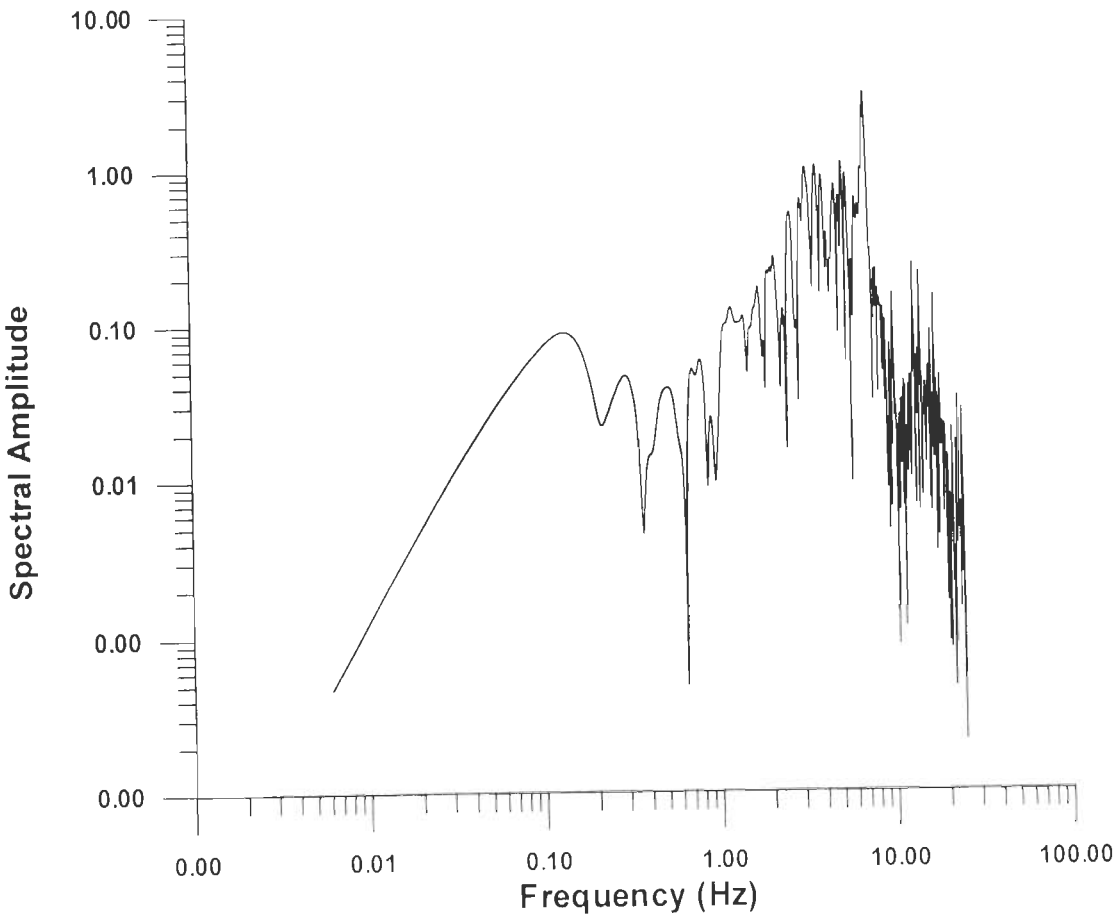

Fig. 3.15 : Amplitude spectrum of ground acceleration
Including random behaviour

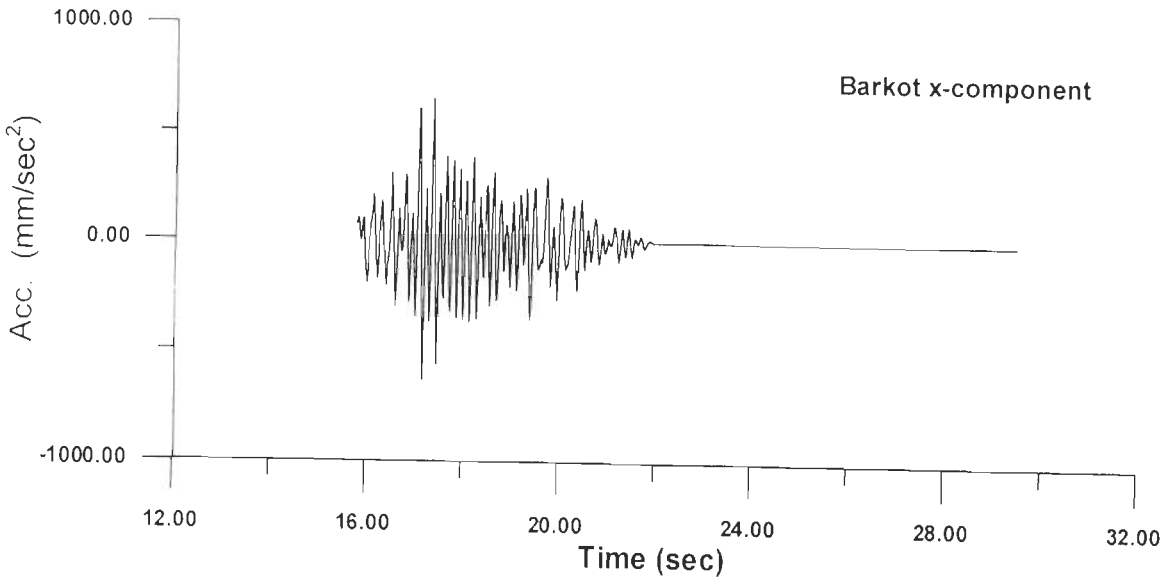

Fig. 3.16 : Ground acceleration when each point on the fault radiates an impulse

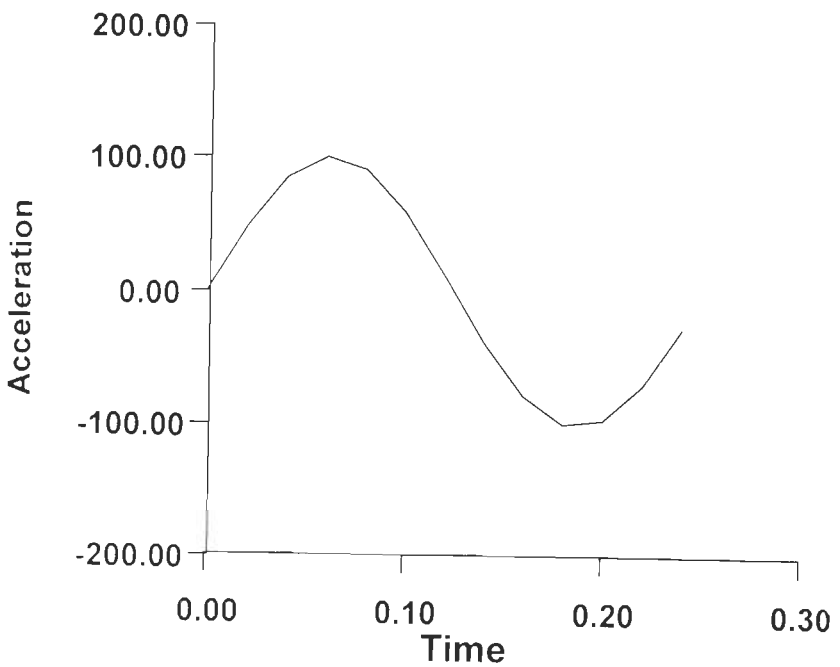

Fig. 3.17 : Acceleration pulse emanating from source

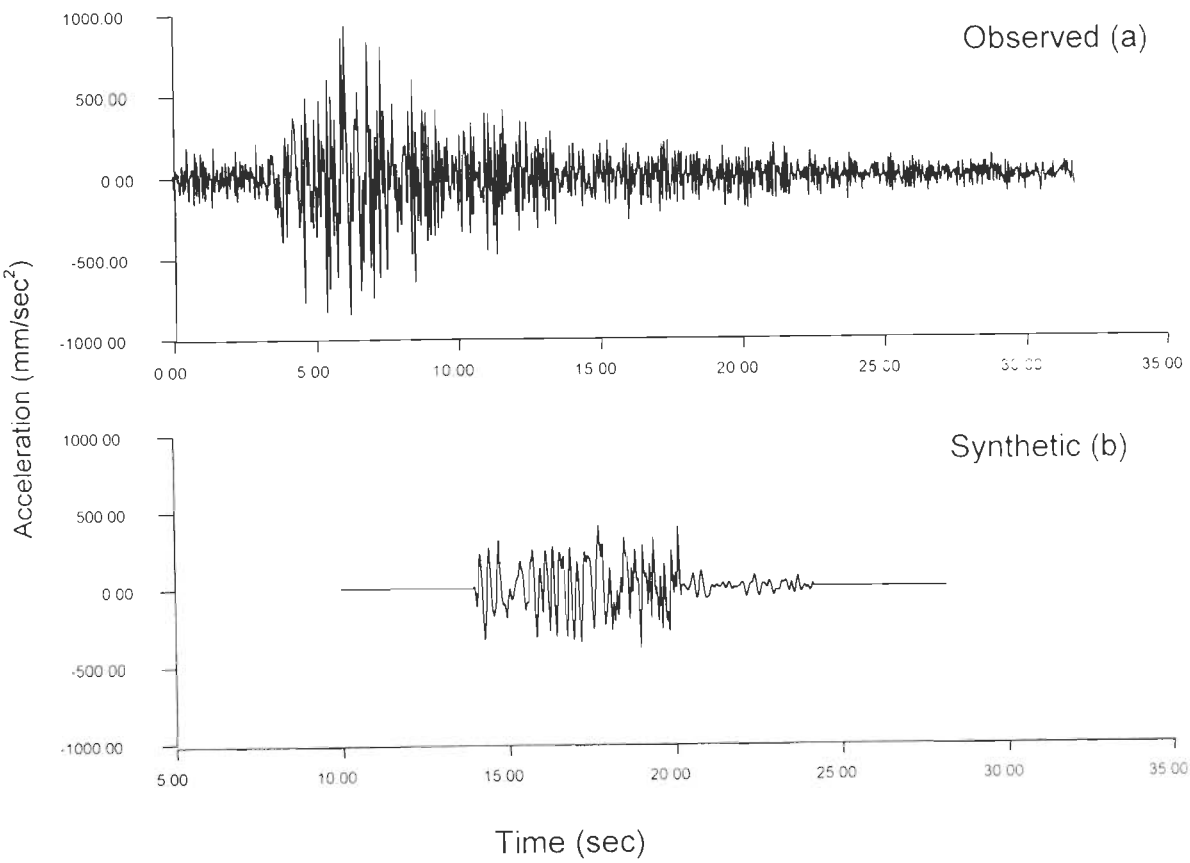

Fig. 3.18 : Observed and Synthetic Accelerograms for N10E component at Barkot (Uttarkashi Earthquake)

CHAPTER 4

Results and Discussion - Synthetic Accelerograms

4.1 Introduction

Following the method described in the last chapter strong motion accelerograms have been synthesized at eight selected sites which recorded the Uttarkashi, 1991 earthquake and at five sites for Chamoli, 1999 earthquake. The locations of these recording sites alongwith the epicentre of the earthquake have been shown in Figs. 2.3 and 2.4.

The objective of this exercise is to examine the usefulness of the proposed method in generating synthetic accelerograms. This has been done by comparing the synthetic accelerograms with the observed ones for two earthquakes in the Himalayan region.

The accelerographs which recorded the two Himalayan earthquakes were analog recording devices. The recording of strong ground motion data was done when these instruments were triggered by a strong pulse. In the case of these two earthquakes the instruments were ~~do~~ not seen to have triggered by the first P-wave. The later arriving S-waves are clearly seen on most records. The arrival of P and S waves in observed and synthetic accelerograms are given in Table 4.1 and 4.2 for both the earthquakes. It may have been due to the fact that the first P-wave was quite weak or the trigger level of instrument was some what higher. As a result the starting pulse on the observed accelerograms can not be taken to be the first P-arrival. This is borne out the computations carried out in the present study. It has been found that calculated S-P intervals match the hypocentral distances from known values of earthquake parameters, whereas the S-arrivals

on observed accelerograms occur at smaller intervals after the initiation of the record. Consequently the interval on the synthetic accelerograms before the arrival of S-waves is of longer duration than that of observed accelerograms.

4.2 Results and Discussion

Figs. 4.1(a) to (d) to Figs. 4.8(a) to (d) show the synthetic and observed accelerograms and the synthetic accelerograms superimposed over the observed ones for Uttarkashi, 1991 earthquake. Figs. 4.9(a) to (d) to Figs.4.13(a) to (d) show the synthetic and observed accelerograms and the synthetic accelerograms superimposed over the observed ones for Chamoli,1999 earthquake.

In Figs. 4.1(a) & (c) to Figs. 4.13(a) & (c) the synthetic accelerograms begin earlier than that the observed ones. Both the synthetic and observed accelerograms are plotted on the same time scale. The match between the two sets of accelerograms is quite good. The details of the superimposed accelerograms for observed over the synthetic one are given in Table 4.3 and 4.4 for both the earthquakes. The Figs. 4.1(b) & (d) to Figs. 4.13(b) & (d) showing the synthetic accelrograms over the observed ones show nearly complete matching of a number of peaks. The peaks which nearly match have been marked with an arrow. The amplitudes and shapes matched pulses do not agree entirely but their position on the accelerogram does. In order to determine the degree to which the two sets of accelerograms match, root mean square erros (rmse) have been determined over the portion on which the two sets of accelerograms have been superimposed. These errors in percentage (%) are given in Table 4.5 and 4.6. None of these exceed 20% and of the 26 sets of accelerograms compared,

15 have r.m.s. errors less than 10%. The differences in the two sets of accelerograms can be ascribed to following causes:

1. The effect of amplification of ground motion by near surface unconsolidated materials has not been taken into account. The earth model chosen for the present study is that of a uniform and homogeneous half space. In real earth there are number of inhomogeneties which lead to scattering of high frequency energy. Such scattering effects have been ignored.

2. The tail of the accelerogram consists of surface waves and back scattered waves. Such effects have not been taken into account.

3. In the Himalayan region effects of topography in the vicinity of recording station are likely to be important on recorded ground motion. The record of ground motion of a recording station located on the side or bottom of a valley will be influenced by the shape of the valley. These effects are not easy to predict and have not been considered in the present study.

4. The recorded accelerogram is influenced by closeness of the causative fault, its size, the pattern of slip distribution, the form of source time function, rise time, rupture velocity and model of rupture propagation (unilateral, bilateral, circular or other). The size of the fault can be estimated. However other properties of the source are not known in advance. To match the synthetic accelerograms with the observed ones, a set of values for the parameters are tried in a systematic manner before an acceptable match between synthetic and observed data is obtained. There are likely to be several possible combinations of these parameters which may give rise to an acceptable match. No unique set of values can, perhaps, ever be

determined because of the non-unique nature of geophysical inverse problems. There are likely to be some other parameters which are unknown but may be important. These factors that have not been accounted for in synthetic experiments will result in the mismatch between synthetic and observed data.

As stated earlier the objective of the present study is to determine the usefulness of a method of synthetic seismogram generation proposed herein. The synthetic accelerograms generated in the present study show a good match with the observed ones demonstrating the usefulness of the method of synthetic seismogram generation described in the present thesis.

4.3 Synthetic Accelerograms for a Hypothetical Earthquake

The Himalayan region is a highly active seismic region. To mitigate risk from future earthquakes all buildings especially the larger structures such as dams, should account for earthquake forces in their design. For this purpose a knowledge of probable time history of strong motion at the site of construction is a must. The method proposed in the present study has been used to generate accelerograms at a few selected sites produced by a hypothetical earthquakes of magnitude.7.0. The source region of this earthquake lies along the main central thrust near Rudraprayag as shown in Fig. 4.14. The epicentral location has been taken to be 30.50° N 79.00° E with a focal depth of 12 km. The other source parameters have been setup and listed in Table 4.5. The locations of six sites at which the synthetics have been are given in Table 4.8 and shown in Fig. 4.14.

The synthesized accelerograms for all the six sites are shown in Figs. 4.15 to 4.21 for one horizontal component. The peak ground

acceleration has the highest value of 405.72 cm/sec^2 at Rudrapyayag. The synthetic accelerograms can be taken to be a realistic depiction of the probable ground motion in the region and can be used for earthquake resistant design of important civil structures.

Table 4.1 : Arrivals of P and S waves in observed and synthetic accelerograms for Uttarkashi earthquake

Sl. No.	Station	Hypocentral Distance Δ (km)	Observed		Synthetic	
			t_p	t_s	t_p	t_s
1.	Almora	165.35	0.0	14.20	35.73	55.20
2.	Barkot	61.55	0.0	3.84	12.12	20.57
3.	Bhatwari	19.40	0.0	2.60	3.75	6.48
4.	Karnprayag	77.75	0.0	7.25	16.75	25.96
5.	Koteshwar	65.03	0.0	6.66	13.20	21.81
6.	Purola	77.78	0.0	4.26	16.77	26.00
7.	Tehri	55.61	0.0	5.82	11.21	18.54
8.	Uttarkashi	36.41	0.0	3.20	7.52	12.15

Table 4.2 : Arrivals of P and S waves in observed and synthetic accelerograms for Chamoli earthquake

Sl. No.	Station	Hypocentral Distance Δ (km.)	Observed		Synthetic	
			t_p	t_s	t_p	t_s
1.	Almora	96.33	0.0	9.18	19.42	32.13
2.	Barkot	142.85	0.0	11.52	28.81	47.62
3.	Gopeshwar	31.69	0.0	2.90	6.39	13.90
4.	Ukhimath	50.47	0.0	4.01	10.92	16.86
5.	Tehri	103.74	0.0	9.82	20.81	34.57

Table 4.3 : Details of the superimposed accelrograms for Uttarkashi, 1991 earthquake

Sl. No.	Station	Shown in Figures	Observed (s)		Synthetic (s)	
			from -	to	from -	to
1.	Almora	Figs. 4.1(b) & 4.1(d)	0.50	10.50	39.50	49.50
2.	Barkot	Figs. 4.2(b) & 4.2(d)	2.50	10.50	16.50	24.50
3.	Bhatwari	Figs. 4.3(b) & 4.3(d)	4.00	10.50	7.50	14.00
4.	Karnprayag	Figs. 4.4(b) & 4.4(d)	0.50	8.00	25.00	32.50
5.	Koteshwar	Figs. 4.5(b) & 4.5(d)	7.00	17.00	19.50	29.50
6.	Purola	Figs. 4.6(b) & 4.6(d)	2.50	10.50	18.00	26.50
7.	Tehri	Figs. 4.7(b) & 4.7(d)	5.50	14.50	16.00	25.00
8.	Uttarkashi	Figs. 4.8(b) & 4.8(d)	3.50	7.50	9.80	13.80

Table 4.4 : Details of the superimposed accelrograms for Chamoli, 1999 earthquake

Sl. No.	Station	Shown in Figures	Observed		Synthetic	
			from	to	from	to
1.	Almora	Figs. 4.9(b) & 4.9(d)	0.00	9.00	30.50	39.50
2.	Barkot	Figs. 4.10(b) & 4.10(d)	0.50	36.50	7.50	43.50
3.	Gopeshwar	Figs. 4.11(b) & 4.11(d)	3.00	9.00	8.00	14.00
4.	Ukhimath	Figs. 4.12(b) & 4.12(d)	0.00	16.50	4.00	20.50
5.	Tehri	Figs. 4.13(b) & 4.13(d)	0.00	30.50	6.00	36.50

Table 4.5 : RMS errors (%) for superimposed portion of the accelrograms for Uttarkashi, 1991 earthquake

Sl. No.	Station	Hypocentral Distance Δ (km)	L Component	T Component
1.	Almora	165.35	6.225312	2.961601
2.	Barkot	61.55	7.419318	7.870909
3.	Bhatwari	19.40	6.126514	11.370815
4.	Karnprayag	77.75	11.385312	8.063941
5.	Koteshwar	65.03	17.350282	10.035124
6.	Purola	77.78	8.958166	4.560196
7.	Tehri	55.61	19.729436	14.768013
8.	Uttarkashi	36.41	8.075476	8.309871

Table 4.6 : RMS errors (%) for superimposed portion of the accelrograms for Chamoli, 1999 earthquake

Sl. No.	Station	Hypocentral Distance Δ (km)	L Component	T Component
1.	Almora	96.33	15.043584	11.410245
2.	Barkot	142.85	11.380425	8.887654
3.	Gopeshwar	31.69	9.631586	8.526439
4.	Ukhimath	50.47	4.195476	5.648671
5.	Tehri	103.74	11.621656	14.921087

Table 4.7 : Source parameters of hypothetical earthquake of magnitude = 7.0

Sl. No.	Parameter	Value
1	Length of the Fault	60 km
2	Width of the Fault	16 km
3	Focal depth	12 km
3	Dip of the Fault	8°
4	Strike of the Fault	287° N
5	Rise Time	0.30 sec
6	Rupture Velocity	2.30 km/sec
7	Slip Angle	120°
8	Rupture Model	Circular Rupture
9	Source Time Function	Modulated Ramp
10	Average Slip	90 cm.
11	Maximum Slip	175 cm.

Table 4.8 : Details of the selected stations for hypothetical earthquake

Epicentral Location : 30.50° N 79.00° E

Sl. No.	Station	Station Coordinates	Epicentral Distance Δ (km.)	Components
1.	Bhatwari	30.80° N 78.60° E	55.61	L N85E T N05W
2.	Ghansali	30.42° N 78.65° E	40.25	L N00E T N90W
3.	Karnprayag	30.25° N 79.23° E	36.25	L N05W T N85E
4.	Rudraprayag	30.27° N 78.98° E	25.60	L N53E T N37W
5.	Tehri	30.36° N 78.50° E	57.83	L N63W T N27E
6.	Uttarkashi	30.73° N 78.45° E	66.37	L N15W T N75E

Δ : Epicentral distance, L : Longitudinal, T : Transverse

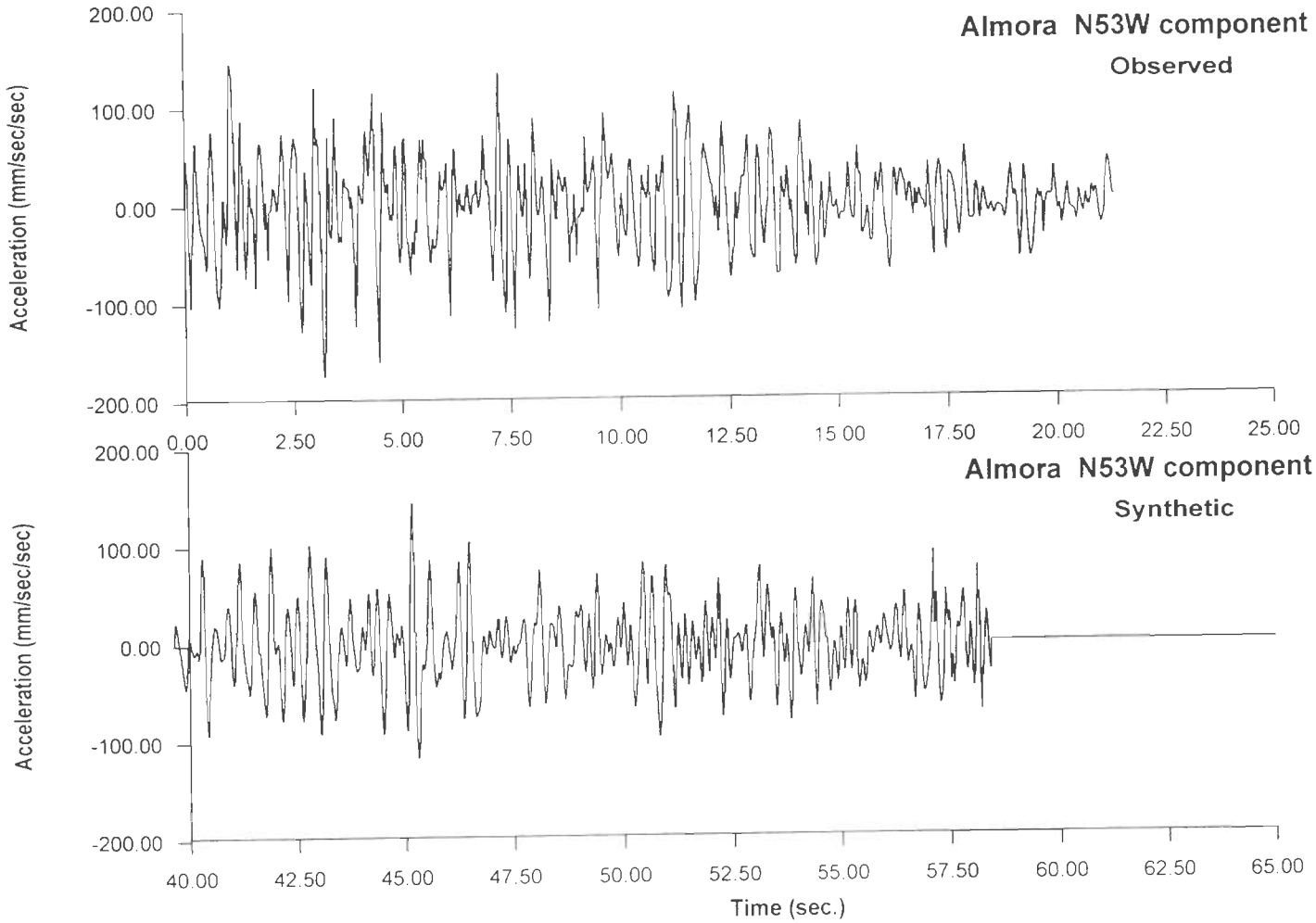

Fig. 4.1(a) : Observed and Synthetic accelerograms for N53W component at Almora (Uttarkashi Earthquake)

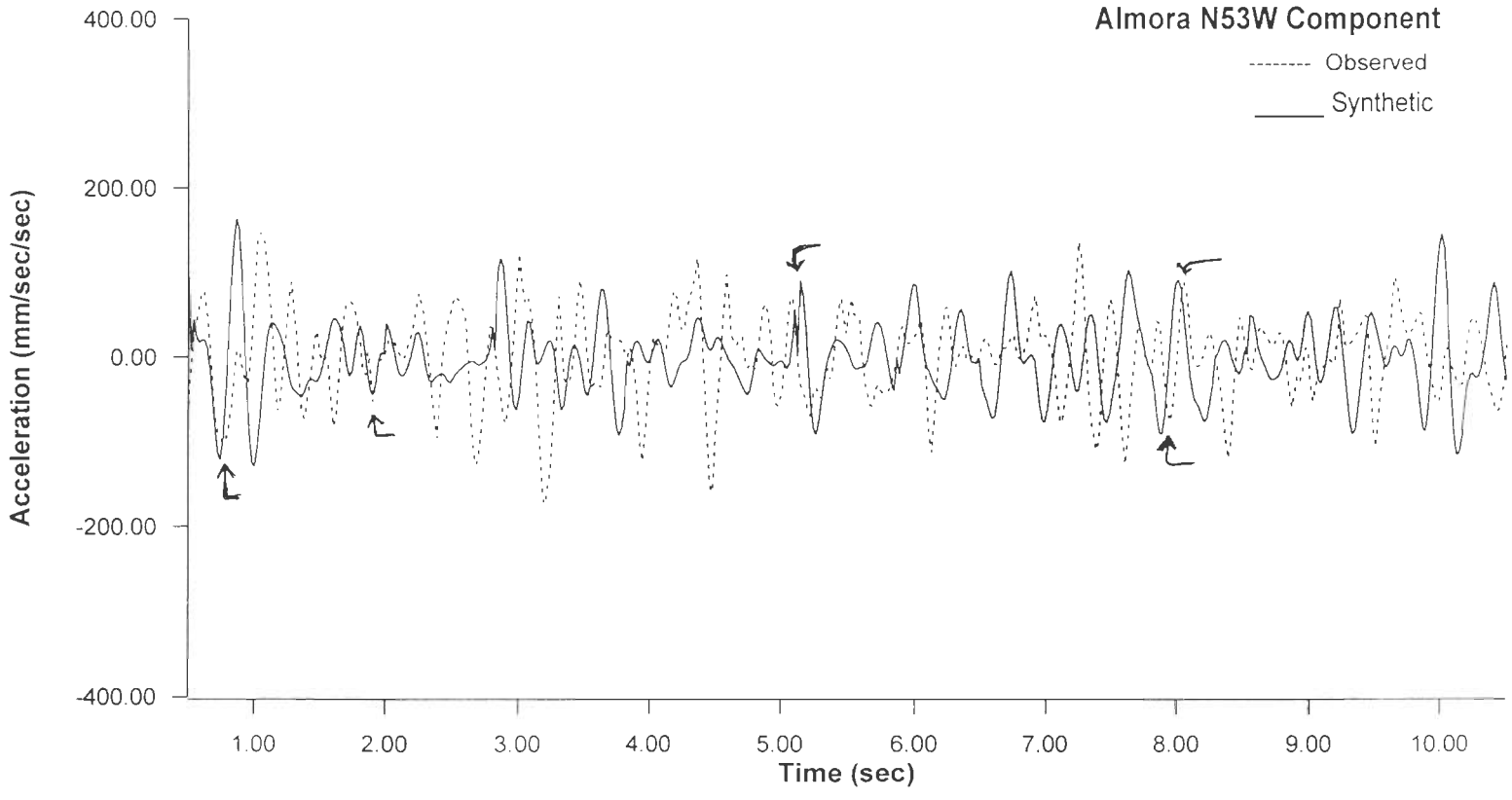

Fig. 4.1(b) : Synthetic accelerogram superimposed over the observed accelerogram for N53W component at Almora (Uttarkashi Earthquake)

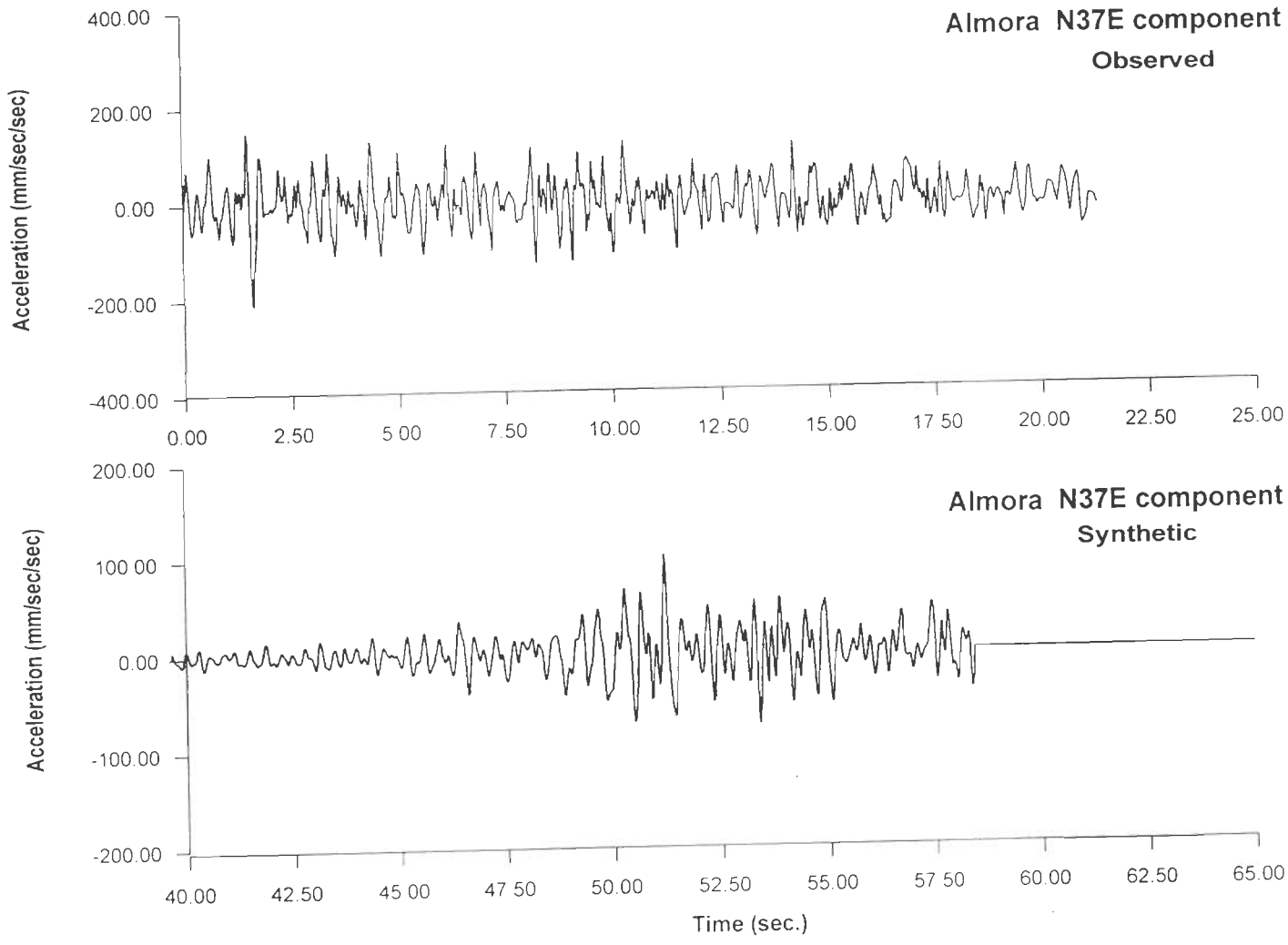

Fig. 4.1(c) : Observed and Synthetic accelerograms for N37E component at Almora (Uttarkashi Earthquake)

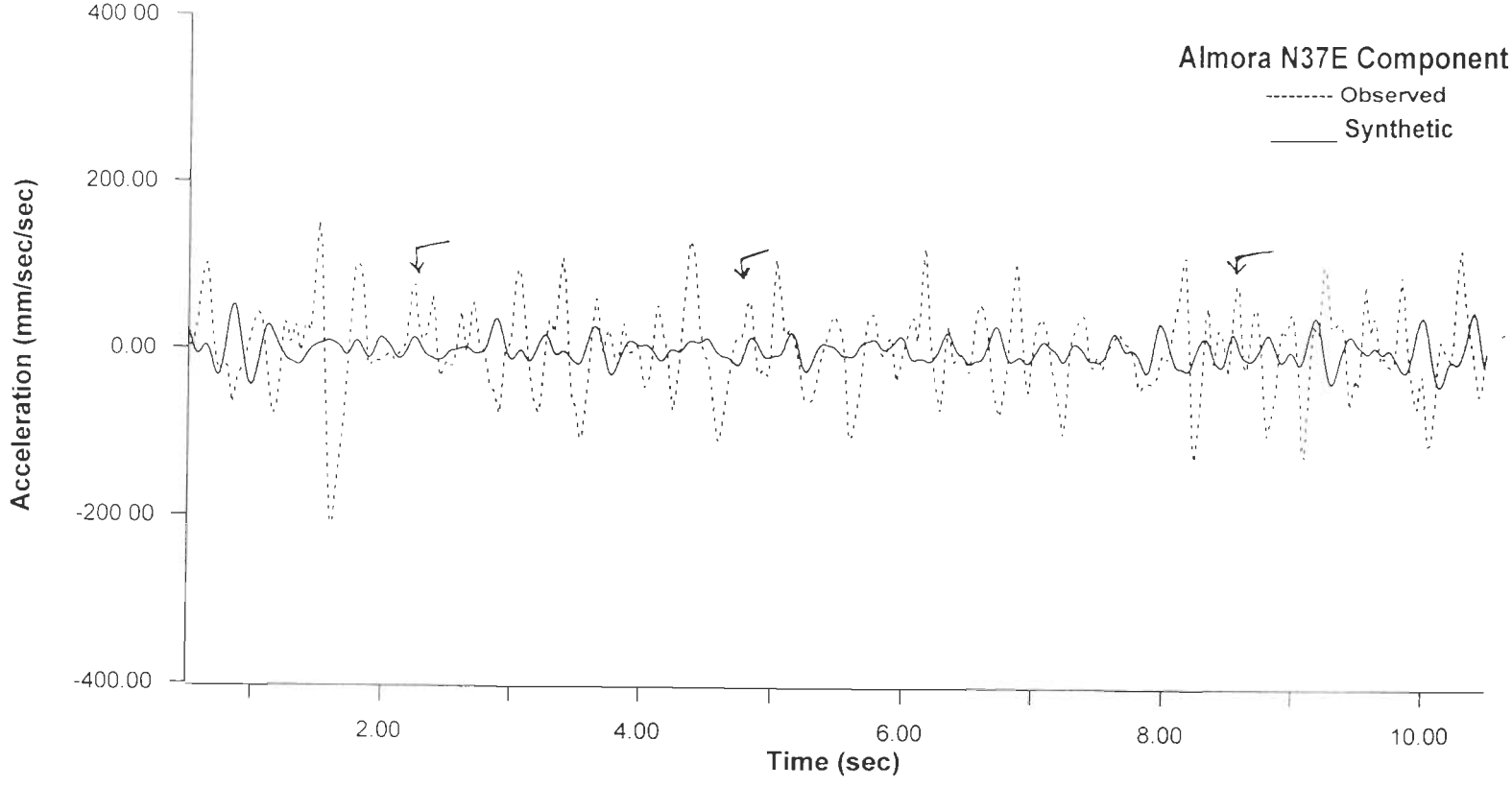

Fig. 4.1(d) : Synthetic accelerogram superimposed over the observed accelerogram for N37E component at Almora (Uttarkashi Earthquake)

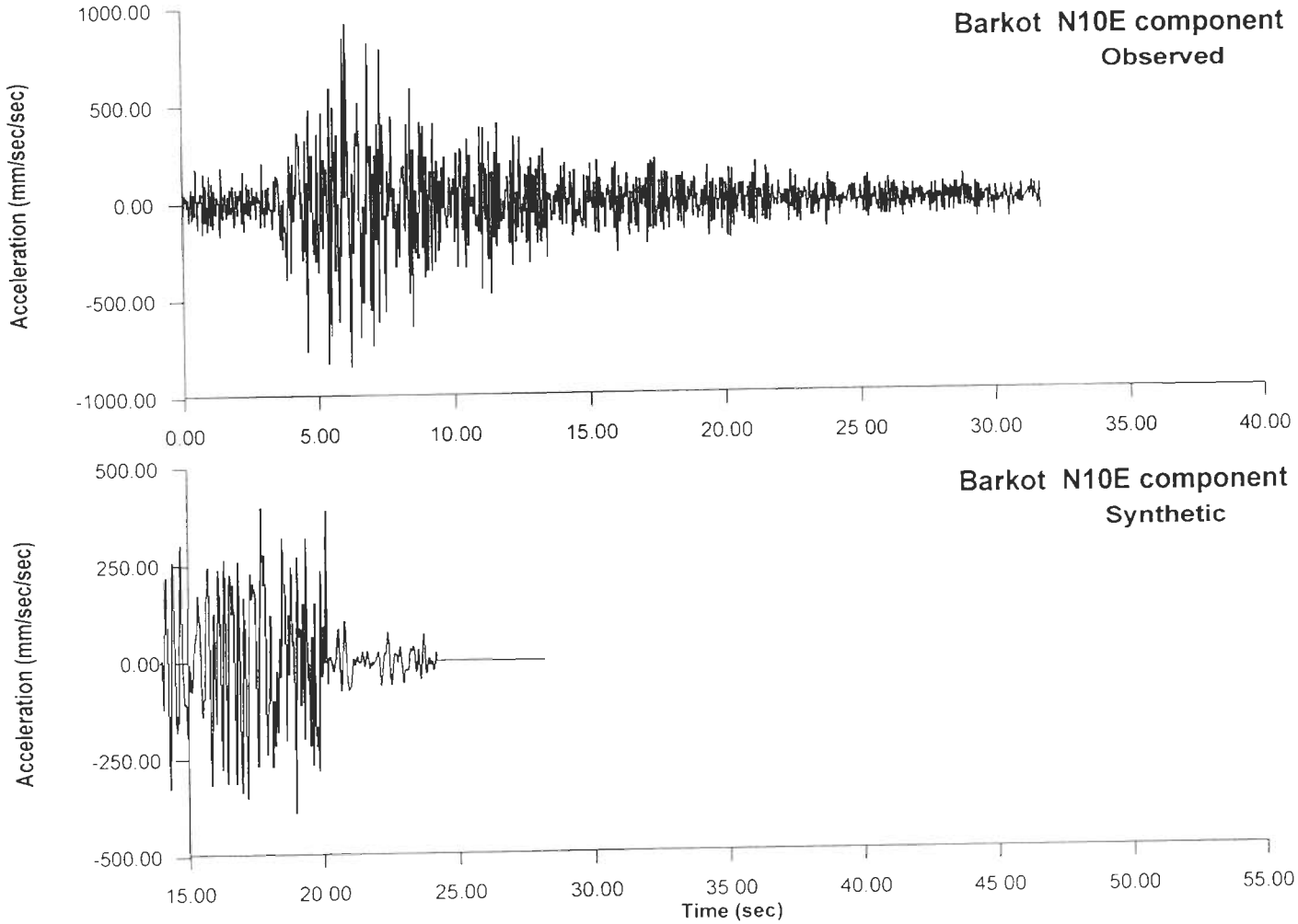

Fig. 4.2(a) : Observed and Synthetic accelerograms for N10E component at Barkot (Uttarkashi Earthquake)

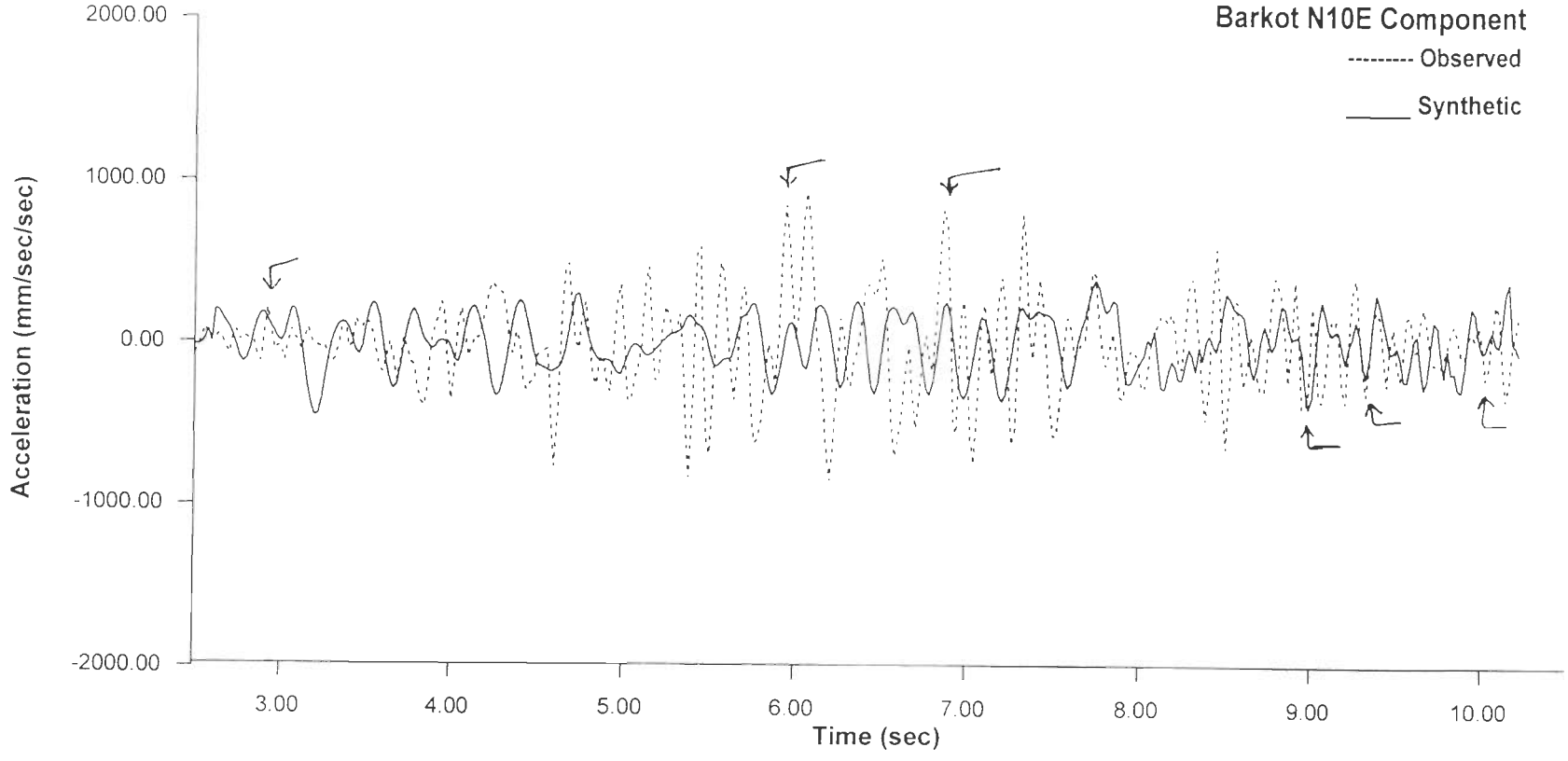

Fig. 4.2(b) : Synthetic accelerogram superimposed over the observed accelerogram for N10E component at Barkot (Uttarkashi Earthquake)

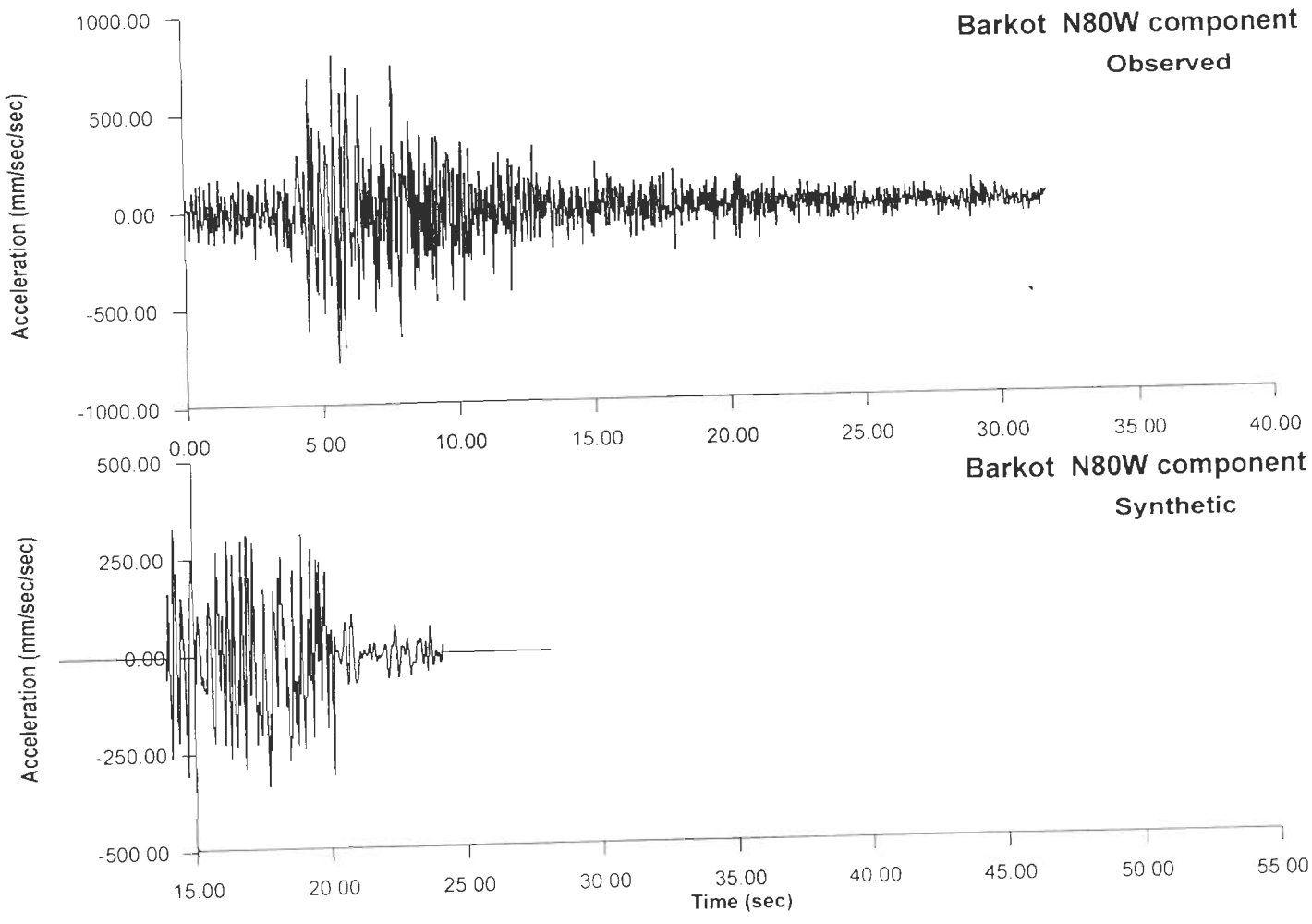

Fig. 4.2(c) : Observed and Synthetic accelerograms for N80W component at Barkot (Uttarkashi Earthquake)

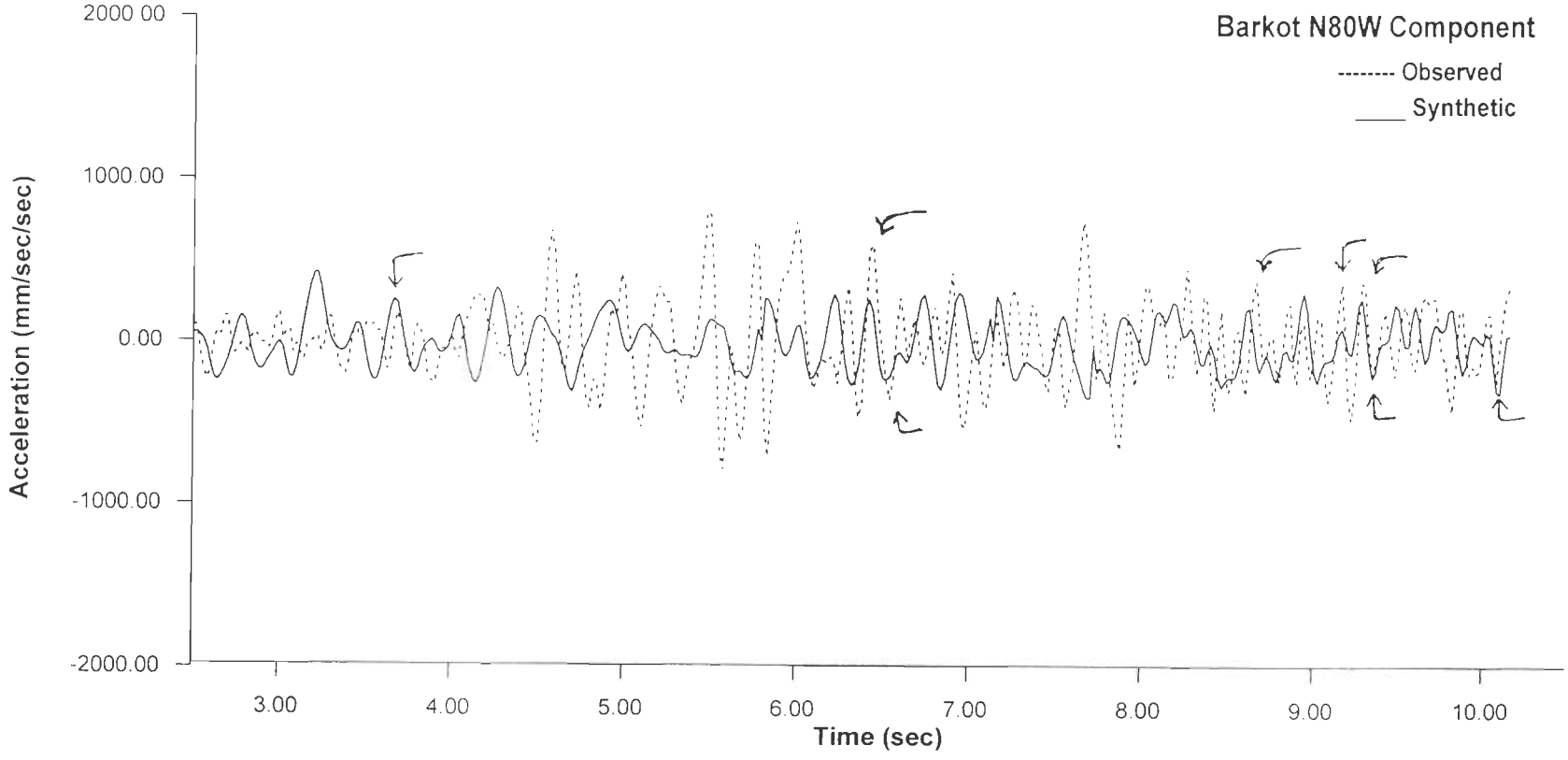

Fig. 4.2(d) : Synthetic accelerogram superimposed over the observed accelerogram for N80W component at Barkot (Uttarkashi Earthquake)

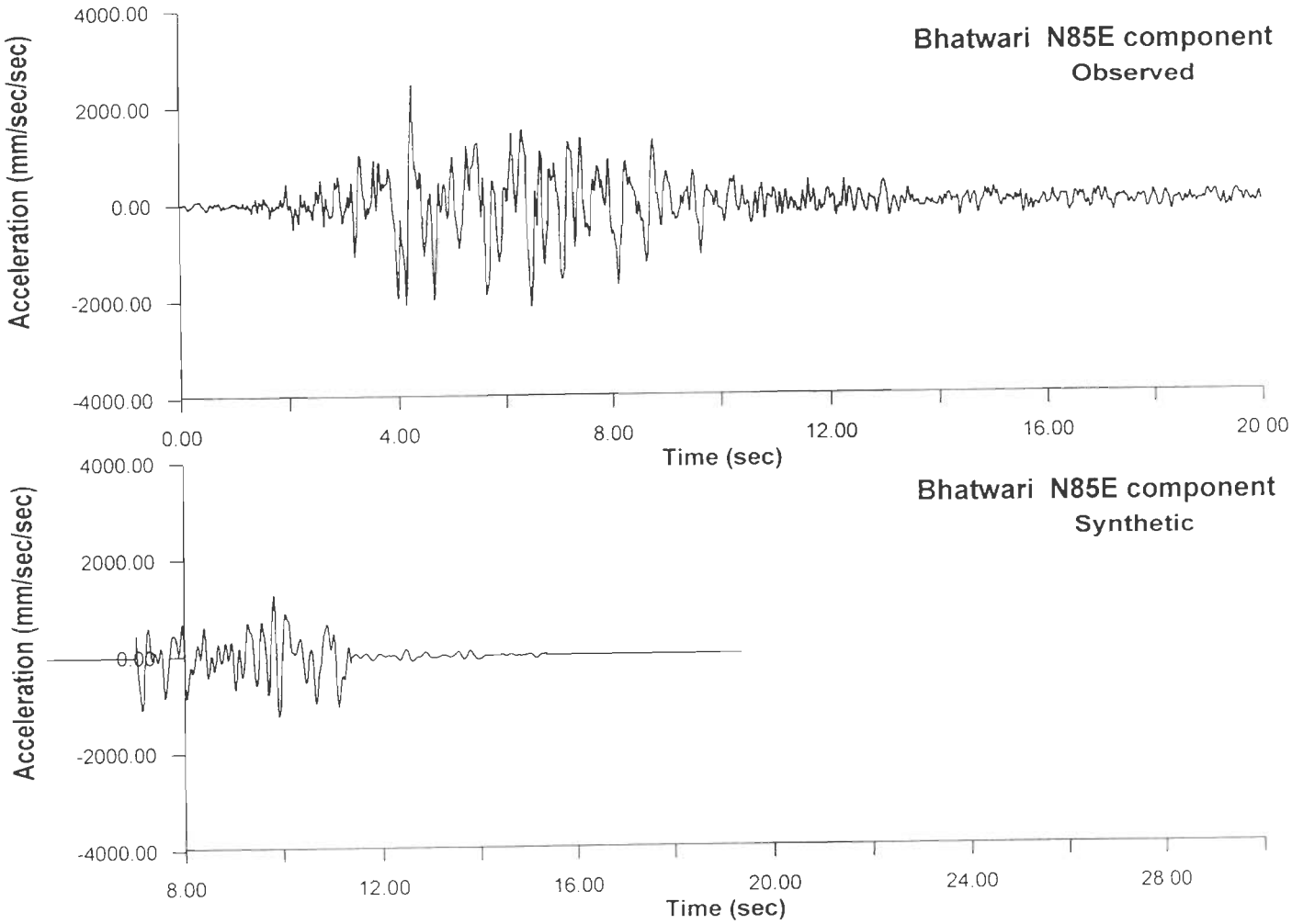

Fig. 4.3(a) : Observed and Synthetic accelerograms for N85E component at Bhatwari (Uttarkashi Earthquake)

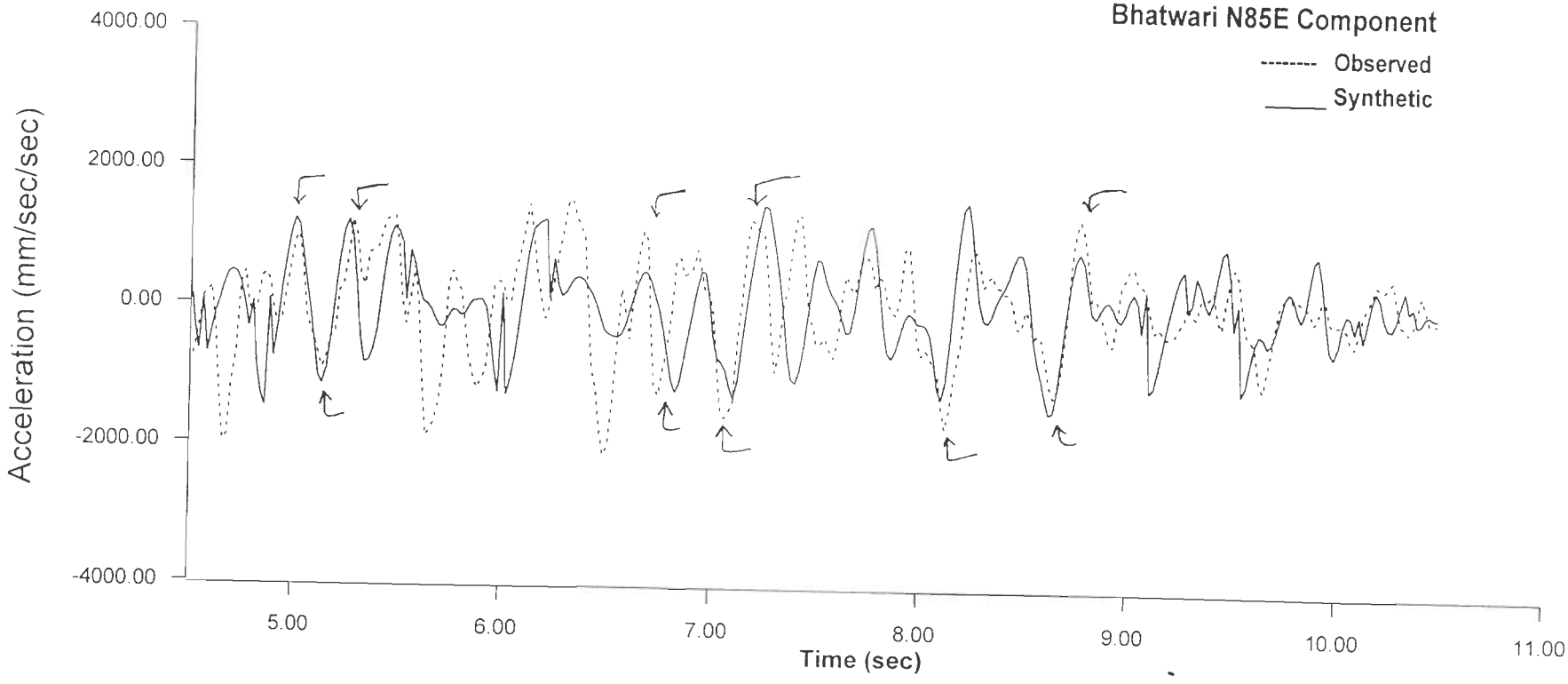

Fig. 4.3(b) : Synthetic accelerogram superimposed over the observed accelerogram for N85E component at Bhatwari (Uttarkashi Earthquake)

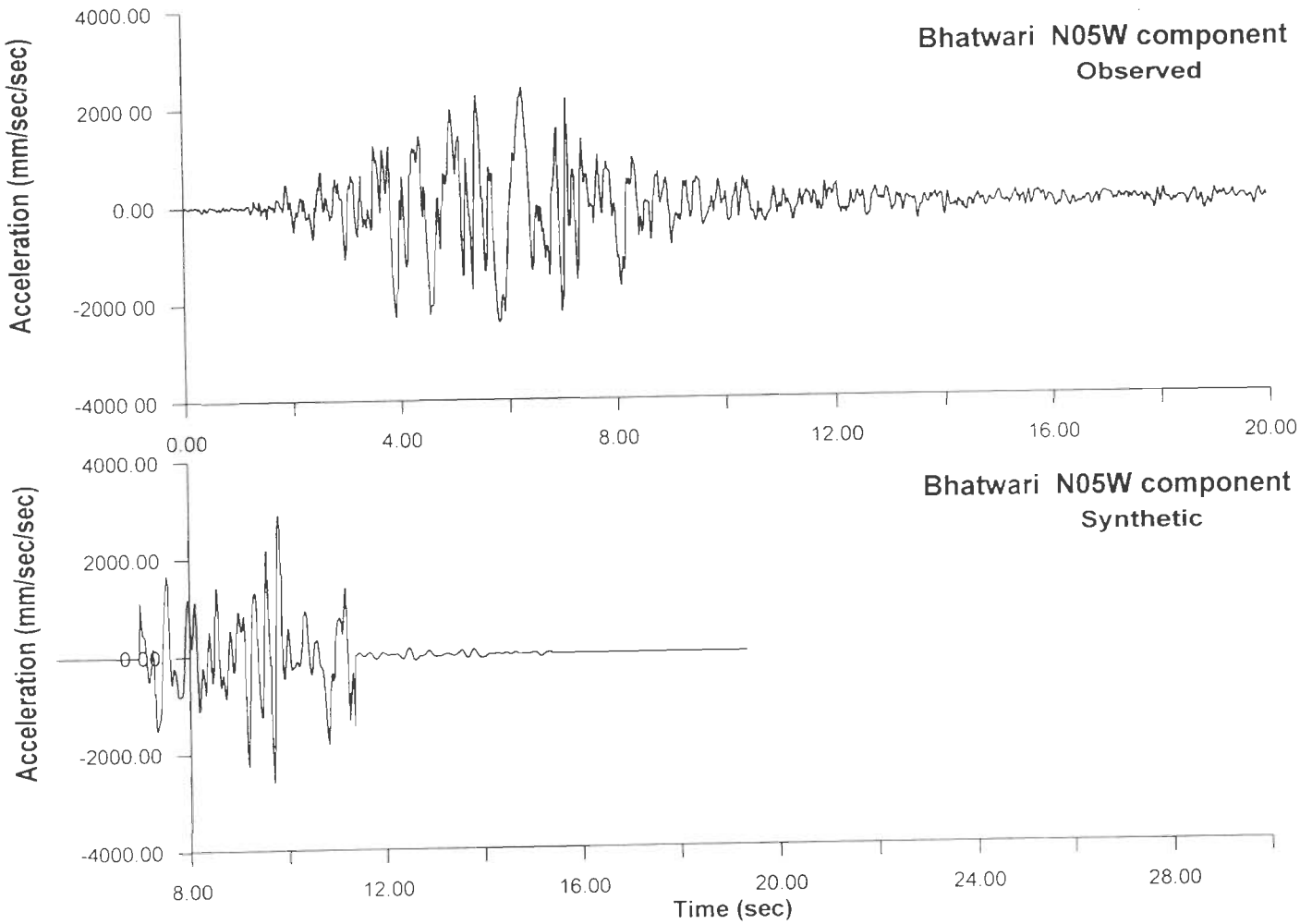

Fig. 4.3(c) : Observed and Synthetic accelerograms for N05W component at Bhatwari (Uttarkashi Earthquake)

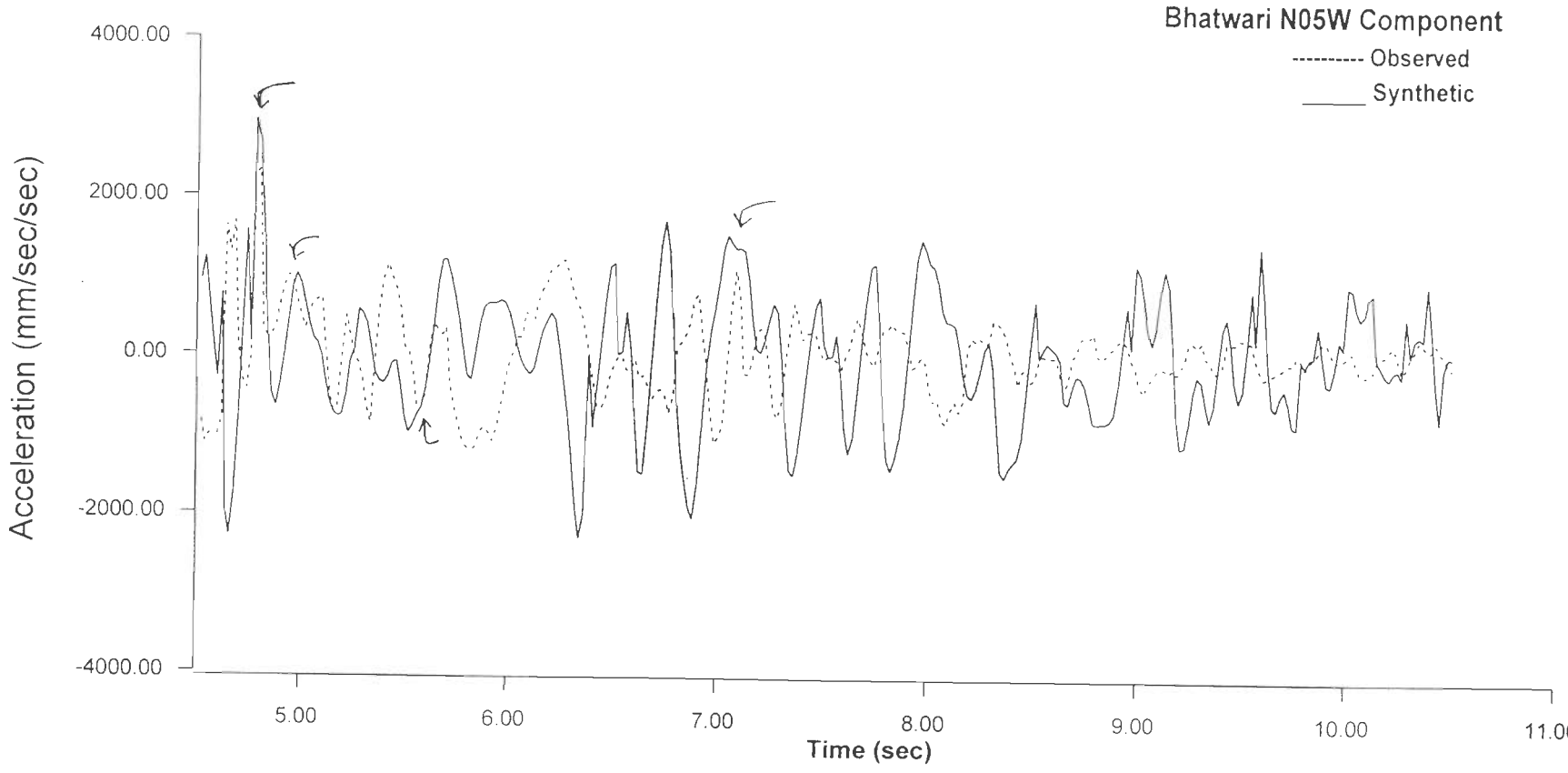

Fig. 4.3(d) : Synthetic accelerogram superimposed over the observed accelerogram for N05W component at Bhatwari (Uttarkashi Earthquake)

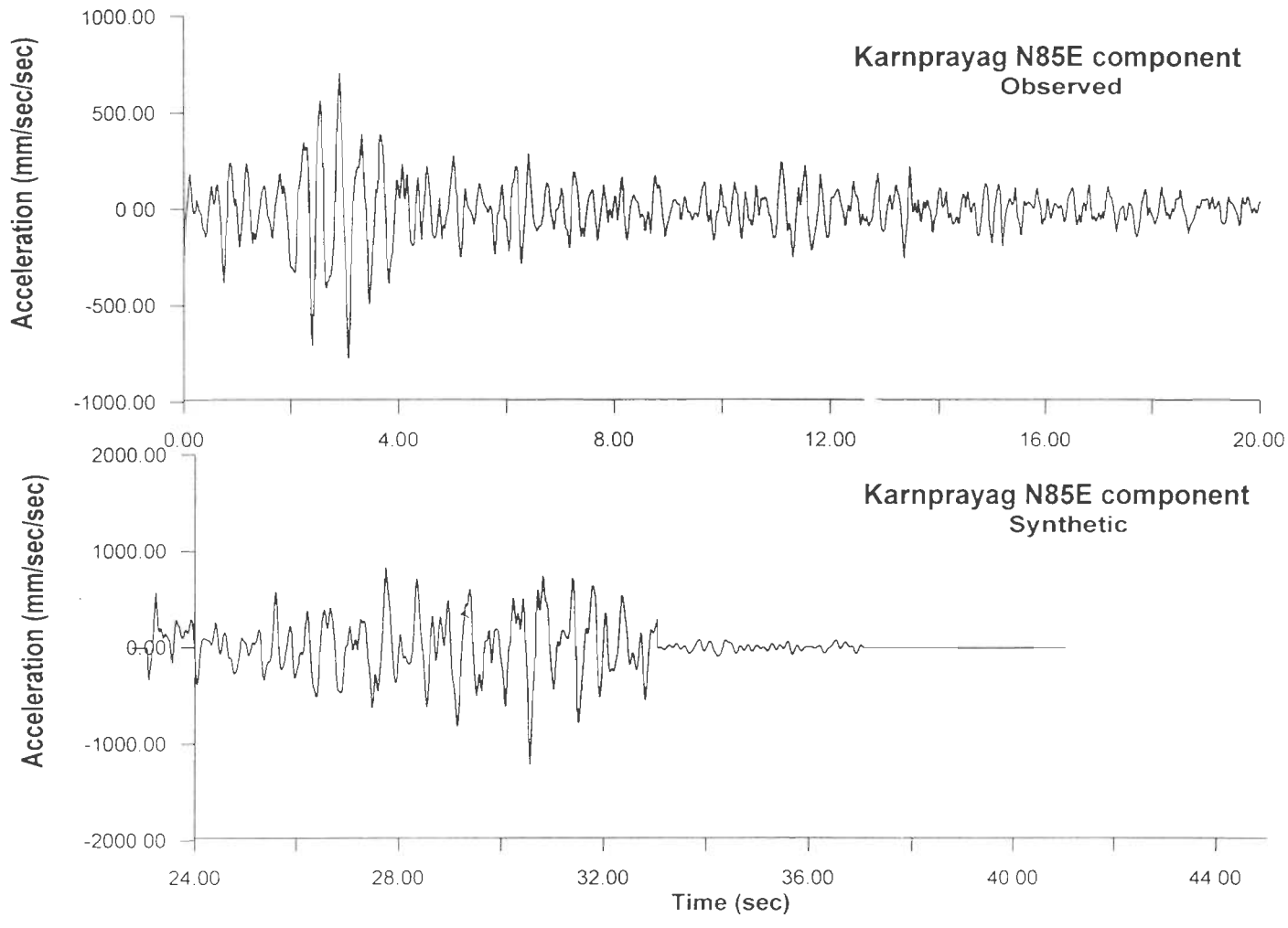

Fig. 4.4(a) : Observed and Synthetic accelerograms for N85E component at Karnprayag (Uttarkashi Earthquake)

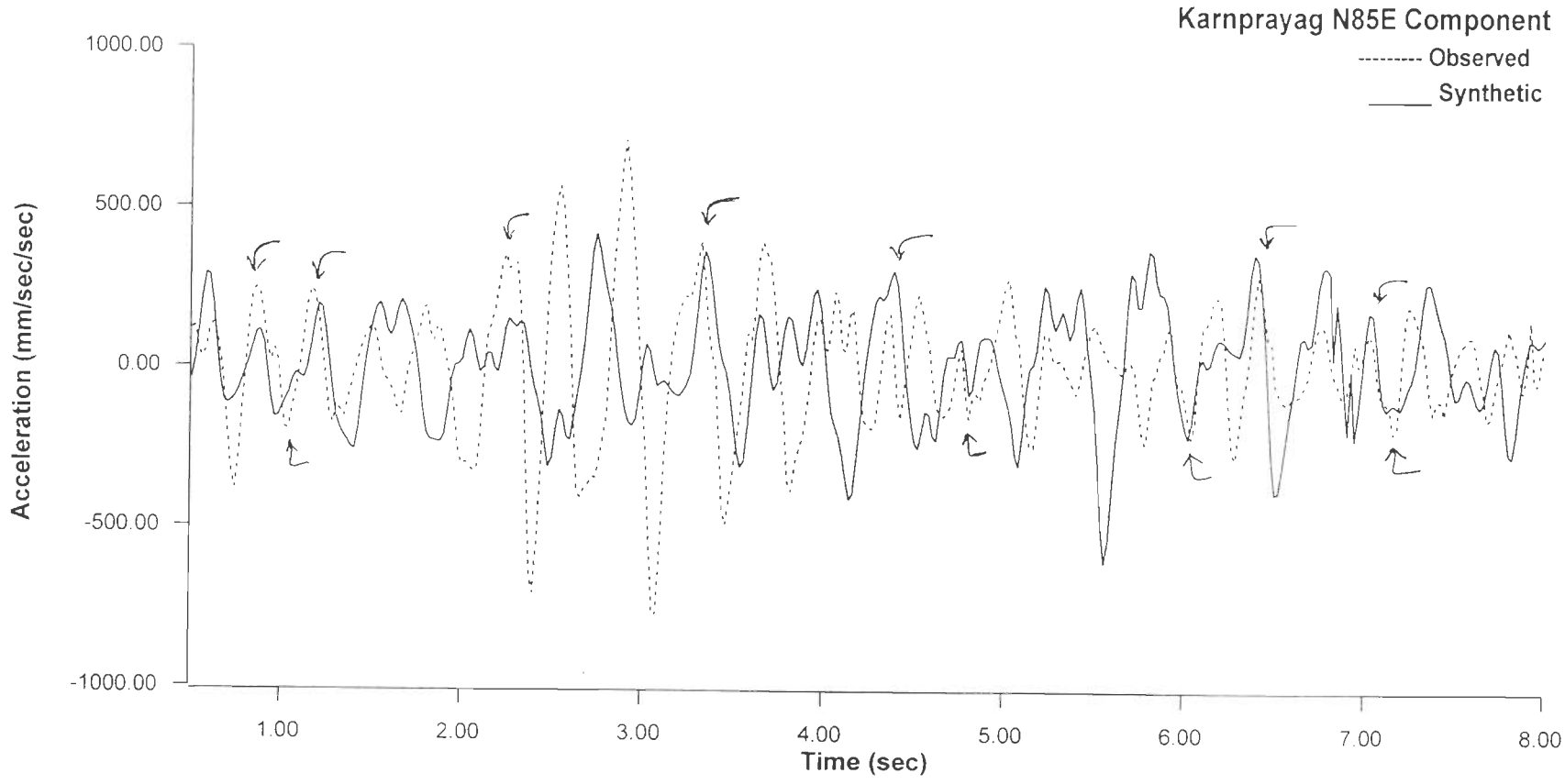

Fig. 4.4(b) : Synthetic accelerogram superimposed over the observed accelerogram for N85E component at Karnprayag (Uttarkashi Earthquake)

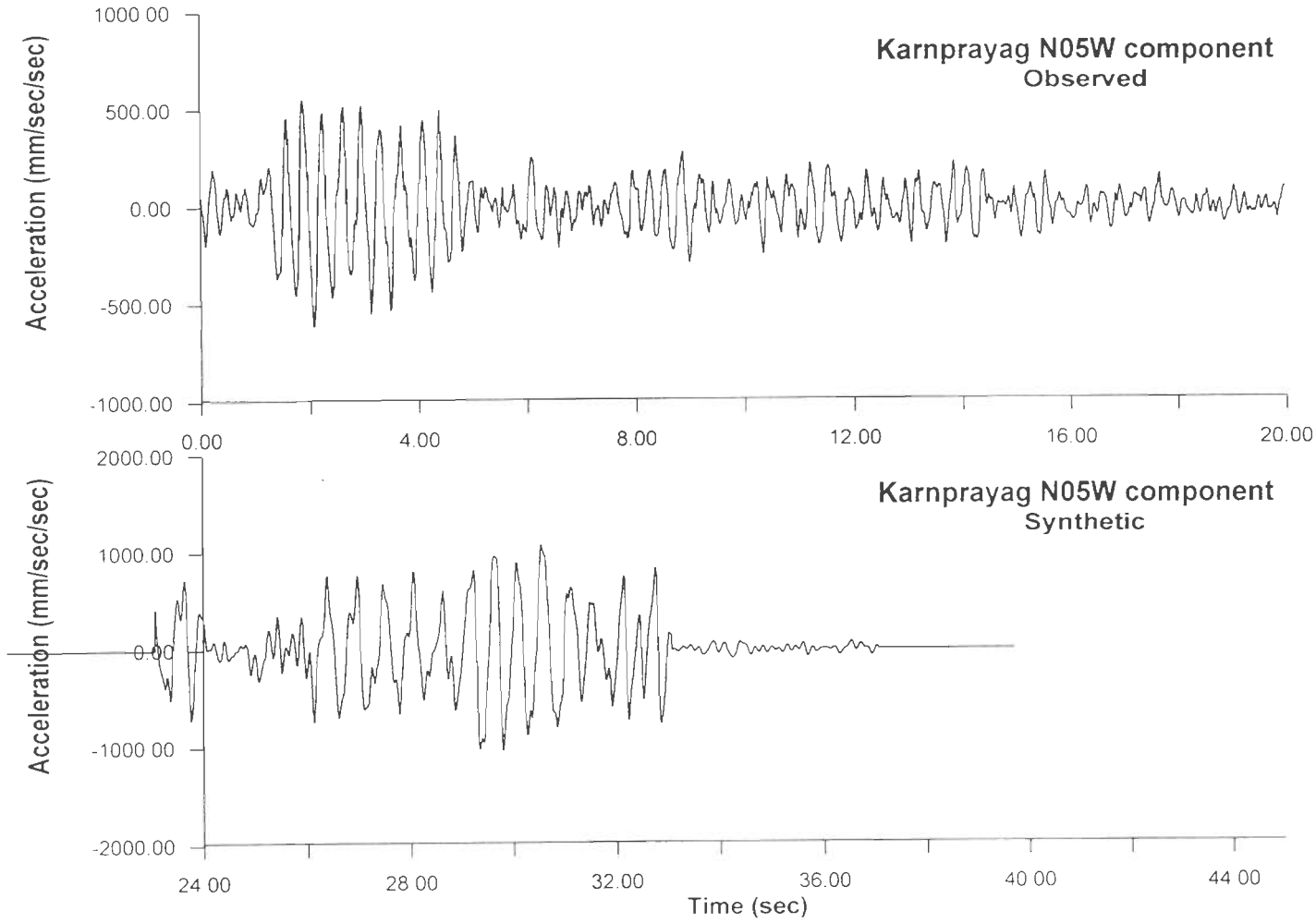

Fig. 4.4(c) : Observed and Synthetic accelerograms for N05W component at Karnprayag (Uttarkashi Earthquake)

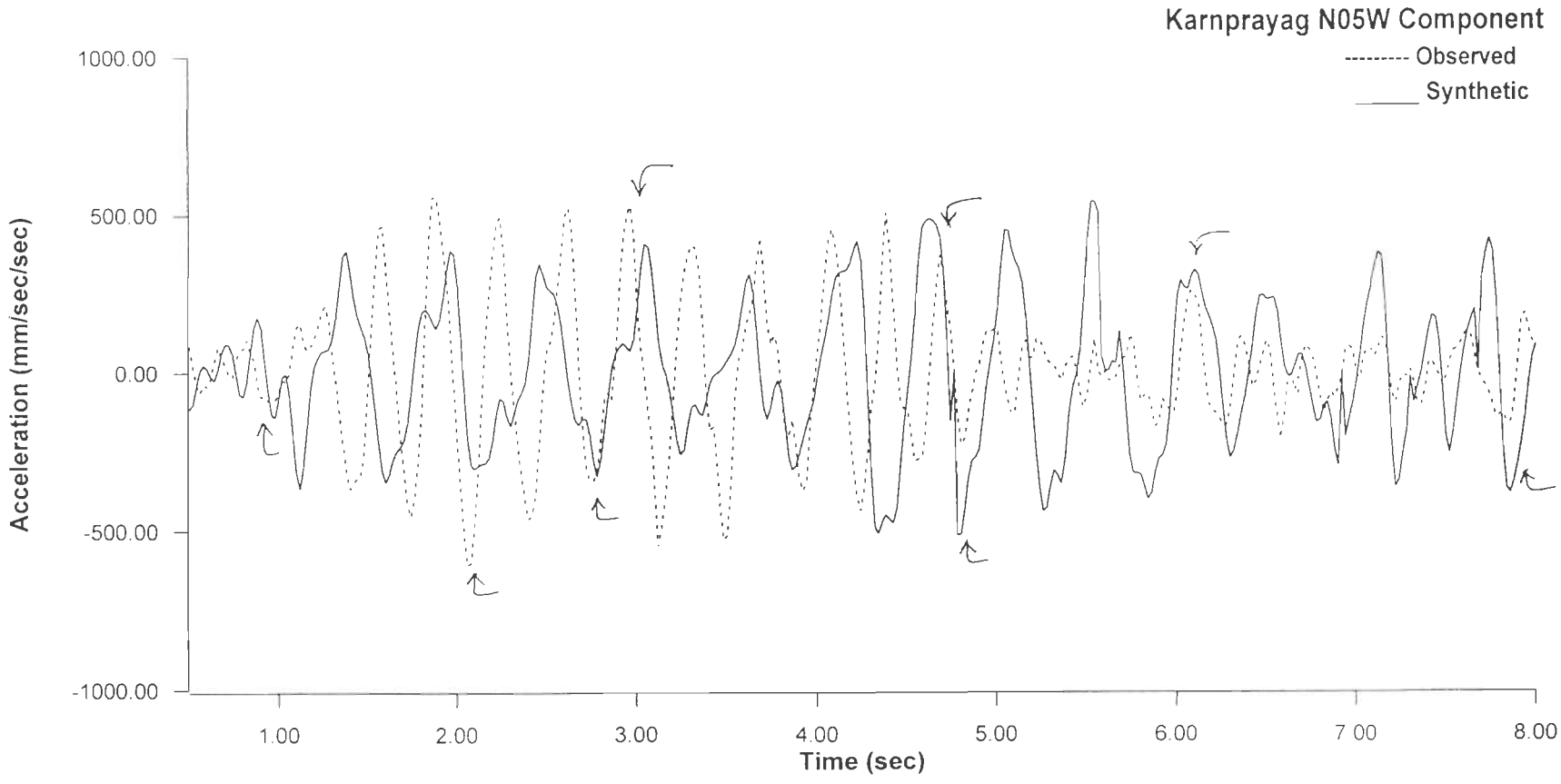

Fig. 4.4(d) : Synthetic accelerogram superimposed over the observed accelerogram for N05W component at Karnprayag (Uttarkashi Earthquake)

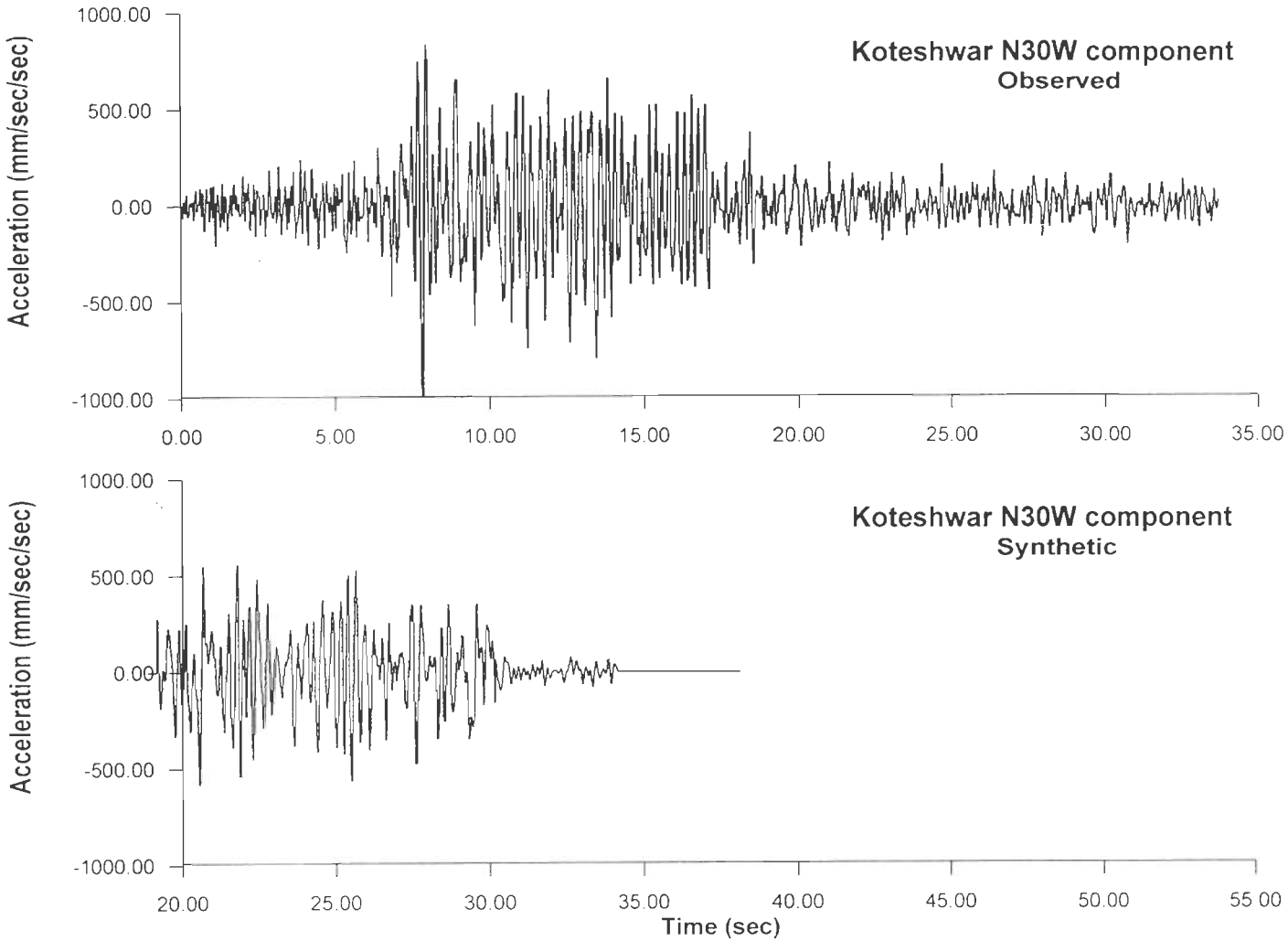

Fig. 4.5(a) : Observed and Synthetic accelerograms for N30W component at Koteshwar (Uttarkashi Earthquake)

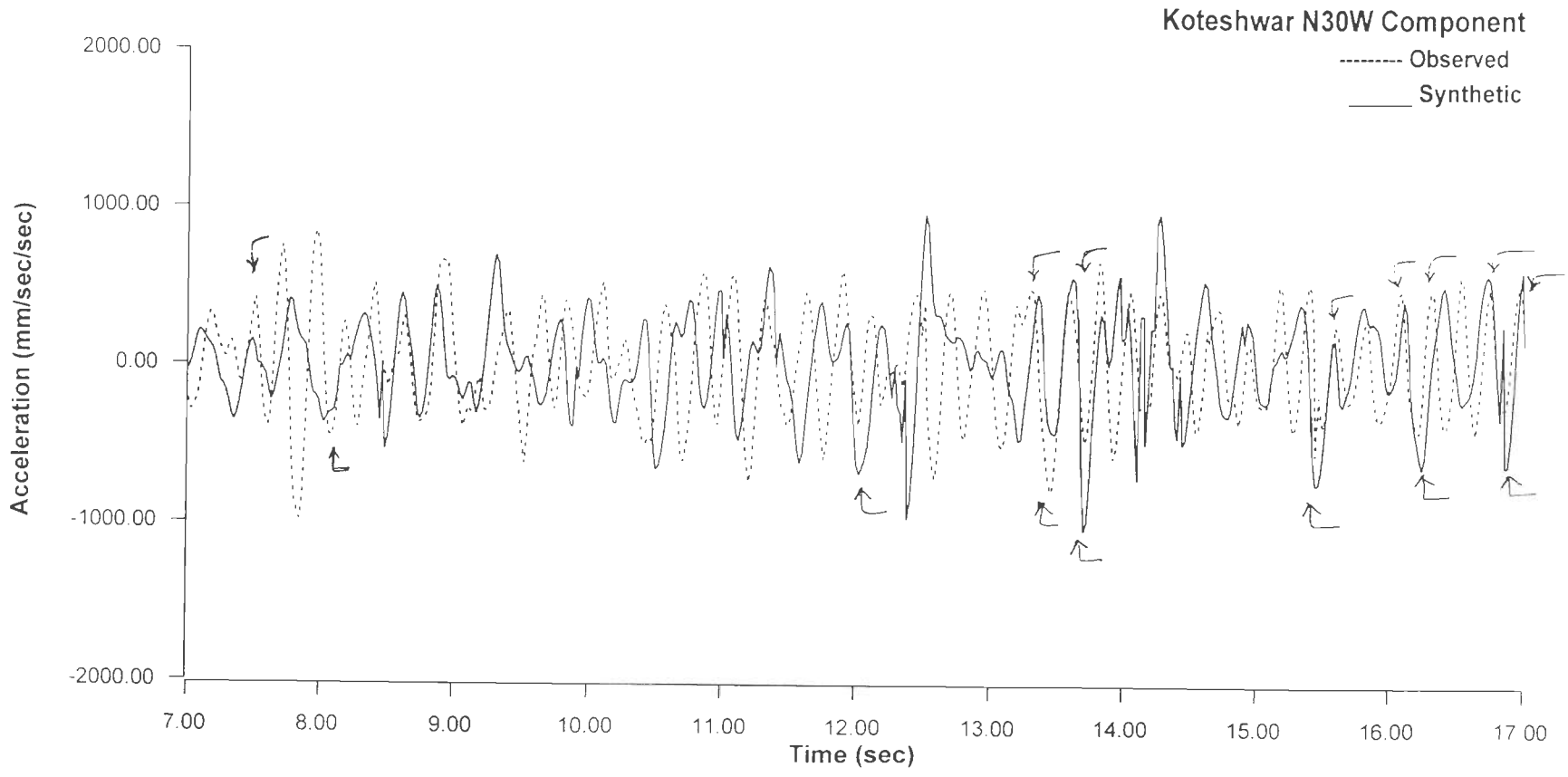

Fig. 4.5(b) : Synthetic accelerogram superimposed over the observed accelerogram for N30W component at Koteshwar (Uttarkashi Earthquake)

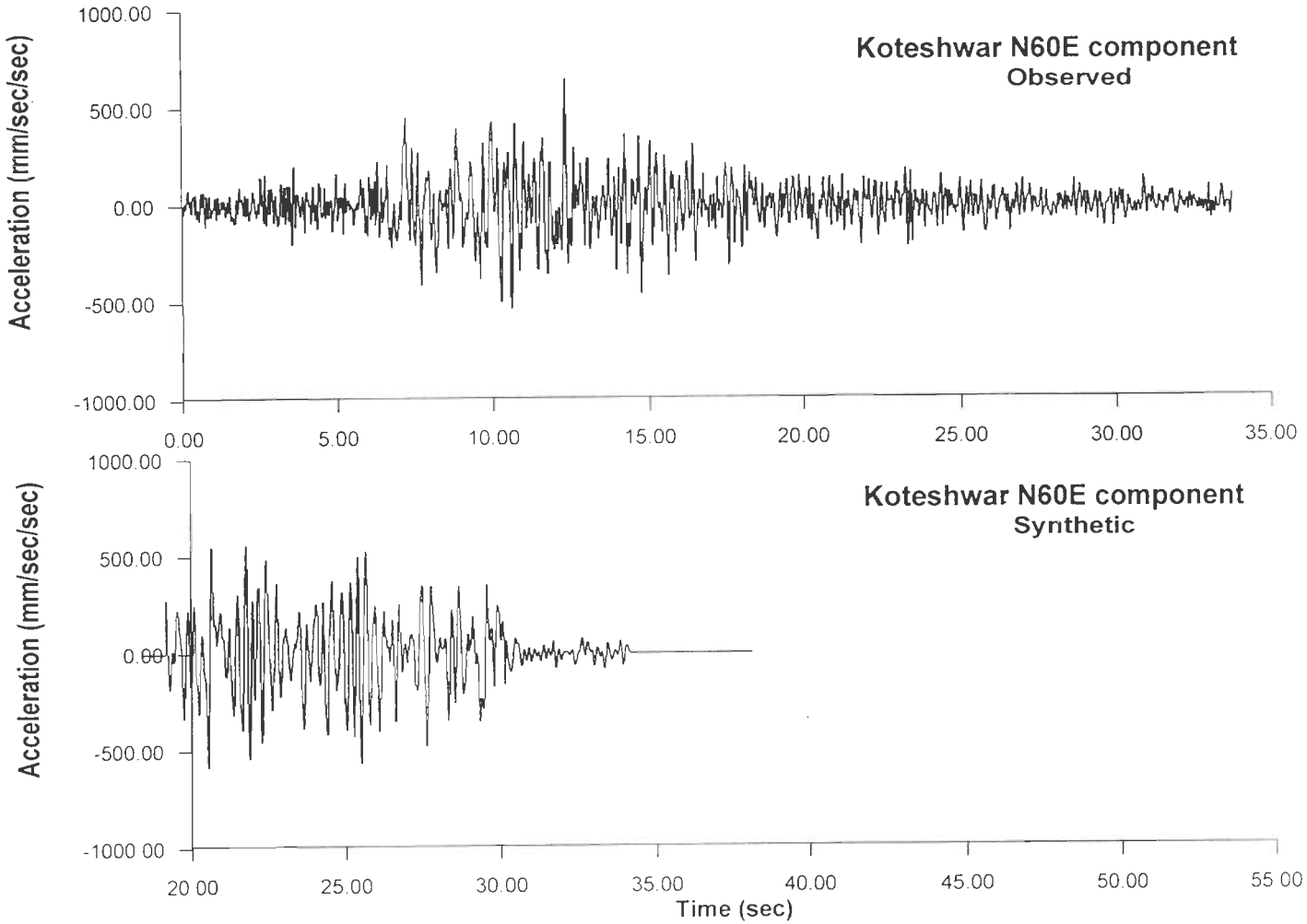

Fig. 4.5(c) : Observed and Synthetic accelerograms for N60E component at Koteshwar (Uttarkashi Earthquake)

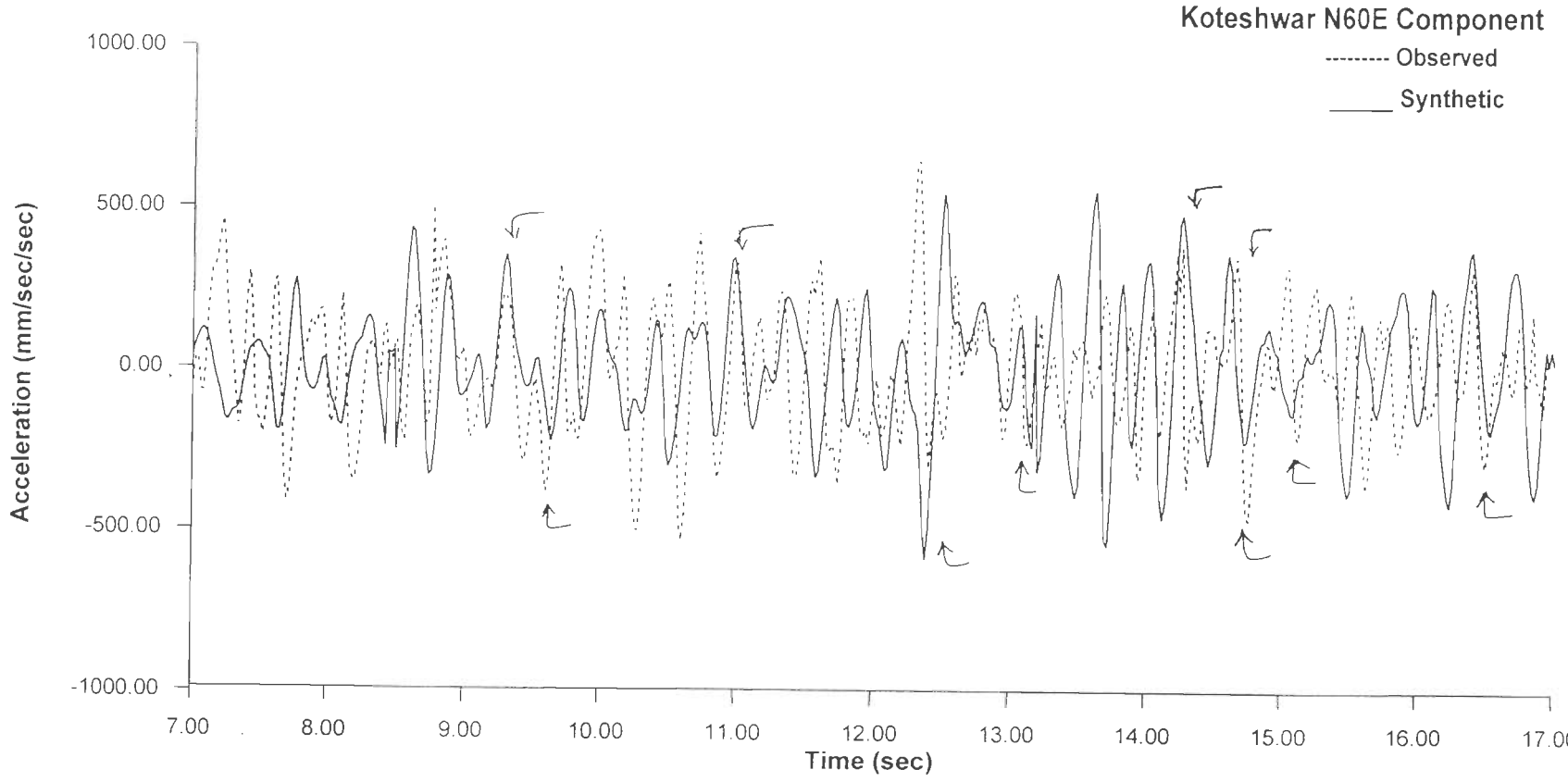

Fig. 4.5(d) : Synthetic accelerogram superimposed over the observed accelerogram for N60E component at Koteshwar (Uttarkashi Earthquake)

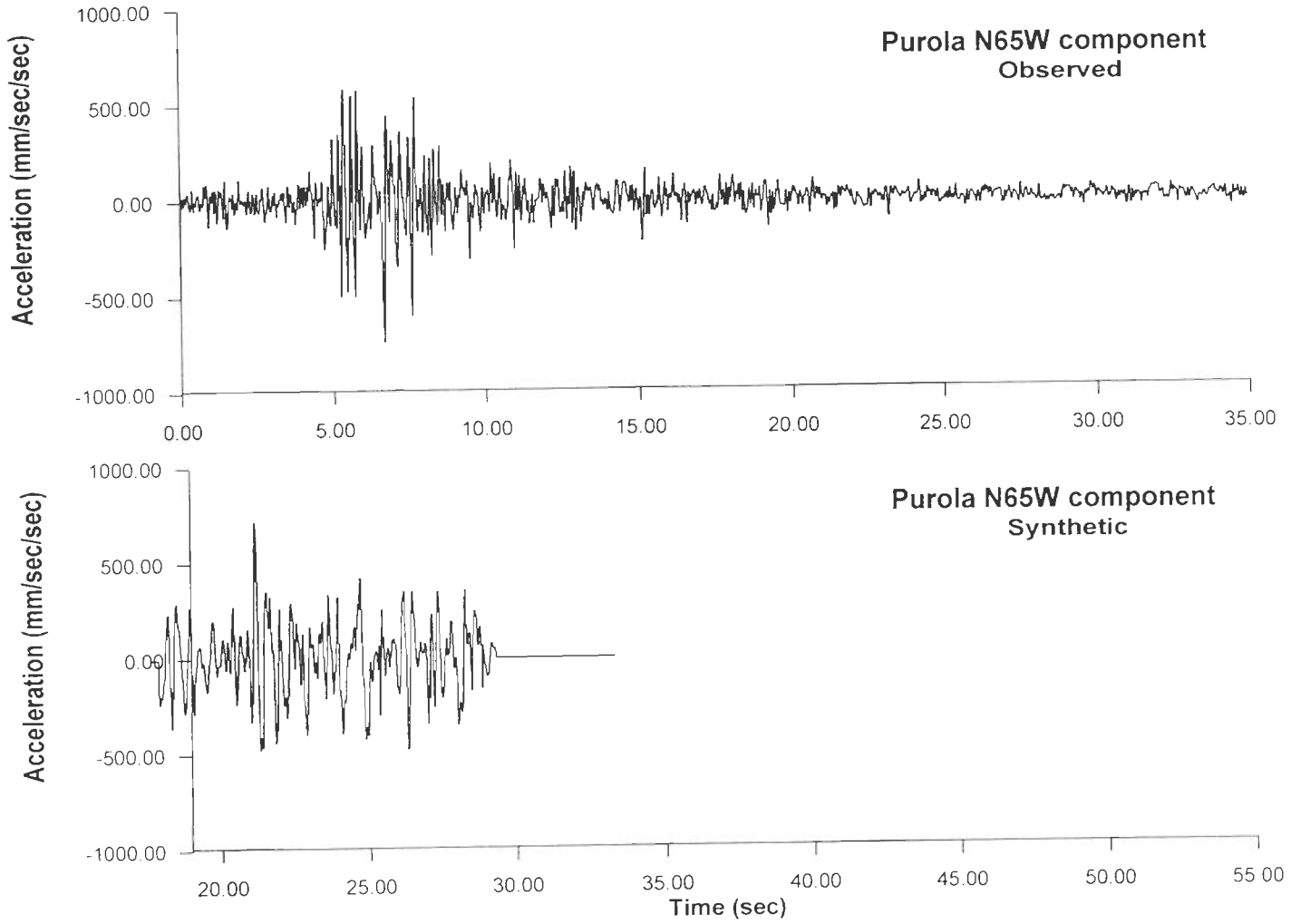

Fig. 4.6(a) : Observed and Synthetic accelerograms for N65W component at Purola (Uttarkashi Earthquake)

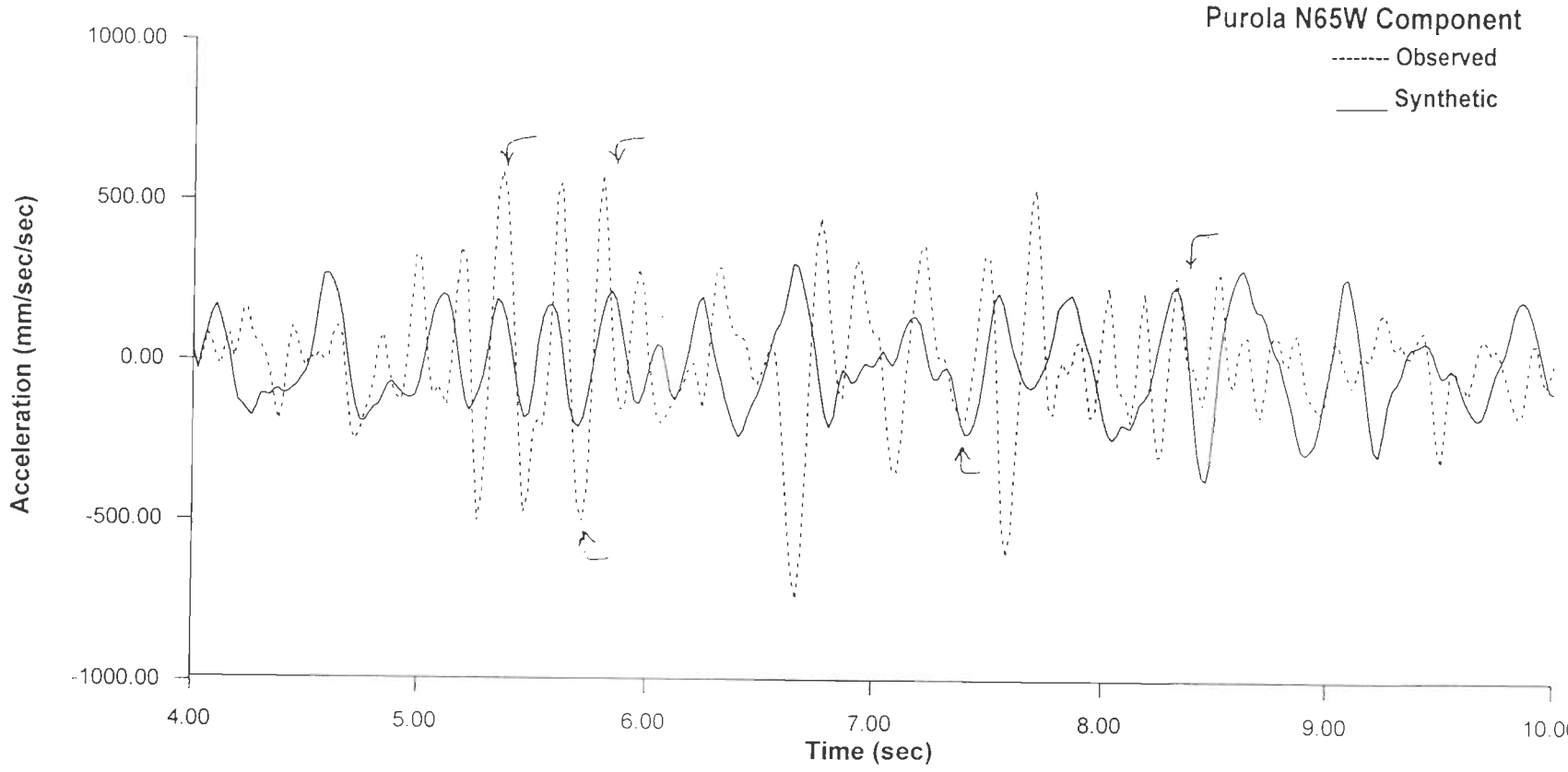

Fig. 4.6(b) : Synthetic accelerogram superimposed over the observed accelerogram for N65W component at Purola (Uttarkashi Earthquake)

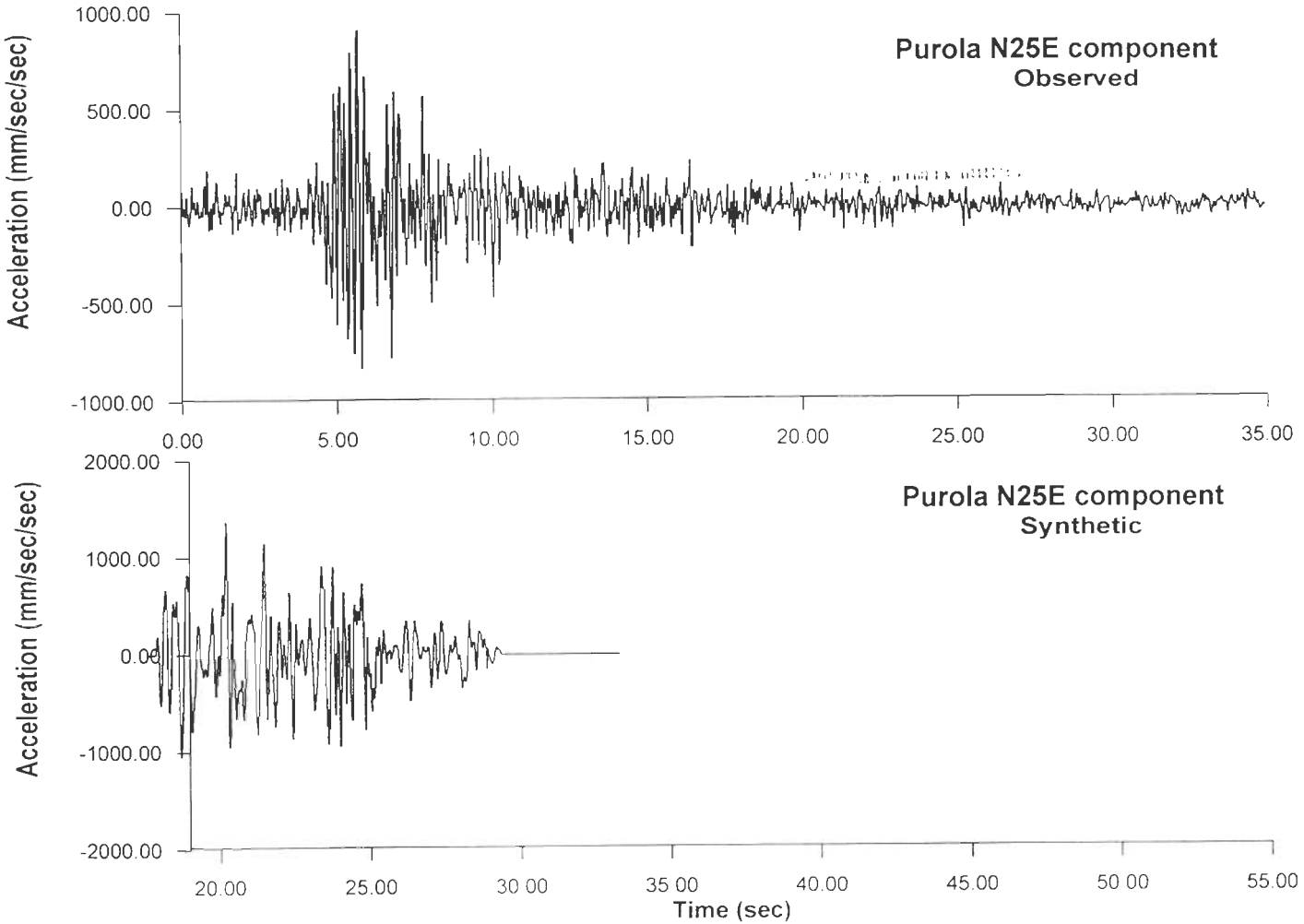

Fig. 4.6(c) : Observed and Synthetic accelerograms for N25E component at Purola (Uttarkashi Earthquake)

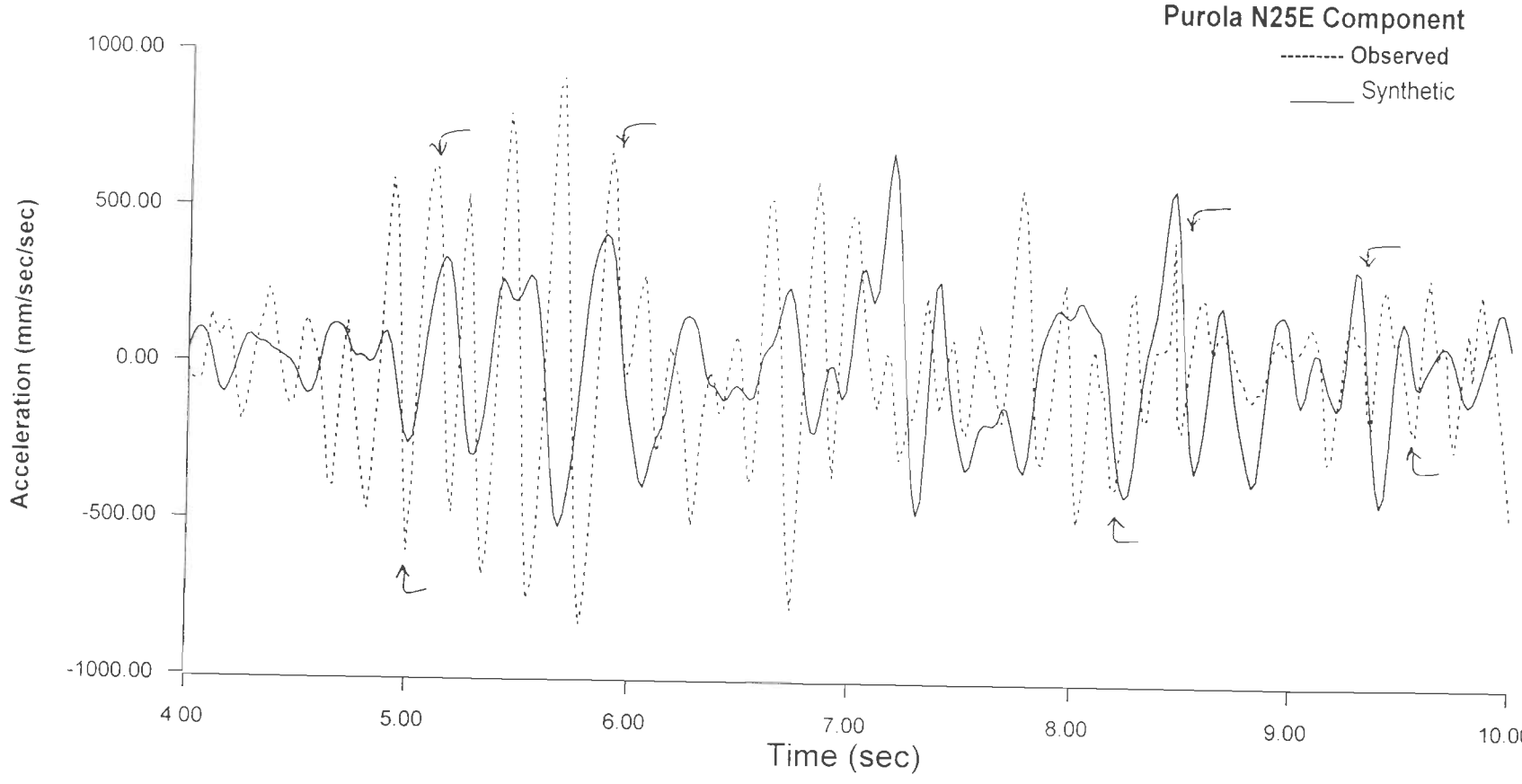

Fig. 4.6(d) : Synthetic accelerogram superimposed over the observed accelerogram for N25E component at Purola (Uttarkashi Earthquake)

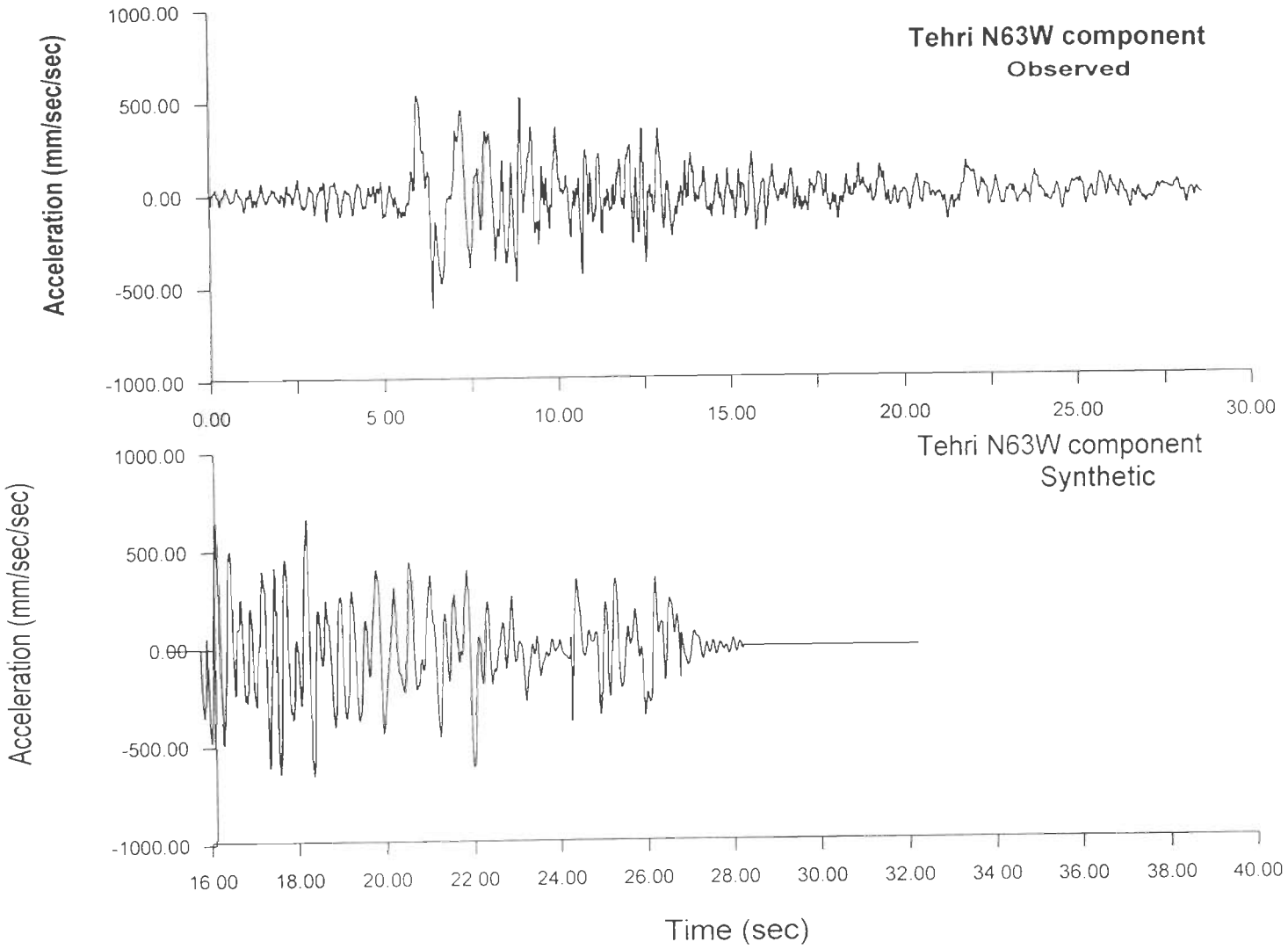

Fig. 4.7(a) : Observed and Synthetic accelerograms for N63W component at Tehri (Uttarkashi Earthquake)

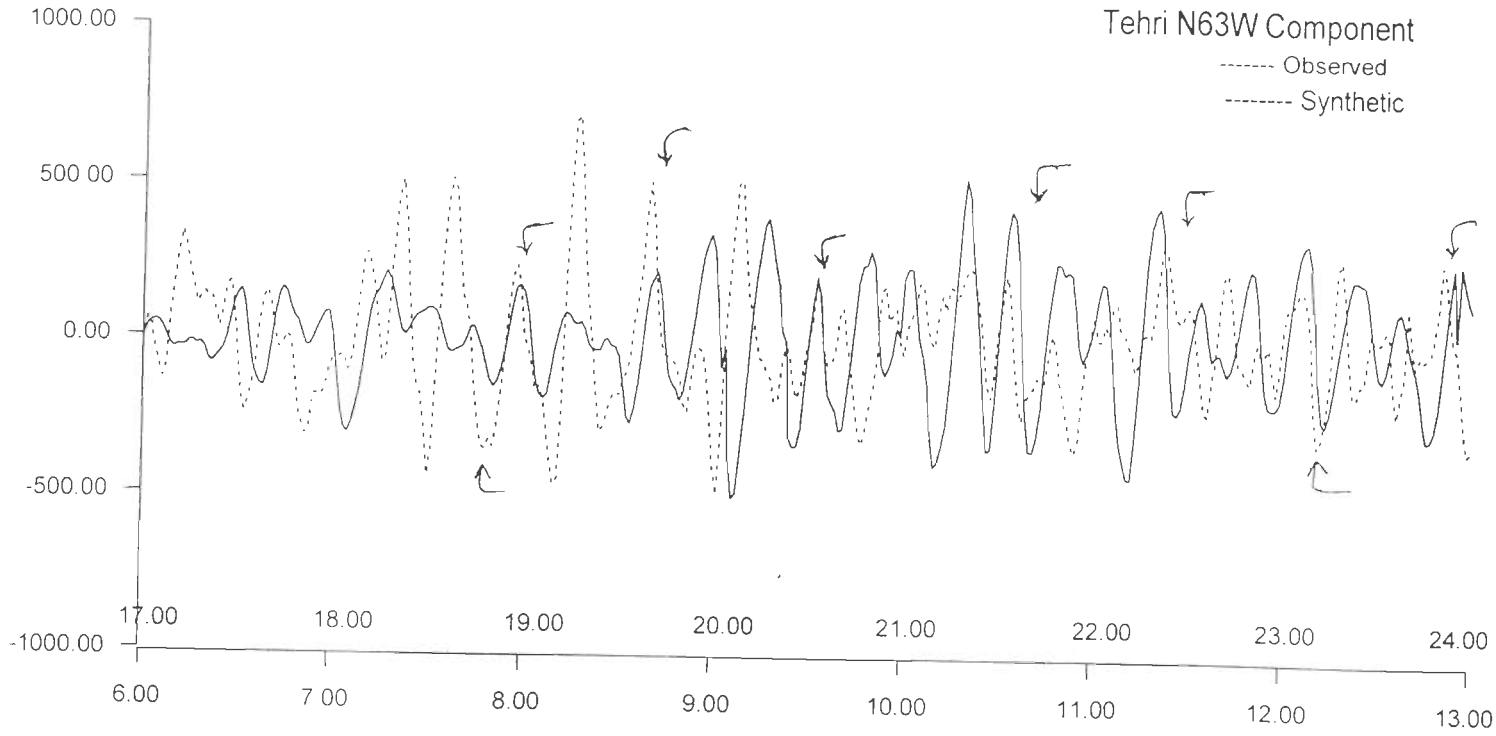

Fig. 4.7(b) : Synthetic accelerogram superimposed over the observed accelerogram for N63W component at Tehri (Uttarkashi Earthquake)

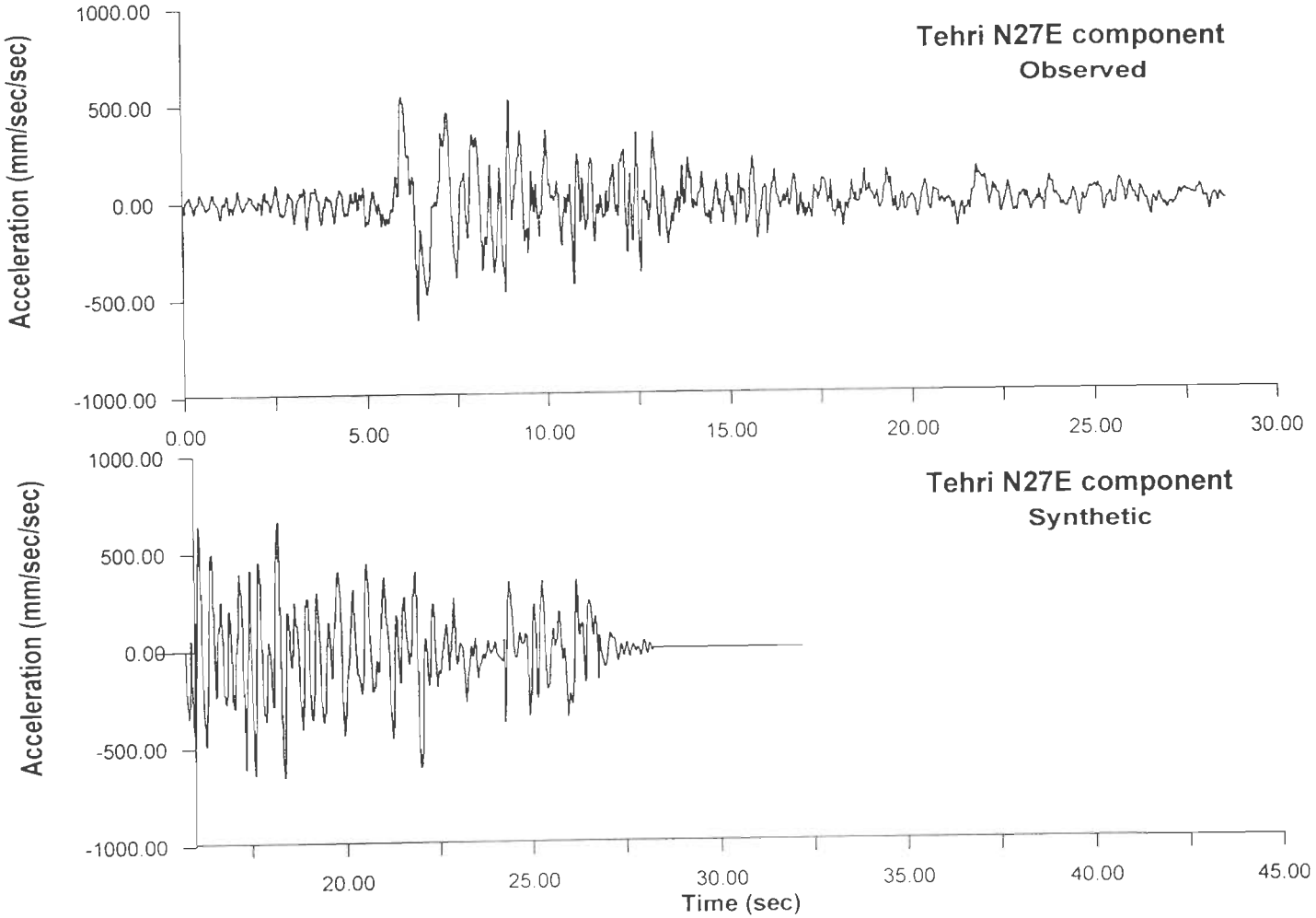

Fig. 4.7(c) : Observed and Synthetic accelerograms for N27E component at Tehri (Uttarkashi Earthquake)

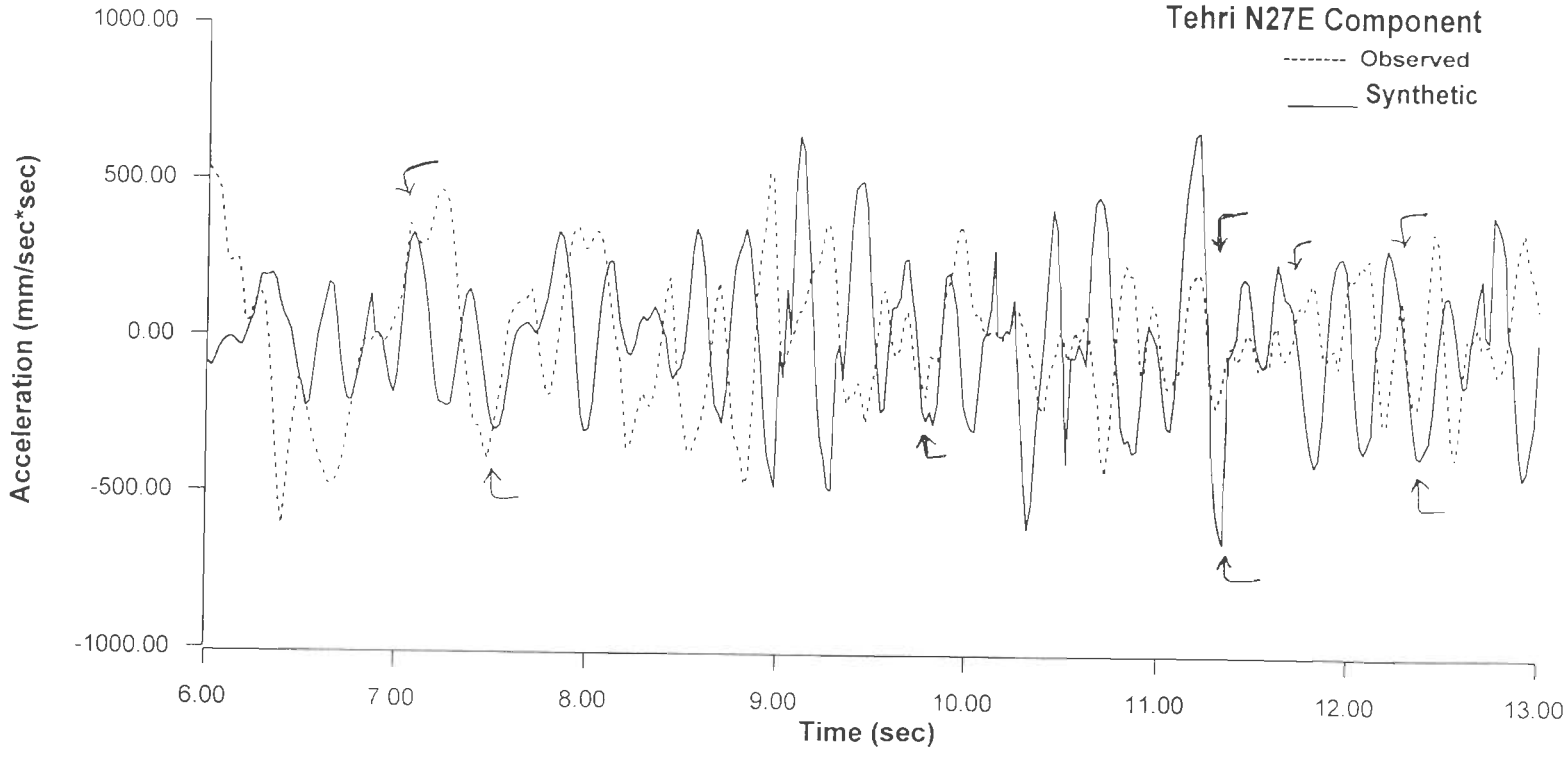

Fig. 4.7(d) : Synthetic accelerogram superimposed over the observed accelerogram for N27E component at Tehri (Uttarkashi Earthquake)

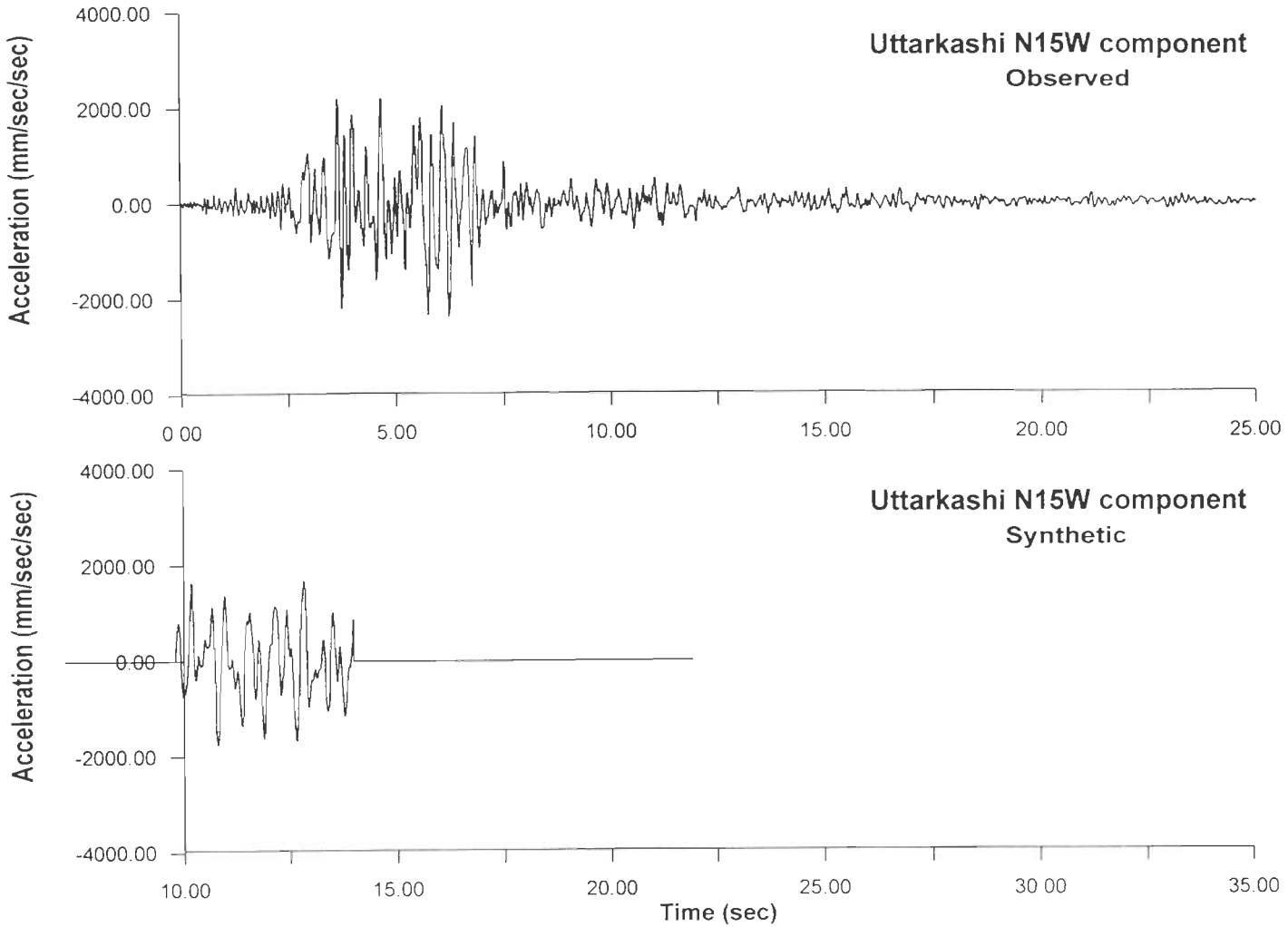

Fig. 4.8(a) : Observed and Synthetic accelerograms for N15W component at Uttarkashi (Uttarkashi Earthquake)

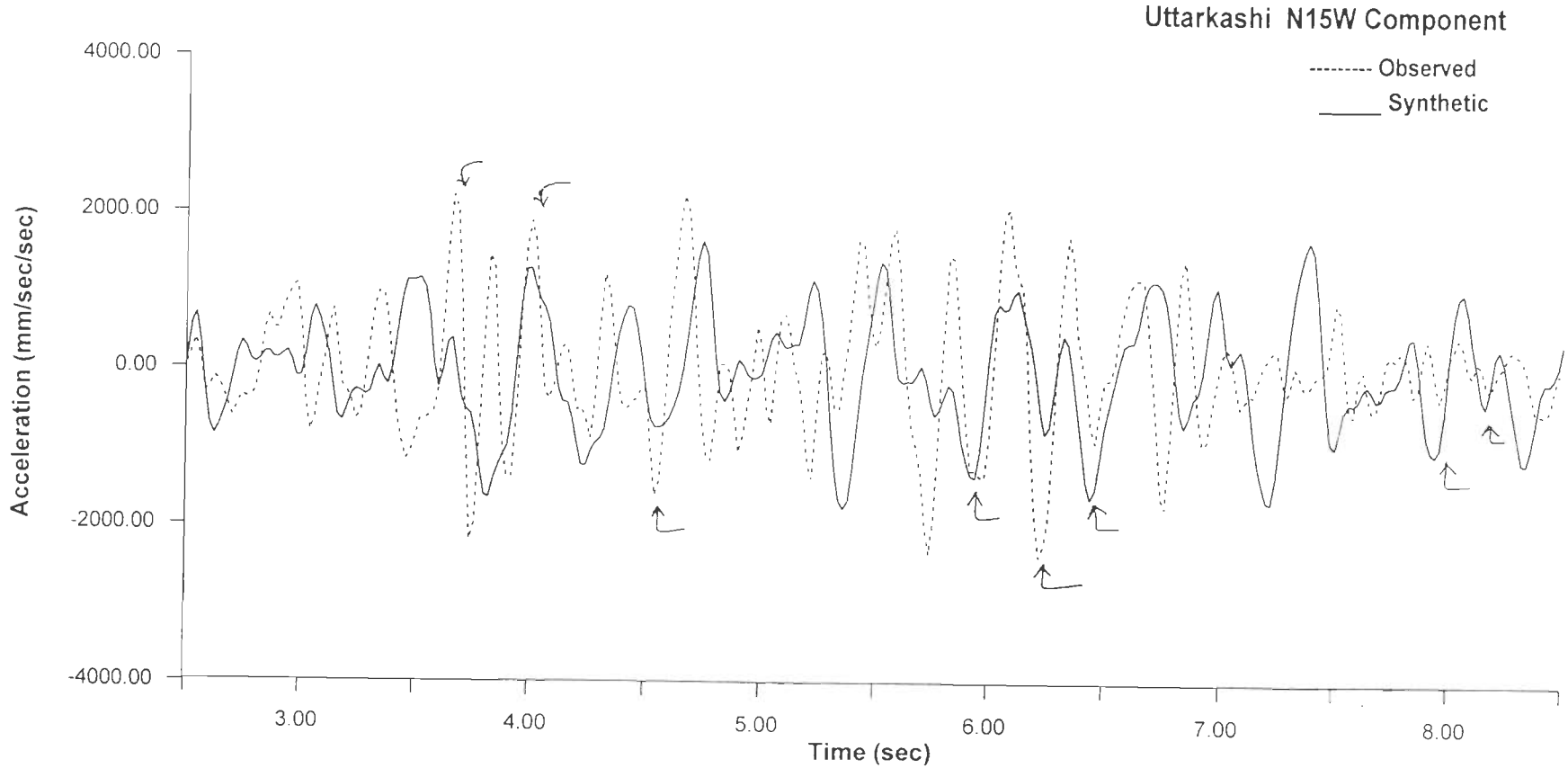

Fig. 4.8(b) : Synthetic accelerogram superimposed over the observed accelerogram for N15W component at Uttarkashi (Uttarkashi Earthquake)

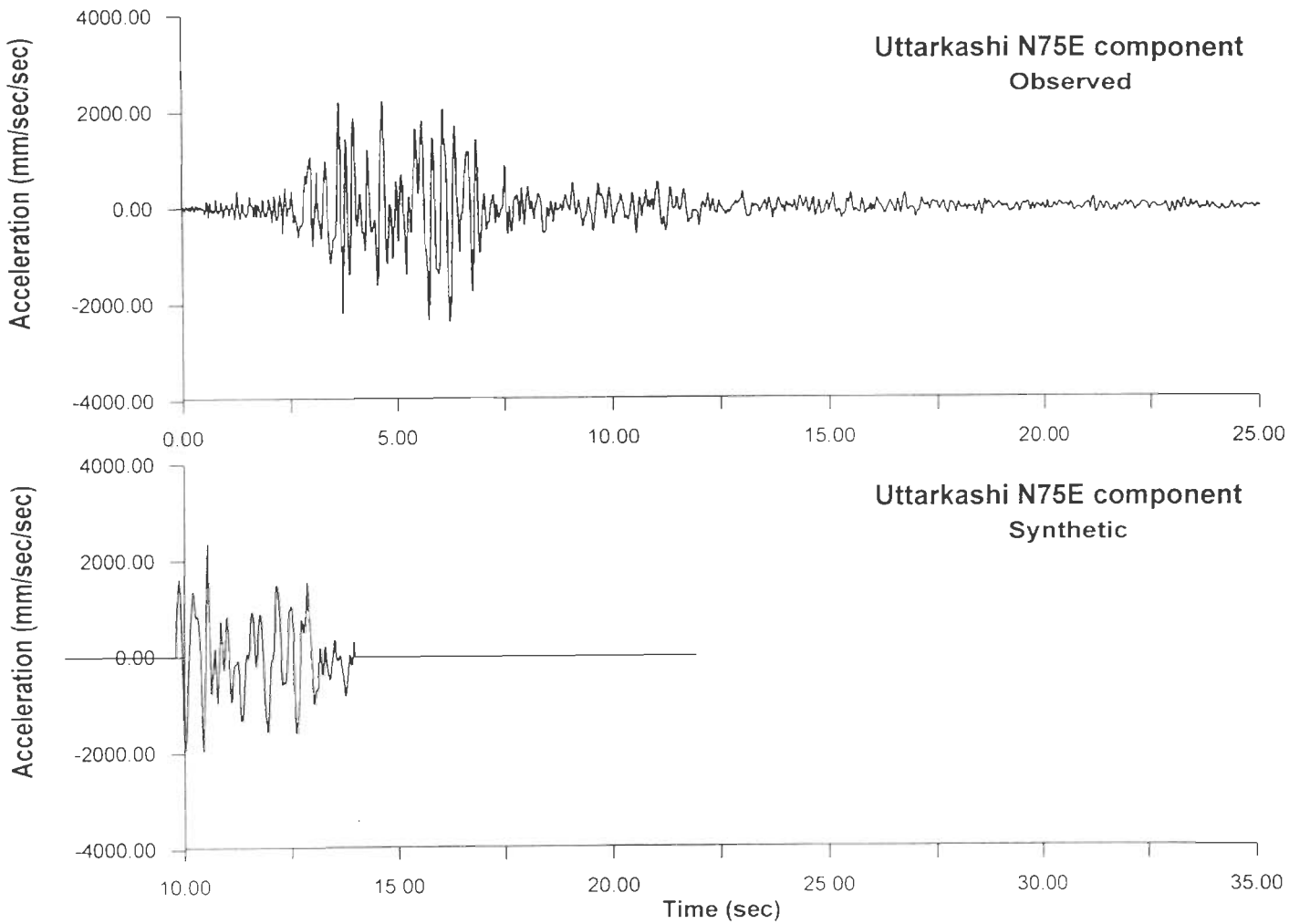

Fig. 4.8(c) : Observed and Synthetic accelerograms for N75E component at Uttarkashi (Uttarkashi Earthquake)

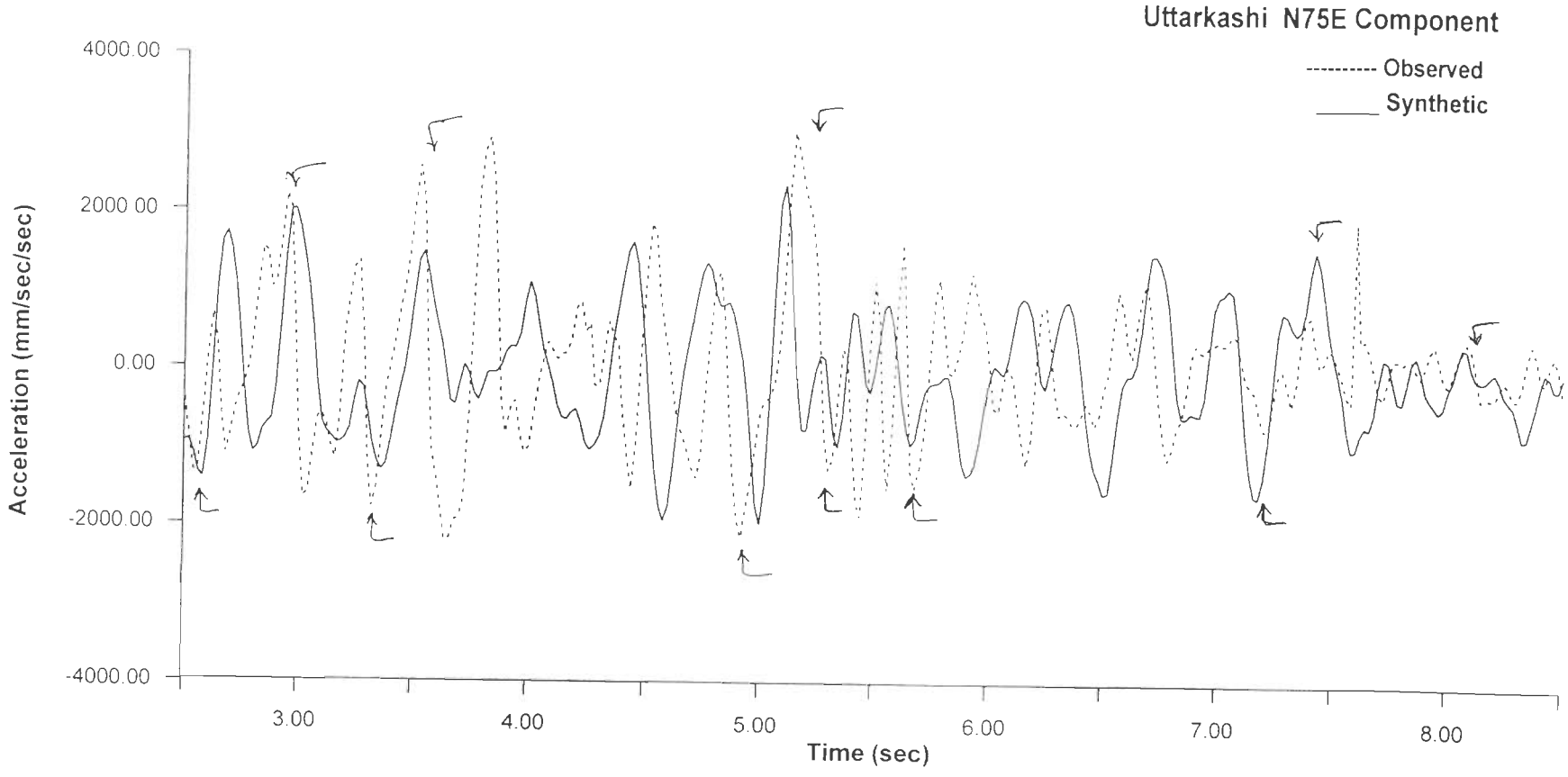

Fig. 4.8(d) : Synthetic accelerogram superimposed over the observed accelerogram for N75E component at Uttarkashi (Uttarkashi Earthquake)

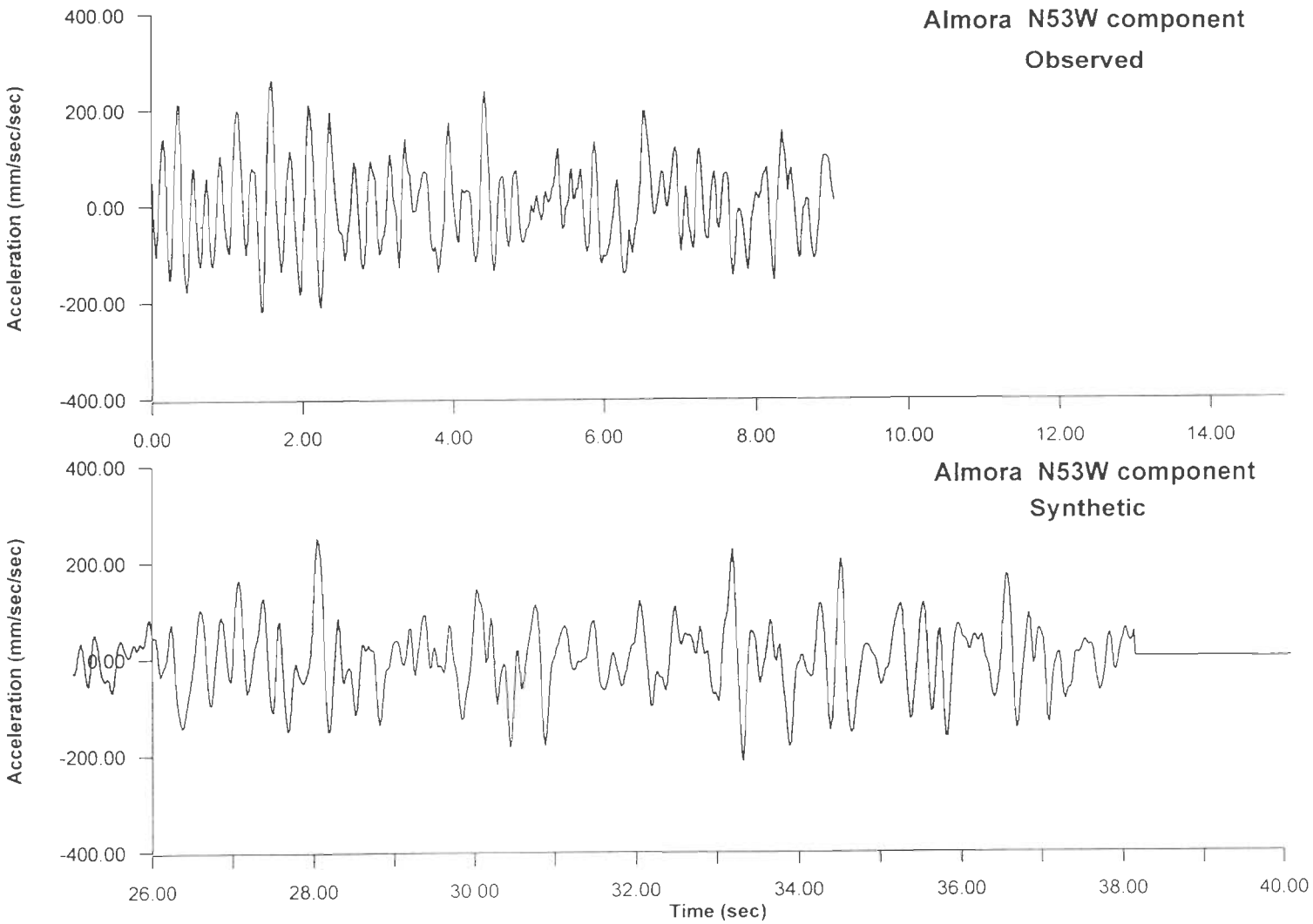

Fig. 4.9(a) : Observed and Synthetic accelerograms for N53W component at Almora (Chamoli Earthquake)

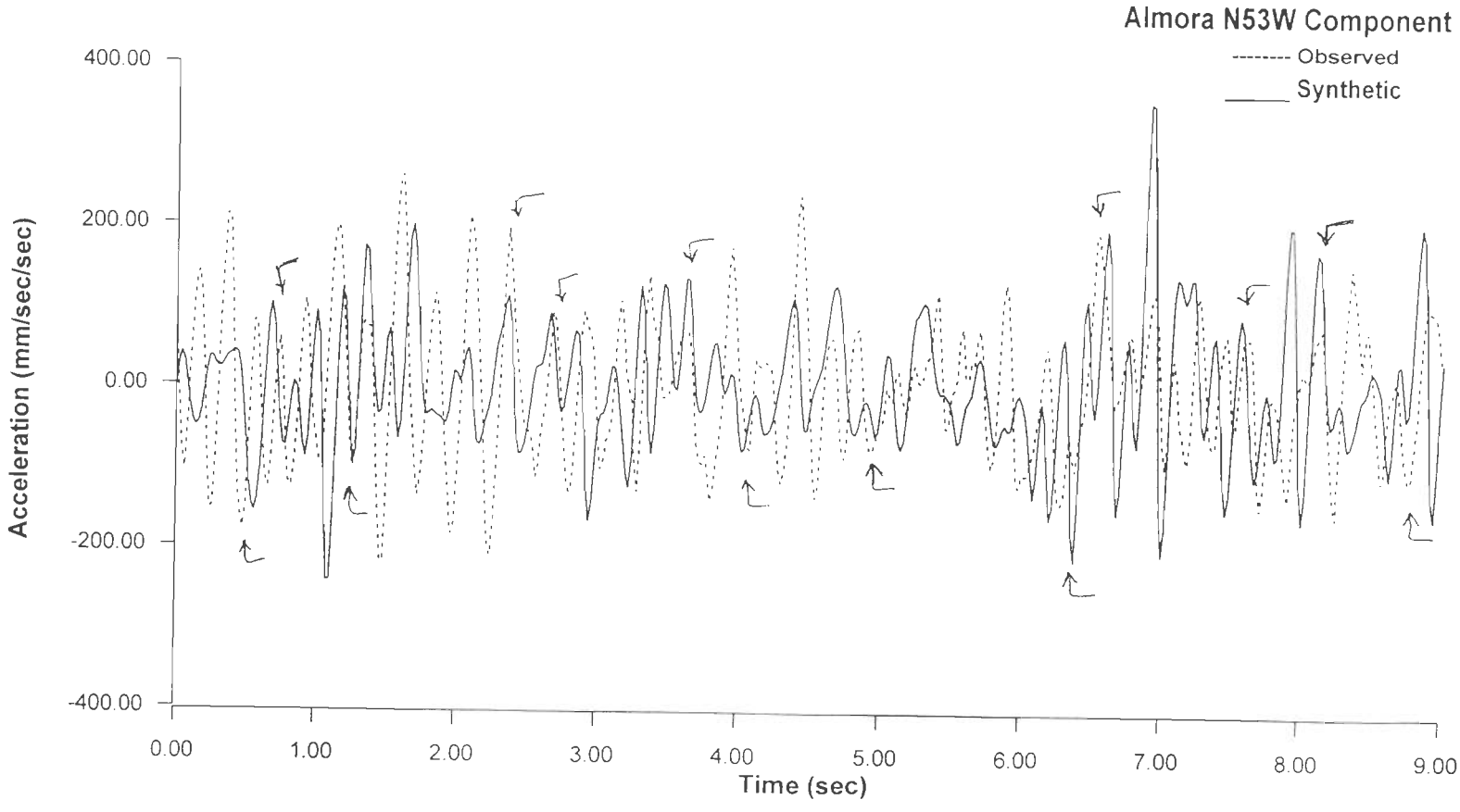

Fig. 4.9(b) : Synthetic accelerogram superimposed over the observed accelerogram for N53W component at Almora (Chamoli Earthquake)

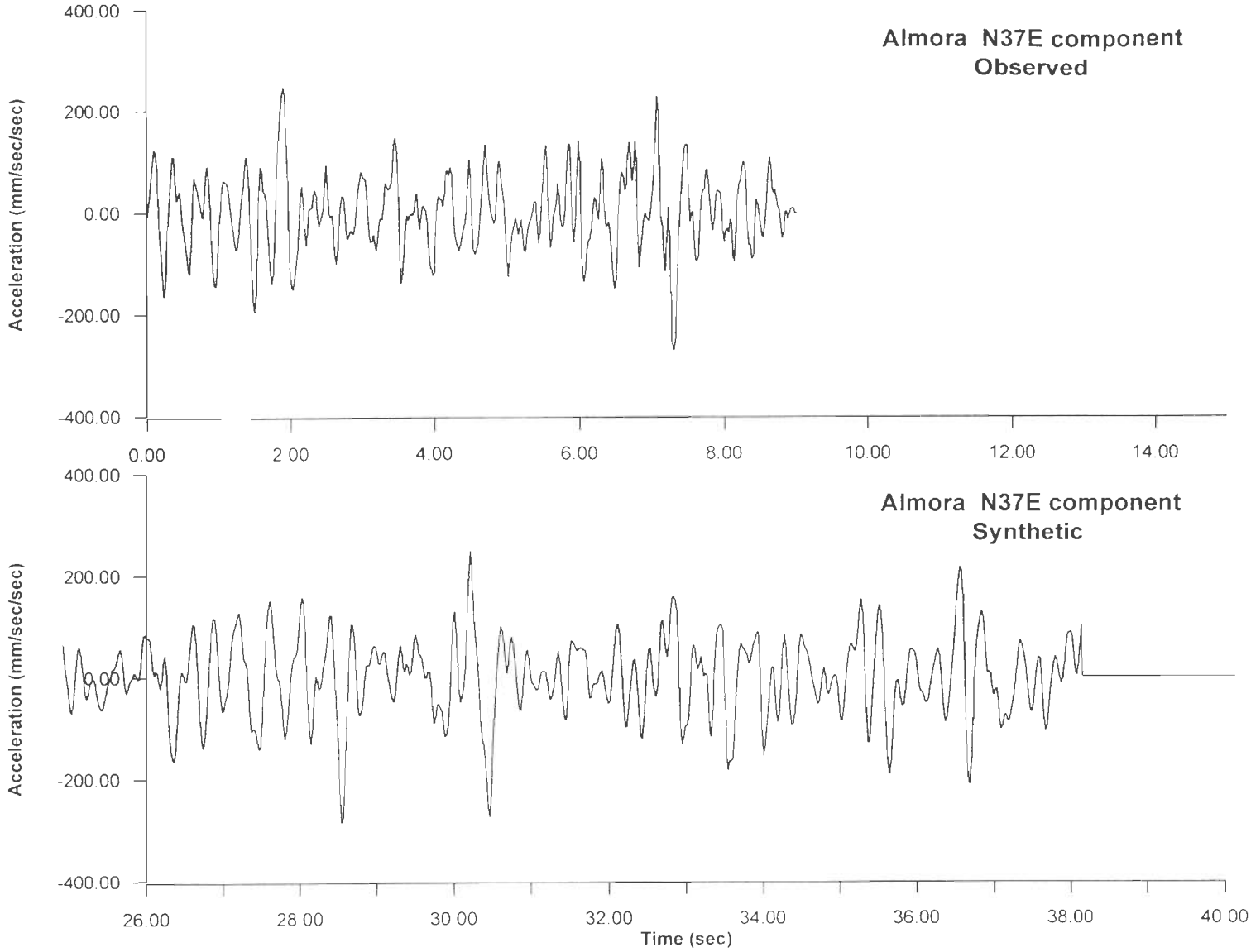

Fig. 4.9(c) : Observed and Synthetic accelerograms for N37E component at Almora (Chamoli Earthquake)

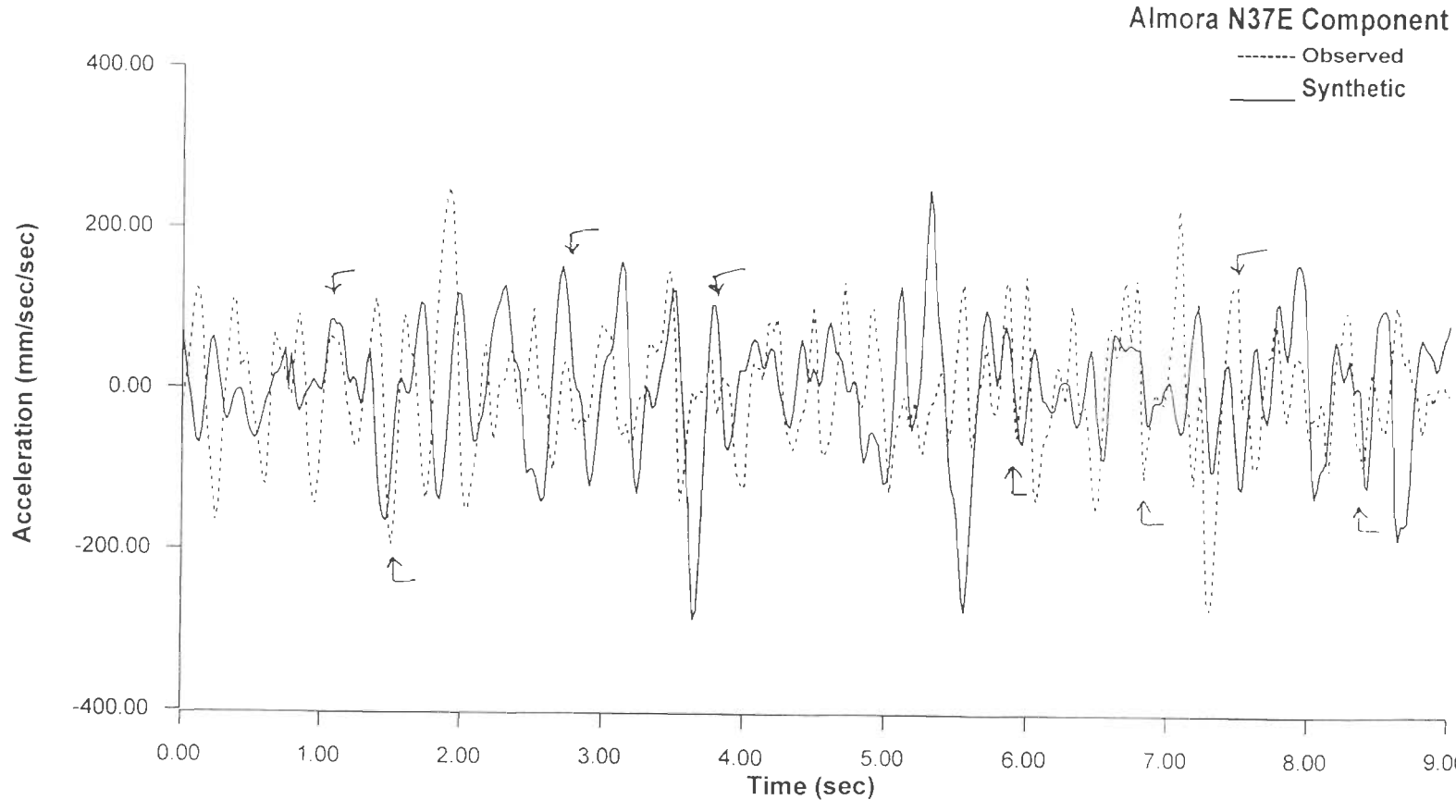

Fig. 4.9(d) : Synthetic accelerogram superimposed over the observed accelerogram for N37E component at Almora (Chamoli Earthquake)

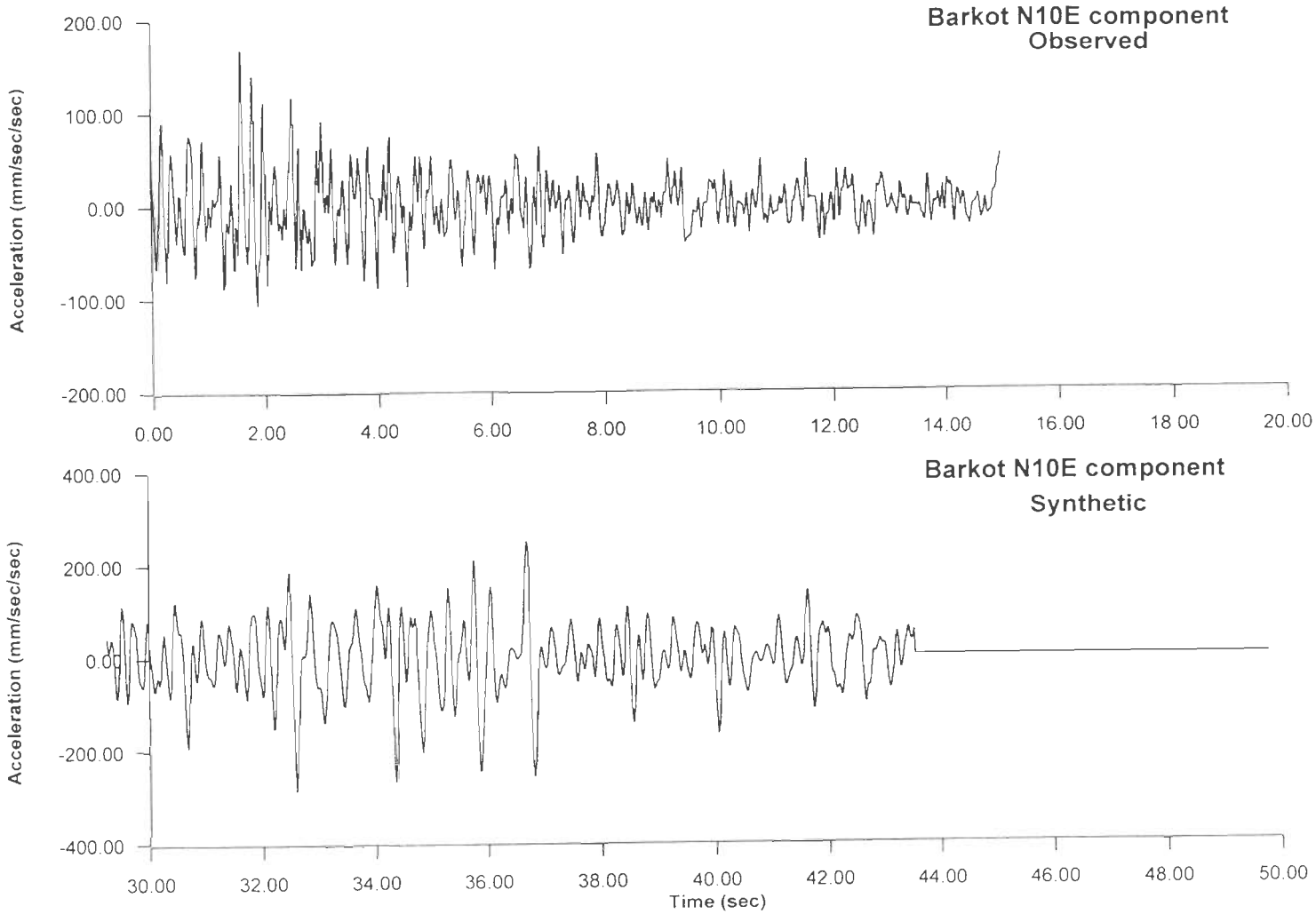

Fig. 4.10(a) : Observed and Synthetic accelerograms for N10E component at Barkot (Chamoli Earthquake)

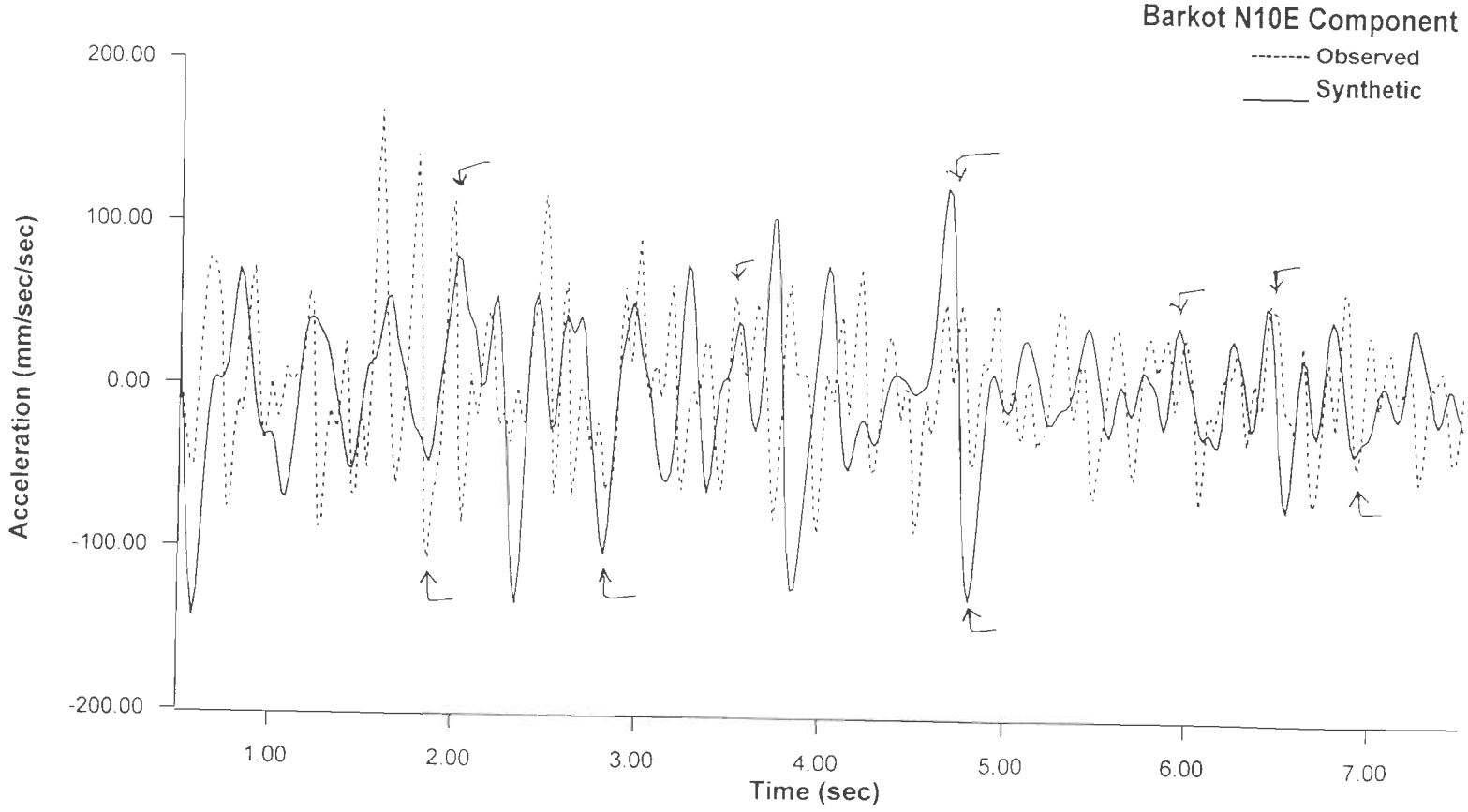

Fig. 4.10(b) : Synthetic accelerogram superimposed over the observed accelerogram for N10E component at Barkot (Chamoli Earthquake)

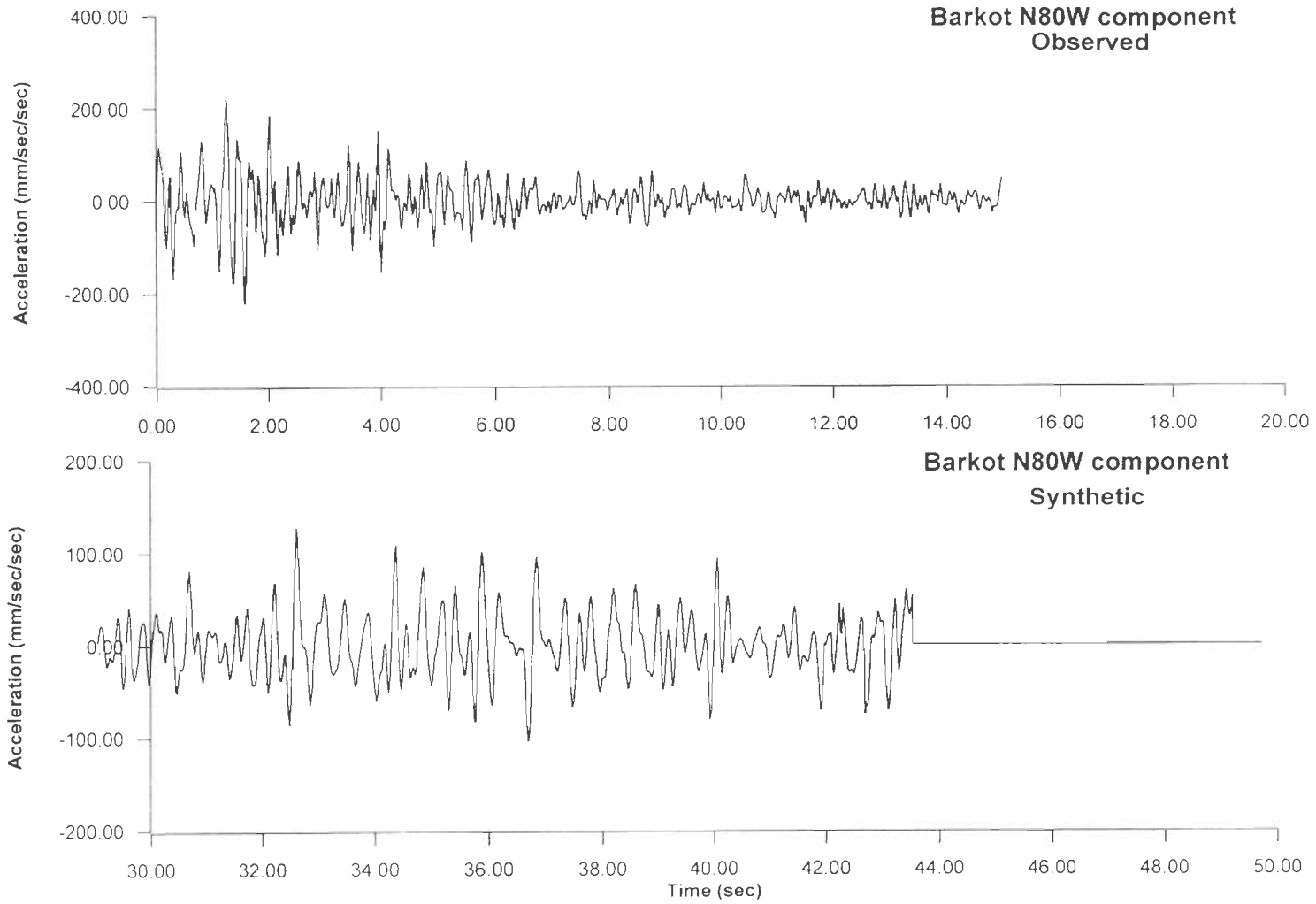

Fig. 4.10(c) : Observed and Synthetic accelerograms for N80W component at Barkot (Chamoli Earthquake)

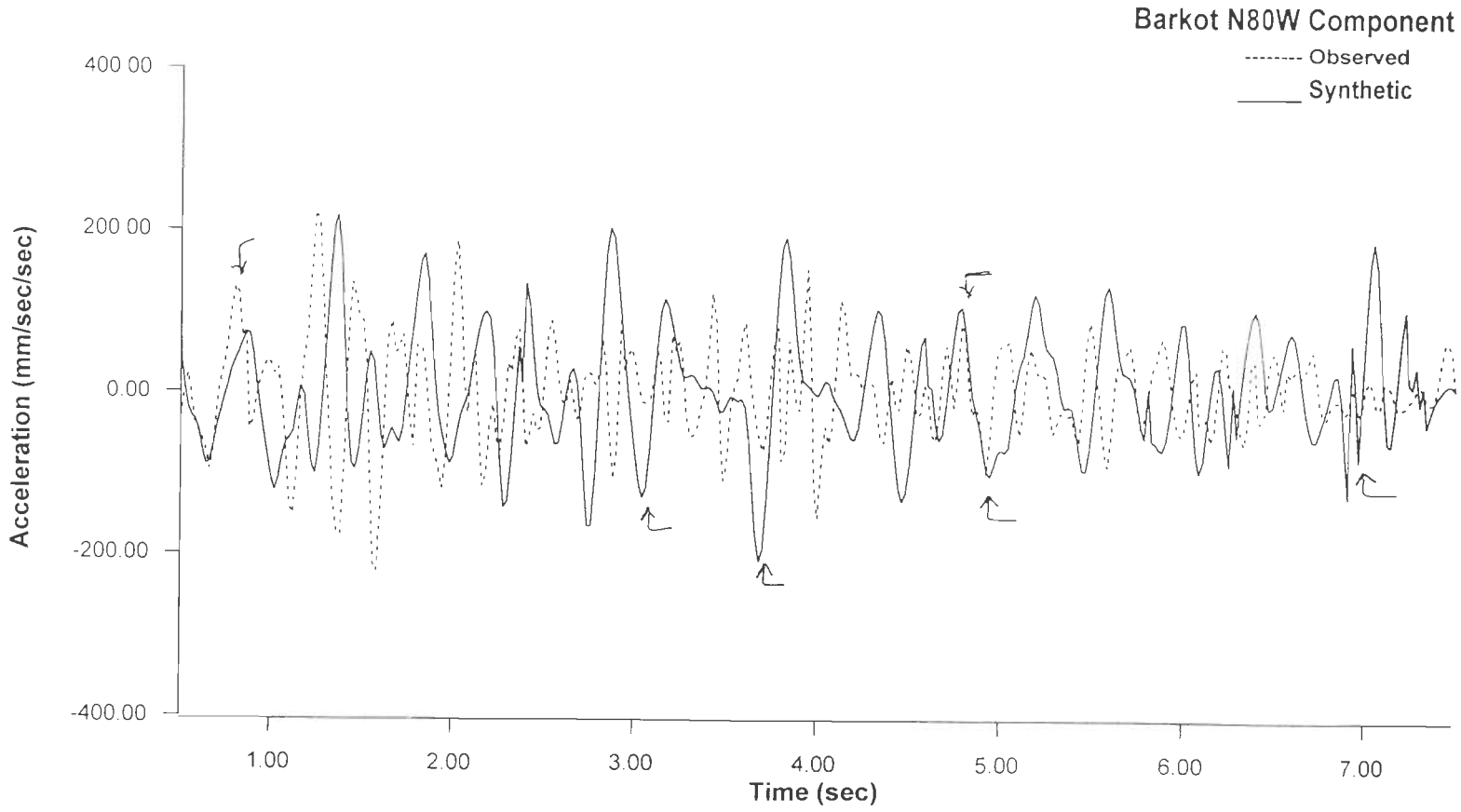

Fig. 4.10(d) : Synthetic accelerogram superimposed over the observed accelerogram for N80W component at Barkot (Chamoli Earthquake)

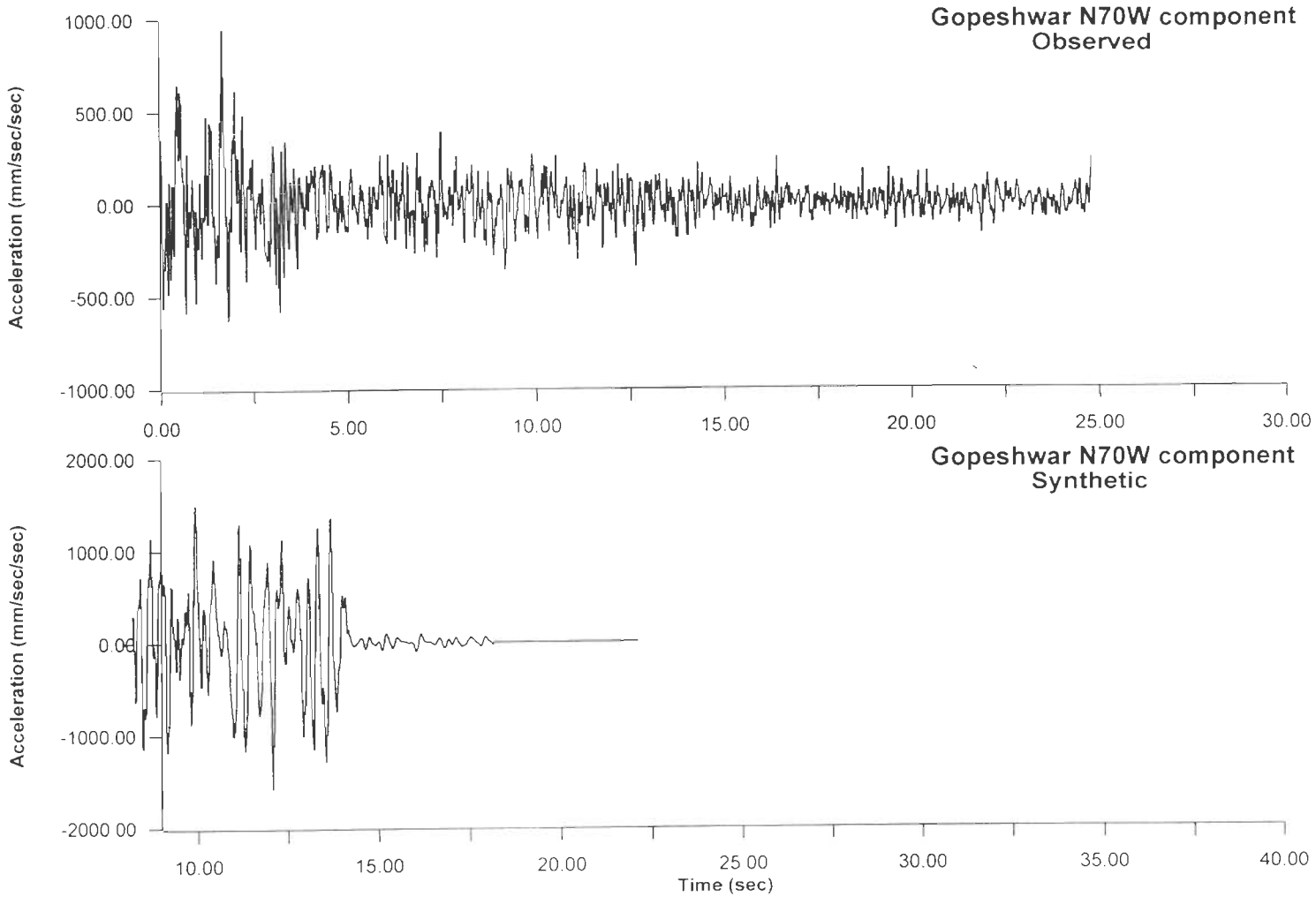

Fig. 4.11(a) : Observed and Synthetic accelerograms for N70W component at Gopeshwar (Chamoli Earthquake)

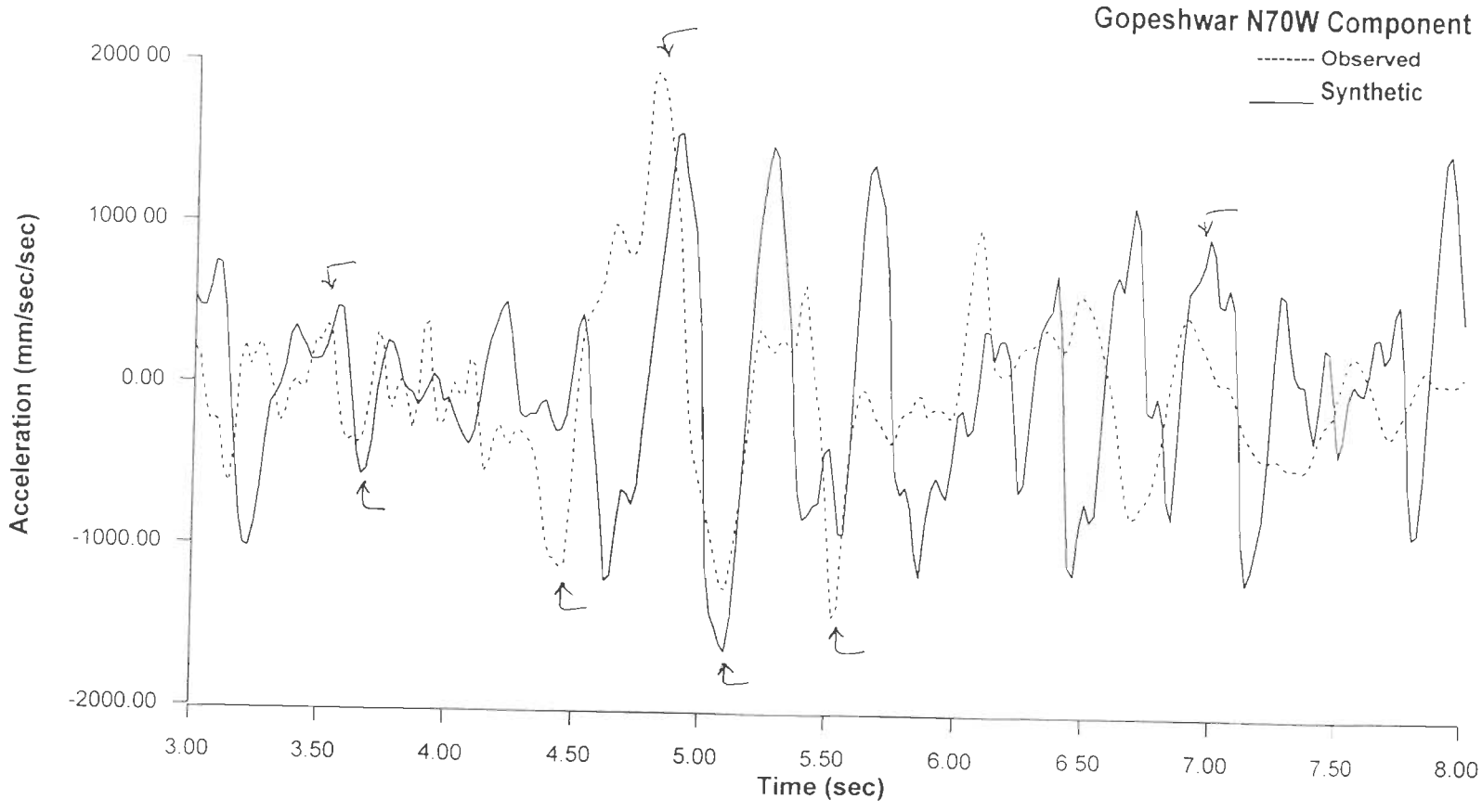

Fig. 4.11(b) : Synthetic accelerogram superimposed over the observed accelerogram for N70W component at Gopeshwar (Chamoli Earthquake)

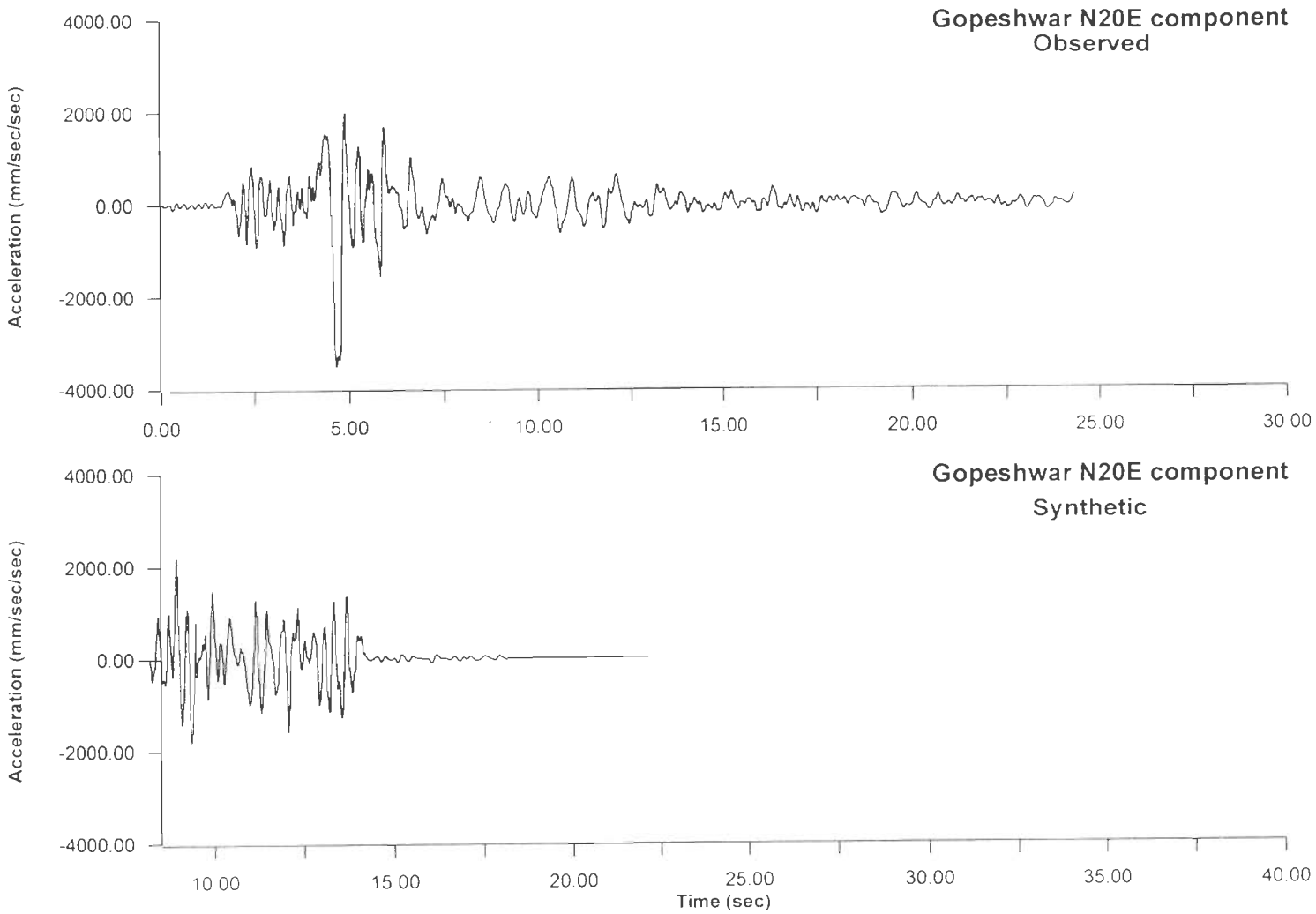

Fig. 4.11(c) : Observed and Synthetic accelerograms for N20E component at Gopeshwar (Chamoli Earthquake)

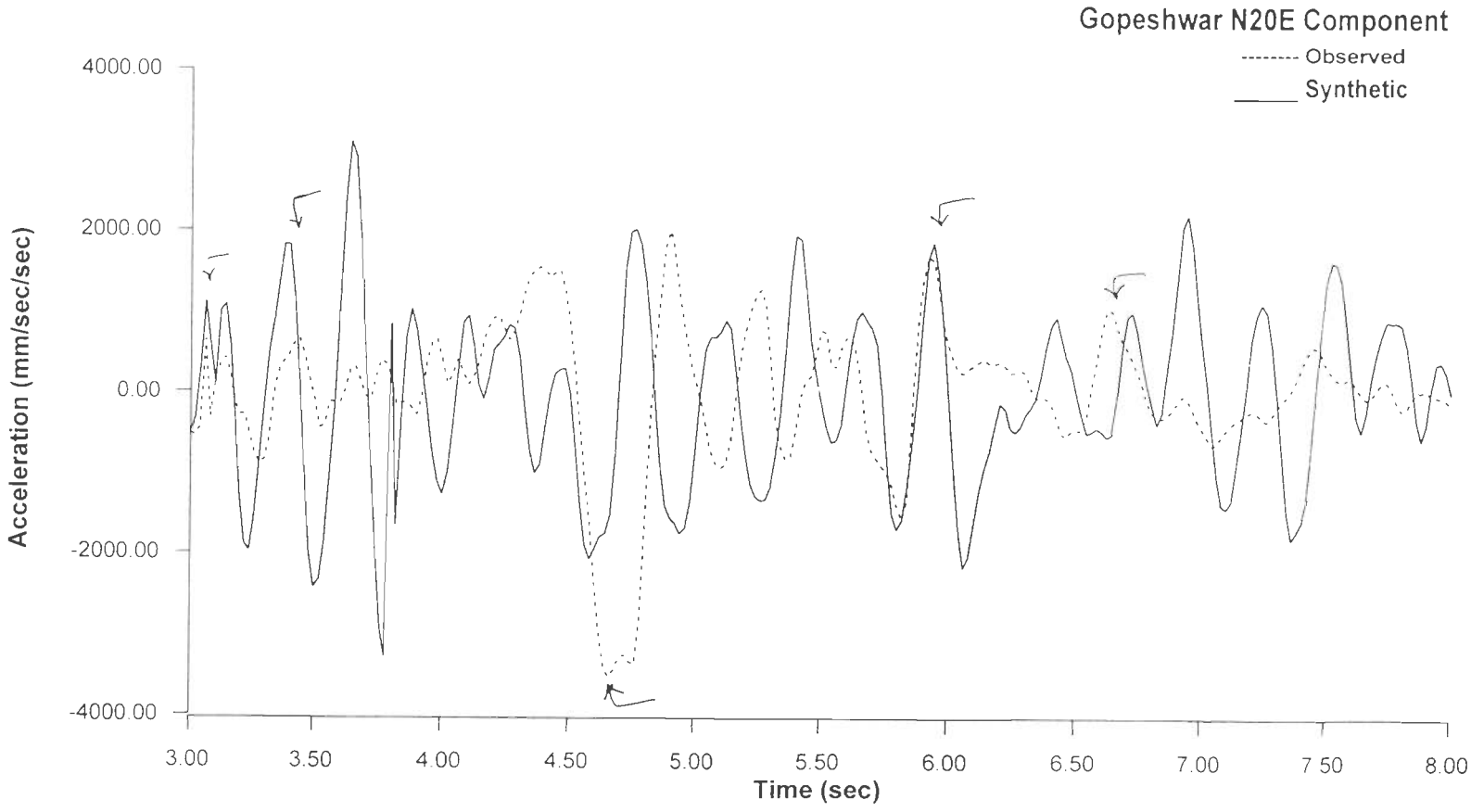

Fig. 4.11(d) : Synthetic accelerogram superimposed over the observed accelerogram for N20E component at Gopeshwar (Chamoli Earthquake)

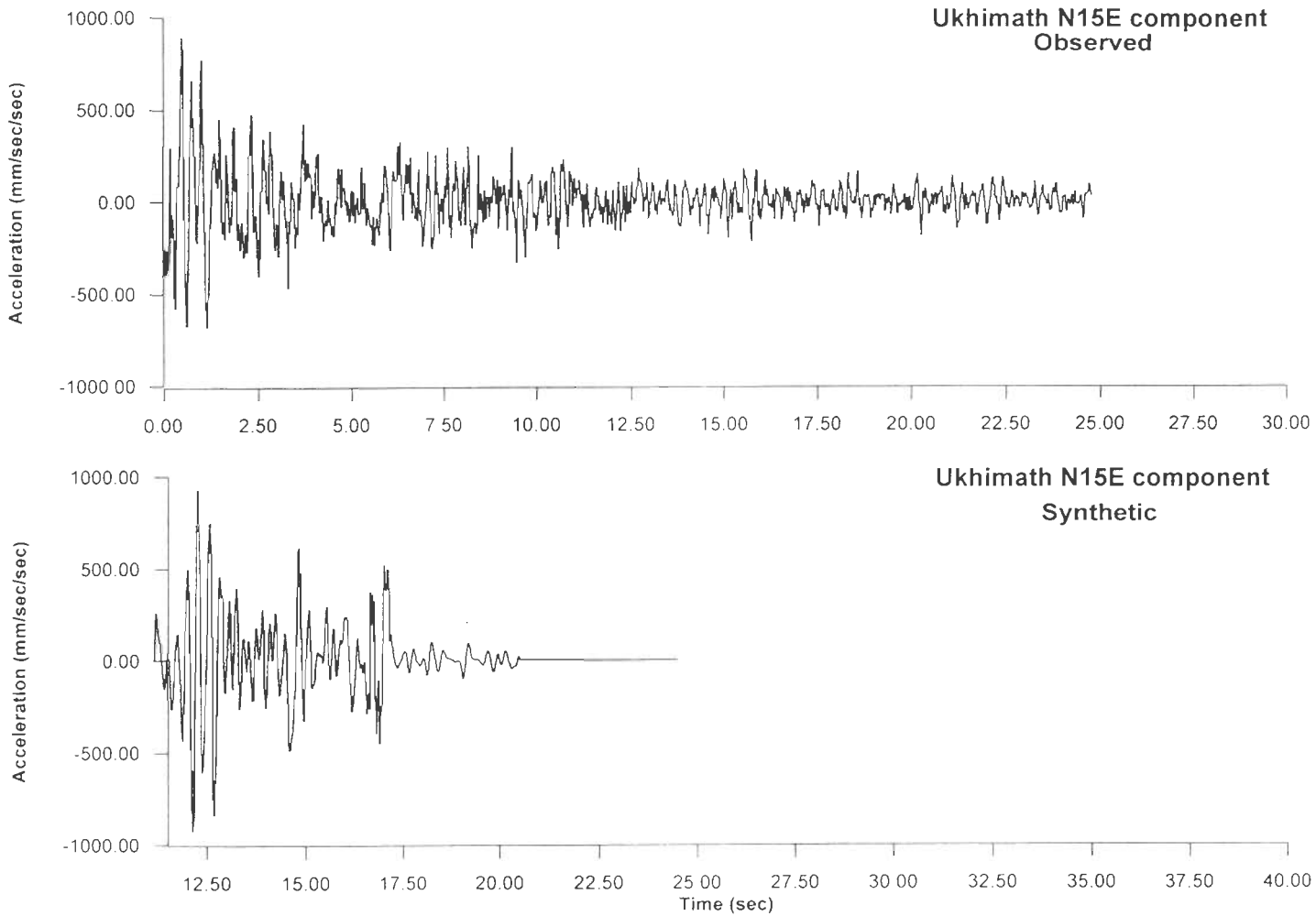

Fig. 4.12(a) : Observed and Synthetic accelerograms for N15E component at Ukhimath (Chamoli Earthquake)

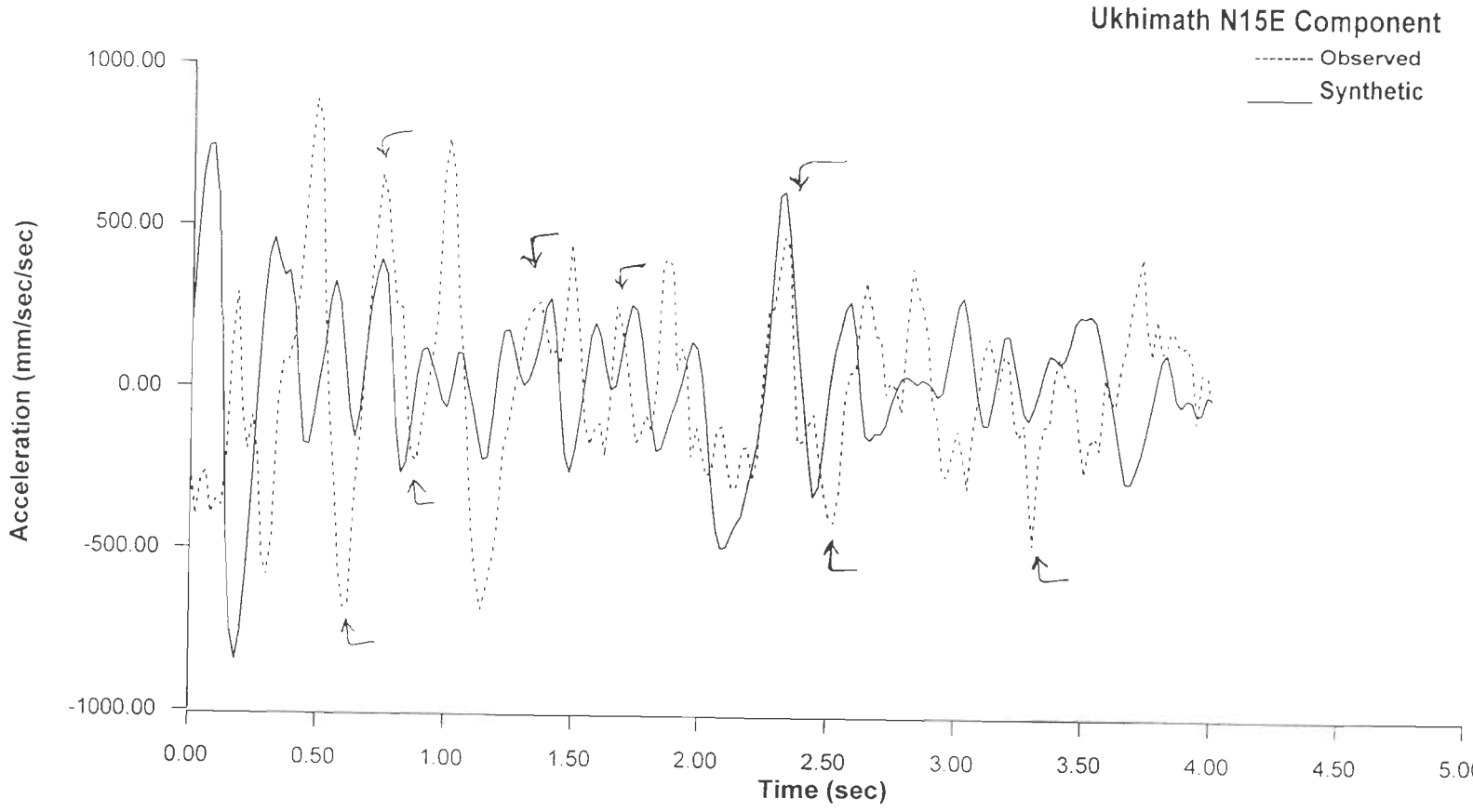

Fig. 4.12(b) : Synthetic accelerogram superimposed over the observed accelerogram for N15E component at Ukhimath (Chamoli Earthquake)

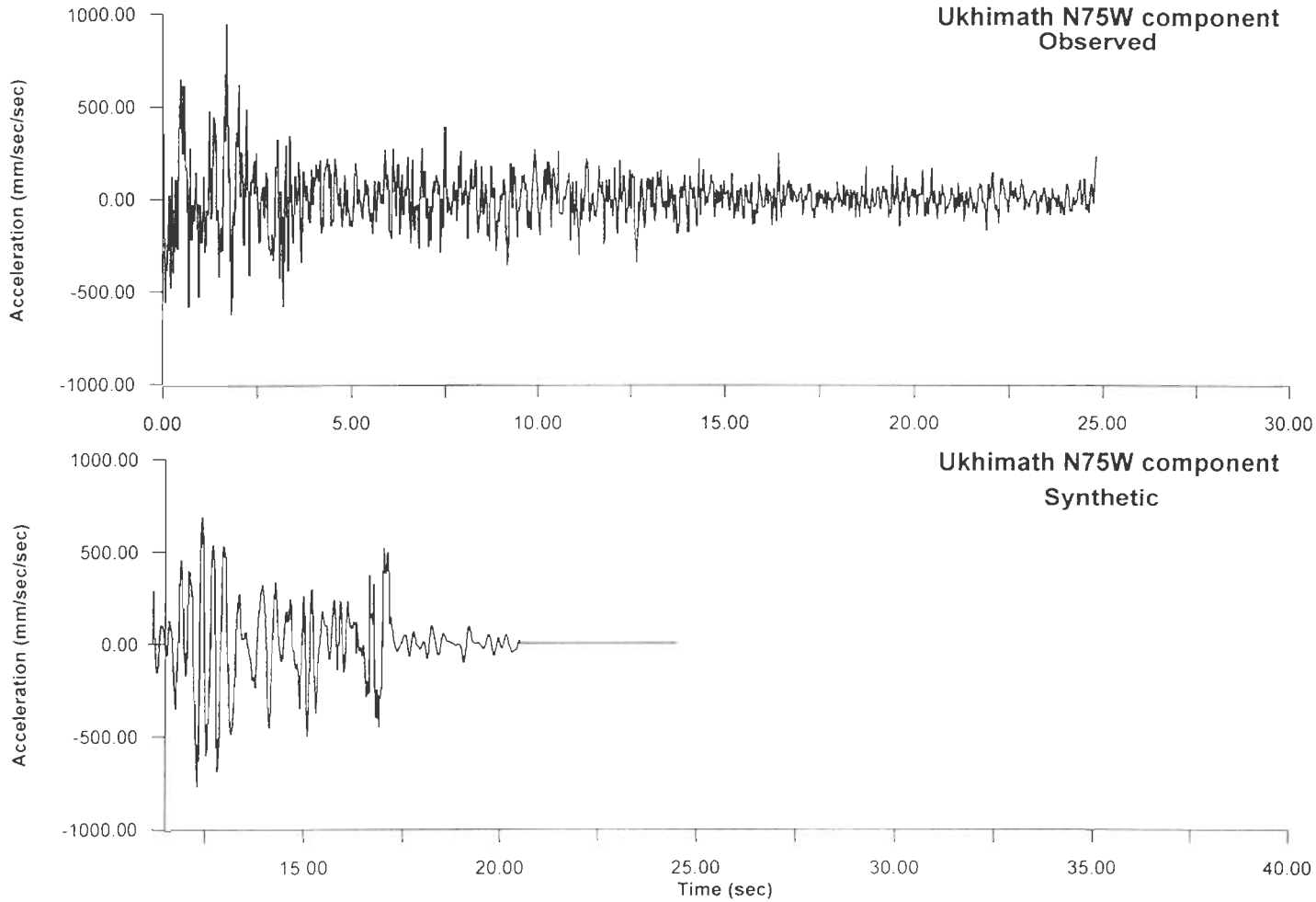

Fig. 4.12(c) : Observed and Synthetic accelerograms for N75W component at Ukhimath (Chamoli Earthquake)

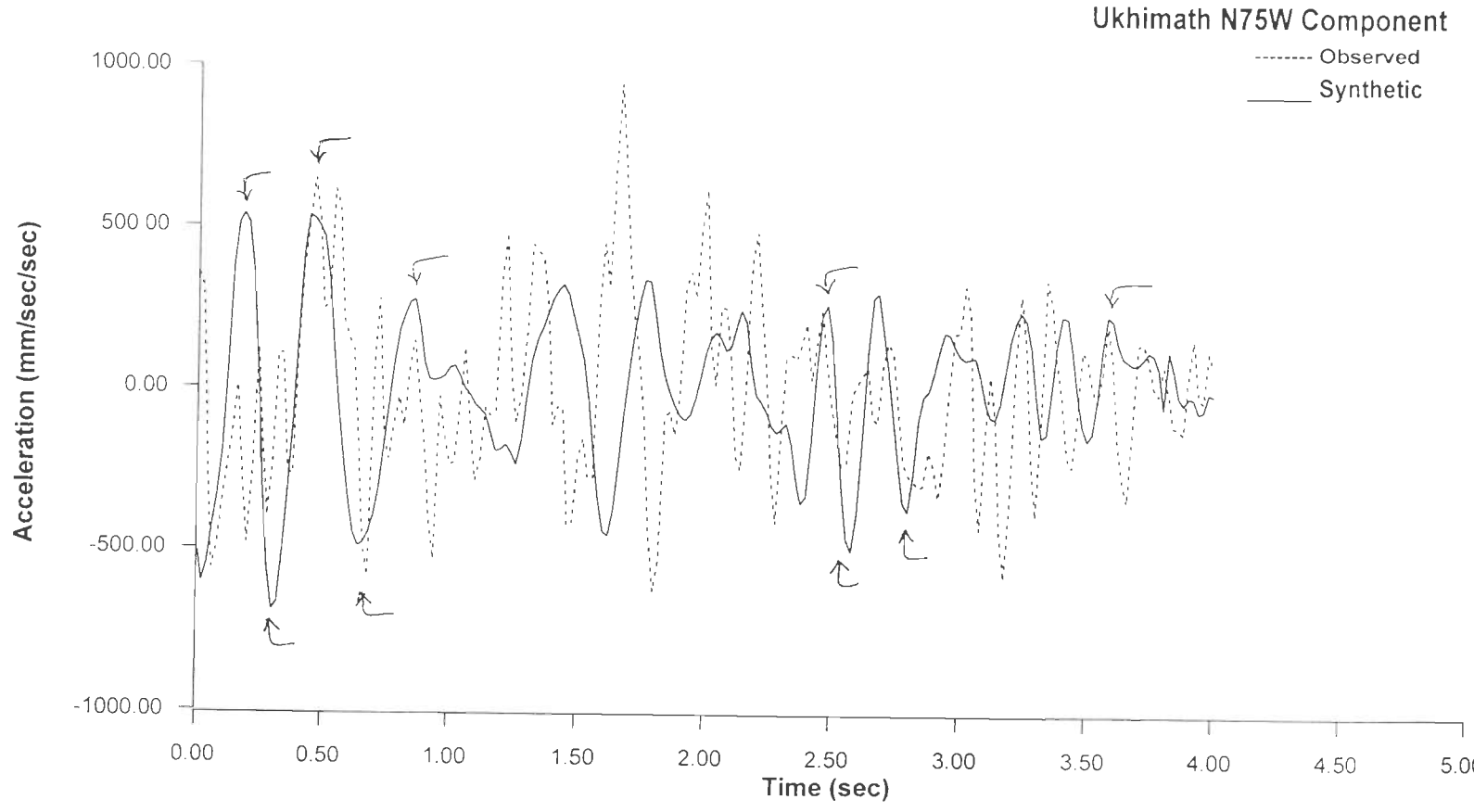

Fig. 4.12(d) : Synthetic accelerogram superimposed over the observed accelerogram for N75W component at Ukhimath (Chamoli Earthquake)

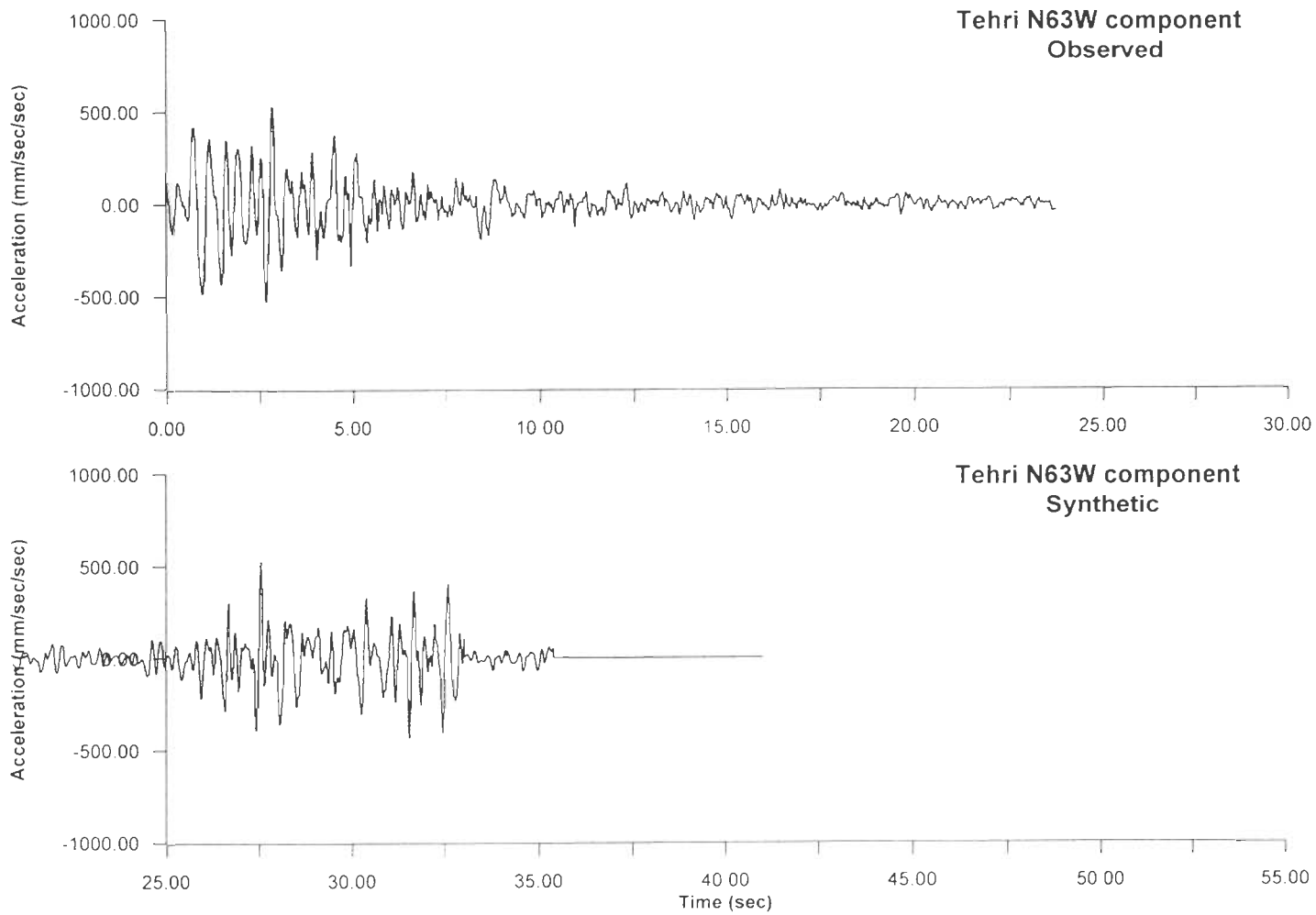

Fig. 4.13(a) : Observed and Synthetic accelerograms for N63W component at Tehri (Chamoli Earthquake)

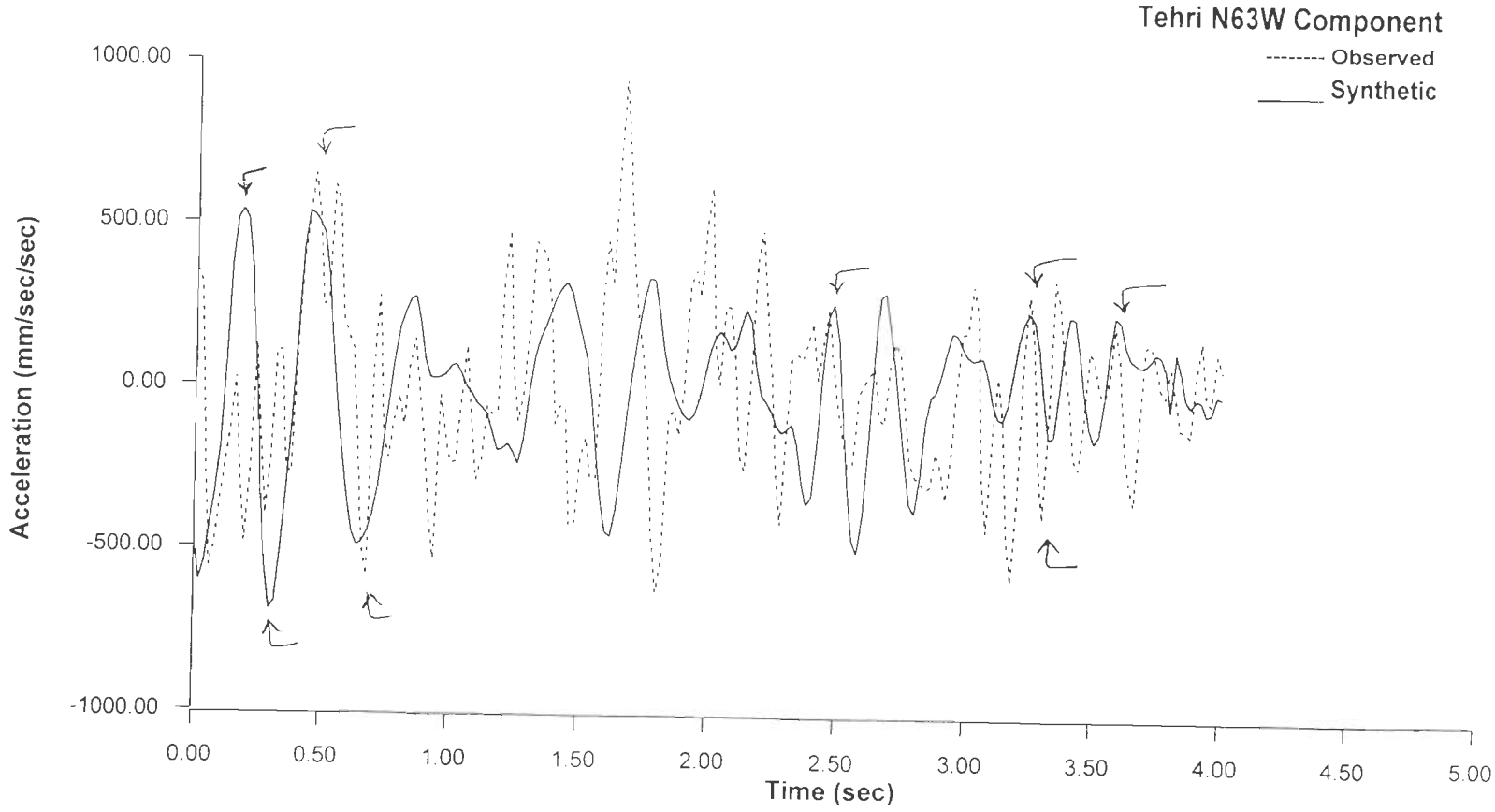

Fig. 4.13(b) : Synthetic accelerogram superimposed over the observed accelerogram for N63W component at Tehri (Chamoli Earthquake)

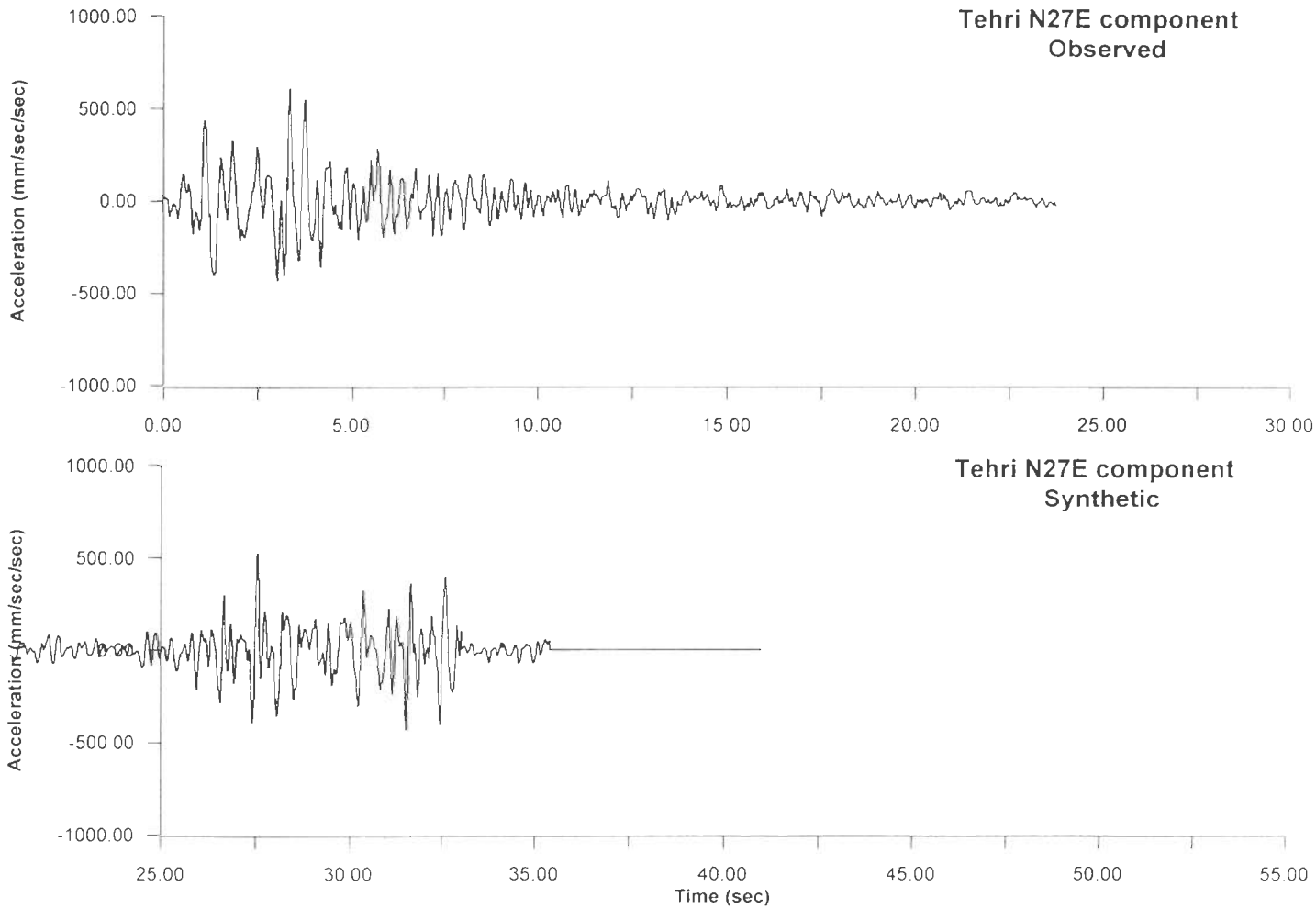

Fig. 4.13(c) : Observed and Synthetic accelerograms for N27E component at Tehri (Chamoli Earthquake)

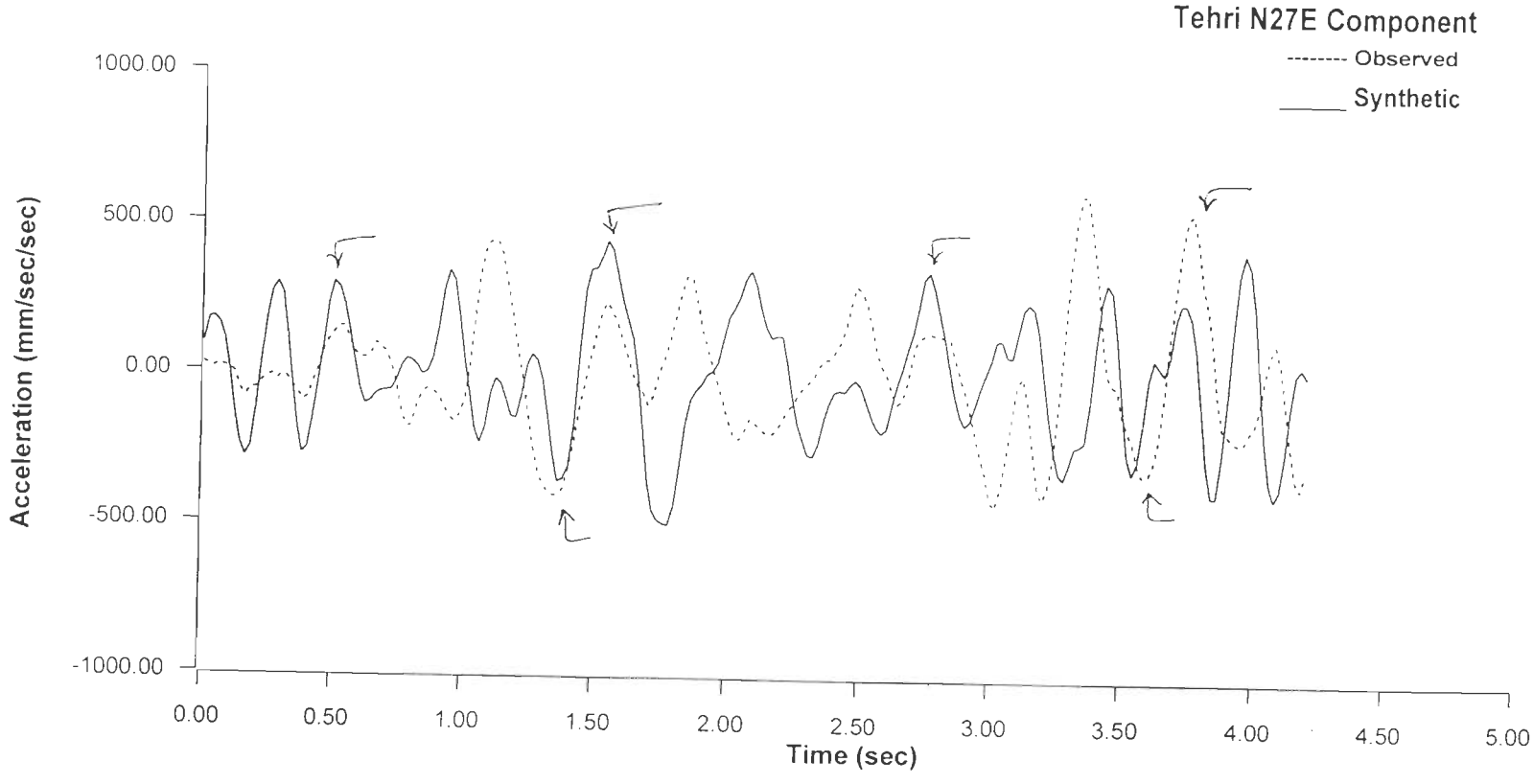

Fig. 4.13(d) : Synthetic accelerogram superimposed over the observed accelerogram for N27E component at Tehri (Chamoli Earthquake)

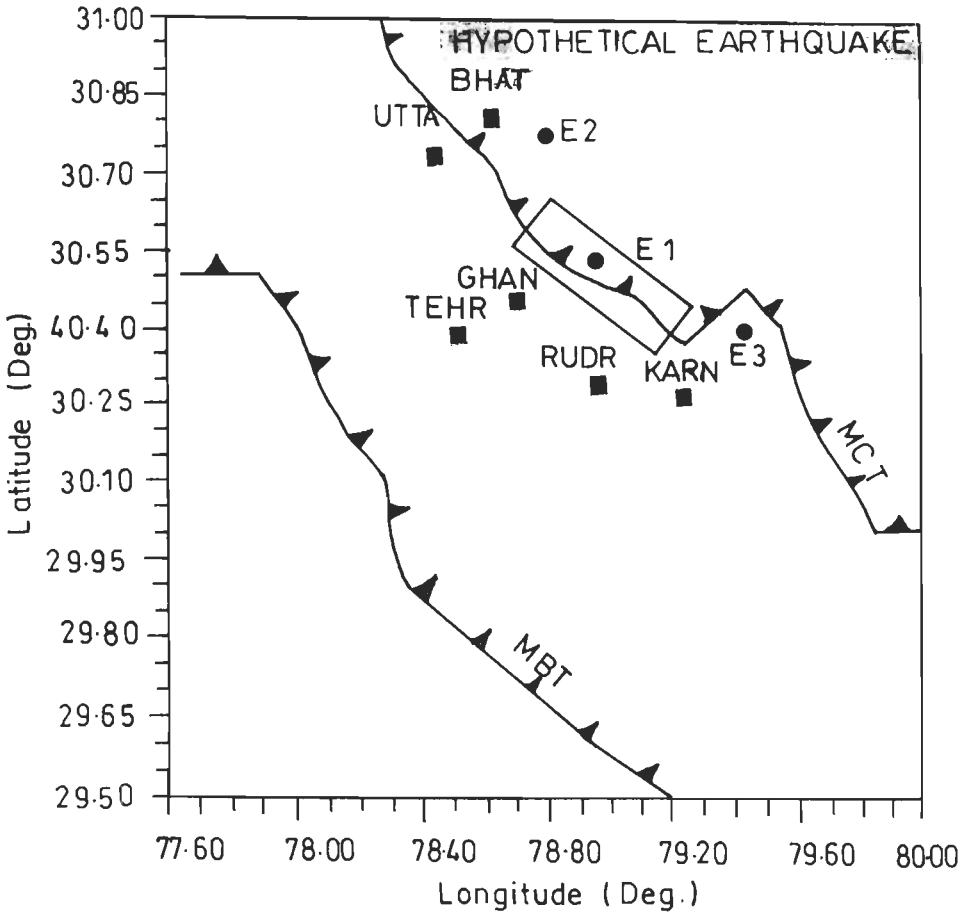

E1 : epicentre (Hypothetical earthquake)
E2 : epicentre (Uttarkashi earthquake)
E3 : epicentre (Chamoli earthquake)

Fig. 4.14 : Location of the epicentre and recording stations of hypothetical earthquake

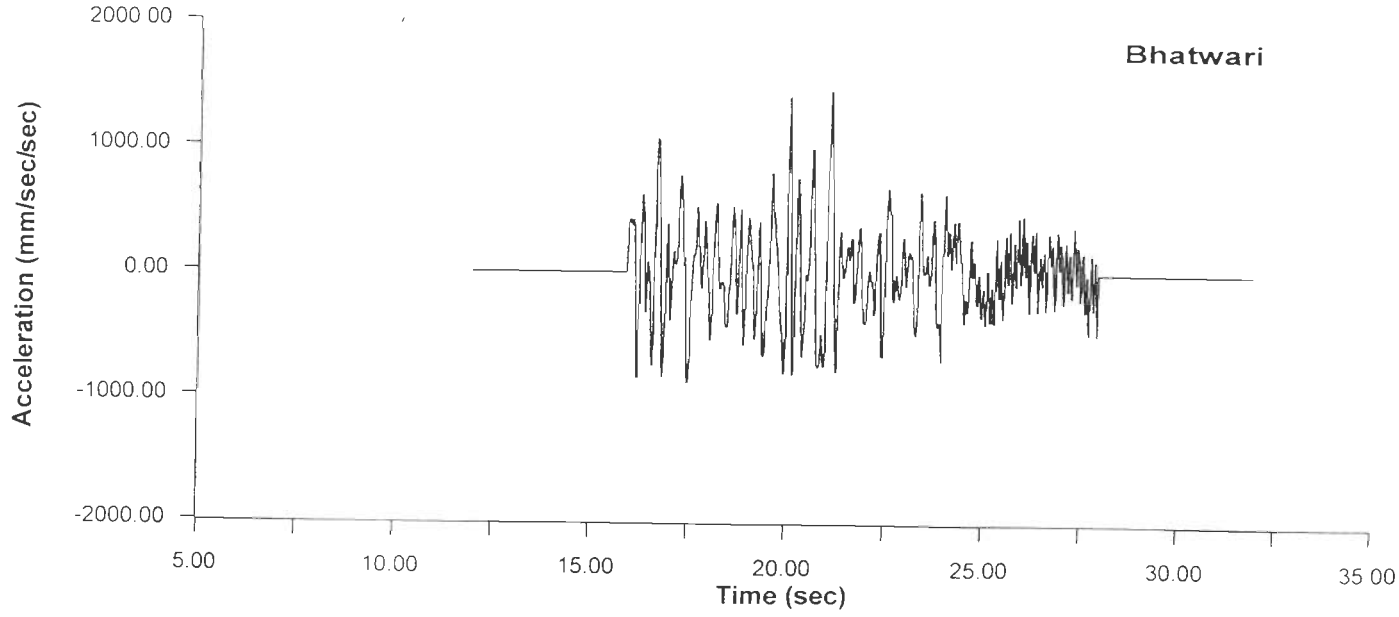

Fig. 4.15 : Synthetic accelerogram for one horizontal component at Bhatwari (Hypothetical earthquake)

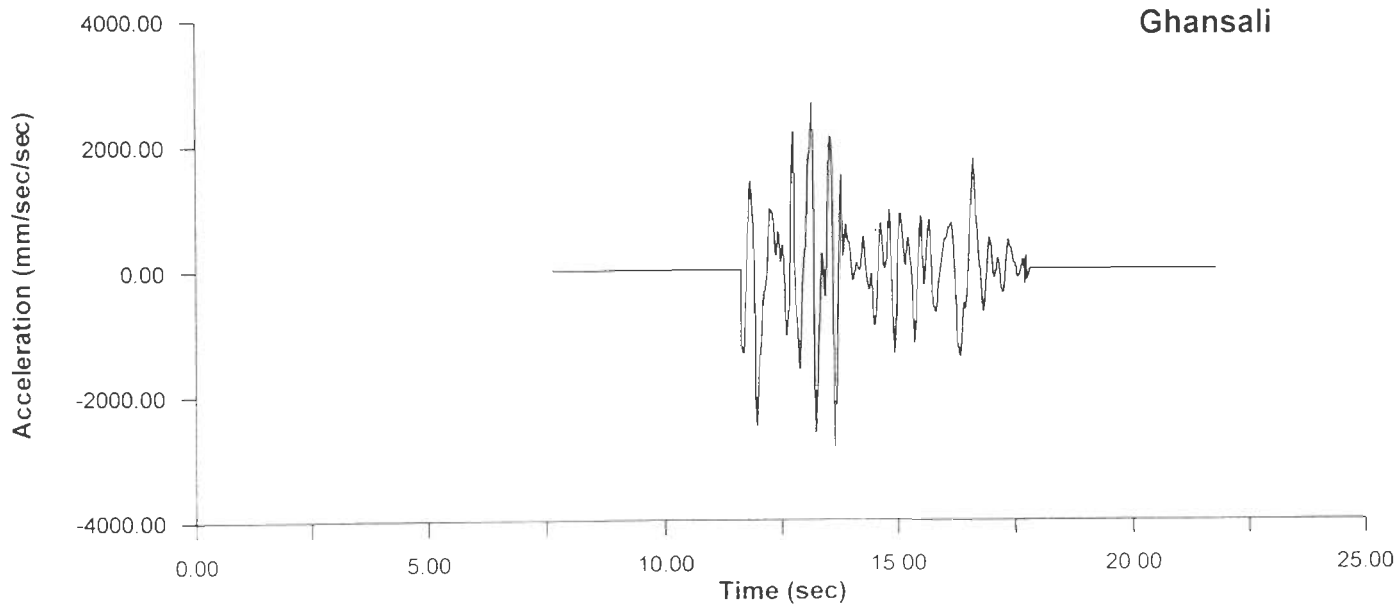

Fig. 4.16 : Synthetic accelerogram for one horizontal component at Ghansali (Hypothetical earthquake)

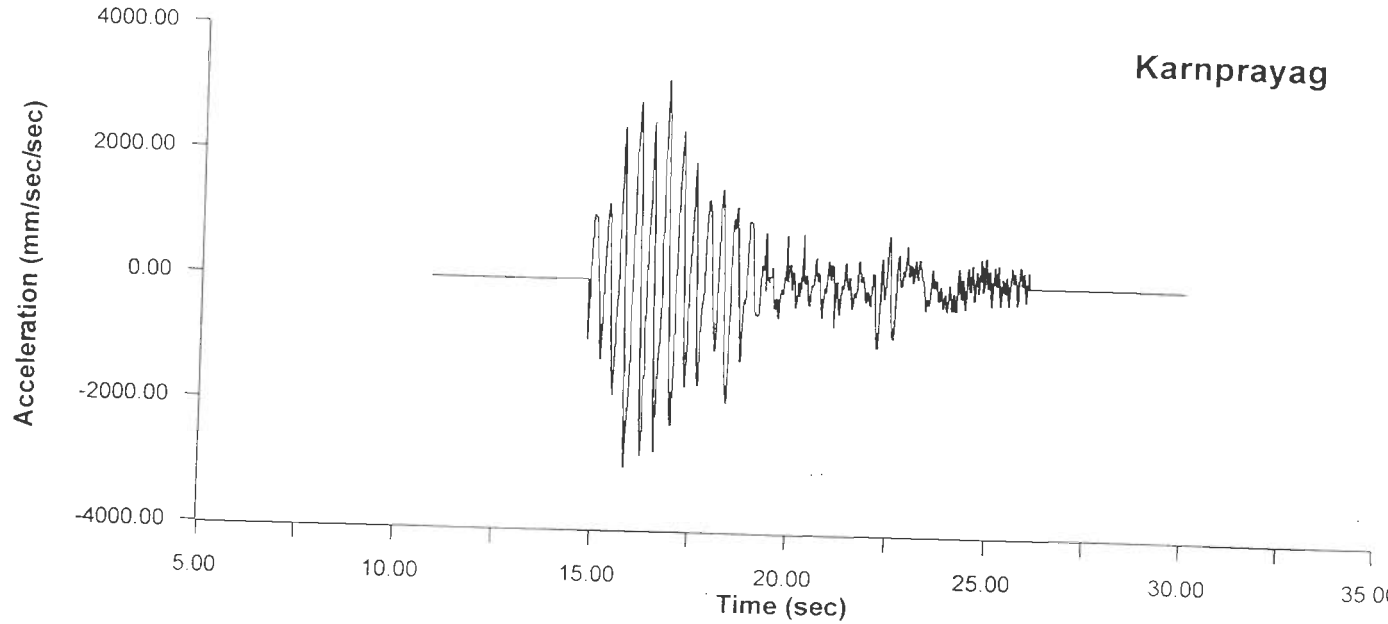

Fig. 4.17 : Synthetic accelerogram for one horizontal component at Karnprayag (Hypothetical earthquake)

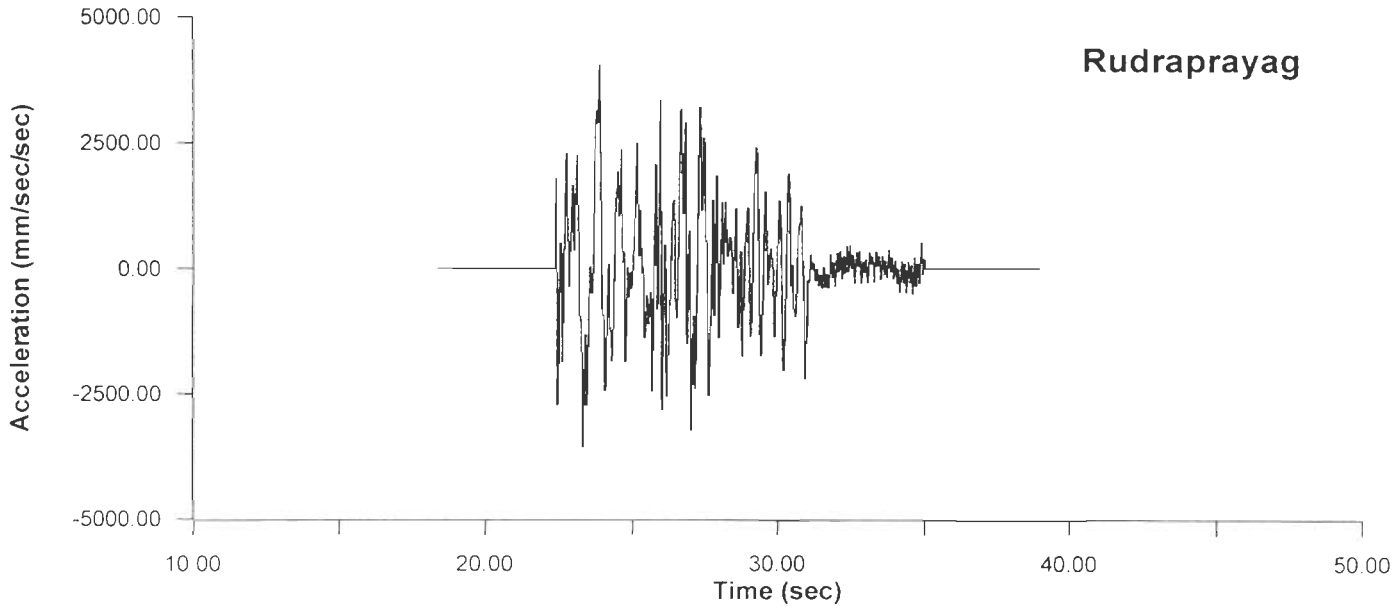

Fig. 4.18 : Synthetic accelerogram for one horizontal component at Rudraprayag (Hypothetical earthquake)

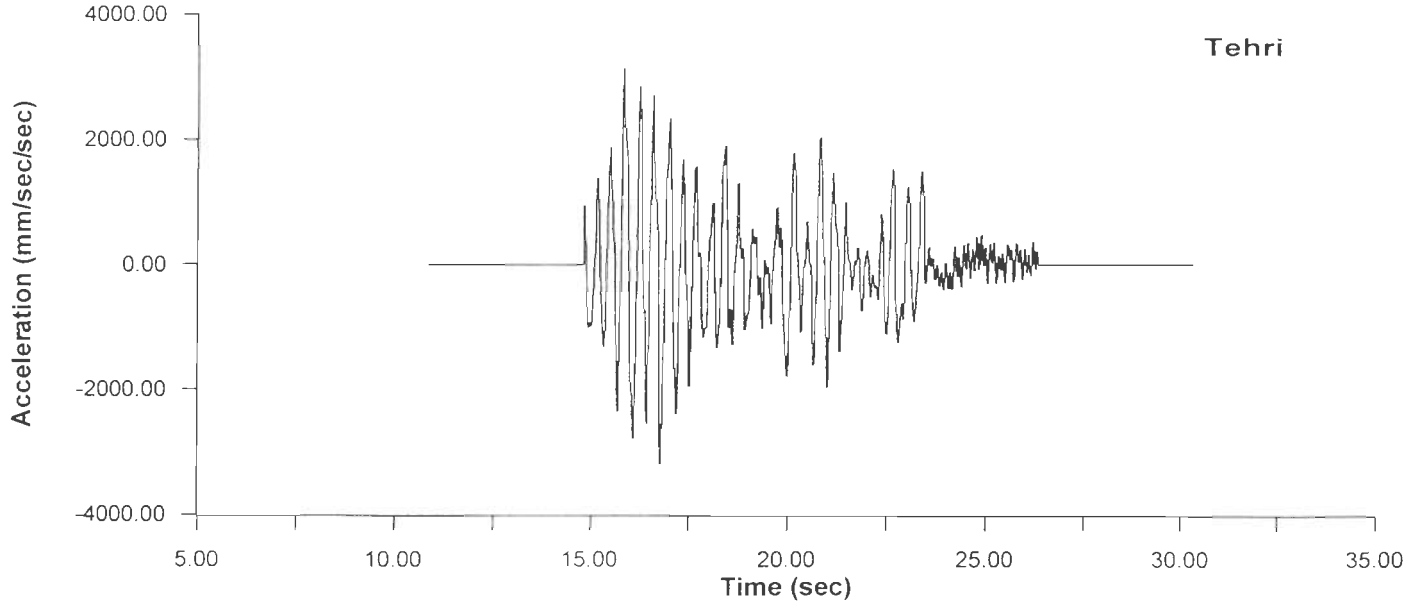

Fig. 4.19 : Synthetic accelerogram for one horizontal component at Tehri (Hypothetical earthquake)

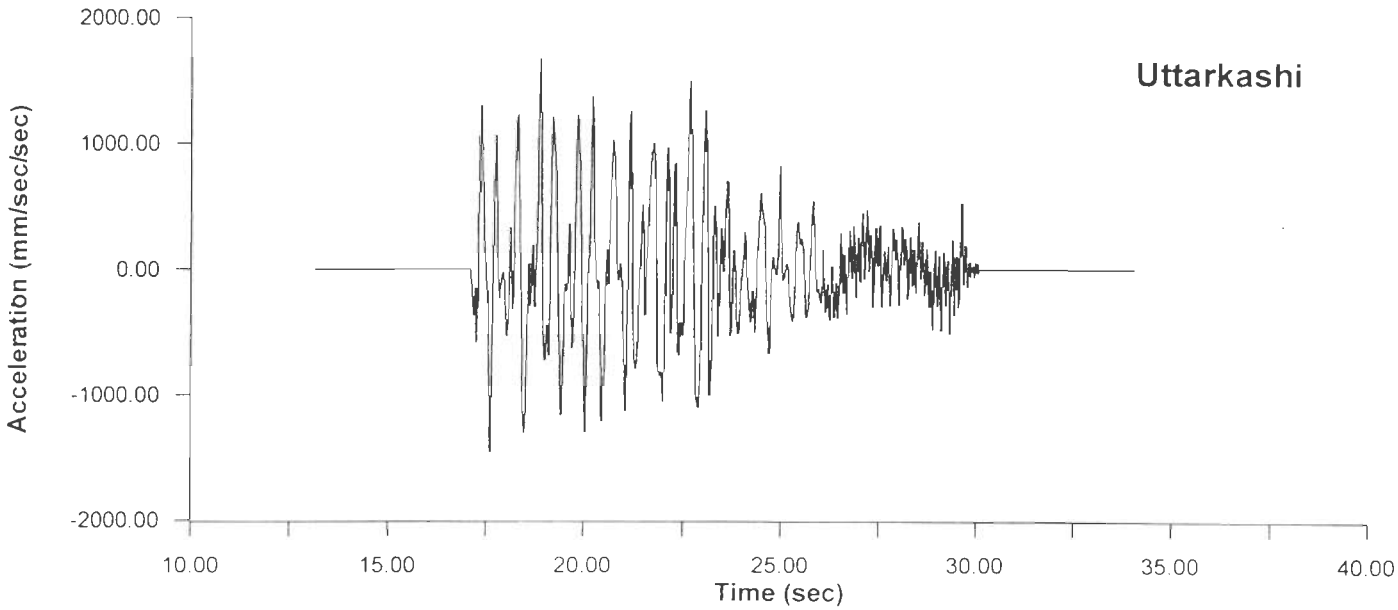

Fig. 4.20 : Synthetic accelerogram for one horizontal component at Uttarkashi (Hypothetical earthquake)

CHAPTER 5

Summary and Conclusions

5.1 Summary

In the present work two empirical relationships have been developed based on the strong motion data for Himalayan and northeast region of India. In addition a fresh approach has been presented for obtaining synthetic accelerograms. Its suitability has been demonstrated successfully by modelling the accelerograms from two Himalyan earthquakes i.e. Uttarkashi, 1991 and Chamoli, 1999 earthquakes. Synthetic accelerograms have been compared with the observed ones for some of the recording stations.

In Chapter 2, two empirical attenuation relationship have been developed, one for Himalayan and the other for northeast region. The available data for eight earthquakes, three from Himalayan region and five from northeast region of India have been used to develop these relationships. These predict the peak ground acceleration in the absence of strong motion data. The data to be provided are magnitude of earthquake and source to site distance (epicentral distance).

An integrated attenuation relationship has also been developed based on the various relationships available in the literature. The root mean square errors have been calculated with the observed acceleration values for all the eight earthquakes with the developed relationships and integrated relationship. These errors have been found to be less than 5% in all cases.

In Chapter 3, a simple method has been discussed and presented for generating synthetic accelerograms based on the convolution model of the seismogram. The spectrum of the ground motion expected at recording site is first computed from the knowledge of source parameters (source mechanism, size, geometry, time function, slip distribution on fault plane) for a source buried in a half space. This spectrum is then inverse Fourier transformed to yield the desired synthetic accelerogram.

In Chapter 4, the suitability of the method has been demonstrated by comparing the synthetic accelerograms with the observed ones for two earthquakes, Uttarkashi, 1991 and Chamoli, 1999. The extent of matching has been quantitatively expressed by computing the r.m.s. errors. It has been found that synthetic accelerograms match fairly well with the observed ones, r.m.s. errors being less than 20% in all cases.

The synthetic accelerograms have also been generated at six sites of Garhwal Himalaya region for a hypothetical earthquake of magnitude 7.0 in the Himalayan region.

5.2 Conclusions

1. The empirical attenuation relationships derived in the present study for predicting PGA values give good fit with the observed peak acceleration values of strong motion data.

2. The integrated (generalized) relationship is at par with the other relationships of the same type and can be used for computing PGA values at sites and regions where strong motion data is not available.

3. The method presented in the present thesis for generating the synthetic accelrograms, though simple, successfully tested with the observed data of two earthquakes events that occurred in the Himalayan region.

4. The method presented is found to be quite suitable for generating the synthetic accelerograms for earthquakes up to moderate magnitudes (~ 7.0).

5. Inclusion of new features in the spectral modelling method presented here has made it computationally very efficient and can be applied to simulate strong ground motion for sites in seismically active regions.

5.2 Suggestions for Further Research

1. The strong motion arrays installed in India should be further strengthened by installing more seismographs in the northern Himalayan belt. As and when more strong motion data is available the attenuation relations will be further modified. More parameters like topographical effect, local site geology etc. should be taken into account for developing the attenuation relationships.

2. The convolution method for generating the synthetic accelerograms can be further modified by incorporating the effect of surface inhomogeneous layers, effect of topography near the recording station, stochastic variability in the rupture process thereby making the model more in tune with the natural phenomenon.

References

1. Abrahamson N.P., P.G.Somerville, and C.A. Cornell (1990). "Goodness of Fit for Numerical Strong Motion Simulations and Uncertainty in Numerical Strong Motion Simulations predictions", *Proc. 4th US National Conference on Earthquake Engineering , Palm Springs, California*, Vol.1, pp. 317-326.

2. Abrahamson, N.A. and J.J. Litehiser (1989), "Attenuation of Vertical Peak Acceleration", *Bulletin of the Seismological Society of America*, 79 (3), pp. 549- 580.

3. Abrahamson, N.A. and W.J. Silva (1997), "Empirical Response Spectral Attenuation Relations for Shallow Crustal Earthquakes", *seismological research letters* Vol. 68, pp. 94-127.

4. Aki, K. (1968), "Seismic Displacement near a Fault", *Journal of Geophysics Research*, Vol. 73, 5359-5376.

5. Aki, K. and P.G. Richards (1980), "Quantitative Seismology : Theory and Methods", *W.H. Freeman and Company, San Fransisco*, Volumes 1 & 2.

6. Ambraseys, N.M. and J.J. Bommer (1991), "The Attenuation of Ground Acceleration in Europe", *Earthquake Engineering and Structural Dynamics*, 20, 1179- 1202

7. Amin, M. and A.H.S. Ang (1968) "Non-stationary Stochastic Model of Earthquake Motions", *Journal of Engineering Mechanics Division, ASCE*, Vol. 94(2), pp. 559-583.

8. Anderson, J.G. and Y. Lei (1994), "Non-parametric Description of Peak Acceleration as a Function of Magnitude, Distance and Site in Guerrero, Mexico", *Bulletin of the Seismological Society of America*, 84(4), 1003-1017.

9. Anderson, J.G. (1996), "Non-parametric Description of Peak Acceleration above a Sub-duction Thrust", *Seismological Research Letters*, Vol.68, pp. 86-93.

10. Atkinson, G.M. and D.M. Boore (1997a). "Some Comparison Between Recent Ground Motion Relations", *seismological research letters*, Vol.68, pp. 24-40.

11. Atkinson, G.M. and D.M. Boore (1997b). "Stochastic Point Source Modeling of Ground Motions in the Cascadia Region", *seismological research letters*, Vol.68 pp.74-85.

12. Barker, J.S.,P.G.Somerville and J.P.McLaren, (1988), "Modelling of Ground Motion Attenuation in Eastern North America", *Electric Power Research Institute Report* NP-5577, 414p.

13. Barker, J.S.,P.G.Somerville and J.P.McLaren, (1989), "Modelling of Ground Motion Attenuation in Eastern North America", *Tectonophysics,* Vol. 167, pp. 139-149.

14. Bath, M. (1975), "Seismicity of the Tanzania Region", *Tectonophysics*, Vol. 27, pp. 353- 379.

15. Battis, J. (1981), "Regional Modification Acceleration Functions", *Bulletin of the Seismological Society of America*, Vol. 71, pp. 1309-1321.

16. Ben-Menahem, Ari and Sarva Jit Singh, (1981), "Seismic Waves and Sources", *Springer-Verlag New York Inc.* PP. 1108.

17. Bolotin, V.V. (1960), "Statistical Theory of Aseismic Design of Structures", *Proceedings of Second World Conference on Earthquake Engineering, Tokyo*, pp. 1365-1374.

18. Boore, D.M. (1983), "Stochastic Simulation of High Frequency Ground Motions based on Seismological Models of the Radiated Spectra", *Bulletin of the Seismological Society of America*, Vol. 73, pp. 1865-1894.

19. Boore, D.M. (1986), "Short-period P- and S-wave Radiation from Large Earthquakes : Implications for Spectral Scaling Relations", *Bulletin of the Seismological Society of America*, Vol. 76, pp. 43-64.

20. Boore, D.M. (1987). "The Prediction of Strong Ground Motion", in *Strong Ground Motion Seismology,* M.Erdik and M.N.Toksoz, Editors, NATO Advanced Studies Institute series, D.Reidel Publishing Company, Dordrecht, The Netherlands, pp. 109-141.

21. Boore, D.M. and Atkinson G.M. (1986), "Stochastic Prediction of Ground Motion and Spectral Response Parameters at Hard Rock Sites in Eastern North America", *Bulletin of Seismological Society of America*, Vol. 76, pp. 440-467.

22. Bouchon, M.,(1979), "Predictability of Ground Displacement and Velocity Near an Earthquake Fault : an example : the Parfield Earthquake 1966", *Journal of Geophysical Research*, Vol.84, pp.6149-6156.

23. Brune, J.N. (1970), "Tectonic Stress and the Spectra of Seismic Shear Waves from Earthquakes", *Journal of Geophysical Research*, Vol. 75, pp. 4997-5009.

24. Brune, J.N. (1971), "Correction (to Brune 1970)", *Journal of Geophysical Research*, Vol. 76, pp. 5002.

25. Burridge, R. and L. Knopoff, (1964), "Body Force Equivalents for Seismic Dislocation", *Bulletin of the Seismological Society of America*, Vol. 54, pp. 1875-1888.

26. Bycroft, G.N. (1960) "White Noise Representation of Earthquakes," *Journal of Engineering Mechanics Division, ASCE*, Vol. 86(2), pp. 1-16.

27. Campbell, K.W. (1981), "Near- source attenuation of peak horizontal acceleration", *Bulletin of the Seismological Society of America*, Vol. 71, pp. 2029- 2070.

28. Campbell, K.W.(1991), "An Empirical Analysis of Peak Horizontal Acceleration for the Loma Prieta, California, Earthquake of 18 October 1989", *Bulletin of the Seismological Society of America*, Vol. 81, pp. 1838-1858.

29. Campbell, K.W.(1985), "Strong Motion Attenuation Relations: A Ten-year Prospective", *Earthquake Spectra*, Vol. 1(4), pp. 759- 804.

30. Chandrasekaran, A.R. and Das J.D. (1990), "Strong Motion Arrays in India and Characteristics of Recent Recorded Arrays," *Bulletin of The Indian Society of Earthquake Technology* , Vol. 27(1), March, pp. 1-66.

31. Chandrasekaran, A.R. and Das J.D. (1995), "Strong Motion Records from Uttarkashi Earthquake", *Memoir Geological Society of India*, No. 30, pp. 133-147.

32. Cornell, C.A., H. Banon and A.F. Shakal (1979). "Seismic Motion and Response Predication Alternatives", *Earthquake Engineering. and Structural Dynamics*, Vol. 7, pp. 295- 315.

33. Das, S. and K. Aki, (1977a), "A Numerical Study of Two-dimensional Spontaneous Rupture Prorogation", *Geophys.Jour. R.A.Soc.*, Vol.50, pp. 643-668.

34. Das, S. and K. Aki, (1977b), "Fault Plane With Barriers : A Versatile Earthquake Model", *Geophys. Jour.R.A. Soc.*, Vol.82, pp. 5658-5670.

35. Davenport, A.G. (1972). "A Statistical Relationship Between Rock Amplitude Magnitude and Epicentral Distance and its Application to Seismic Zoning", *Univ. of Western Ontario, Faculty of Engineering Science*, BLWT-4-72.

36. Donovan, N.C. (1973). "A Statistical Evaluation of Strong Motion Data Including the Feb. 9, 1971 San Fernando Earthquake", *Proceedings, Fifth World Conference on Earthq. Engineering, Rome,* Vol. 1, pp. 1252- 1261.

37. Esteva, L. (1970), "Seismic Risk and Seismic Design Decisions, in Simple Design for Nuclear Power Plants", R.J.Hanson, editor, *M.I.T.Press, Cambridge, Massachusetts*, pp. 142-182.

38. Esteva, L. and Rosenblueth (1963), "Espectros de Temblores a Distancias Moderasr Grandes", *Proc. Chilean Conf. on Seis. and Earthq. Engg.*, 1, Univ. of Chile.

39. Fukushima, Y. and T. Tanaka (1990). "A New Attenuation Relation for Peak Horizontal Acceleration of Strong Earthquake Ground Motion in Japan", *Bulletin of the Seismological Society of America*, Vol. 80(4), pp.757- 783.

40. Gupta I.D., Rambabu and B.M. Rame Gowda (1997), "An Integrated Attenuation Relationship", *Bulletin of Indian Society of Earthquake Technology*, Vol. 34, No. 3, Sept. 1997, pp 137-158.

41. Gupta I.D., Rambabu and R.G. Joshi (1991), "Attenuation of Peak Acceleration, Velocity and Displacement at Small Distance in Koyna Dam Region, India", *Proceedings First International Conference on Seismological and Earthquake Engineering, 27- 29 May, 1991, Tehran, Iran,* pp. 307- 316.

42. Hanks, T.C. (1982). "fmax", *Bulletin of the Seismological Society of America*, Vol. 72, pp. 1867-1879

43. Hanks, T.C. and D.M.Boore (1984). "Moment-magnitude Relations in Theory and Practice", *Jour. of Geophysical Research*, Vol. 89, pp. 6229-6235.

44. Hanks, T.C. and Maguire, R.K., (1981) "The Character of High Frequency Strong Ground Motion," *Bulletin of the Seismological Society of America*, Vol. 71(6), December, pp. 2071-2095.

45. Hartzell, S.H.,(1978), "Earthquake Aftershocks as Green's Function", *Geophys. Res. Letter*, Vol.5, pp.1-4.

46. Hasagewa, H.S., P.W. Basham and M.J. Berry (1981), "Attenuation Relation for Strong Seismic Ground Motion", *Bulletin of the Seismological Society of America*, Vol. 71, pp. 2071- 2095.

47. Haskell, N.A., (1966). "Total Energy and Energy Spectral Density of Elastic Wave Radiation from Propagating Faults", *Bulletin of the Seismological Society of America*, Vol.59, pp.865-908.

48. Haskell, N.A., (1969). "Elastic Displacements in the Near Field of a Propagating Fault", *Bulletin of the Seismological Society of America*, Vol.59, pp. 865-908.

49. Heaton, T.H., and D.V.Helmberger, (1977), "A Study of the Strong Motion of the Borrego Mountain, California Earthquake", *Bulletin of the Seismological Society of America*, Vol.67, pp. 315-330

50. Heaton, T.H., and D.V.Helmberger, (1978), "Predictability of Strong Ground Motion in the Imperial Valley : Modelling the M 4.9 November 4, 1976 Brawley Earthquake", *Bulletin of the Seismological Society of America*, Vol.68, pp. 31-48.

51. Helmberger, D.V., (1968), "The Crust-mantle Transition in the Bering Sea", *Bull. Of Seism. Soc. America,* Vol.58, pp. 179-214.

52. Herrmann, R.B., (1977), "Final Rep.", *Contact DACW 39-76-C-0058. Waterways Exp. Stn., Vicksburg, Mississipi.*

53. Housner, G.Q. (1947), "Calculating the Response of an Oscillator to Arbitrary Ground Motion", *Bulletin of the Seismological Society fo America*, vol. 31, No. 2, April, pp. 133-149.

54. Housner, G.W. (1955), "Properties of Strong Ground Motion Earthquakes," *Bulletin of the Seismological Society of America*, Vol. 45, No.3, pp. 197-218.

55. Housner, G.W. (1959), "Behaviour of Structures during earthquakes", *Journal of Engineering Mechanics Division, ASCE,* Vol. 85(4), pp. 109-129.

56. Housner, G.W. and Jennings, P.C. (1964) "Generation of Artificial Earthquakes, " *Journal of the engineering grams Systems-Problems & Prospect, " Proceedings of Eight Conference on Earthquake Engineering*, Vol. 2, 1984, pp. 39-45.

57. Houston, H. and h. Kanamori (1986). "Source Spectra of Great Earthquakes : Teleseismic Constraints on Rupture Processes and Strong Motion", *Bulletin of the Seismological Society of America*, 76, 19-42.

58. Hudson, D.E. (1956), "Response Spectrum Techniques in Engineering Seismology", *World Conference on Earthquake Engineering, Berkeley, California.*

59. Idriss, I.M. (1979). "Characteristics of Earthquake Ground Motions, in Earthquake Engineering and Soil Dynamics", *Proc. Am. Soc. Civil Eng. Div. Specialty Conf., June 19-21, 1978, Pasadena, California,* 3, pp. 1151-1265.

60. IMD, (2000), "Chamoli Earthquake of March 29, 1999 and its Aftershocks", *Indian Meteorological Department, Government of India, Seismology No.* 2/2000, pp. 70.

61. Iyengar, R.N. and Iyengar K.T.S. (1969) "A non-stationary Random Process Model for Earthquake Accelerograms", *Bulletin of the Seismological Society of America*, Vol. 59, pp. 1163-1188.

62. Jaikrishana, Chandrashekharan, A.R. and Saini, S.S. (1969) "Analysis of Koyna Accelerograms of Dec.11, 1967," *Bulletin of the Seismological Society of America,* Vol.59(4), Aug. 1969, pp.1719-1732.

63. Joyner, W.B. and D. M. Boore (1981), "Peak horizontal acceleration and velocity from strong motion records including records from the 1970 Imperial Valley, California, Earthquake", *Bulletin of the Seismological Society of America,* Vol. 71, pp. 2011- 2038.

64. Kasahara, K. (1981), "Earthquake Mechanics", Cambridge University Press.

65. Khattri, K.N., Yu, G., Anderson, J.G., Brune, J.N,. and Zeng, Y. (1994 a), " Seismic Hazard Estimation Using Modeling of Earthquake Strong Ground Motions: A brief analysis of 1991 Uttarkashi Earthquake, Himalaya and Prognostication for a Great Earthquake in the region," *Current Science*, Vol. 67(5), September, pp. 343-353.

66. Khattri, K.N., Zeng, Y. Anderson, J.G., Brune, J. (1994 b), "Inversion of Strong Motion Waveforms for Source Slip Function of 1991 Uttarkashi Earthquake, Himalaya", *Journal of Himalayan Geology,* Vol. 5 (2), pp. 163-191.

67. Kumar Dinesh, S.S. Teotia and K.N. Khattri (1997). "The Representability of Attenuation Characteristics of Strong Ground Motions Observed in the 1986 Dharmsala and 1991 Uttarkashi Earthquakes by Available Empirical Relations", *Current Science*, Vol. 73, No. 6, pp 543-548.

68. Kumar, D., Khattri, K.N., Teotia, S.S. and Rai, S.S. (1999) "Modeling of Accelerograms of Two Himalayan Earthquakes Using a Novel Semi-Empirical Method and Estimation of Accelerograms for a Hypothetical Great Earthquake in the Himalaya," *Current Science*, Vol. 76, No. 6, March, 1999, pp. 819-830

69. Kumar, G. (1981) "Stratigraphy & Tectonic of Lesser Himalayas of Kumaon, U.P.", *Contemporary GeoSc. Res. Himalaya*, VI, pp 61-70.

70. Makaris, D.I., G.N.Stavrakakis and J.C.Drakopoulos, (1992), "Expected Ground Motion at a Site Based on Hypothetical Fault Models", *Earthquake Engineering, Tenth World Conference,* Vol.2, Balkema, Rotterdam, pp. 703-708.

71. Maruyama, T,(1963), "On the Force Equivalents of Dynamic Elastic Dislocations with Reference to the Earthquake Mechanism", *Bulletin of Earthquake Research Institute, Tokyo University*, Vol. 41, pp. 467-486.

72. McGuire, R.K.(1977). "Seismic Design Spectra and Mapping Procedures using Hazard Analysis Based on Oscillator Response", *Earthquake Engineering and Structural Dynamics*, Vol. 5, pp. 211- 234.

73. McGuire, R.K.(1978). "Seismic Ground Motion Parameter Relation", *Journal of Geotechnical Engineering Division, ASCE,* Vol. 104, pp. 481-490.

74. Milne, W.G. and A.G.Davenport (1969). "Distribution of Earthquake Risk in Canada", *Bulletin of the Seismological Society of America*, Vol. 59(2), pp. 729-754.

75. Nuttli, O.W. and R.B. Herrmann (1984). "Ground Motion of Mississippi Valley Earthquake", *Journal of Technical Topics in Civil Engineering ASCE,* Vol. 110, pp. 54- 69.

76. Olson, A.H., (1982), "Ph.D. Thesis, Univ. of California, San Diego PDE, (1991)", *Preliminary Determination of Epicenters,* No. 42-91, U.S. Department of the Interior, Geological Survey.

77. Orphal, D.L. and J.A. Lahoud (1974), "Prediction of Peak Ground Motion from Earthquakes", *Bulletin of the Seismological Society of America*, Vol. 64(5), pp. 1563- 1554.

78. Papageorgiou, A. and K. Aki (1983a). "A Specific Barrier Model for the Quantitative Description of Inhomogeneous Faulting and the Prediction of Strong Ground Motion. Part I. Description of the Model", *Bull, Seism. Soc. Am.* Vol. 73, pp. 693-722.

79. Papageorgiou, A. and K. Aki (1983b). "A Specific Barrier Model for the Quantitative Description of Inhomogeneous Faulting and the Prediction of Strong Ground Motion. Part II. Applications of the Model", *Bulletin of the Seismological Society of America*, Vol. *73*, pp. 953-978.

80. Peng, K.Z., F.T. Wu and L. Song (1985). "Attenuation Characteristics of Peak Horizontal Acceleration in Northeast and Northern China", *Earthquake Engineering and Structural Dynamics*, Vol. 13, pp. 337- 350.

81. Penzien, J. and Liu, S.C. (1969), "Non-deterministic Analysis of Non-linear Structures Subjected to Earthquake Excitation", *Proceedings of Fourth World Conference on Earthquake Engineering, Chile*, pp. 114-129.

82. Richter, C.F. (1958), "Elementary Seismology", *W.H. Freeman & Company, San Francisco.*

83. Rosenblueth, E. (1956), "Some Applications of Probability Theory of A seismic Design", *World Conference on Earthquake Engineering, Berkeley, California.*

84. Rovelli, A.(1987). "Strong Ground Motion in Italy : Accelerogram spectral properties and prediction of peak values", in *Strong Ground Motion Seismology,* M.Erdik and M.N.Toksoz, Editors, NATO Advanced Studies Institute series, D.Reidel Publishing Company, Dordrecht, The Netherlands, pp 333-354.

85. Sabetta, F. and A. Pugliese (1987). "Attenuation of Peak Horizontal Acceleration and Velocity from Italian Strong- Motion Records", *Bulletin of the Seismological Society of America,* Vol. 77, pp. 1491- 1513.

86. Sadigh, K., C.Y.Chang, J.A Egan, F. Makdisi, and R.R. Youngs (1997), "Attenuation Relationships for Shallow Crustal Earthquakes Based on California Strong Motion Data", *seismological research letters*, Vol. 68, pp. 180-189.

87. Seeber, L. and J.G. Armbruster (1981). "Great Detachment Earthquakes along the Himalayan Arc and Long term Forecasting, in Earthquake Prediction : An International Review, Maurice Ewing Series, 4", *American Geophysical Union, Washington. D.C.,* pp. 259-277.

88. Sharma M.L. (1998), "Attenuation Relationship for Estimation of Peak Ground Acceleration using Data from Strong Motion Arrays in India", *Bulletin of the Seismological Society of America*, Vol 88, No. 4, pp.1063-1069.

89. Shinozuka, H. and Sato, Y. (1967). "Simulation of Non-stationary Random Process," *Journal of Engineering Mechanics Division, ASCE*, Vol. 93(1), pp. 11-40.

90. Singh R.P., E.Aman and Y.J. Prasad (1996). "Attenuation Relations for Strong Seismic Ground Motion in the Himalayan Region", *Pure and Applied Geophysics*, Vol. 147, pp 161-180.

91. Somerville, Paul G., James P. McLaren, Chandan K Saikia and Donald V. Helmberger, (1990), "The 25 November 1988 Saguenay, Quebec, Earthquake : Source Parameters and the Attenuation of Strong Ground Motion", *Bulletin of the Seismological Society of America*, Vol.80, No.5, pp.1118-1143.

92. Somerville, Paul G., M.Sen and B.Cohee, (1991), "Simulation of Strong Ground Motions Recording During the 1985 Michocan Mexico, and Valpazaiso Chili Earthquake", *Bulletin of the Seismological Society of America*, Vol.81, No.1, pp.1-27

93. Swanger, H.J., and D.M.Boore, (1978), "Stimulation of Strong Motion Displacements using Surface Wave Model Superposition", *Bulletin of the Seismological Society of America*, Vol.68, pp.907-922.

94. Trifunac, M.D. and V.W.Lee (1990). "Frequency Dependent Attenuation of Strong Earthquake Ground Motion", *Soil Dyn. and Earthq. Engg.*,9(1), pp. 3-15.

95. Valdiya, K.S. (1988). "Tectonics and Evolution of the Central Sector of the Himalaya", *Philos. Trans.R.Soc. London* 4326, pp. 151-175.

96. Wald, David J, Donald V. Helmberger and Thomas H.Heaton, (1991), "Rupture Model of the 1989 Loma Prieta Earthquake From the Inversion of Strong Motion and Broadband and Teleseismic data", *Bulletin of the Seismological Society of America*, Vol.81, No.5, pp. 1540-1572.

97. Youngs, R.R.,S.J.Chiou, W.J. Silva and J.R.Humphery, (1997), "Strong Ground Motion Attenuation Relationship for Sub-duction Zone Earthquakes", *Seismological Research Letters*, Vol. 68, pp. 58-73.

98. Yu, G., Khattri, K.N. Anderson, J.G., Brune, J.N. and Zeng, Y. (1995) " Strong Ground Motion from the Uttarkashi, Himalaya, India, Earthquake: Comparison of Observations with Synthetics Using the Composite Source Model", *Bulletin of the Seismological Society of America*, Vol. 85(1), pp. 31-50.

99. Zeng, Y., Anderson, J.G. and Yu, G. (1994a) " A Composite Source Model for Computing Realistic Synthetic Strong Motions," *Geophys. Research Letters,* Vol. 21, pp. 725-728.

100. Zeng, Y., Anderson, and F.Su (1994b). "Source and Path Effects in Realistic Strong Ground Motion Simulation (abstract)," *Seism. Research Letters* pp. 65, 36.

101. Zeng, Y., K. Aki, and L. Teng (1993a). "Source Inversion of the 1987 Whittier Narrows Earthquake, California, Using the Isochron Method, *Bulletin of the Seismological Society of America*, Vol. 83, pp. 358-377.

102. Zeng, Y., K. Aki, and L. Teng (1993b) " Mapping of the High Frequency Source Radiation for the Loma prieta Earthquake. *California, Journal Geophys. Res.* Vol. 98, pp. 11981-11993.

APPENDICES

APPENDIX A

Earthquake Locations with their Peak Ground Horizontal Accelerations etc.

Earthquake stations	PGA (cm/s*s)	Epicentral Distance (km)	Magni-tude (Mb)	Depth (km)	Site Type (R/S)
Dharamsala,1986 Earthquake					
Bandlakhas	142.90	24.18	5.5	7	R
Baroh	61.80	21.21	5.5	7	R
Bhawarna	39.30	24.50	5.5	7	R
Dharamsala	244.30	437	5.5	7	R
Jawali	19.70	26.73	5.5	7	R
Kangra	160.40	9.33	5.5	7	R
Nagrota-Bagwan	147.10	12.29	5.5	7	R
Shahpur	265.00	9.98	5.5	7	R
Sihunta	57.20	23.06	5.5	7	R
Shillong Earthquake					
Baithalangso	45.41	79.50	5.5	28	S
Dauki	93.52	27.16	5.5	28	R
Khliehrait	50.85	30.15	5.5	28	R
Nongkhlaw	92.33	52.76	5.5	28	R
Nongpoh	66.15	57.01	5.5	28	R
Nongstoin	20.53	81.80	5.5	28	R
Panimur	59.05	76.63	5.5	28	S
Pynursla	102.07	21.68	5.5	28	R
Saitsama	147.97	44.79	5.5	28	S
Ummulong	112.56	12.83	5.5	28	R
Umrongo	38.15	55.92	5.5	28	S
Umsning	124.43	39.39	5.5	28	R
N.E. Earthquake (May 1987)					
Baithalangso	33.94	178.30	5.7	50	S
Bamungao	21.82	137.83	5.7	50	S
Berlongfer	88.49	110.36	5.7	50	S
Bokajan	68.74	93.88	5.7	50	S
Diphu	85.55	105.03	5.7	50	S
Gunjung	53.48	119.76	5.7	50	S
Haflong	60.32	119.22	5.7	50	R

Hajadisa	86.87	91.28	5.7	50	S
Hathikhali	38.30	117.30	5.7	50	S
Laisong	63.35	89.76	5.7	50	S
Nongpoh	19.02	243.29	5.7	50	R
Panimur	46.45	147.08	5.7	50	S
Saitsama	48.74	188.42	5.7	50	S
Umrongso	28.48	159.95	5.7	50	S
N.E. Earthquake (Feb. 1988)					
Baigao	25.53	159.27	5.8	15	S
Baithalangso	33.67	182.55	5.8	15	S
Bamungao	17.27	203.60	5.8	15	S
Dauki	29.98	79.06	5.8	15	S
Gunjung	42.26	167.63	5.8	15	R
Haflong	36.19	161.94	5.8	15	S
Hatikhali	24.91	194.87	5.8	15	R
Katakhal	9.57	114.86	5.8	15	S
Khliehriat	78.43	116.49	5.8	15	S
Mawphlang	87.61	93.52	5.8	15	R
Nongkhlaw	138.70	116.27	5.8	15	R
Nongpoh	84.61	144.70	5.8	15	R
Pynursla	51.67	83.25	5.8	15	R
Saitsama	77.33	147.71	5.8	15	S
Shillong	46.87	109.22	5.8	15	R
Ummulong	63.00	116.24	5.8	15	R
Umrongso	46.59	147.11	5.8	15	S
Umsning	60.49	126.79	5.8	15	R
N.E. Earthquake (August 1988)					
Baigao	247.47	230.05	6.8	91	S
Baithalangso	179.64	269.65	6.8	91	S
Bamungao	105.52	228.08	6.8	91	S
Bearlongfer	344.57	200.93	6.8	91	S
Bokajan	219.99	167.21	6.8	91	S
Cherrapunji	58.38	341.26	6.8	91	
Dauki	107.71	311.97	6.8	91	R
Diphu	366.00	189.94	6.8	91	R
Doloo	64.25	237.12	6.8	91	S
Gunjung	135.58	214.06	6.8	91	S
Hajadisa	105.29	185.78	6.8	91	S
Harengajao	77.53	228.55	6.8	91	S
Hojai	144.87	246.08	6.8	91	S
Jellalpur	31.68	269.40	6.8	91	S
Jhirighat	118.62	207.07	6.8	91	R
Kalain	59.40	257.52	6.8	91	S
Katakhal	74.29	253.44	6.8	91	S
Khliehriat	73.12	278.52	6.8	91	R

Koombur	49.38	213.58	6.8	91	S
Loharghat	57.98	377.51	6.8	91	S
Mawkyrwat	50.98	368.81	6.8	91	R
Mawphlang	115.09	339.47	6.8	91	R
Mawsynram	85.88	357.43	6.8	91	R
Nongkhlaw	144.52	355.55	6.8	91	R
Nongstoin	61.84	289.93	6.8	91	R
Panimur	166.71	240.78	6.8	91	S
Pynursla	58.75	324.34	6.8	91	R
Saitsama	262.22	282.32	6.8	91	S
Shillong	83.17	327.85	6.8	91	R
Silchar	89.72	237.49	6.8	91	S
Ummulong	159.88	301.27	6.8	91	R
Umrongso	88.44	254.41	6.8	91	S
Umsning	152.40	331.83	6.8	91	R
N.E. Earthquake (January 1990)					
Baigao	63.51	250.65	6.1	119	S
Baithalangso	88.42	297.90	6.1	119	S
Bamungao	33.28	257.48	6.1	119	S
Berlongfer	177.06	230.01	6.1	119	S
Diphu	103.72	222.81	6.1	119	S
Gunjung	71.90	233.42	6.1	119	S
Hajadisa	85.12	207.57	6.1	119	S
Hojai	42.29	275.99	6.1	119	S
Laisong	70.98	201.13	6.1	119	S
Maibang	74.67	220.54	6.1	119	S
Panimur	78.26	265.49	6.1	119	S
Saitsama	68.94	306.24	6.1	119	S
Ummulong	51.54	321.61	6.1	119	R
Umrongso	35.90	275.98	6.1	119	S
Uttarkashi, 1991 Earthquake					
Almora	22.27	150.64	6.6	12	R
Barkot	103.88	61.40	6.6	12	R
Bhatwari	871.63	25.45	6.6	12	R
Ghansiali	141.98	41.84	6.6	12	R
Karnprayag	84.74	65.94	6.6	12	R
Koteshwar	99.08	64.15	6.6	12	R
Kosani	31.58	144.86	6.6	12	R
Koti	41.09	105.01	6.6	12	R
Purola	96.13	75.68	6.6	12	R
Rudraprayag	65.27	54.60	6.6	12	R
Srinagar	65.77	59.56	6.6	12	R
Tehri	73.63	54.53	6.6	12	R
Uttarkashi	313.09	39.25	6.6	12	R

Chamoli, 1999 Earthquake					
Almora	95.03	27.24	6.1	21	R
Barkot	155.78	22.26	6.1	21	R
Chinyalisur	145.57	81.84	6.1	21	R
Ghansali	123.81	50.65	6.1	21	R
Gopeshwar	33.78	352.83	6.1	21	R
Joshimath	23.01	69.55	6.1	21	R
Karnprayag	40.54	31.08	6.1	21	R
Lansdown	143.19	11.01	6.1	21	R
Tehri	50.31	94.71	6.1	21	R
Ukhimath	133.73	61.06	6.1	21	R

APPENDIX B

Attenuation Relations available in Literature

1. Esteva, L. (1970)
   $a(cm/s^2) = 1230\, e^{0.8M} (R + 25)^{-2}$; Firm ground condition

2. Mickey, W.V. (1971)
   $\log a(cm/s^2) = 1.325 + 0.466M - 1.4 \log R$; Not applicable for $R \leq 15$ km.

3. Denham, D.G. and G.R. Small (1971)
   $\log a(cm/s^2) = 2.80 + 0.20\, M - 1.10 \log R$;Australia, unconsolidated soil

4. Devenport, A.G. (1972).
   $a(cm/s^2) = 274\ e^{0.8M} R^{-1.64}$;
   Not applicable for $R \leq 15$ km.

5. Denovan, N.C. (1973).
   $a(cm/s^2) = 1080\, e^{0.5M} (R + 25)^{-1..32}$; Rocky ground.

6. Esteva, L. and R. Villaverde (1973).

   $a(cm/s^2) = 5600\, e^{0.8M} (R + 40)^{-2}$; $\sigma_{\ln a} = 0.64, R \geq 15$ km.

7. Merz, H.A. and C.A. Cornell (1973).
   $a(cm/s^2) = 1200\ e^{0.8M} R^{-2}$; $\sigma_{\ln a} = 0.2$,

8. Orphal, D.L. and J.A. Lahoud (1974).
   $a(cm/s^2) = 64.75 \times 10^{0.4M} R^{-1..39}$; $\sigma_{\ln a} = 0.69$
   California region, Rock and Alluvium, Not applicable for $R \leq 15$ km.

9. Bath, M. (1975).
   $a(cm/s^2) = 1.03\, h^{0.6} \times 10^{0..54\, M} R^{-1..5}$;
   Tanzania region, $R \geq 15$ km.

10. Trifunac, M.D. (1976)

$\log a(cm/s^2) = M + \log A_o(R) + 0.898_P + 1.789M - 6.217 - 0.06s - 0.186M^2$

Applicable for M= 4.8- 7.5, $\log A_o$ (R) is Richter's attenuation function, p is confidence level, s=0 for alluvium, 2 for rock and 1 for intermediate type of geology.

11. McGuire R.K. (1977)

$a(cm/s^2) = 472.0 \times 10^{0..278M} (R+25^{-1..301};$ $\sigma_{\ln a} = 0.62$

Rock and Allluvium, Not applicable for $R \leq 15km$

12. Ohashi et al (1977).

$a(cm/s^2) = 46 \times 10^{0.208} (R+10)^{-0.686}$; Rock sites

$a(cm/s^2) = 24.5 \times 10^{0.333M} (R+10)^{0..924}$; Stiff soil

Based on Japanese data.

13. Donovan, N.C. and A.E. Bornstein (1978).

$a(g) = 2198e^{(0.046 + 0.193 \ln R) M} R^{-2.1} (R+25)^{-2.515 + 0.21 \ln R}$

California region, Rock and stiff soil sites.

14. McGuire, R.K. (1978).

$a(g) = 0.0306e^{0.89M} R^{-1.17} e^{-0.020s}$; $\sigma_{\ln a} = 0.62$

s= 0 for rock and 1 for soil sites in Western U.S.

15. Cornell, C.A. , H. Banon and A. F. Shakal (1979).

$a(g) = 0.863e^{0.86M} (R+25)^{-1..8}$; $\sigma_{\ln a} = 0.57$, Western U.S.

16. Espinosa, A. F. (1980).

$a(g) = 1.119 \times 10^{-6} e^{2..3M} R^{-0.11-0.22 \ln R}$; Western U.S.

17. Battis, J. (1981) .

$a(g) = 0.3480e^{1.21M} (R+25)^{-2.08}$; $\sigma_{\ln a} = 0.71$, California region.

$a(g) = 0.0239e^{1.24M} (R+25)^{-1.24}$; $\sigma_{\ln a} = 0.71$, Central U.S.

18. Campbell K.W. (1981).

$a(g) = 0.0159e^{0.868M} (R+0.0606e^{0.7M})^{-1.09}$; $\sigma_{\ln a} = 0.37$,

World wide data, Rock sites, R< 50km

19. Hasegawa, H.S., P.W. Basham and M.J. Berry (1981).

$a(g) = 1.02 \times 10^2 e^{1..3M} R^{-1..5}$; Western Canada

$a(g) = 3.47 \times 10^{3e\ 1.3M} R^{-1.1}$; Eastern Canada

20. Joyner, W.B. and D.M. Boore (1981).
$a(g) = 0.0955e^{0.573\,M}\ R_1^{-0.5}e^{-0.00587\,R1\,0..5}$; $\sigma_{\ln a} = 0.60$
$R_1 = (R^2+7.3^2)^{0.5}$;
Western North America.

21. Nuttli, O.W. and R.B. Herrmann (1984)
$a(g) = 3.79 \times 10^{-3}e^{1.15\,M}(R^2 + 0.000346e^{2.1\,M})^{-0.415}e^{-0\,00159R}$; $\sigma_{\ln a} = 0.55$
Mississippi Valley

22. Sabetta, F. and A. Pugliese (1987)
$\log a(g) = -1.562 + 0.306M - \log (R^2 + 5.8^2)^{0\,5} + 0.\,169s$;
s=0 for rock sites and 1 for soft sites, Italian data.

23. Peng K.Z., F.T. Wu and L. Song (1985)
$\log a(cm/s^2) = -0.474 + 0.613M - 0.873 \log R - 0.00206\ R$; NE China
$\log a(cm/s^2) = -0.437 + 0.454M - 0.739 \log R - 0.00279\ R$; NW China

24. Abrahamson, N.A. and J.J. Litehiser (1989)
$\log (g) = -0.62 + 0.177M - 0.982 \log (R + e^{0.284M}) + 0.132F - 0.0008E_r$;
$\sigma_{\ln a} = 0.277$, F=1 for reverse or reverse oblique events, 0 otherwise
Er = 1 for interplate events and 0 for intraplate events.

25. Fukushima, Y and T. Tanaga (1990).
$\log a(cm/s^2) = 0.41M - \log (R + 0.032 \times 10^{0.41M}) - 0.0034R + 1.30$;
Japan region

26. Gupta I.D., V. Rambabu and R.G. Joshi (1991).
$\log a(cm/s^2) = 2.64 - 0.01197\ R - 0.0995 \log R - 0.6476M + 0.10634M^2$
Koyna region, India

27. Crouse, C.B. (1991)
$\ln a(cm/s^2) = 6.36 + 1.76M - 2.731 \ln (R + 1.58e^{0.608\,M}) + 0.00916h$;
$\sigma_{\ln a} = 0.773$
Cascadia subduction zone

28. Ambraseys, N.M. and J.J. Bommer(1991)
$\log a(g) = -0.87 + 0.217M - \log R - 0.00117R$; $\sigma_{\log a} = 0.26$,
Europian data

29. Theodulidin, N.P. and B.C. Papazachos (1992)
$\ln a(cm/s^2) = 3.88 + 1.12M - 1.65\ln(R+15) + 0.41s$; $\sigma_{\ln a} = 0.71$
s=1 for rock and 0 for alluvial sites, Greece.

30. Niazi, M. and Y. Bozorgnia (1991)
ln a(g) = - 5.503 + 0.936M- 0.816ln (R_h + 0.407e $^{0.455M}$); $\sigma_{\ln a}$ =0.461,
NE Taiwan.

31. Tento, A., L. Franceschina and A. Marcellini (1992)
ln a(cm/s^2) = 4.73 + 0.52M- ln R – 0.002R; $\sigma_{\ln a}$ = 0.67,
Italian sites.

32. Singh et.al. (1996)
log a(cm/s^2) = 1.140 + 0.31M- 0.6151log R ;
Himalayan region of India.

33. Sharma M.L. (1998)
log a(cm/s^2) = - 1.072 + 0.39M- 01.210 log (R + e $^{0.587M}$);
Himalayan region of India.

APPENDIX C

Radiation Pattern in Terms of Fault Parameters

The radiation pattern terms in equation (3.3) should be expressed in terms of parameters of the fault having arbitrary orientation. These parameters are the dip and the strike of the fault. The direction of slip is expressed in the form of slip angle or rake. The fault has two surfaces, called hanging wall and foot wall. Slip u the direction in which hanging wall moves relative to foot wall. Rake λ is the angle between strike direction and slip. This is illustrated in Fig. C.1, in which X_1 – axis is taken positive towards north, X_2-axis positive towards east and X_3-axis positive downwards. The origin of the cartesian coordinate system is taken to coincide with the epicentre E of the earthquake with focus F lying on the fault. The strike of the fault is denoted by ϕ_s and dip by δ. Rake λ is measured on the fault plane in the counter clockwise direction.

For a strike slip fault, $\delta = \pi/2$ and $\lambda=0$ or π corresponding to left lateral or right lateral strike slip fault respectively. For a dip-slip fault $\delta = \pi/2$ and $\lambda = \pi/2$ or 3 $\pi/2$. If δ is less than $\pi/4$ and λ is within the range $(0, \pi)$ the fault is termed thrust fault. For $\delta >$ /4, it is termed reverse fault if $0 < \lambda < \pi$ and normal fault if $\pi < \lambda < 2\pi$.

The expressions for R^P, R^{SV} and R^{SH} in terms of various angles are given below (aki and Richards, 1980) :

$$R^P = \cos\lambda \sin\delta \sin^2 i_o \sin 2(\phi-\phi_s) + \sin\lambda \cos 2\delta \sin 2i_o \sin(\phi-\phi_s) + \sin\lambda \sin 2\delta [\cos 2i_o - \sin 2i_o \sin^2(\phi-\phi_s)] - \cos\lambda \cos\delta \sin 2i_o \cos(\phi-\phi_s) \quad \ldots (C.1)$$

$$R^{SV} = +\tfrac{1}{2}(\cos\lambda \sin\delta \sin 2i_o \sin 2(\phi-\phi_s) + \sin\lambda \cos 2\delta \cos 2i_o \sin(\phi-\phi_s) - \tfrac{1}{2}\sin\lambda \sin 2\delta \sin 2i_o (1+\sin^2(\phi-\phi_s) - \cos\lambda \cos\delta \cos 2i_o \cos(\phi-\phi_s) \quad \ldots (C.2)$$

$$R^{SH} = \cos\lambda \sin\delta \sin i_o \cos 2(\phi-\phi_s) + \sin\lambda \cos 2\delta \cos i_o \cos(\phi-\phi_s) - \tfrac{1}{2}\sin\lambda \sin 2\delta \sin i_o \sin 2(\phi-\phi_s) + \cos\lambda \cos\delta \cos i_o \sin(\phi-\phi_s) \quad \ldots (C.3)$$

The expressions for R^P, R^{SV} and R^{SH} can also be expressed in matrix form as follows:

$$\begin{bmatrix} R^P \\ R^{SV} \\ R^{SH} \end{bmatrix} = \begin{bmatrix} P_1 & P_2 & P_3 & P_4 \\ S_1 & S_2 & S_3 & S_4 \\ T_1 & T_2 & T_3 & T_4 \end{bmatrix} \begin{bmatrix} \cos\lambda \sin\delta \\ \sin\lambda \cos 2\delta \\ \sin\lambda \sin 2\delta \\ \cos\lambda \cos\delta \end{bmatrix} \quad \ldots (C.4)$$

where P_1, P_2, etc. are coefficients of corresponding terms in the column vector on the R.H.S. and can be obtained from equations (C.1) to (C.3), e.g.

$$P_1 = \sin^2 i_o \sin 2(\phi-\phi_s),\ S_2 = \cos 2i_o \sin(\phi-\phi_s),\ T_3 = -(1/2)\sin i_o \sin 2(\phi-\phi_s),\ \text{etc.}$$

The radiation pattern terms are thus seen to be made up of contributions from four elementary faults. If $\lambda=0$, $\delta=\pi/2$ (vertical strike slip fault), only the first column of the matrix (C.4) contributes to the radiation pattern, since all but the first element of the column vector on R.H.S. of the equation (C.4) are zero. Four cases arise: (a) for $\lambda=0$, $\delta=\pi/2$ (vertical strike slip fault) only first column contributes; (b) for $\lambda=3\pi/2$, $\delta=\pi/2$ (vertical dip slip fault) only the

second column contributes; (c) for $\lambda = \pi/2$, $\delta = \pi/4$ (reverse slip on a 45° dipping fault plane) only the fourth column contributes; and (d) for $\lambda=0$, $\delta=0$ (slip on a horizontal plane) only the fourth column contributes. For arbitrary λ and δ, all the 12 elements of the matrix contribute. When $i = \pi/2$, it corresponds to surface focus. For a point strike slip fault with surface focus, the radiation pattern is given by $\text{Sin}2(\phi-\phi_s)$ which gives the familiar four lobe radiation pattern for P waves.

For the four elementary faults the radiation pattern for P-, SV- and SH- are shown in Fig. C.2 for surface focus (i.e., $i_o=0$). Due to this reason there will be no radiation of P and SH for cases (b) and (d) and no radiation of SV for cases (a) and (c).

Strong ground motion records are obtained by accelerographs placed on earth's surface. The free surface of the earth modifies the amplitudes of waves incident from below.

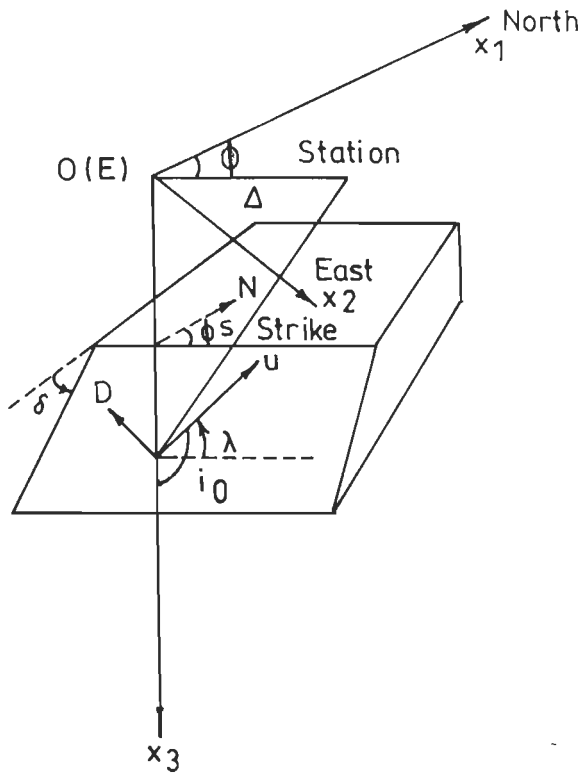

Fig. C.1 : Notations used to obtain explicit dependence of Radiation Pattern terms on (ϕ_s, δ, λ, i, ϕ) (Modified after Aki and Richards, 1980)

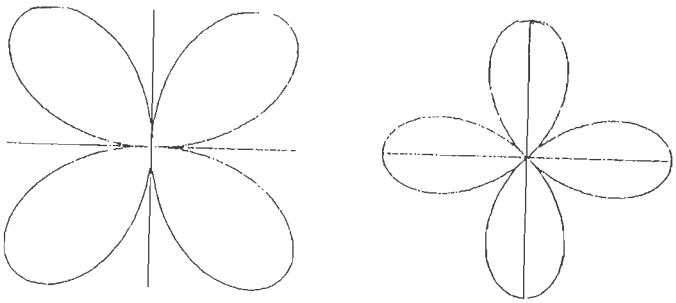

(a) Vertical strike slip fault

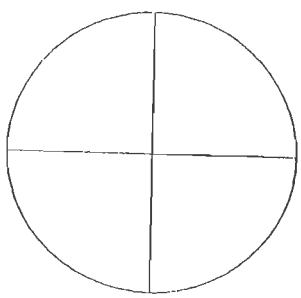

(b) Vertical dip slip fault

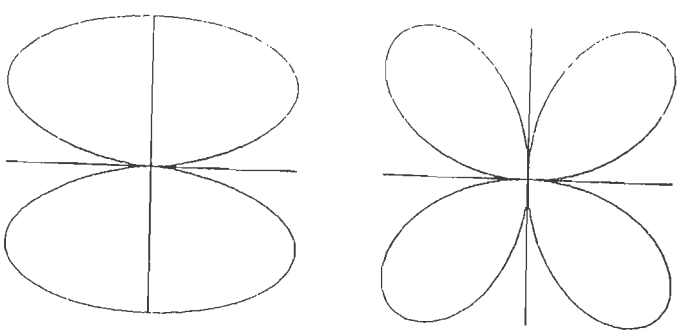

(c) Reverse slip on a 45° dipping plane

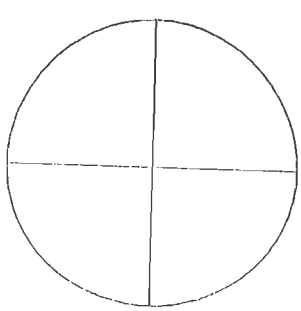

(d) Slip on a horizontal fault

Fig. C.2 : Radiation Pattern terms for P, SV and SH waves for four elementary faults for an earthquake with focus on the surface

APPENDIX D

Free Surface Effect

In Fig. D.1 a receiver R is placed below the free surface which receives direct P, reflected PP and reflected PS waves from a buried focus F. The record of ground motion made by this receiver shows three distinct events. When the depth of the receiver below the surface is decreased the three events are observed at shorter time intervals. When the receiver lies at the free surface the three events coalesce giving a single event, which then expresses the effect which the presence of free surface has on the wave incident from below. In a similar way incident SV waves are also affected by the presence of free surface. The amplitude of SH waves is doubled as a consequence of the presence of the free surface.

The formula for computing free surface effect on incident P-waves are given below in terms of horizontal u_H and vertical u_3 components of P-wave displacement (Aki and Richards, 1980).

$$u_H^P = A[\sin i + R_{pp} \sin i + R_{ps} \cos j] \quad \ldots (D.1)$$

$$u_3^P = A[-\cos i + R_{pp} \cos i + R_{ps} \sin j] \quad \ldots (D.2)$$

and those for incident SV waves are

$$u_H^{SV} = B[\cos j + R_{sp} \sin i + R_{ss} \cos j] \quad \ldots (D.3)$$

$$u_3^{SV} = B[\sin j + R_{sp} \cos i + R_{ss} \sin j] \quad \ldots (D.4)$$

where A, B are the amplitude of P and SV waves in an infinite medium.

In the above formulae the horizontal component of the displacement is in the plane of incidence containing the receiving station, ray path and the focus. The angle i is the angle of incidence for the P waves and j for the SV waves at the free surface. These angles are related by Snell's law.

$$\frac{\sin i}{\alpha} = \frac{\sin j}{\beta} \qquad \ldots (D.5)$$

where α and β are P and S wave velocities in the half space. R_{PP}, R_{ps} are reflection coefficients for incident P waves and R_{ss}, R_{sp} those for incident SV waves when waves are incident on the surface of half space from below. These are given below:

$$R_{PP} = \frac{-(1/\beta^2 - 2p^2)^2 + 4p^2[(\cos i/\alpha][(\cos j/\beta]}{+(1/\beta^2 - 2p^2)^2 + 4p^2[(\cos i)/\alpha][(\cos j/\beta]} \qquad \ldots (D.6)$$

$$R_{PS} = \frac{4(\alpha/\beta)p(\cos i/\alpha)(1/\beta^2 - 2p^2)}{(1/\beta^2 - 2p^2)^2 + 4p^2(\cos i/\alpha)(\cos j/\beta)} \qquad \ldots (D.7)$$

$$R_{SP} = \frac{4(\beta/\alpha)p(\cos j/\beta)(1/\beta^2 - 2p^2)}{(1/\beta^2 - 2p^2)^2 + 4p^2(\cos i/\alpha)(\cos j/\beta)} \qquad \ldots (D.8)$$

$$R_{SS} = \frac{(1/\beta^2 - 2p^2)^2 - 4p^2(\cos i/\alpha)(\cos j/\beta)}{(1/\beta^2 - 2p^2)^2 + 4p^2(\cos i/\alpha)(\cos j/\beta)} \qquad \ldots (D.9)$$

The formula (D.3) and (D.4) for incident SV waves are valid only for $j \leq j_c$ where $j_c = \sin^{-1}(\beta/\alpha)$ is the critical angle for incident SV waves. When $j \geq j_c$, the reflected wave becomes inhomogeneous travelling along the free surface and decaying in the vertical direction. The reflection coefficient R_{sp} becomes complex. The reflected S wave does not decay with depth. However, R_{ss} is complex and its magnitude becomes unity for all angles $j \geq j_c$. In formula (D.6) and (D.7), R_{ps} and R_{ss} are evaluated as complex numbers treating cos i as imaginary quantity given by $i\sqrt{(p^2\alpha^2-1)}$ where $p=\sin j/\beta$ is the ray parameter.

The horizontal and vertical components of SV- displacement at the free surface are also given by (D.8) and (D.9) with the difference that R_{sp} and R_{ss} must now be treated as complex quantities.

For incident SH waves the displacement are simply doubled to take into account the free surface effect. The P, SV and SH wave displacements on free surface are now given by

$$u^P = u_H^P \cos\phi \; e_1 + u_H^P \sin\phi \; e_2 + u_3^P \; e_3 \qquad \ldots (D.10)$$

$$u^{SV} = u_H^{SV} \cos\phi \; e_1 + u_H^{SV} \sin\phi \; e_2 + u_3^{SV} \; e_3 \qquad \ldots (D.11)$$

$$u^{SH} = -c \sin\phi + c \cos\phi \qquad \ldots (D.12)$$

where c is the amplitude of the SH wave in an infinite medium. The formula given by equations (D.10) to (D.12) yield P, SV and SH wave displacements on the surface of a half space due to a point shear dislocation with radiation pattern of the source and free surface effect having been taken into account. For a moving source the effect of rupture propagation has to be taken into account. A rectangular fault of length L and width W is considered as shown in Fig. D.2. The rupture initiates along the side AB of the fault and propagates perpendicular to AB at the speed of rupture propagation v_r.

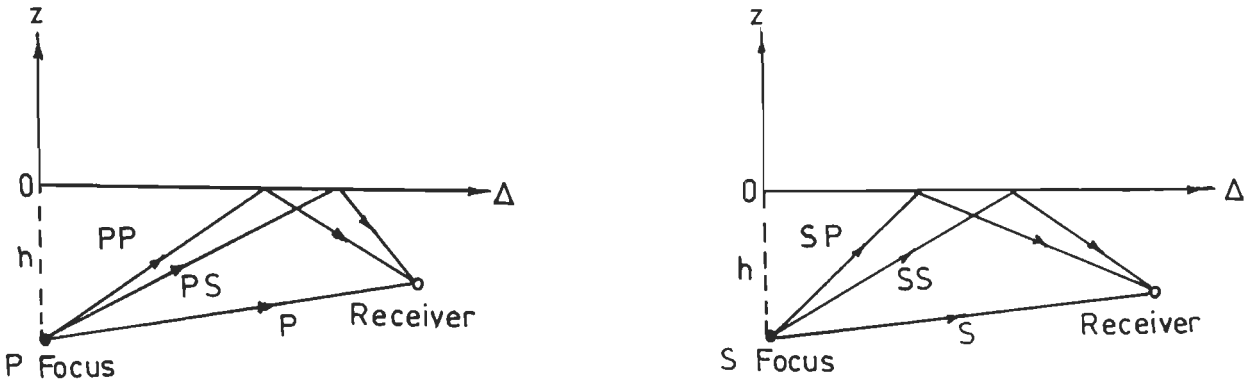

Fig. D.1 : Direct and reflected rays emanating from a buried source and received at a buried receiver

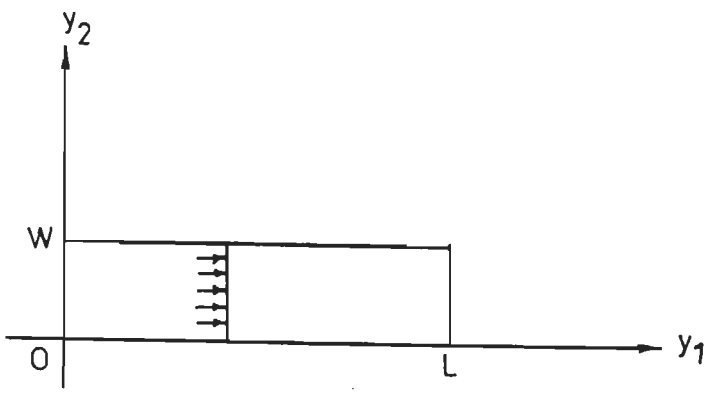

Fig. D.2 : Unilateral faulting on a rectangular fault plane

Errata of the thesis

Chapter II

Page 23 : The epicentre of fifth earthquake is out of range from the figure on Page 23. Corrected figure is attached herewith.

Page 27 : There is only one '+' sign before last variable in equation 2.6.

Page 28 : There is only one '+' sign before last variable in equation 2.8. There is one extra ')' in equation 2.9.

Page 33 : There is '-' sign before last variable in place of '+' sign in equation 2.12.

Page 63 : Corrected Fig. 2.21(i-viii) is attached.

Page 64 : Corrected Fig. 2.21(ix-xvi) is attached.

Page 74 : Corrected Fig. 2.31 is attached.

Chapter III

Page 75 : The reference referred on the page is added as

Abrahamson N.A. and Bolt B.A. (1986),Array Analysis and Synthesis Mapping of Strong Seismic Motion, Ch. 2 in Seismic Strong Motion Synthetics, B.A. Bolt (Ed.), Academic Press, INC. (London), pp 55-88.

Page 79 : The denominator term in equation 3.8 should be

$$[(\omega^2 - \omega_r^2) + 4\eta^2 \omega^2 \omega_r^2]^{1/2}$$

Page 82 : "top later" should be "top layer" in the second paragraph of the page.

Page 87 : The reference referred on the page is added as

Stearns S.D. and David R.A., Signal Processing Algorithm, Published in 1988.

Chapter IV

Page 112 The word "do" is omitted from the fourth line of the second paragraph.

Page 176 At Y-axis the value is 30.40 in place of 40.40.

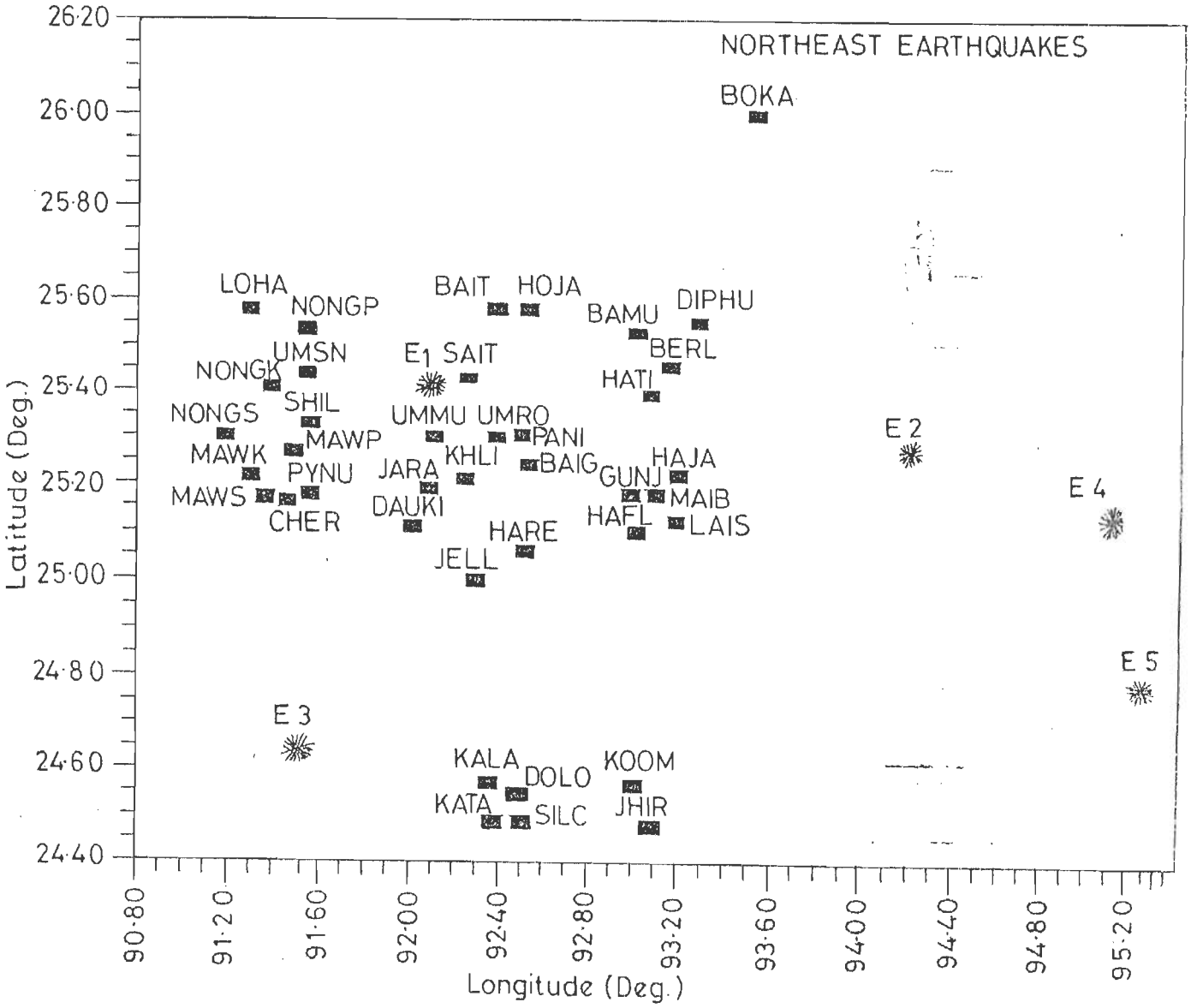

Fig. 2.6: Locations of the five earthquakes and recording stations of the northeast region

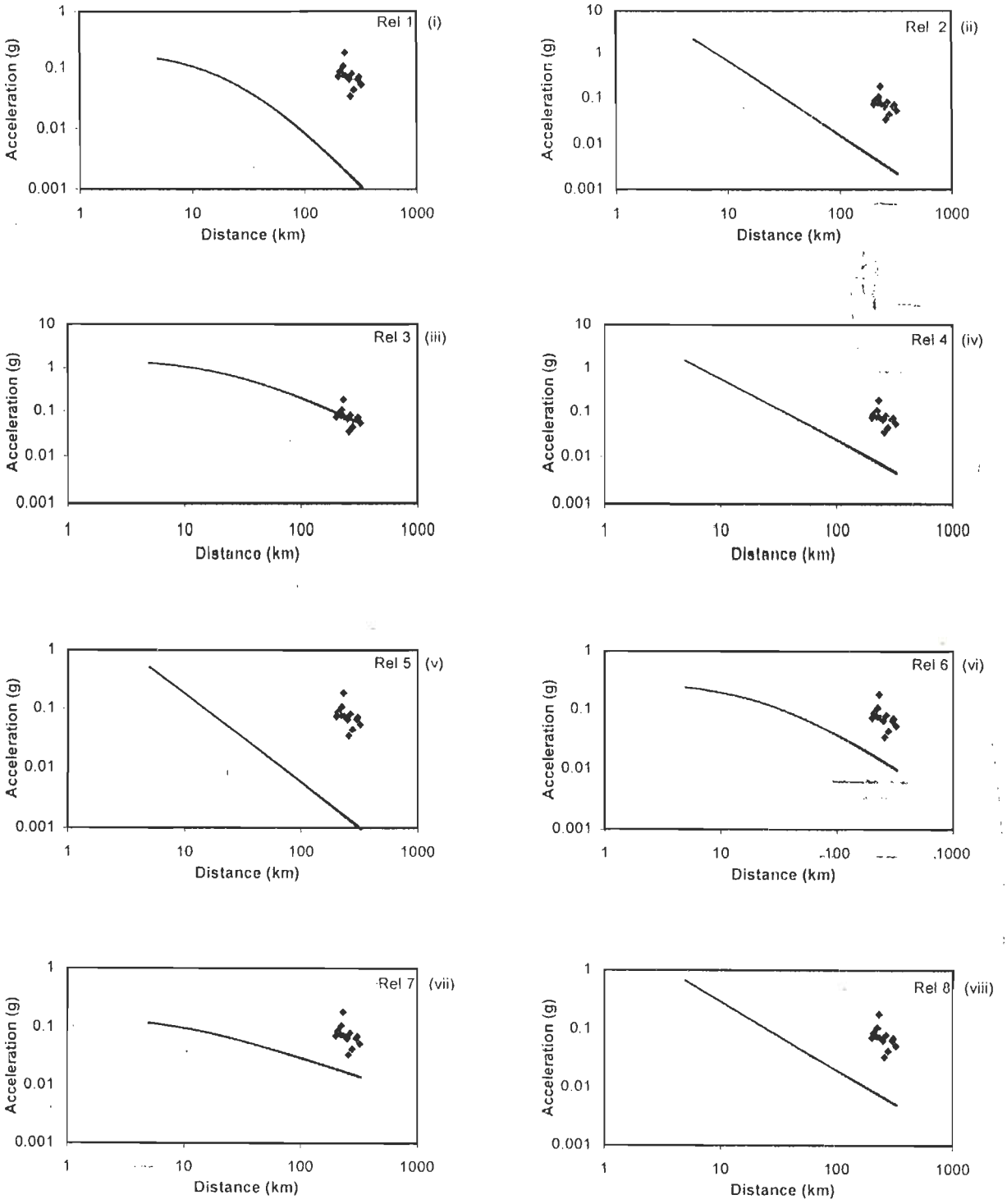

Fig. 2.21(i-viii) : Plot of the observed acceleration with distance for Northeast earthquake of Jan.1990 and the regression curves of the empirical relations for Table 2.6

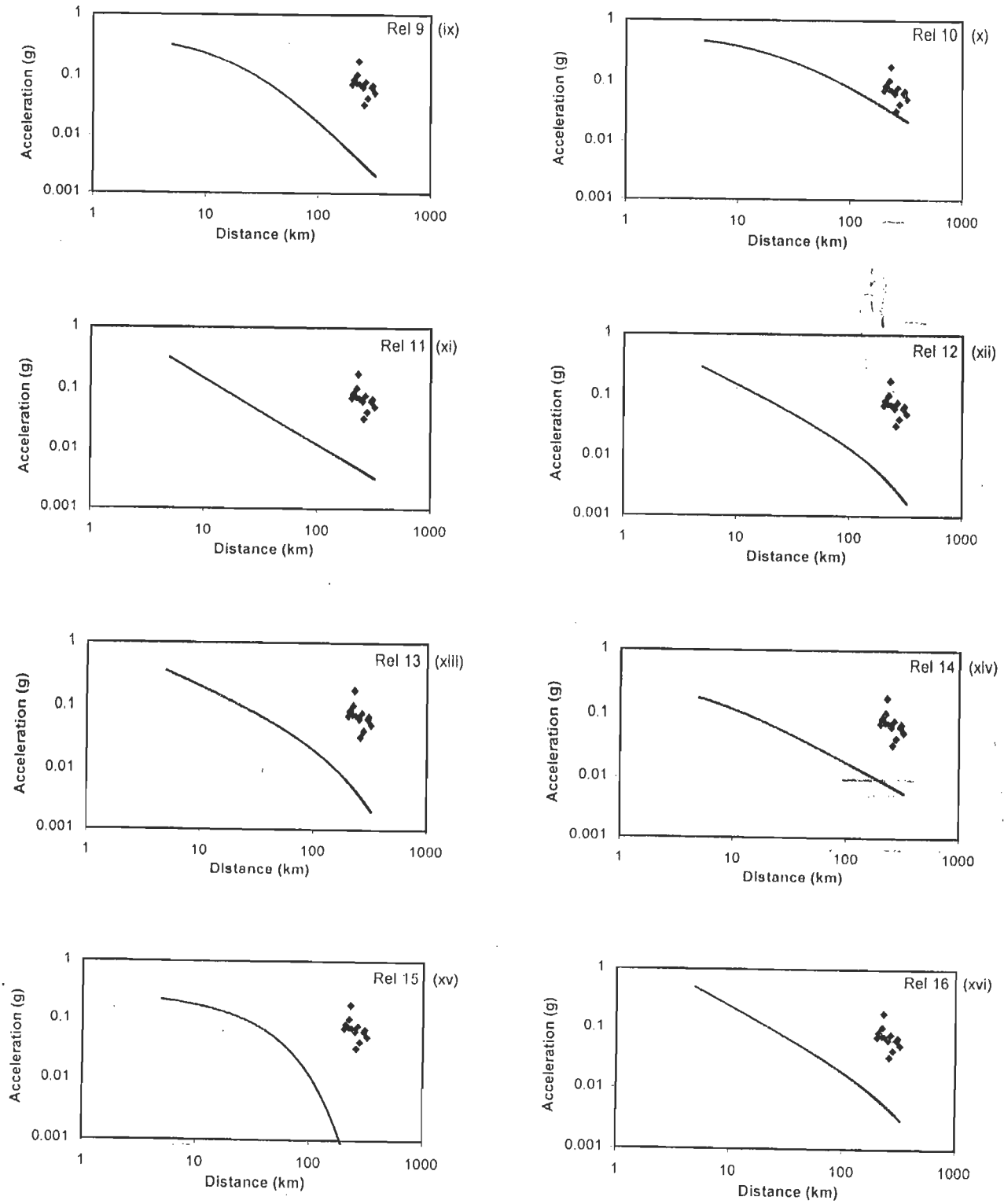

Fig. 2.21(ix-xvi) : Plot of the observed acceleration with distance for Northeast earthquake of Jan.1990 and the regression curves of the empirical relations for Table 2.6

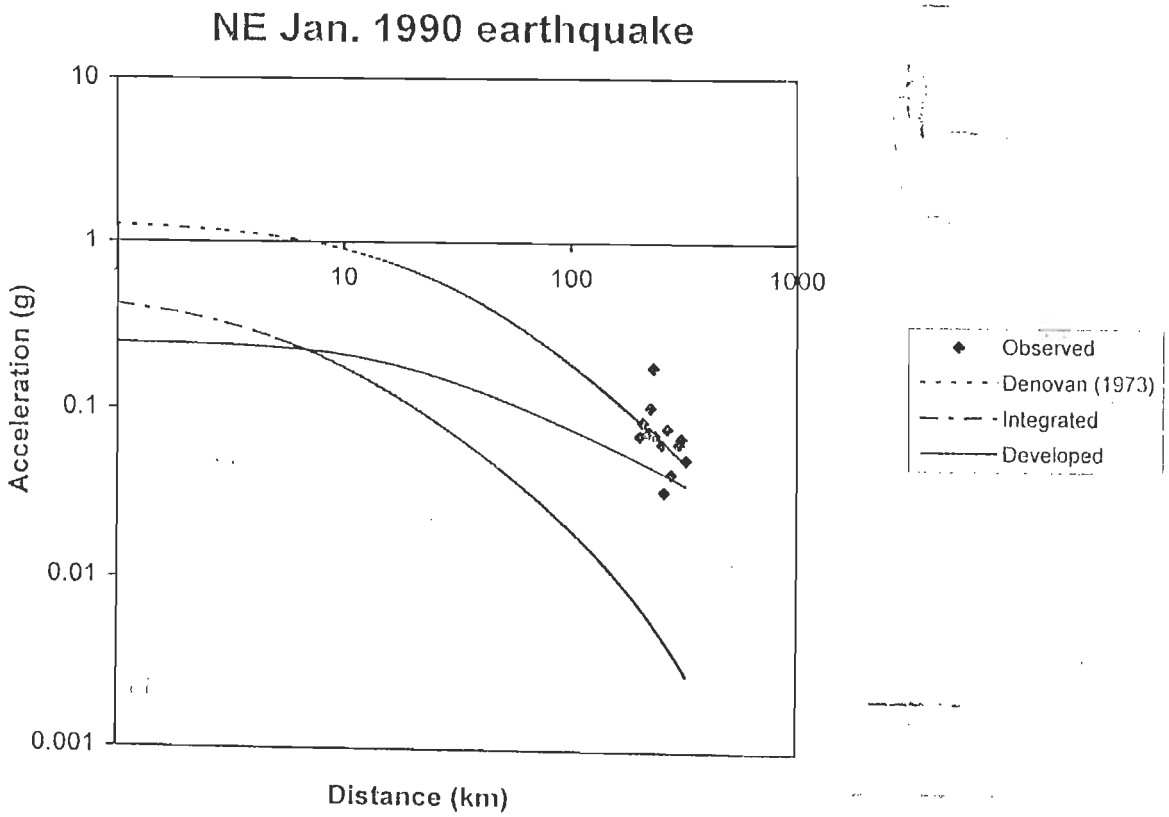

Fig. 2.31 : Comparison of observed data with developed relationship, integrated relationship and relationship from literature found min rmse (Northeast earthquake of Jan.1990)